The Design and Evaluation of Microelectrode Patterns on a Multilayer Biochip Platform for Trapping Single Cells using Dielectrophoresis

Siti Noorjannah Ibrahim

A thesis presented for the degree of

DOCTOR OF PHILOSOPHY (PhD)
In Nanostructure Sciences and Technology

Department of Electrical and Computer Engineering
University of Canterbury, New Zealand

July 2012

For my beloved husband, Shamsul Mazalan
and
my sweet little girl who was born
during my Phd journey, Ilham Najihah.

Abstract

Trapping ability on a biochip device is useful for systematic cell addressing and real-time observation of single cells analysis, however, precise control over the cell movements remains challenging. This thesis addresses the problem of controlling movement of single cells on a biochip platform by a technique called the Dielectrophoretic (DEP) force. Existing researches showed that the DEP force offers precise control of cell movements through various microelectrode designs which generate strong polarization effects i.e., DEP forces, but with the expense of damaging cell's structure.

The thesis contribute three new microelectrode designs for trapping single cells: the dipole, the quadrupole and the adaptive octupole, structured on a metal-insulator-metal (multilayer) biochip platform called the Sandwiched Insulator with Back Contact (SIBC) biochip. Cores of the study lie on the microelectrode designs that are capable of generating strong DEP holding forces, the back contact to enhance trapping of single cells and the fabrication process of creating a metal-insulator-metal structure. This thesis also presents details on the experimental setups of the trapping experiments and the numerical analysis of the microelectrode designs.

The SIBC biochip comprises of the back contact on the first metal layer, the microcavity (cell trap) on the insulator layer and the three microelectrodes on the second metal layer. Together, the three microelectrodes and the back contact generate DEP forces that attract particles/single cells toward microcavities and maintain their positioning in the traps. Prior to the fabrication, profiles of the DEP force generated by the microelectrodes are studied using COMSOL3.5a software. Simulation results suggest that the DEP trapping region can be created surrounding the microcavity if the microelectrode and the back contact are connected with AC signals that have different phases. The strongest DEP force can be obtained by setting the back contact and the microelectrodes with AC signals that have 180° phase difference.

Evaluations on the trapping functionality for the three microelectrodes were conducted using polystyrene microbeads and Ishikawa cancer cells line suspended in various medium. Trapping capability of the three microelectrodes was demonstrated through experiments with 22 percent of the Ishikawa cancer cells and 17 percent of the polystyrene microbeads were successfully trapped. With these promising results, the new microelectrode designs together with the SIBC biochip structure have huge potentials for biomedical applications particularly in the field of diagnosis and identification of diseases.

Acknowledgments

This PhD thesis would not have been possible without the tremendous help and support from my supervisors, the research group, my colleagues, my friends and my family. Above all, I would like to thank my husband for his personal support and great patience at all times. Not to forget, my parents, sisters and brothers who have given me their unequivocal supports throughout my PhD journey.

I am greatly thankful to my supervisor, Assoc. Prof. Maan Alkaisi for his guidance, encouragement and advise to this project. In fact, the last couple of years have been very challenging for me, but his patience and dedication to this research have encouraged me countless times to work on the SIBC biochip's thin films adhesion problem and proceed towards the completion of this thesis. I was honoured to have him as my supervisor and mentor.

I would like to thank my other supervisor, Assoc. Prof. John Evans for his biological expertise and insights to the study. Without his advices, details on the biological aspects of the research will be left untold. Ultimately the thesis was a result of the strong collaborative efforts between both supervisors. I also would like to thank Mr. Mike Arnold of Industrial Research, for his helps and practical advices that have improved my work tremendously.

I would like to express my gratitude to the people who involves in this thesis: Volker Nock for teaching and introducing me to the worlds of microfluidic and SU-8, Fahmi Samsuri, Lynn Murray and Muthanna Majid for the continuous supply of Ishikawa cancer cells, Xianming Liu for advice on SU-8 etching, Suzanne Furkert for her advise on NiCr and Au depositions, Jessica Chai, Khairudin Mohamed and for their advices on fabrication processes.

Special thanks to Gary Turner and Helen Devereux for teaching me how to use the machines and tips and tricks in the fabrication processes. Not to forget, room A217 people: Ciaran Moore, Prateek Mehrorta, David Kim, John Foulkes, Mikkel Scholer, and my fellow postgraduate friends: Rezaul Bari, Senthuran and Shazlina Johari for their supports.

I would also like to acknowledge the financial support of the Ministry of Higher Education of Malaysia and the International Islamic University Malaysia and its staff, particularly in the award of a Postgraduate Scholarship that provided the necessary financial support for my study in New Zealand. Finally, I would like to acknowledge the support from the MacDiarmid Institute for Advanced Materials, New Zealand.

Table Of Content

List of Figures

List of Tables

Chapter One

Introduction

1.1 The Emergence of Bionanotechnology

The miniaturisation of diagnostic instruments can benefit clinical diagnosis activities by improving the efficiency and reliability of experiments, and enhancing the accuracy of results. Smaller diagnostic devices also mean smaller sample sizes are required in the diagnosis process. Therefore, the miniaturisation concept can reduce the cost of a single device particularly when using fabricated using the microelectronics technology.

In recent years, many studies have been conducted to improve the process of device miniaturisation despite of many constraints available [1-2].The constraints are materials compatibilities, specimen sensitivities, lengthy procedures, undesired chemical reactions, lifespan of the instruments and specimens, contaminations and temperature effects [1-5]. These constraints, which sometimes co-related with each other, will affect the diagnosis and degrade the results.

Recent trends in biochip design have increased the need to encapsulate bulky diagnostic system onto a single platform, which is called the Lab on a Chip (LOC) concept. A biochip can be described as a device for detecting biological components through a physicochemical detector. It can be divided into three components:

1) The lives elements: The lives elements are the biological materials such as tissues, microorganisms, organelles, cell receptors, enzymes, antibodies, nucleic acids or a biologically derived material (biomimic).

2) The detector: A detector can be in a form of physicochemical technique such as optical, piezoelectric, electrochemical, thermometric or magnetic components, used to detect signals and interpret those signals into useful and understandable information.

3) The transducer: A transducer is the component that associates biological materials with the detector element.

Clearly, designs of any biochip platform need to accommodate the biological element for the results to be consistent, accurate and reliable. One factor that needs to be considered in a biochip design is the Scaling Law [5]. As shown in Fig.1.1, animal cells such as the red blood cells, muscle cells, pancreas cells or even cancer cells lie in the range of 1 μm to 30 μm. Taking the size of human cells into consideration, the design of microelectrode on biochip platform has to be on the same scale of these cells i.e., in the micrometer scale. Biochip platforms that are proportional to the target specimens will result in improved throughputs and performances [5].

To imitate the natural condition of a biological specimen, recent studies have demonstrated the possibilities of integration between biochip devices and microfluidic components [6-8]. Moreover, the immense potentials due to this integration have driven many researches to design new platforms for trapping cells that also have capability of cells addressing.

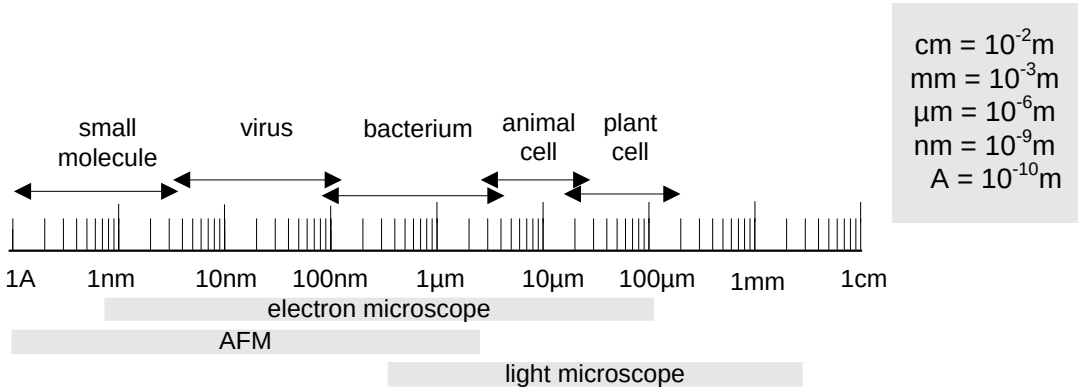

Figure 1.1: Size of biological elements in comparable with the scaling law and the means of imaging [5].

1.2 Research Objectives

The motivation of this research is to design a bio-analysis platform which uses the dielectrophoretic (DEP) force for trapping single cells. The main focus is to investigate ways to control movement of single cells on biochip platform and ways to trap them at specific locations by using a new microelectrode design and/or biochip platform structure. In this work, a multilayer biochip structure called the Sandwiched Insulator with Back Contact (SIBC) biochip is developed together with three new microelectrode designs. This thesis also presents descriptions on the SIBC design and issues regarding the fabrication of the SIBC's multilayer structure, experimental setup as well as the DEP trapping results.

In brief, to structure the SIBC biochip involves several stages. At first, studies on the microelectrode designs were conducted using the Matlab7.7.0(2008b) and COMSOL3.5a software. This is followed by the fabrication stage using the photolithography and

softlithography techniques. Subsequent to the fabrication stage, functionality test is conducted on the SIBC biochip using polystyrene microbeads and Ishikawa cancer cells.

Despite the great potentials in live sciences analysis, studies on single cells trapping remain challenging. There are many confounding factors that need thorough investigation particularly the cell's unique structure and membrane components that are highly responsive to its surroundings. One issue afflicting any DEP-based biochip is the over-heating of microelectrodes which in turn can affect cell viability. It occurs when the microelectrode generates high non-uniform electric fields in order to produce strong DEP holding forces. Therefore, numerical analysis of the microelectrode designs is essential as DEP profiles of the designed microelectrode can be thoroughly studied.

Another way to maintain a cell's viability is by incorporating a microcavity on the SIBC platform. By using the microcavity structure, a minimum DEP force is needed to control cell's positions after a cell is trapped. Studies have also shown that placing microcavities will influence cells to be in a statutory position, when feasible amount of DEP force is supplied to the platform [9-11].

Integration with microfluidic channel also reduces cell damage during the DEP trapping experiments. Thus, cell immobilization and monitoring cell's responses toward various treatments can be performed concurrently on the same platform. Nevertheless, trapping single cells at a specific location requires a trade-off between the DEP force's strength and cell's viability.

1.3 Thesis Outline and Contributions

1.3.1 Thesis Outline

The thesis starts with an introduction to the emerging area of bionanotechnology and the principal of biochip design for biological analysis. In this opening chapter, the motivation behind this study is described, the research contributions are highlighted, and publications based on the research are listed.

Chapter Two details the convergence of biological cell analysis and microfabrication technology which becomes the essence of this thesis. The chapter starts with an introduction to the single cell structure, the cell membrane transport mechanism and the microfabrication application in single cell analysis. This is followed by the microfabrication technology in single cell studies in section 2.2 where the literature reviews on cell manipulation techniques are presented in subsection 2.2.1. Meanwhile, section 2.3 focuses on the type of DEP manipulations on biochip. The chapter ends with descriptions on the development of SIBC biochip in section 2.4.

In Chapter Three, the effects of DEP force on cell movements, the DEP force trapping mechanisms and the effects of hydrodynamic force on a biochip are presented. The chapter starts by explaining the dipole force concept, followed by describing the DEP trapping mechanisms employed on the SIBC biochip. The idea of precise trapping of single cells on the SIBC biochip is highlighted in subsection 3.3.1. This is followed by the theoretical aspects of the hydrodynamic force. The chapter ends with a brief description on the SIBC biochip concept in section 3.5.

The methodology for designing the SIBC biochip is explained in two chapters. Chapter Four details the numerical analysis of the three microelectrodes using a finite element software i.e., COMSOL3.5a. In this chapter, the electric field distributions and DEP force profiles generated by the three designed microelectrodes were examined. Subsection 4.2 presents studies on the horizontal plane of the SIBC biochip while subsection 4.3 describes studies on the vertical plane of the microcavity.

Chapter Five comprises of the fabrication processes of the SIBC biochip and the microfluidic channels. This chapter covers the general photolithography and softlithography processes used for creating the SIBC biochip and its microfluidic channel. Here, issues regarding the fabrication processes together with its possible solutions are discussed. The fabrication process of the SIBC biochip is detailed in section 5.1, and followed by the processes for the microfluidic channels in section 5.2. The chapter ends with details on the integration of SIBC biochip and microfluidic system as presented in section 5.3.

Chapter Six details the experimental setup and the DEP trapping results. The first part of this chapter looked into the differences between conducting DEP experiments on an open platform and a close platform setup. Then, section 6.2 presents the results of DEP trapping experiments conducted on the three microelectrodes. Here, single cells trapping ability for the three designs microelectrode were observed through experiments with polystyrene microbeads and Ishikawa cancer cells line. Meanwhile, the comparison on trapping ability between the SIBC biochip and the planar two-layer biochip is detailed in subsection 6.2.6. The chapter ends with discussions on the DEP experiments trapping results.

Chapter Seven concludes this thesis with summary of the research. This chapter covers research contributions and suggestions for future works that can be integrated with the microelectrode designs and the SIBC biochip.

1.3.2 Thesis Contributions

The originality of this research stems from the development of SIBC biochip's microelectrode designs which involves several crucial stages: the design using numerical analysis, the fabrication process and the experiments with biological cells stage. The research contributions on the SIBC biochip study are as follows:

1) Three novel microelectrode patterns for single cells trapping using the DEP force. They are the dipole, the quadrupole, and the adaptive octupole microelectrodes.

2) A biochip platform consists of a multilayer structure that allows DEP force to be generated inside the microcavity, which in turn enhanced the overall DEP force on the platform. The significant of having DEP force inside the microcavity has on trapping single cells was demonstrated by conducting experiment on the SIBC and planar two-layer biochips using the same type of particles i.e., the polystyrene microbeads and the Ishikawa cancer cells.

3) The numerical analysis of the three novel microelectrode designs and the multilayer structure conducted using Matlab7.7.0(2008b) and COMSOL3.5a software. In the analysis, other factors that contributed to DEP force such as AC signals potential (φ) configurations, amplitude and phase are also studied. Results from these studies suggested that the designed microelectrodes were capable of producing DEP holding force to maintain cell positioning inside the microcavity.

4) The development of a fabrication process for multilayer thin films, consisting of metal-insulator-metal layer on a substrate, which is unique in itself due to the materials and the deposition technique used. Here, the fabrication process of microcavity layer on a metal using SU-8-2005 was developed and characterized.

5) The Integration process with the microfluidic channels which details the techniques on reversible and irreversible bonding between SU-8 and PDMS material. The integration has increased the SIBC biochip potentials for other cell manipulation techniques.

6) A set of useful DEP force trapping parameter, in particular the trapping frequency for polystyrene microbeads and Ishikawa cancer cell lines suspended in medium of different conductivity. During the experiments, the amplitude and frequency of φ are varied and their effects on the SIBC biochip are also observed. These parameters are useful and relevant in DEP manipulation for the adherent-type of cells, and in profiling cell type in other clinical stimulus.

7) In this study, a planar two-layer biochip equipped with the three microelectrode patterns is fabricated to distinct cell's movements on the SIBC biochip.

8) Finally, the different approach used for cell loading and handling on top of the SIBC biochip resulted with different experimental results. Experimental results showed that by integrating microfluidic channels on top of the biochip, observations on movement of single cells can be facilitated.

The following are peer-reviewed journals and conference proceedings publications resulted from works conducted in this thesis:

1) S. Noorjannah Ibrahim, L. Murray, V. Nock, John J. Evans and Maan M. Alkaisi, "The Quadrupole Microelectrode Design of Multilayer Biochip", in Special Issue: Micro and Nano Engineering, Journal of Microelectronics Engineering, Vol.97,pp.369-374. (2012).

2) S. Noorjannah Ibrahim, L. Murray, John J. Evans and Maan M. Alkaisi, "Trapping Single Cells: Comparison between Sandwiched Insulation with Back Contact (SIBC) and Planar Biochip", Advanced Material and Nanotechnology in the Journal of Materials Science Forum, Vol. 700, pp.188. (2012).

3) S.Noorjannah Ibrahim, L. Murray, V. Nock, John J. Evans and Maan M. Alkaisi, "Trapping Single Cells on a Sandwiched Insulator with Back Contact (SIBC) Biochip", short paper in the conference proceeding of the 2012 International Conference on Nanoscience and Nanotechnology (ICONN2012), (Perth, Australia, February 2012).

4) S.Noorjannah Ibrahim, John J. Evans and Maan M. Alkaisi, "The Quadrupole Microelectrode Design of Multilayer Biochip", abstract in the conference proceeding of the 37th International Conference on Micro and Nano Engineering (MNE2011), (Berlin, Germany, September 2011).

5) S.Noorjannah Ibrahim and Maan M. Alkaisi, "The Comparative study of Dipole, Quadrupole and Octupole Microelectrodes for Trapping Cell", abstract in the conference proceeding of the 36th International Conference on Micro and Nano Engineering (MNE2010), (Genoa, Italy, September 2010).

The work described in this thesis has also been presented in various forms i.e., Oral and Poster Presentations:

1) Oral Presentation on "Trapping Single Cells on a Sandwiched Insulator with Back Contact (SIBC) Biochip", at the 2012 International Conference on Nanoscience and Nanotechnology (ICONN2012), (Perth, Australia, February 2012).

2) Oral Presentation on "The Quadrupole Microelectrode Design of Multilayer Biochip", at the 37th International Conference on Micro and Nano Engineering (MNE-2011), (Berlin, Germany, September 2011).

3) Poster presentation on "Trapping Single Cell in Microfluidic Channel using AC Electrokinetics", at the Fifth International Conference on Advanced Materials and Nanotechnology (AMN-5), (Wellington, New Zealand, February 2011).

4) Poster presentation on "Lab on Chip: Trapping Single Cell with AC Superposition", MacDiarmid Institute Student Symposium (Wellington, NZ, November 2010).

5) Poster presentation on "Patterns that Trap Cells: Comparative Study of Dipole, Quadrupole and Octupole Trapping Behaviour", at the 36th International Conference on Micro and Nano Engineering (MNE 2010), (Genoa, Italy, September 2010).

6) Poster presentation on "Lab on Chip: Trapping Single Cell with AC Superposition", at the Engineering Research Poster Competition, University of Canterbury (Christchurch, New Zealand, August 2010).

7) Poster presentation on "Controlling Single Cell Positions on Biochip: using quadrupole microelectrode and back contact arrangements to enhance dielectrophoretic force efficiency", at the 2010 International Conference on Nanoscience and Nanotechnology (ICONN 2010), (Sydney, Australia, February 2010) and **Award for the Author of the Best Poster.**

8) Poster presentation on, “Trapping Single Cell: A Biochip Design for Cell Analysis”, at the Canterbury Health Research Poster Expo (Christchurch, New Zealand, June 2009).

9) Poster presentation on, “Catching Single Cell using Dielectrophoresis”, at the Engineering Research Poster Competition, University of Canterbury (Christchurch, New Zealand, September2008).

Chapter Two

Introduction to Single Cells Manipulation

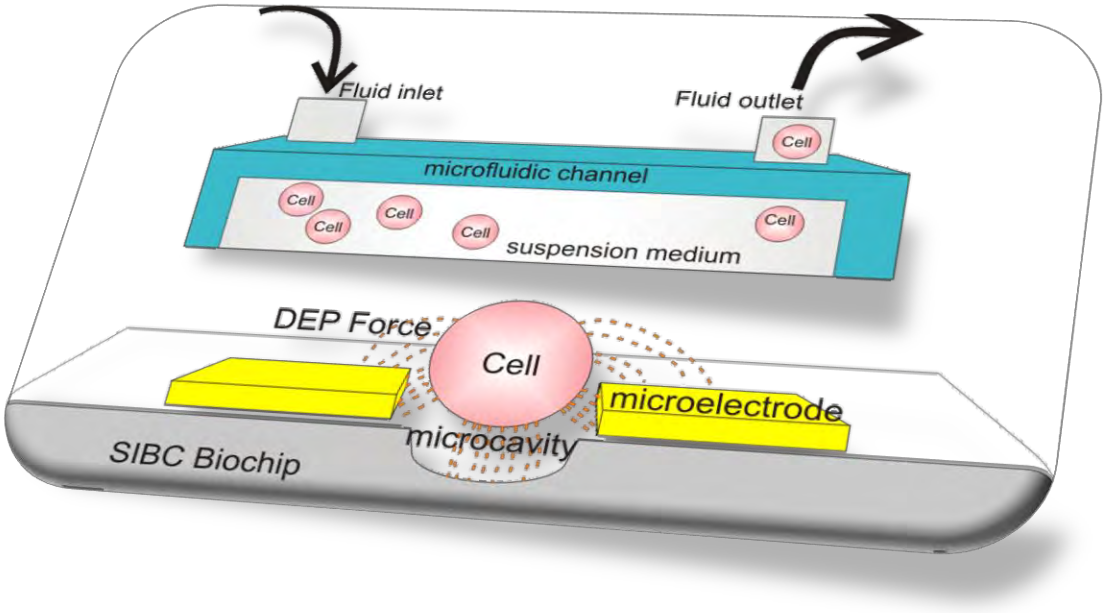

Chapter One has highlighted in brief the motivation, objective and achievements of this research. In this chapter, background details on the work are discussed. Here, the contributions of microfabrication technology and the different manipulation techniques in single cell studies are presented. The chapter starts with a brief introduction on cell structure and is followed by descriptions of the cell membrane transport mechanism. Then, section 2.2 summarizes the microfabrication technology used in single cells studies. Here, reviews on the cell manipulation techniques are also presented. This is followed by section 2.3, where details of cell sorting/trapping applications using the DEP force are discussed. The chapter ends with details on the development of the SIBC (Sandwiched Insulator with Back Contact).

2.1 Single Cell Structure and Physiology

2.1.1 Introduction

At present, research on human diseases returns to the fundamental of biological sciences and focuses down to the single cell studies. Undoubtedly, knowledge in cell physiology is crucial to address any integration issues between the biochip fabrication process and single cell analysis function. A cell is the basic building blocks of living things. In the human body there are about 75 trillion to 100 trillion cells, and each type of cells is dedicated to executing a different type of task [12]. For example, the red blood cell acts as the oxygen carrier to the lungs and tissues in our bodies while the beta cells in the pancreas are responsible for releasing insulin hormone into the body.

The nucleus and the cytoplasm are two major components of the cell, separated by a nuclear membrane. The cytoplasm however, is isolated from the surrounding fluids by an elastic barrier called the cell membrane. As illustrated in Fig. 2.1, cytoplasm contains organelles, each has an important role in the cell's biochemical processes. The mitochondria for example, extract energy from nutrients and oxygen, and act as the main energy supplier to the cell. Therefore, inadequate energy resulting from malfunctioning mitochondria will hinder cell to function efficiently.

Cell gateway to the extracellular world is through the 7.5 nm to 10 nm thick cell

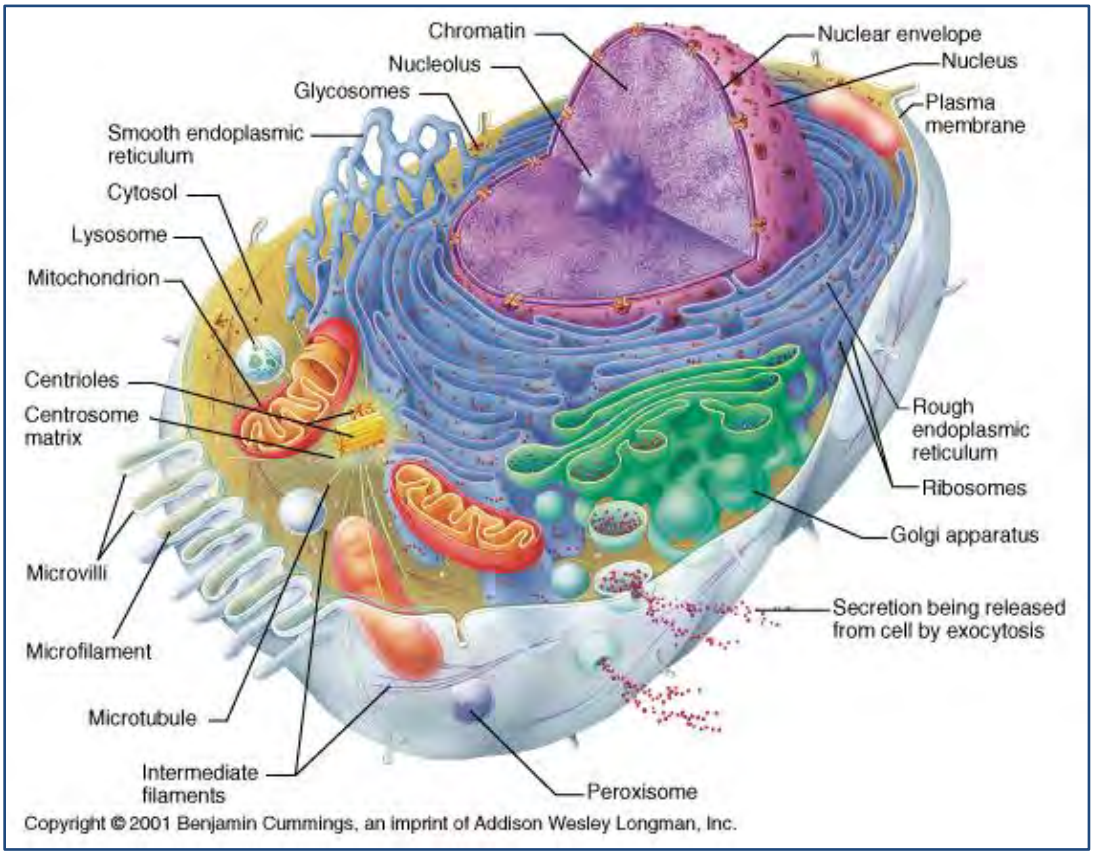

Figure 2.1: An illustration of the cell and its internal components adapted from [13].

membrane [12]. It functions as the input and output controller for water and water soluble components while maintaining the cell's shape. It has a lipid bilayer that filters ions, glucose, urea and other water soluble substances from entering the cell, yet allows fat soluble substances such as oxygen, carbon dioxide and alcohol to penetrate into it. The lipid bilayer is physically fluid not a solid structure [12], hence some parts of the membrane are seen as flowing from one point to another along the membrane surface. This fact points out the reason why fluidic components are incorporated in cell analysis biochips. Ideally, results from any cell manipulations are representations of the actual cell behaviours in its natural environments.

2.1.2 Cell Membrane Transport Mechanisms

As a living organism, a cell has several basic functions. It must obtain nutrients from surrounding environments to accommodate its needs and regulate unwanted substances from the cytoplasm. There are two ways for substances to flow through the cell membrane; diffusion and active transport. They relay the electrical and biochemical signals of cell systems and thus, knowledge of the membrane's transport mechanism is crucial in disease studies. Diffusion describes the random movements of uncharged substances either through molecule by molecule interactions or combinations of molecules and a carrier protein. An active transport illustrated in Fig. 2.2(a) on the other hand, is referring to the movement of ions or substances across the membrane against an energy gradient such as from a low concentration state to a high concentration state, hence requires an additional source of energy.

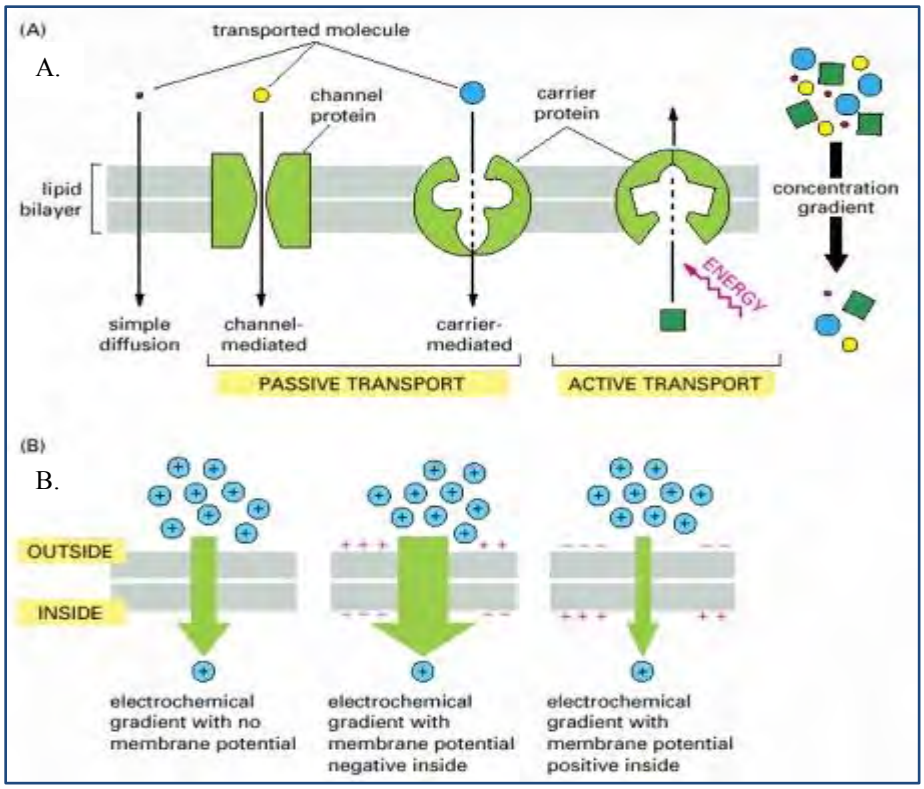

Figure 2.2: (a)The difference between passive and active transports. (b) The driving force on an ion across a cell membrane is enhanced by combinations of the membrane potential and cell's concentration gradient[14].

In a medium with net charges as in Fig. 2.2(b), the active transport mechanism can be stimulated by different factors such as the concentration gradient, the electrical potential difference across the membrane and the membrane potential. This effect points out the possibility of using external source such as voltage supply, to stimulate cellular transport mechanism and observe cell behaviour. Under such experimental setups, the cell membrane acts as an electrical capacitor with an approximate value of around $1\mu F/cm^2$ [12]. Any changes to the cell membrane from these manipulations are transformed into measureable electric signals. Another important character of an active mechanism is that the cell membrane's potential difference induces positively charged ions into the cell, and at the same time opposes the entry of

negatively charged ions [14], unless the cell is suspended in a medium with specific concentrations that reverse the charged ions' directions.

Alternatively, large particles can enter the cell using a special process called endocytosis or ingestion by cell. There are two forms of endocytosis, the picocytosis and the phagocytosis. The picocytosis creates vesicles around 100 nm to 200 nm in diameter on the cell membrane which allows protein molecules to enter the cell. This process requires energy supplied by ATP (Adinosine-5'-Triphosphate) from the cell and calcium ions from the extracellular fluid. Meanwhile, the phagocytosis process involves much larger particles than molecules such as bacteria, cells or tissue debris. However, not all cells are capable of phagocytosis, only a few types of cells such as tissue macrophages and some of the white blood cells are known to have this capability [12] .

The cell transport mechanism has essential information that can be used in the development of new drug treatments and tool for diagnosis of diseases. For instance, by applying the knowledge of the ion channels across cell membrane, the intracellular and extracellular electrical recordings can be made which may provide the foundations for cell-based biosensor designs. In order to record electrical signals, the ion permeability of protein pores on the membrane surface is charged by exerting an electric field along the ion channel or by binding ligand to the protein channel [15]. Another example is the patch clamp, a method used for recording current flow through a single protein channel, was made possible by understanding how the cell diffusion process works.

An interesting question worth exploring is whether these electrically measured transport mechanism occurrences, really resemble changes on membrane surfaces. Efforts on profiling

changes in cell membrane surfaces using optical microscopy are not without challenges. The CLM (confocal laser microscopy) for instance, is capable of surface profiling but required specific preparation and florescence staining on cell before the imaging process. Excellent high resolution images using AFM (atomic force microscopy) scanning are considered to be the best approach to capture the cellular transport mechanism. However, concerns over the sharp tip used in scanning microscopy, which can protrude and rupture cell membrane structure, impedes direct imaging on biological cells [16].

Another issue with AFM imaging is the maximum depth (z-limit) of scanning which is limited by the shape and size of the AFM tip. Hence, profiles of exocytosis pits using direct AFM scanning might not represent the pit's actual depth [9]. Imaging biological cells in a vacuum or in air environments as required by TEM (Transmission Electron Microscopy) or SEM (Scanning Electron Microscopy) has its drawbacks. Cells have to go through a dehydration process, and must be immobilised on a platform through cell fixation processes. Not only are these procedures time consuming but they may also alter the cell's morphology and structure [16].

To address these limitations on tools and methods in cell imaging, an integrated approach with microfabrication technology called Bioimprint was introduced [17]. It uses nanoimprint technology by using a polymerised monomer mixture to profile cell surfaces. A replica of the cellular profiles, obtained through careful selection of monomer polymer and specific solidification process, are scanned using AFM. However, accurate cell replication requires the cell to be in its original structure, with minimal changes from its culture conditions or cellular

environments. This in turn has motivated this research to develop a cell handling device dedicated for trapping single cells.

2.2 Microfabrication Technology in Single Cells Study

Efforts to understand an individual cell's behaviour in a complex organism system often approaches using a minimal concept. Therefore, microfabrication technology is used to create boundaries that localize a cell in specifically designed environments. Using the microfabrication technology, the designed environment can also be used to isolate selected cells in preparation for clinical analysis [18]. Furthermore, the cell analysis platform can be integrated with various sensing techniques which provide high throughput analysis and precise characterization of biological samples. For instance, a biochip can be incorporated with image-based analysis and biochemical techniques for expressing gene and protein analysis of cancer cell lysates [19] .

In conventional cell studies, where cell activities are observed in large batches, results obtained sometimes do not truly represent a single cell activity due to the cellular heterogeneity being masked [20]. Moreover, the quantitative measurements obtained, are average results derived from large cell colonies. In contrary to the previous method, one to one analysis of cells is possible in microfabricated devices, allowing insights of a biological cell to become more visible.

Single cell analysis allows researchers to discern how disease originated. Results from these cell studies are useful in defining the role of a cell in an organism, to predict an organism's normal functions and pathological changes. In diabetes type II disease for example, problem

starts when the beta cells which are responsible for producing adequate insulin hormone in response to the glucose levels become unresponsive [12]. These cells do not necessarily lose their function all at once, but the problem progresses through time. Finally, the problem results in the pancreas being incapable of regulating the insulin hormone. Through single cell study on a biochip, researchers can develop an effective way to combat this disease by observing cell responses towards the studied drugs or chemical stimulus in a well-controlled environment.

A cell is also known to behave differently depending on whether it is alone or part of a cell culture. Interactions between one cell to another, present actual insights of the intercellular activities of biochemistry signals and mechanical interactions which are relayed by multiple signals such as cytokinesis, protein secretions etc. [21]. However, in mass cell populations, the relative signals could be misinterpreted as a response of an individual cell to another cell. For that matter, a microfabricated analysis platform is useful in single cell studies as the biochemical signal relays are facilitated in controllable and reproducible manners.

Detection of abnormalities in cell membrane structure may benefit cancer cell studies. Usually, cancer cells are the results of oncogenes i.e., mutation or abnormal activation of cellular genes which affected the ability to control cell's growth and mitosis, and these changes can be observed on cell membrane surfaces. This also points out that cell membrane transport mechanisms might have significant changes due to these abnormalities. One significant aspect of this disease is the cancer cell's heterogeneity, meaning that there is a range of characteristics of an individual cancer cells which makes identifying the cause of progression of this disease persistently challenging [22].

A biochip can offer a flexible environment for cell study, as cellular heterogeneity can be designed and controlled according to the required specifications. For example, heterogeneous cell populations can be fractionated into homogeneous populations or selected single cells, so that different cell types can be analysed separately [20]. Due to the possibilities to integrate the microfabrication technology with cellular analysis in biological studies, it is increasingly difficult to ignore the technology benefits. These considerations justified the use of the microfabrication methods in designing a single cells analysis platform or a biochip.

2.2.1 Cell Manipulation Techniques

There are many cell analysis techniques that can be used on a biochip. As shown in Table 2.1, these techniques usually evolve from a basic physics phenomenon, the nature of cells and their compatibility with a new technology. A bioanalytic device is designed according to its requirements such as the objective of cell studies, cost benefits, processing time, reproducibility of device and portability. In general, a simple biochip provides the facility for a single manipulation process while a complex design provides integration of one or more manipulation techniques. Hence, these cell manipulation techniques must be thoroughly reviewed before incorporating it on a single cell analysis biochip.

Surface chemistry is one technique commonly used in cell manipulations in which substrate surfaces are modified with materials i.e., metals, polymers, self-assembly monolayers, proteins and bioactive molecules through microfabrication processes. The technique uses matched chemical interactions between cell membrane receptors and substrates to bind cells at specific locations. The main advantage of this technique is that researchers are able to control changes on surface roughness, surface structures or chemical bonding, thus allowing for

intercellular activities to be monitored in a controlled environment [23-25]. Figure 2.3 depicts an example of the usage of surface chemistry on cell's growth in a confined environment.

Table 2.1: Cell manipulation techniques in microfabrication technology.

Technique	Single/ Many Cells Manipulation	Parallel process	Suitable for SIBC	References
Surface Chemistry	Many cells	Yes	No	[23-26]
Hydrodynamic Traps	Single cell and many cells	Yes	Yes	Suction [27-30] Laminar [31] Electroosmotic [32]
Optical	Single cell and many cells (limited manipulation)	Yes	No	[31, 33-34]
Acoustic	Many cells	Yes	No	[31]
Dielectrophoresis	Single cell and many cells	Yes	Yes	[35]
Grippers	Single cell	N/A	No	[36-38]
Hydrogel	Single cell and many cells	yes	No	[39-41]

Despite being widely used in cell patterning, cell adhesion to a surface is usually irreversible [29] and leads to cell death. Therefore, a means to release cells from the substrates is

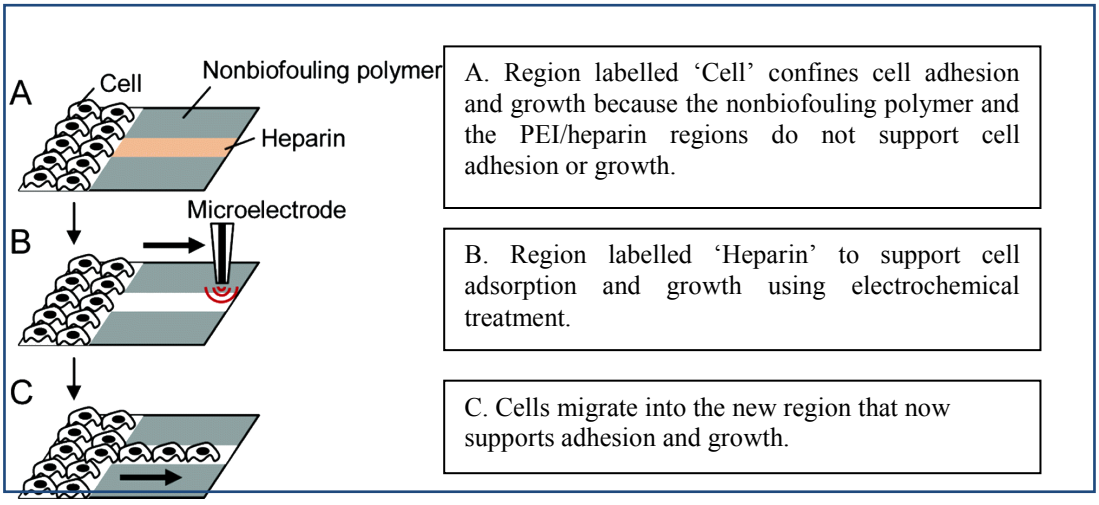

Figure 2.3: Surface chemistry modification allows cell patterning in a geometric confined environment [11].

necessary, which is dependent on the selection of the chemical interactions that are involved in trapping a specific cell. Although the technique can be used for immobilising cancer cells [31], the lack of a method reliably and efficiently traps single cells makes directing a cell into a stipulated microcavity or vial very challenging [42]. This issue highlights unsuitability of the surface chemistry technique to be used in this study.

Another common manipulation technique is the hydrodynamic force. This method can be categorised into three main areas: trapping by suction [27-29]; laminar flow segregation [31]; and electroosmotic tweezers [32]. One interesting fact about hydrodynamic force is that it offers smooth loading of cells on biochips with minimum physical interference. This is because, in general, cells are cultured in fluid suspension or in an aqueous medium. Not only is the technique an excellent way to handle mass populations of cell, it is also capable of precise single-cell trapping. A study on an automated hydrodynamic system, using the Escherichia Coli bacterial cells in Luria-Bertanu-LB broth medium, has claimed that the bacterial cells were successfully trapped up to single cells efficacy [43]. The system uses a laminar flow stagnation point at four microchannel junctions, which trapped cell in the centre of the fluid flow.

Next, the hydrodynamic trapping by suction method, which was first introduced in conduit patch clamp in 1945 by Hodgkin and Huxley [44], has inspired many modern fluidic-based analysis systems. Using this hydrodynamic technique, evidence of high throughput single-cell trapping on PDMS arrays and recording of cells' electrochemical activities were reported [27]. Hydrodynamic force has also been used to filter cells from laminar flow using mechanical barriers to trap the cells in microwells [31]. Due to the high probability of traps remained empty

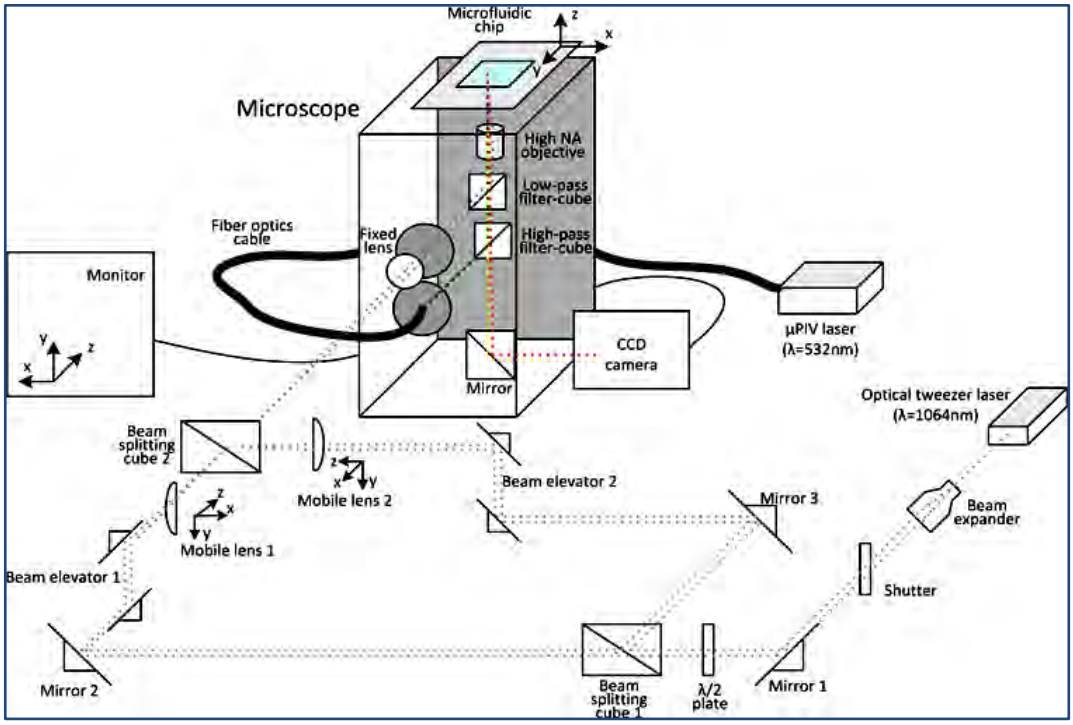

Figure 2.4: Setup for cell manipulation using the optical tweezers method. A laser needs to go through different optical components including beam splitting cubes that can complicate the setup for cell analysis [19].

than filled with single cells [43], the results of trapping by loading mass single cells onto a platform using the laminar flow technique are usually very poor.

Optical tweezers are an excellent technique for cell sorting and separation. This technique uses laser light to exert forces on cells, positions and traps them at a stipulated location [45]. In theory, the trapping mechanism is achieved by passing a laser beam through a microscopic lens and focusing it onto a diffraction limited spot. Different refractive indices of medium and cells create rays of refracted light, which then exerts a force onto the cell, and guides movement of cells on the platform [33]. However, the heat releases from the applied power and wavelength of the focused laser beam might cause some damage to the cells during manipulation process. Figure 2.4 illustrates the setup of an optical cell manipulating techniques.

Another technique that can be used in single cell analysis is the piezoelectric method. The piezoelectric transducers on biochip are used to generate acoustic waves for cell manipulation. Due to the difference of cell's density and cell's suspending medium, the transducer produces ultrasonic standing waves that is capable of moving cells [31]. With this technique, cells aggregate at the nodes of a standing wave, so that cell segregation is possible between different types of cells. As all cells are impacted with the same energy, control over an individual cell is difficult. Due to the complicated setup and the compatibility issue with the Bioimprint [9] process (details are in subsection 2.3.1), the optical tweezers and the acoustic wave techniques are not used in this research.

Microgrippers is a very useful technique for precise trapping of single cells. As shown in Fig. 2.5, this technique can efficiently maintain single cell position, and yet allows for some random movements [38]. However, the inability to perform parallel manipulations on different cells remains as the major limitation of microgrippers. Due to this fact, this method was not chosen to be used in this research. Another downside of this technique is the slow sample loading time, as only one cell can be manipulated at a time.

Another method for cell manipulation is trapping with hydrogel. In this technique, hydrogel encapsulates cells and then needs to be cured under UV light radiation [31]. The cured gel functions as a mechanical support to the cells and maintains their positions until the gel dissolves. However, this is a one shot loading technique, which limits cell mobility after a cell is attached to the gel [39]. It is also difficult to define single cell trapping during a mass loading of cells as the cells are inclined to aggregate on the gel. Moreover, once the gel is solidified,

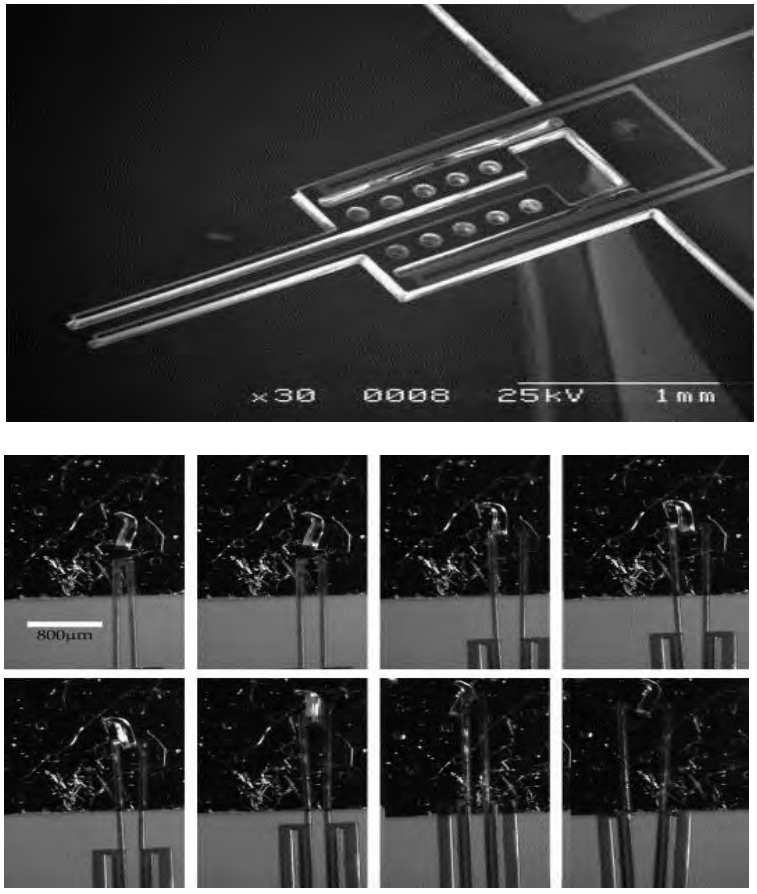

Figure 2.5: Images of microgrippers adapted from [24] used for cell manipulation. (a) The SEM image of microgrippers. (b) Microgrippers in actions; sequence images of microgrippers gripping and place a gold coated SU8 object between its holders.

chemical stimulation cannot be performed on a cell. An example of trapping with gel is shown in Fig.2.6.

Finally, the DEP (Dielectrophoresis) is another widely used technique in single cell manipulations. This method uses DC or AC signals to generate electric fields that trigger cell movements on a biochip platform [46-47]. The DEP force depends on the electrode designs to generate a high gradient of non-uniform electric fields. Due to the nature of DEP, which uses electric fields as its source, presence of any conductors or insulators on the platform will affect

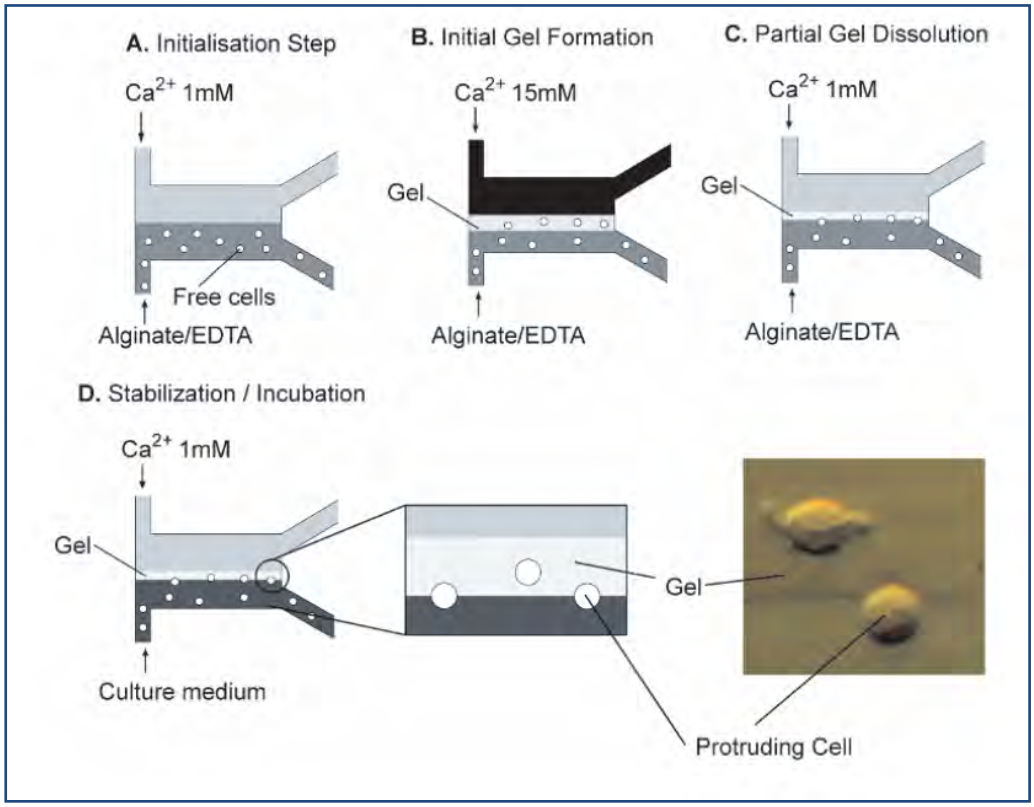

Figure 2.6: Protocols for positioning HEK 293 cell in a microfluidic channel at the gel border [26].

the DEP force. In the context of this research, the design of single cells analysis platform which is called the SIBC (Sandwiched Insulator with Back Contact) biochip, will make use of the DEP technique in combination with hydrodynamic force as the main manipulation technique. In depth discussions on both techniques, which include theoretical aspects and design requirements, are presented in Chapter Three.

2.3 Trends of DEP manipulation on Biochip

A study on DEP force was first initiated by H.A. Pohl in the 1950s. The governing equation of DEP was the result of his observations on homogenous particle movements in non-uniform electric fields [48-49]. In 1966, separation of live and dead cells in non-uniform electric fields was successfully demonstrated using DEP [50] and since then, studies on DEP cell manipulation gained more attention from other researchers. His works also showed the effects of frequency on cells, which became the basis of DEP-based biochips. The studies revealed that dead and live cells have different frequency responses and cells could remain alive after DEP experiments [49] . From then on, DEP has evolved with many early published works focusing on modelling the DEP force in various environments and basic DEP manipulations [51-53].

The advent of microfabrication technology in 1980s and 90s allowed for precise manufacturing of micron-sized electrode and chamber to suit particle sizes. With the help of modern modelling software, the number of research done on particle manipulation and DEP has increased. As a result, an era of application based on biochips for diseases identification [54-56], single cell manipulation [35, 57-58], cell separation [59-62] and particle characterizations [55, 63] has emerged.

In recent years, the concept of cells analysis on a single platform or lab-on-chip [64] has further developed DEP manipulation studies on living organisms. New DEP techniques such as DEP-TW (Travelling wave) [65], DEP-FFF (Field Flow Fractionations) [60] were derived from DEP force and integration with other techniques. Studies on DEP manipulations also began to diverge from single cell [36-37, 59] manipulation to analysing DNA [66-69], and proteins [70-

72] as well as from 2D to 3D microstructures [73-74]. As depicted in Table 2.2, DEP offers versatility in cell manipulation technique, either used solely or integrated with other methods such as hydrodynamics, optics, etc in biochip design.

The main value of using DEP in biochips is the ease of controlling cell movements on the platform. As previously mentioned in subsection 2.1.2, the external electric field imposed on a cell will polarise charges in the cell's membrane, exert a force on the cell and subsequently create cell translational movement on the platform, with respect to the external electric field.

Although the problem of cells remaining localised at electrode edges are evident when using DEP, it is still a widely used technique for cell sorting and separation. Separation of cells is made possible using the fact that a particular type of cell has a unique frequency-dependent dielectric property. Precise separation is observed especially when two cell types have a great difference in their cross over frequency and dielectric properties [60]. It was reported that castellated electrode design demonstrates efficient yeast cell transition between positive DEP and negative DEP [58, 75]. Other examples of successful separations using DEP include separation of live cells and dead cells [63], cancer cells from blood cells [59], malaria cells from normal cells [76], and cells from microbeads [61].

Another DEP application in cell studies is the non-contact trapping of single cells for example trapping of single cells using negative DEP trapping at the centre of polynomial electrodes systems [77]. Hughes and Morgan [78] demonstrated trapping of single sub-micron particles using quadrupole microelectrode structures, which permits individual isolation without mechanical or chemical interferences on particles. Studies by Muller provided further evidence that DEP force is capable of trapping particles down to 14 nm particle size [79].

The main deficiency however, is the electrohydrodynamic forces which are by-product of the DEP force during cell manipulation process. Studies showed that at high frequencies the electrothermal force is more dominant while at low frequencies the electroosmosis force controls particle movements [80], this means generating a stable holding force on a single particle is indeed a challenging process.

In terms of microelectrode designs, the open top of traps of quadrupole microelectrode design causes some particles to not necessarily remain in the trap. The drawback becomes apparent when trapping submicron sized particles and this leads to the introduction of octupole microelectrode design. This design generates octode electric fields that trap a particle in an enclosure [81]. Other methods that can be used to retain single cell in traps include the usage of microwell [11] and an insulator based microstructure [82].

The advent of hydrodynamic manipulation technique generated great interest in designing a biochip using DEP as the trapping mechanism. In hydrodynamic studies, channels of micron size were designed in relation to the scaling law. Reduction of consumables in each run meaning low production costs for a single device without compromising accuracy of the results. Table 2.2 shows the combination of hydrodynamic traps and DEP force that can be used in designing precise single cell trapping platform. The DEP-FFF [60, 83] or DEP-TW [84] are excellent techniques to use to separate and transport cells simultaneously. These methods eliminate the need to flush the platform with fluid once separated cells are localised at the electrodes.

Table 2.2: DEP flexibility suits biochip design with/without integration with other manipulation methods i.e., optical, etc.

Technique	Manipulation Technique	References
DEP	a. Positioning : i. Sorting & Separation, ii. Trapping b. Patterning	[15, 46-47, 85-86] [10, 77, 86] [87-88]
Hydrodynamic & DEP	Trapping	[73, 89-92]
Optical & DEP	Trapping	[15, 64, 93]

Single Cell Measurements and References
Cell Impedance (capacitance) [86, 94-99]

DEP-based cell patterning is very useful in tissue engineering due to its ability to arrange cells into desired patterns. In tissue engineering, the three common ways to cell patterning are: 1) by using cell adhesive substrates micro-patterned by photolithography, 2) micro-contact printing and by applying force to direct cells using optical, magnetic, electrokinetics and hydrodynamic, and 3) a combination of these techniques [87]. By using DEP, a specific type of cell is guided towards the patterned substrates and thus DEP can be further used in developing a new technique for organ reconstruction.

DEP is also useful in real time monitoring of cells. Information on cell viability using DEP-based biochips is measured through cell membrane capacitance exhibited by the cell membrane. This technique is used to distinguish between live and dead cells [95]. For example, the measurement of high crossover frequencies of yeast in a low conductivity medium would

represents the internal cell conductivity, which indirectly can be used to measure the permeability of the cell membrane [97].

2.3.1 Development of Single Cell Imprint Process

In addition to basic cell trapping and sorting, the purpose of this research is to design a single cell trapping biochip that is compatible with the Bioimprint process. Hence it is vital to understand basic concepts of the Bioimprint technique. The technique was developed based on nanoimprint technology. The hot embossing nanoimprint is a method of surface structuring which relies on mechanical deformation of the patterning materials such as polymers, resins, silicon or metal. The technique distinguished itself for its low cost, high throughput and resolution patterning technique for example by using the heat treatment of the media, 3D master mould and process pressure.

Bioimprint, a novel technique for replicating biological cells and their sub-cellular structures, has been previously developed [9]. The method facilitates imaging of individual cell at high resolution and creates a topographical image of cell responses to stimulus. It has the ability to detect features of fusion pores in cells at high resolution using AFM (Atomic Force Microscopy) [16]. Once a single cell is properly trapped at a specific location, the Bioimprint process can take place without the need of cell fixation or further cell immobilization. In other words, cell responses to chemical stimulus can be captured through imprint of its cell membrane without altering cell conditions.

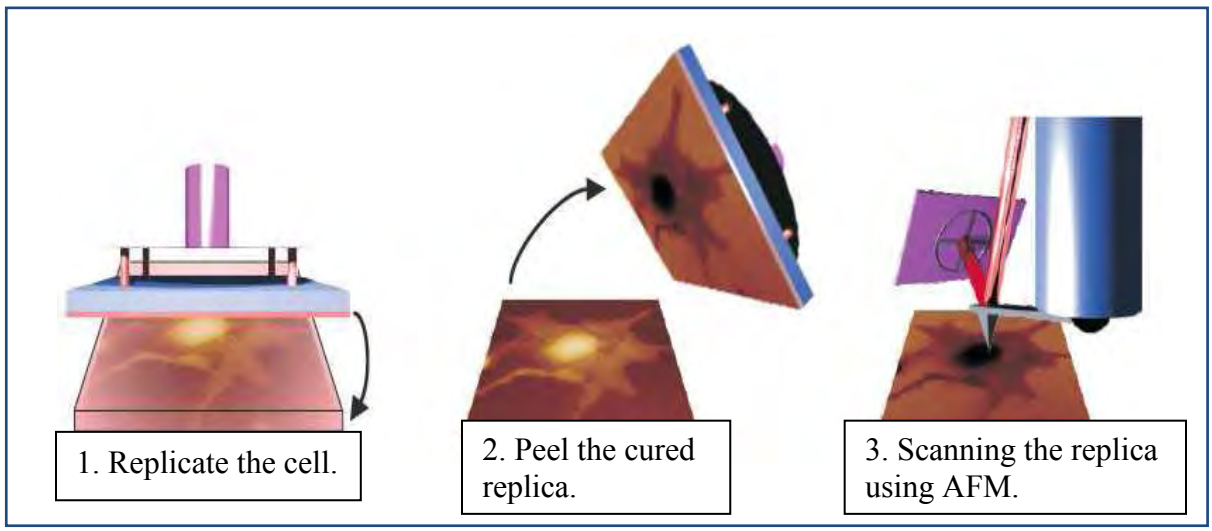

Figure 2.7: The Bioimprint process described in [77].

2.4 Development of the SIBC Biochip

After comprehensive reviews on current trends in single cells studies and manipulation techniques, the chapter continues with the SIBC biochip specific design requirements to fulfil the research gap in this area.

1. The designed platform is required to trap single cells. Therefore, cell's dielectric properties become the critical factors. Ideally, the biochip should be flexible enough to address a wide range of cell types.

2. Cells can be directed into the microcavity and remain trapped before performing the Bioimprint process. Thus, the biochip platform must provide areas for cells to stay permanently in traps by incorporating holes or cavities of appropriate size.

3. Incorporating microfluidic channels on the device for proper loading of samples onto the biochip.

4. Once trapping occur at the stipulated locations, the Bioimprint polymer can be flowed into the microfluidic channels. After the polymer is crosslinked (solidified), impression of membrane cells that describes intercellular activities of cells can be peeled or washed out from the channel (which is called the flow-based Bioimprint).

Figure 2.8 illustrates the development of SIBC biochip and its microfluidic channel. It shows the important aspects of the biochip platform used for trapping single cells. Based on these criteria, and knowledge from literature reviews, the SIBC biochip will be realised in several steps starting with the design process using computer simulation software, followed by fabrication stage and finally testing with microbeads and living cells. Each stage of the implementation of the SIBC biochip will be presented extensively in the following chapters.

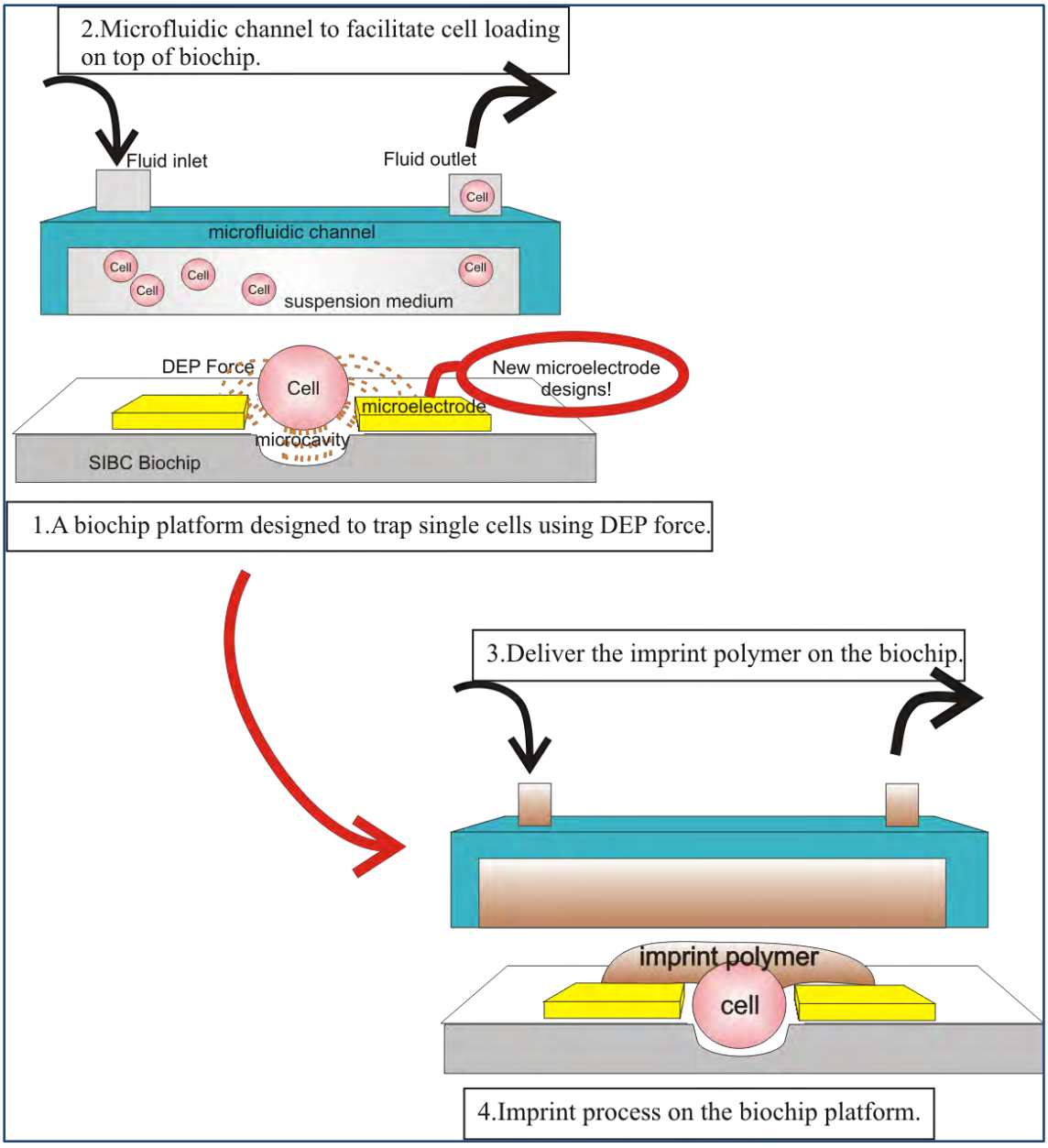

Figure 2.8: The development of SIBC biochip and its microfluidic channel.

2.5 Summary

Understanding the physiology of a cell is very crucial in identifying and analysing disease. In this chapter, various manipulation techniques for single cell analysis have been explored. Each technique was critically analysed, while identifying their strengths and limitations in the context of this research. Subsequently, the synthesis from the critical analysis of previous researches in single cells studies provides a strong justification for using the DEP manipulation method in this research. From here, we developed a biochip platform to meet the requirement of trapping single cells and analysis, and suitable for the Bioimprint application called the Sandwiched Insulator with Back Contact or SIBC biochip.

Chapter Three

Theoretical Background of the Microelectrode Design

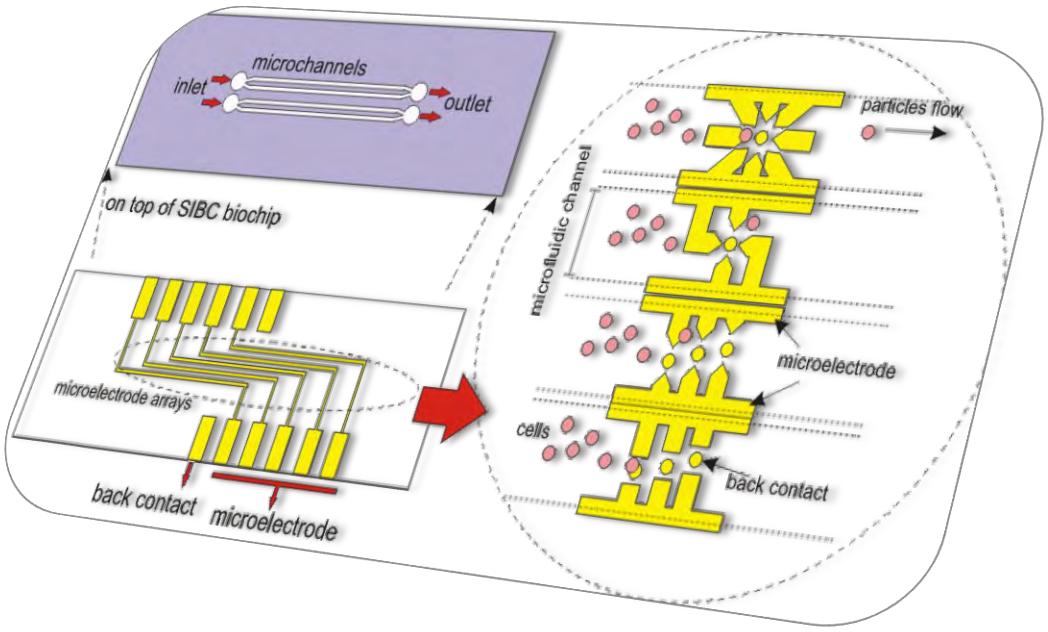

In this chapter, the backgrounds of DEP and hydrodynamic forces highlighted in Chapter Two are explained in details. The chapter starts with the principals of DEP force and followed by the particle trapping mechanisms using DEP force in section 3.2. The three new microelectrode designs (the dipole, the quadrupole and the adaptive octupole) and the multilayer structures for the SIBC biochip are detailed in section 3.3. Then, results of the electric field calculations for the three microelectrodes using Matlab 7.7.0(2008b) are presented in subsection 3.3.1. The chapter ends with an overview on the integration of SIBC biochip and microfluidic channels.

3.1 DEP Force and Cell Movements

Knowledge of the electric field distributions on a biochip is essential when using the DEP force and hydrodynamic techniques for trapping single cells. On a biochip platform, the DEP force is derived from physical interactions between particles or cells with the electric fields generated by micro-size electrodes (microelectrodes). Due to the complexity of force calculations, the physical interactions can be explained according to the dipole force concept [100].

3.1.1 The Dipole Force Concept

The principle of cell manipulation using electric fields lies on the charge displacement and polarization mechanisms. As illustrated in Fig. 3.1, when charge particles are positioned near an electric field $E(\vec{r})$, the net force exerted on $+q$ and $-q$ charges by $E(\vec{r})$ separated by $\vec{d}$, is governed by

$$\vec{F} = q\vec{E}\left(\vec{r} + \vec{d}\right) - q\vec{E}(\vec{r}). \qquad (3.1)$$

Therefore, the microscopic approximation for dipole force can be defined as

$$\vec{F}_{dipole} = q\vec{d}.\nabla\vec{E} \equiv \vec{p}.\nabla\vec{E} \qquad (3.2)$$

with ∇ is the gradient and $\vec{p}$ is the dipole moment. By using Taylor's series approximation and taking the limit of $|\vec{d}| \to 0$, the $q\vec{d}$ in Equation (3.2) stays finite. Therefore, the dipole moment can be defined as $\vec{p} = q\vec{d}$ with units in Coulomb-metre or Debye (1 Debye = 3.33x10^{-30} Cm) [101]. The net dipole force only occurs when the gradient of electric field is non zero or when particles are in inhomogeneous electric fields. In contrary, the dipole moment experiences net electrostatic torque in homogeneous electric fields condition shown in Fig. 3.2. The net electrostatic torque can be derived as

$$\vec{T} = [\tfrac{\vec{d}}{2} \times (q\vec{E})] + [\tfrac{-\vec{d}}{2} \times (-q\vec{E})]. \qquad (3.3)$$

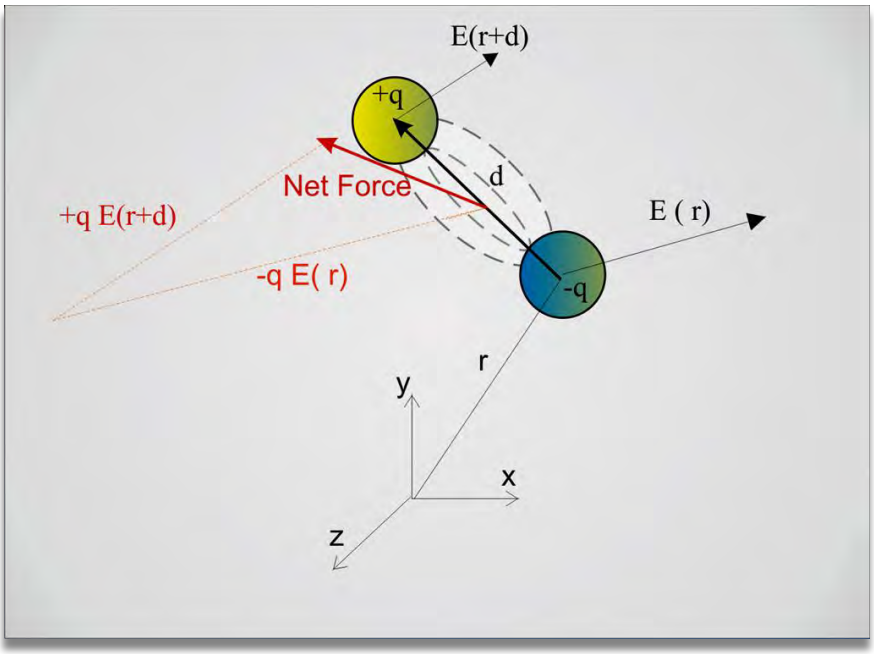

Figure 3.1: The net force on small dipole due to electric field $E(\vec{r})$, is a result from vectors addition of the charges i.e., $qE(\vec{r} + \vec{d}) + [-qE(\vec{r})]$.

Equation (3.3) is rewritten in relation to moment dipole as

$$\vec{T} = q\vec{d} \times \vec{E} \equiv \vec{p} \times \vec{E} \,. \qquad (3.4)$$

The force and the torque on dipole moments in Equations (3.2) and (3.4), are fundamental principles for particle polarization due to the electric fields.

Polarization occurs when charges inside a dielectric material move in short distances within the material's compound. These movements create induced dipoles within the material as illustrated in Fig.3.3. Similar to a dielectric material, a biological cell will polarize and create many small dipoles inside its membrane when subjected to an electric field, $\vec{E}$. During cell manipulation on biochip, the cell radius (R) is usually smaller than the electric field's distance to the cell ($\vec{d}$) or $R << \vec{d}$. Therefore, the dipole moment approximation can be used to simplify the DEP force calculations. The approximation implies that although a cell is subjected to inhomogeneous electric fields within the small vicinity of cell membrane compound, it

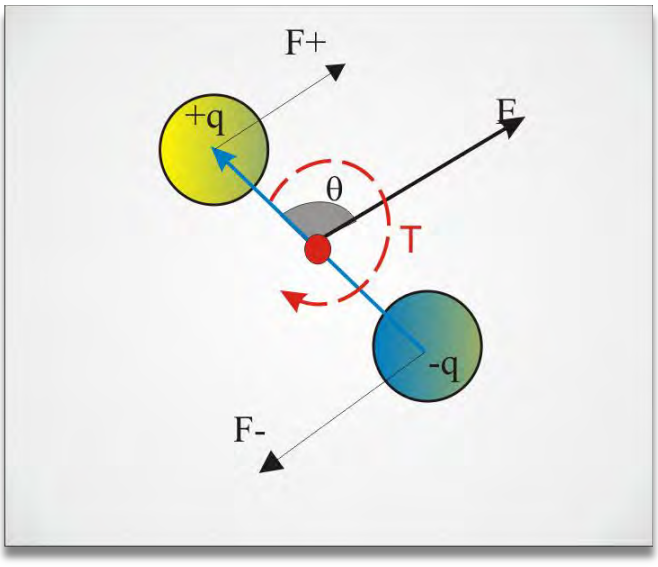

Figure 3.2: The torque (T) on dipole moment is due to homogeneous electric field.

experiences an electric field that is similar to a homogeneous electric field [35].

The induced polarization which occurs inside the cell's membrane will also generate another electric field $(\overrightarrow{E_p})$ that polarizes the cell. Therefore, the net polarization field of cell, $\vec{E}_T$, is equal to the summation of electric field $(\vec{E})$, and cell's polarized electric field $(\vec{E}_p)$. To simplify calculation of the total polarization in space $\vec{E}_T$, the induced polarization $\vec{E}_p$ is assumed to be similar to the electric field generated from a dipole $\vec{p}$ placed at the centre of the sphere [101]. Therefore, the total polarization $\vec{E}_T$ can be assumed to be similar as the induced polarization for a dielectric sphere located in a homogeneous electric field [1]. Using this approximation, the effective dipole $\overrightarrow{p}$, at the centre of the sphere is described as :

$$\vec{p} = 4\pi\varepsilon_m \left(\frac{\varepsilon^* p - \varepsilon^* m}{\varepsilon^* p + 2\varepsilon^* m}\right) R^3 \vec{E} \qquad (3.5)$$

where ε_p, ε_m, and R are the dielectric constant of particle, the dielectric constant of medium and

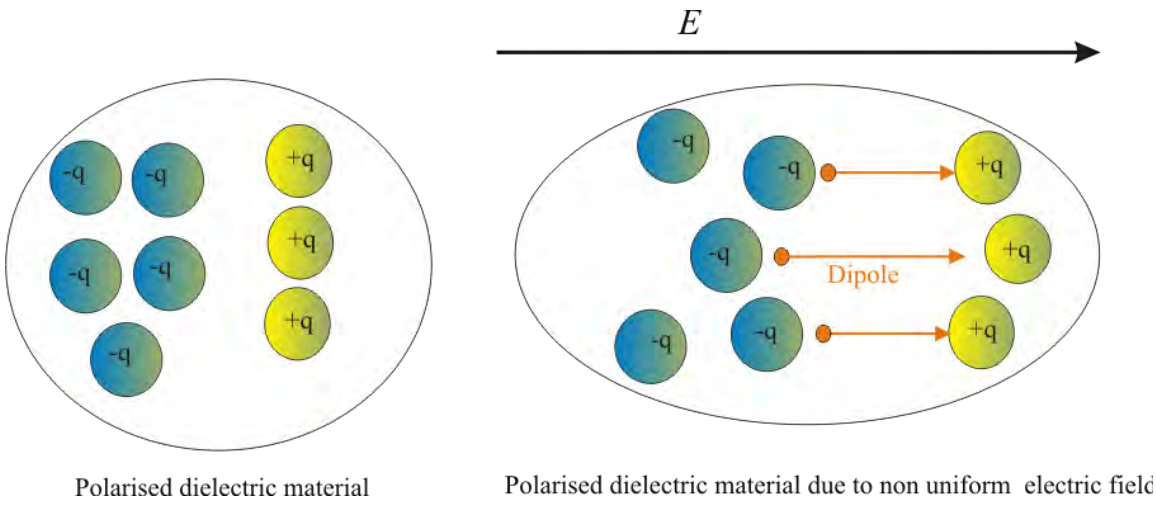

Figure 3.3: The polarization concept of dielectric material is used to understand polarization effects on biological cells.

the particle radius respectively. In Equation (3.5), the direction of total polarization forces or the direction of cell movements on the biochip is determined by the Clausius-Mossotti (CM) factor :

$$K(\omega) = \left(\frac{\varepsilon^*_p - \varepsilon^*_m}{\varepsilon^*_p + 2\varepsilon^*_m}\right) \qquad (3.6)$$

where the ω is the angular frequency, the $\varepsilon^*_p = \varepsilon_p - j\frac{\sigma_p}{\omega}$ and $\varepsilon^*_m = \varepsilon_m - j\frac{\sigma_m}{\omega}$ represent the complex permittivity of both particle and suspension medium. In order to simplify polarization calculations on cells, Equation (3.6) is derived according to the multi-shell equivalent model of Fig.3.4. The model in Fig.3.4(a) uses the homogeneous dielectric effective permittivity ε^*_p instead of the complex calculations of dielectric properties shown in Fig.3.4(b).

Cell manipulation is categorized as nDEP (negative DEP) when the $K(\omega)$ value is less

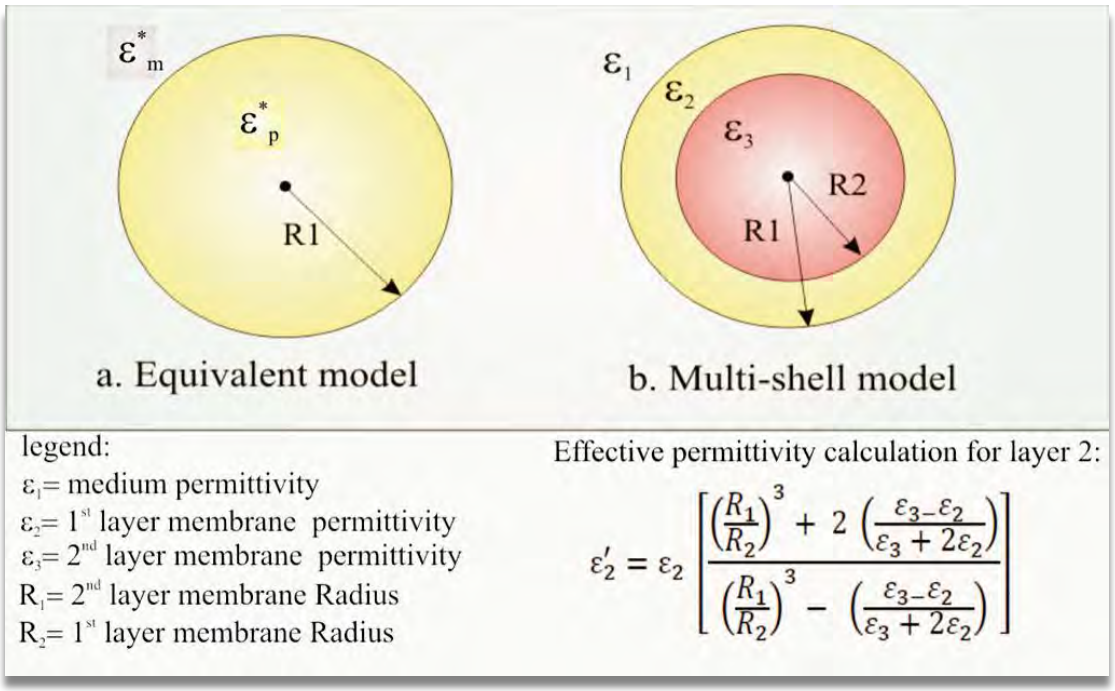

Figure 3.4: (a) The equivalent model used to simplify polarization effects on cell according to the multi-shell model in (b).

than zero and cells are directed to the low electric field regions on a biochip platform [49]. Meanwhile, the pDEP (positive DEP) occurs when the *K(ω)* value is more than zero and cells are directed to the high electric field regions. These distinct operation regions are called the conventional DEP (cDEP) and can be used to trap cells in a controllable manner [35].

Cell polarizability for DEP lies within the real part *Re [K(ω)]* and imaginary part *Im [K(ω)]* of the CM factor. The values of *Re[K(ω)]* is between 1 to -0.5 while *Im [K(ω)]* is between +0.75 to -0.75 [49]. The *Re[K(ω)]* that defines the DEP low frequency limiting value, depends on conductivities of the particle and the suspension medium. The high frequency limiting value however, dominates by permittivities of the particle and the suspension medium. These two key factors are useful in interpreting the DEP experiment results.

An example of the *K(ω)* plot is shown in Fig. 3.5. Here, when *Re[K(ω)]* is less than zero, it means the DEP force is having negative DEP (nDEP). On the other hand, when *Re[K(ω)]* is greater than zero, the DEP force is operating in a positive DEP (pDEP) region. In this plot, the cross-over frequency is at 1.9MHz. Meanwhile, the *Im [K(ω)]* induces cell movements against the travel direction of the electric field when *Im [K(ω)]* >0 or following the direction of electric field when *Im [K(ω)]* <0 [35]. The imaginary part is useful in describing the travelling wave DEP (DEP-TW) situations.

Finally, by using Equation (3.5) and the dipole moment approximation, the net polarization on a cell can be defined as

$$F_{NET} = 4\pi R^3 \varepsilon_m \frac{\varepsilon_p - \varepsilon_m}{\varepsilon_p + 2\varepsilon_m} \vec{E}\left(\nabla . \vec{E}\right)$$

$$= 2\pi R^3 \varepsilon_m K \nabla |E^2| \qquad (3.7)$$

From here onwards, Equation (3.7) is called the dielectrophoretic (DEP) force which manifests into cell translational movements on plane. The direction of DEP either towards regions of high electric field (positive DEP) or regions of low electric field (negative DEP) depends on the frequency of supplied AC signals, and the dielectric properties of cells and suspension medium defined in $K(\omega)$.

In cell manipulations using DEP, AC signals are usually used to preserve cell's viability [1]. Therefore, the time varying electric field of single frequency ω is defined as:

$$E\ (x,t) = E(x)e^{j\omega t}$$
$$= Re\left[\vec{E}(x)e^{j\omega t}\right] \qquad (3.8)$$

with x is the position on a biochip and j is equal to $= \sqrt{-1}$. Equation (3.8) shows that only the real part of the electric field is significant in the calculations. By using Equation (3.2) and Equation (3.8), the time averaged force exerted on a particle can be described as:

$$\langle F_{\mathrm{DEP}} \rangle = \frac{1}{4}\, V\, Re\, [\tilde{\alpha}\,] \nabla |E|^2 \qquad (3.9)$$

where V is the volume of particle, $\tilde{\alpha}$ is the real part of the effective polarisability factor and E is the amplitude of the electric fields. In literature [101], the relations between $\tilde{\alpha}$ and CM factor can be defined as :

$$\tilde{\alpha} = 3\varepsilon_m \qquad (3.10)$$

with ε_m is the permittivity of the medium. By substituting Equation (3.9) into Equation (3.10), the full DEP force expression for a spherical particle is:

$$\langle F_{\mathrm{DEP}} \rangle = \pi\, \varepsilon_m\, R^3 Re\, [K] \nabla |E|^2 \qquad (3.11)$$

and can be rewritten as

$$F_{DEP}\,(x) = \pi \varepsilon_m\, R^3 Re[K(\omega)] \nabla |E(x)^2| \,. \qquad (3.12)$$

Equation (3.12) has highlighted two main points in DEP force effects on cell: 1) the magnitude of the exerted force depends on the particle volume, permittivity of the suspending medium and the gradient of electric fields, and 2) the *K(ω)* defines the direction of force and is dependent on the supplied AC signals frequency. In other words, the frequency of the supplied

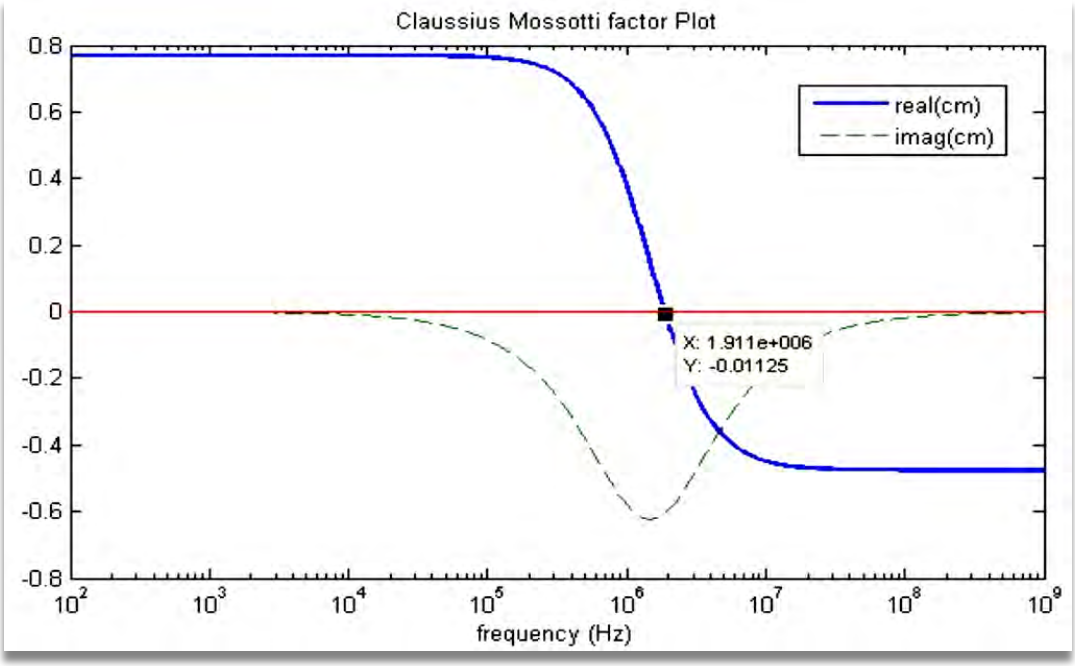

Figure 3.5: The *K(ω)* plot of microbeads showing distinct different of calculated values *Re[K(ω)]* and *Im [K(ω)]* with the cross over frequency *fc* is at 1.9 MHz. The plot is generated using Matlab 7.7.0(2008b) presented in Appendix A.

voltage can change the dielectric characteristics of particle and cell's surrounding medium, and can cause cell to be directed to a specific location.

When two or more electrodes with AC signals with or without phase difference are used for DEP, the imaginary part of the electric field has to be considered. In this condition, cell will experience the DEP-TW force on the biochip. Hence, derivation of the time averaged DEP force becomes [101]:

$$\langle F_{\mathrm{DEP}} \rangle = \frac{1}{4} V\, Re\,[\tilde{\alpha}\,] \nabla \left|\vec{E}\right|^2 - \frac{1}{2} V\, Im\,[\tilde{\alpha}\,] \left(\nabla \times \left(Re\,[\vec{E}] \times Im[\vec{E}]\right)\right) \qquad (3.13)$$

In a nutshell, movements of a single cell are initiated and controlled by changes in frequency of the supply voltage. By referring to Fig.3.5, the positive DEP (pDEP) occurs when cell polarisability is higher than the suspending medium's polarisability ($Re[K] > 0$) and the negative DEP (nDEP) happens when suspending medium polarisability is higher than the cell's polarisability ($Re[K] < 0$). Cell attracts to regions of high electric field intensity due to the pDEP condition, and repels away from it due to the nDEP condition. This striking property of DEP is useful to sort, position and separate cells or its components in a controlled environment such as on a biochip.

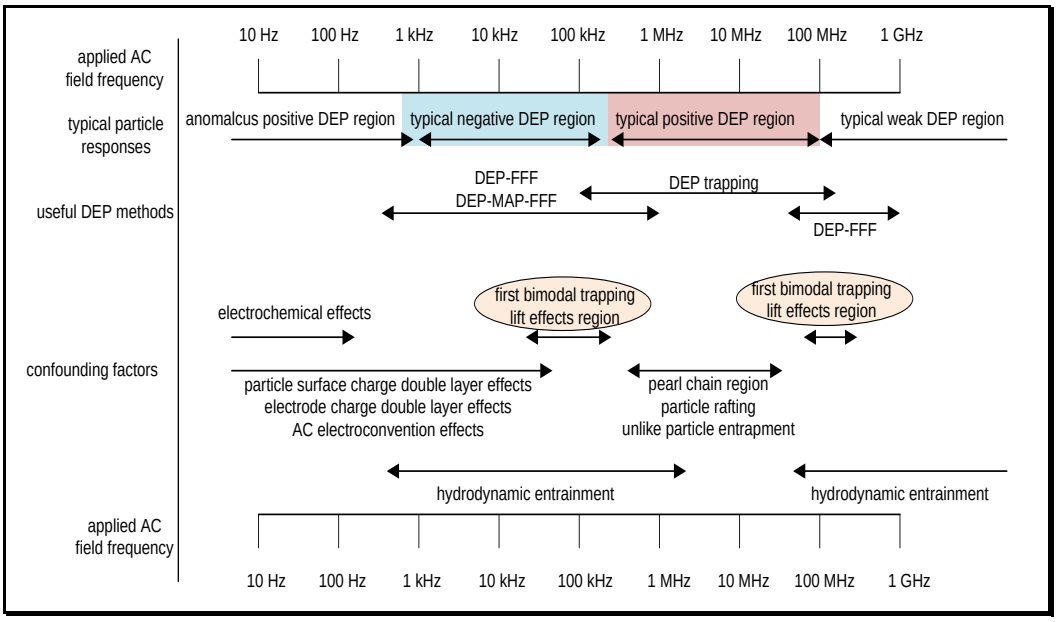

Figure 3.6: An example of DEP force manipulation over a range of frequency. The results are taken from typical mammalian cells conductivity of 50 mS/m which can be used as a reference to many cell studies [102].

Control over cell movements on biochips using DEP force through the frequency of the AC supply were reported in literature [102]. For example, as depicted in Fig.3.6, between 1 kHz to 250 kHz, cell suspended in a 50mS/m media showed the operation of DEP-FFF cell manipulation (DEP-Field Flow Fractionation) but from 250kHz to 100MHz, the DEP trapping method can be used for cell manipulation. From the example of Fig.3.6, characterization of a new biochip design with respect of the trapping frequency of particles/cells is essential and can only be observed through experimental approach.

3.2 DEP Force Trapping Mechanisms

It is now clear that specific frequency of AC supply is the essence of cell mobility and directions on a biochip. The subsequent sections present details on how the DEP force is implemented on the SIBC biochip.

3.2.1 Microelectrode Design and Trapping Regions

The dielectrophoretic (DEP) force offers a non-contact trapping method on a biochip platform. Therefore, single cells can be isolated without the need of invasive physical or/and chemical methods. The DEP trapping event can be either due to nDEP or pDEP depending on responses of the cell dielectric properties and suspension medium, with respect to the electric fields generated on biochip. In this section, critical reviews on the design of microelectrodes used in DEP cell manipulations are presented.

As depicted in Table 3.1, there are various microelectrode designs used for DEP manipulations reported in literature. These microelectrode were designed according to the degree of electric field non-uniformity required for the cell manipulation on biochip platform [103]. The common microelectrode design used for DEP trapping is the ID (interdigitated) or castellated microelectrode. A study done by Wang *et. al,* showed that the Friend Murine Erythroleukemia DS19 cells aggregated at both pDEP and nDEP regions [35]. As shown in Fig.3.7, cells are trapped at the edge of the ID microelectrodes where high electric field intensity occurs for frequency above 140kHz. In contrary, at frequencies below 120kHz, the same type of cell repelled from the edge to the centre and in between the microelectrode showing nDEP

trapping behaviour. Obviously, changes in frequency of the supplied potential resulted with changes in direction and movement of cells on a DEP-based biochip.

Table 3.1: Examples of DEP trapping manipulation on biochip using different microelectrode designs.

DEP Type	Microelectrode Type	Cell Type	Literature
nDEP	U and T shape	Bacteria E.Coli	[104]
Trapping	Planar Quadrupole	HeLa Cell	[11]
pDEP	Planar (floating)	Red Blood Cell	[105-106]
Trapping	Spiral Quadrupole	Human Tumor Cell	[94]
	Planar Quadrupole	DNA	[107]
	Ring Interdigitated	Human Hepatocellular carcinoma cells.	[88]
pDEP and	Planar quadrupole	Latex microbeads	[79]
nDEP	Pyramidal	Latex microbeads	[108]
Trapping	ID (Interdigitated) /Castellated	Friend Murine Erythroleukemia DS19	[35]
Others	Octode Cage	Microbeads	[81]
	Ratchet structure	Microbeads	[109-111]
	Square planar traps	Bovine Pulmonary Arterial Endothelial Cell And Fibroblast Cell	[112]

Cell aggregations in between electrode pitch as shown in Fig.3.7 however, limits the ID microelectrode for single cells trapping. This issue becomes a drawback for trapping single cells especially when the gap is too wide in relative to cell size [47]. Therefore, other microelectrode designs such as the ring interdigitated, planar quadrupole, U and T shaped in Table 3.1 are used to enhance DEP single cell/particle trapping.

Due to cells complex polarization behaviours, there are no definite methods of knowing cell directions, or how to precisely isolate cells at a specific location on a platform using only DEP force. To realise proper positioning on a biochip, trapping location has to be physically or chemically outlined. Cells can be isolated physically through platform design such as in between electrode gaps, on top of microelectrode or in holes or microwells [42, 85]. On the other hand, areas of biochip platform can be functionalised with gels or protein to bind cells chemically at the specific locations. An example in Fig.3.8 illustrates how the Bovine Pulmonary Arterial Endothelial cell And Fibroblast cell were isolated and positioned on arrays of planar-square type Au (gold) and fibronectin protein microelectrodes [112].

Another type of microelectrode commonly used in single cells trapping is the quadrupole microelectrodes. The design consists of four electrodes arranged together towards a common point or area. A high trapping force is created at the central region when an AC supply of one electrode is out of phase or has a different phase from the AC supply of its neighbouring electrode. Examples of the AC supply arrangements used for trapping single cells are presented

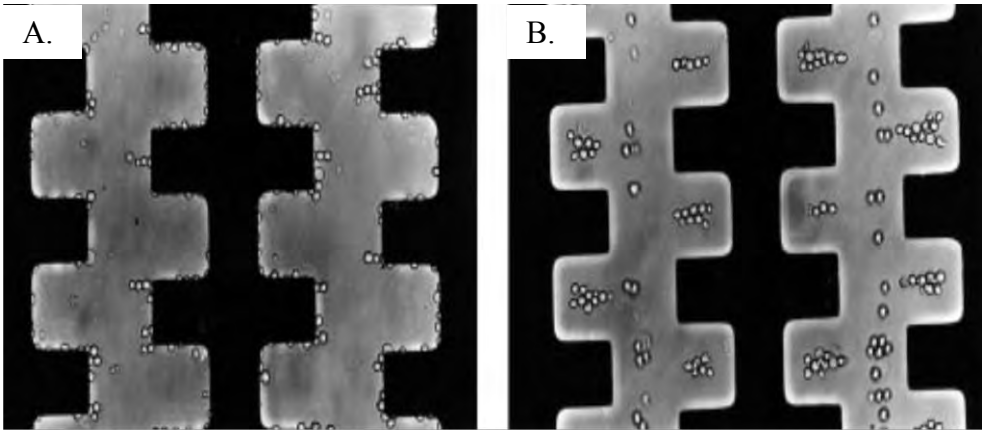

Figure 3.7: Experiments on Friend Murine Erythroleukemia DS19 cells using the Interdigitated (ID) microelectrode in [35] with the height and width of the microelectrode are 80 µm.

in Fig. 3.9. The planar quadrupole in Fig. 3.9(b) for instance, uses AC supply that has 180° phase difference between the two neighbouring electrodes to single out a 20nm microbead. However, in Fig. 3.9(a), the supplied AC signals phase different is 90° and creates electrorotation and DEP force on particles.

The existence of a well-defined electric field minimum surrounded by maximum field at the edge of a quadrupole electrode or the quadrupole DEP holding force [113], benefits single cells positioning especially when trapping sub-micron particles. The electric field minimum or the 'null field' can levitate particle and overcomes the Brownian effect on a biochip. Nonetheless, the rule of thumb for this design is that microelectrode dimensions have to be proportional with respect to cell sizes [114]. Extremely high DEP force at the central region will end up rupturing cell membrane and leads to cell death. In contrast, cells are unable to move on a biochip if the exerted DEP force is too low.

Another way to establish the cell trapping region is by observing the cross-over frequency during experiments. The cross-over frequency is defined as [101]:

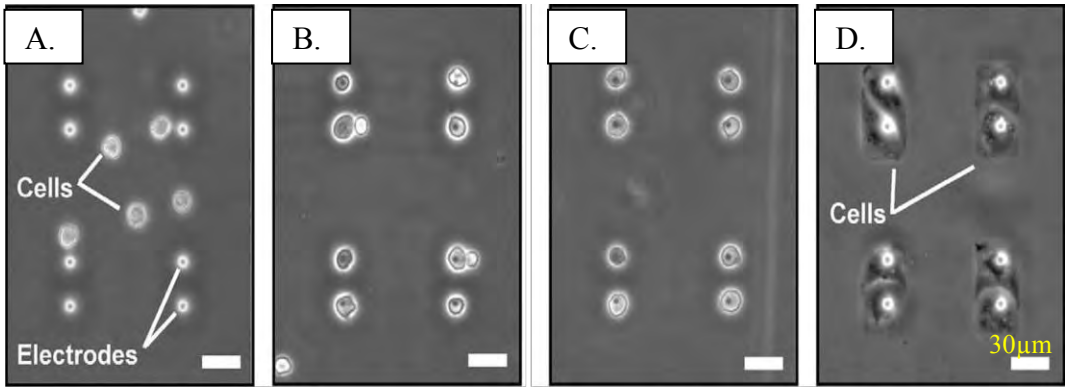

Figure 3.8: Trapping and positioning cells on planar square microelectrodes in [112]. (a) The cells are flowed on the square electrode. (b) & (c) show the trapping events on the platform and (d) cells adhere to the electrodes.

$$f_{crossover} = \frac{1}{2\pi}\sqrt{-\frac{(\sigma_p-\sigma_m)(\sigma_p+2\sigma_m)}{(\varepsilon_p-\varepsilon_m)(\varepsilon_p+2\varepsilon_m)}} \qquad (3.14)$$

The $f_{crossover}$ occurs when the *Re [K]* in Equation (3.11) is equal to zero or when the real part of effective polarisability is equal to the suspending medium. At this frequency, the cell remains stationary, meaning it does not repel from the microelectrode or attracts to the microelectrode. From Equation (3.14), if the dielectric properties of suspending medium are known, the effective complex permittivity of cell $\varepsilon_{p,}$ can be calculated. The method is valid for homogeneous particle like microbeads however, several assumptions have to be made for living cells [101]. In reality, living cells have layers of different component with different permittivitty values and therefore an equivalent relative permittivity in Fig.3.4 is used in calculations.

In order to fully understand cell trapping behaviour, regions of high or/and low electric

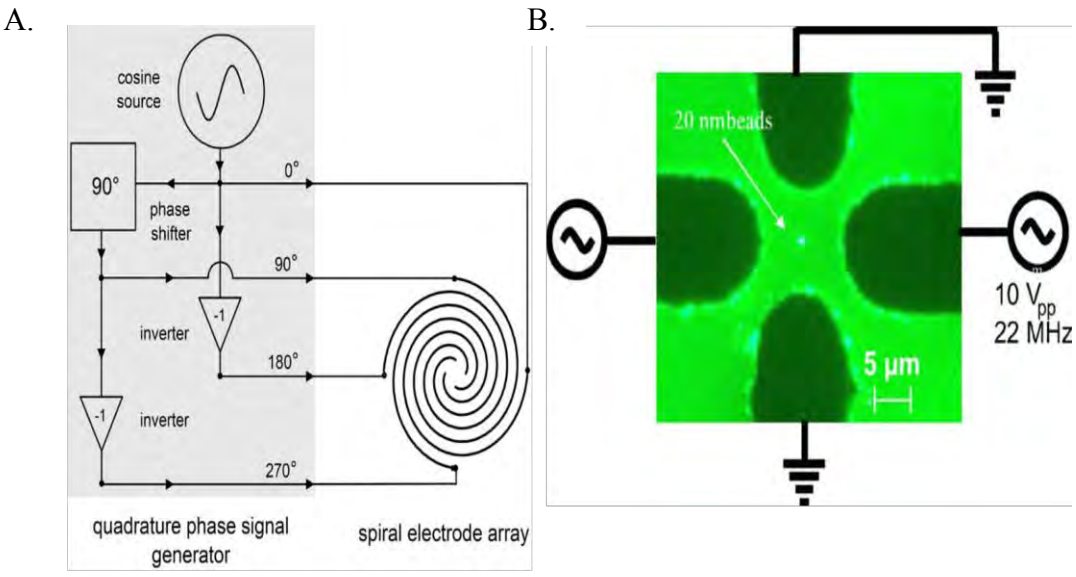

Figure 3.9: Two examples of quadrupole AC signals arrangements : (a) the spiral quadrupole design with 90°phase difference [94] and (b) the planar quadrupole with 180° phase difference [107].

field intensity generated by microelectrodes have to be identified using the numerical simulation analysis. Then, cell trappings at these regions are verified through experiments by using particles or cells. In this thesis, discussions on microelectrode electric field intensity using finite element software COMSOL3.5a, are presented in Chapter Four. Meanwhile, details on the SIBC microelectrode structure and inspiration behind the designs are discussed in section 3.3.

3.3 SIBC Microelectrode Design

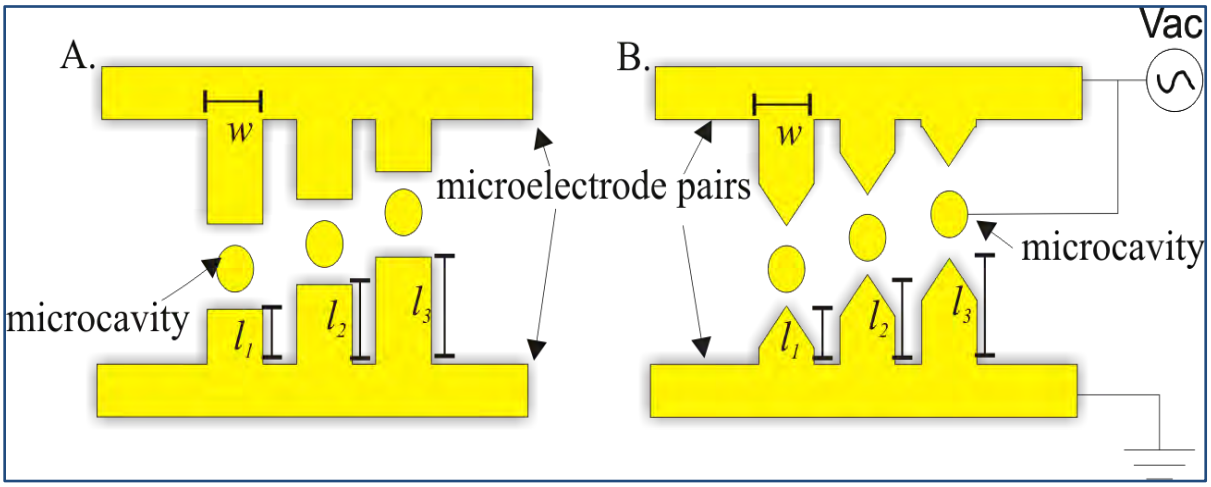

Figure 3.10: The SIBC biochip microelectrode geometry: (a) the flat tip dipole and (b) the sharp tip dipole.

In this work, three types of microelectrode are designed to be implemented on the SIBC biochip. They were developed based on the DEP force principle and the microelectrode designs explained previously in subsection 3.2.1. The three designs are: the dipole flat and sharp tips; the quadrupole; and the adaptive octupole. These microelectrode designs are named due to the number of induced moments force generated inside a particle subjected to non uniform electric fields. The objective is to trap single cells or particles at specific locations. With suitable AC

signals connection to these microelectrodes, single cells will move and reside at the central region or inside a microcavity for a successful trapping event.

Figure 3.10 depicts the schematic of the dipole microelectrode design for the SIBC biochip. In order to compare high electric field region at the edge of electrode, two dipole designs are studied i.e., the flat tips dipole microelectrode and the sharp tips dipole microelectrode. The dipole design consists of three microelectrode arms with the width *w*, of each small electrode arm is approximately 40µm to 60µm while the lengths l_1 , l_2 and l_3 are 20µm, 40µm and 60µm respectively.

These electrode arms resemble the common ID microelectrode design, except for the different length of the electrode arms. Different length is used for generating asymmetric electric fields as shown in Fig. 3.11. Based on the ratchet structure in [111], the asymmetric electric field along the horizontal axis induces polarized particles' movements to regions of high electric field i.e., at the tips of microelectrode. Once the cells are located at the tips of electrode, cells can be driven into the microcavity by using appropriate AC signals.

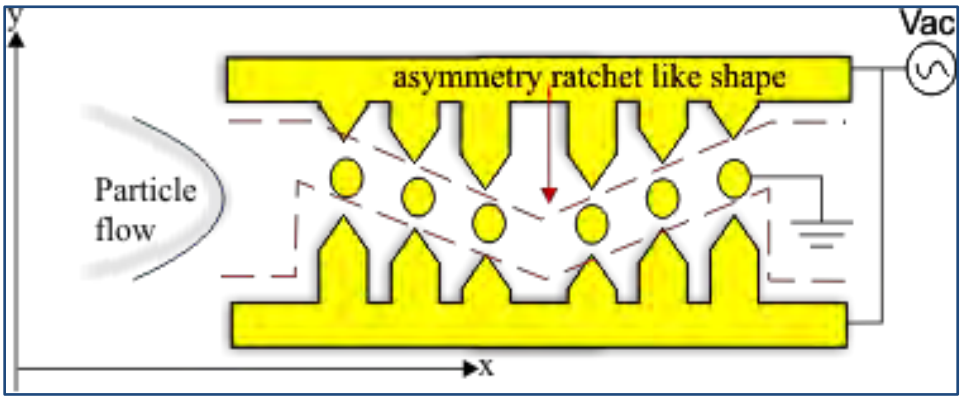

Figure 3.11: Array of dipole microelectrode showing the asymmetric ratchet shape which generates high and low electric field and induces particle motion to the microcavity.

As illustrated in Fig. 3.12, the new quadrupole microelectrode is structured with two neighbouring electrode arms connected together as oppose to the common quadrupole electrode configuration in Fig. 3.9. Since arrays of quadrupole microelectrode need to be fabricated on the same layer of the SIBC biochip, design in Fig.3.12 reduces the complexity of the biochip fabrication process since the interlayer electrical connections for the microcavity can be eliminated. Similar to the common quadrupole design, the four electrode arms will create minima electric field at the central region. Thus, trapping single cells is expected to happen at both pDEP and nDEP regions. Dimensions of this electrode are designed to be proportional to the size of a human cell, with the width w of the electrode arm approximately 40µm while the arm length toward the central area l_1, is 60µm respectively.

The final geometry is called adaptive octupole electrode, as shown in Fig. 3.13. The term 'adaptive' is due to the combination of 2-floating-electrode and 3-arm electrode pair arrangement creating an octupole holding effects on cell. Microelectrode design of a high order moment such

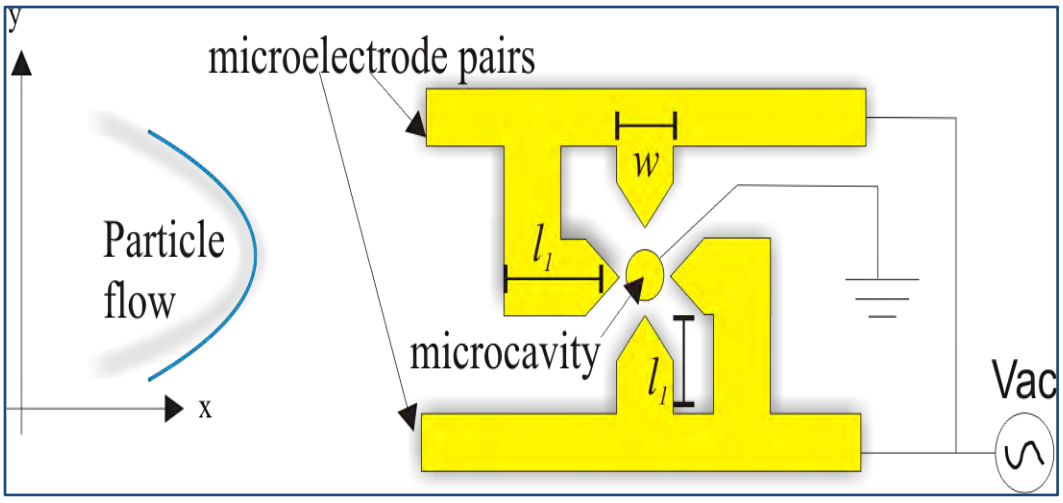

Figure 3.12: The new quadrupole design for SIBC biochip is expected to equivalent holding force to trap single cells as the common quadrupole design in Fig.3.9.

as the adaptive octupole design is dedicated to create a strong DEP holding force [81]. The purpose of 2-floating-electrode is to reduce electric fields intensities at the central region, which may rupture cell's membrane and lead to cell death, by minimizing the electrothermal effects without compromising the DEP trapping force [105]. Dimensions for this design are 40µm in width (w) and 80µm of the longest length (l_1) of microelectrode arms respectively.

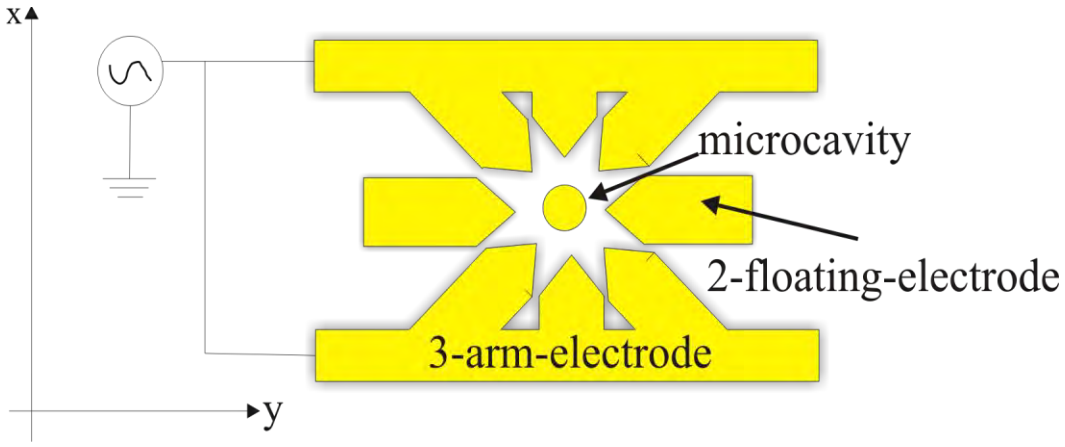

Figure 3.13: The octupole design consists of 3-arm-electrode pair connected to AC source and 2-floating-electrode.

The main objective of the three designs is to trap single cell at a specific location i.e., inside the microcavity. To locate the microcavity at the centre region of each pattern requires complex electrical interconnections layout, if the microelectrodes are to be structured in arrays on the same layer as illustrated in Fig. 3.14(a). A more practical approach is to construct microcavity on a different layer than the microelectrode shown in Fig. 3.14(b). Here, the microcavity not only acts as a cell holder, but also as an electrode that generating the DEP force to hold cell inside the microcavity.

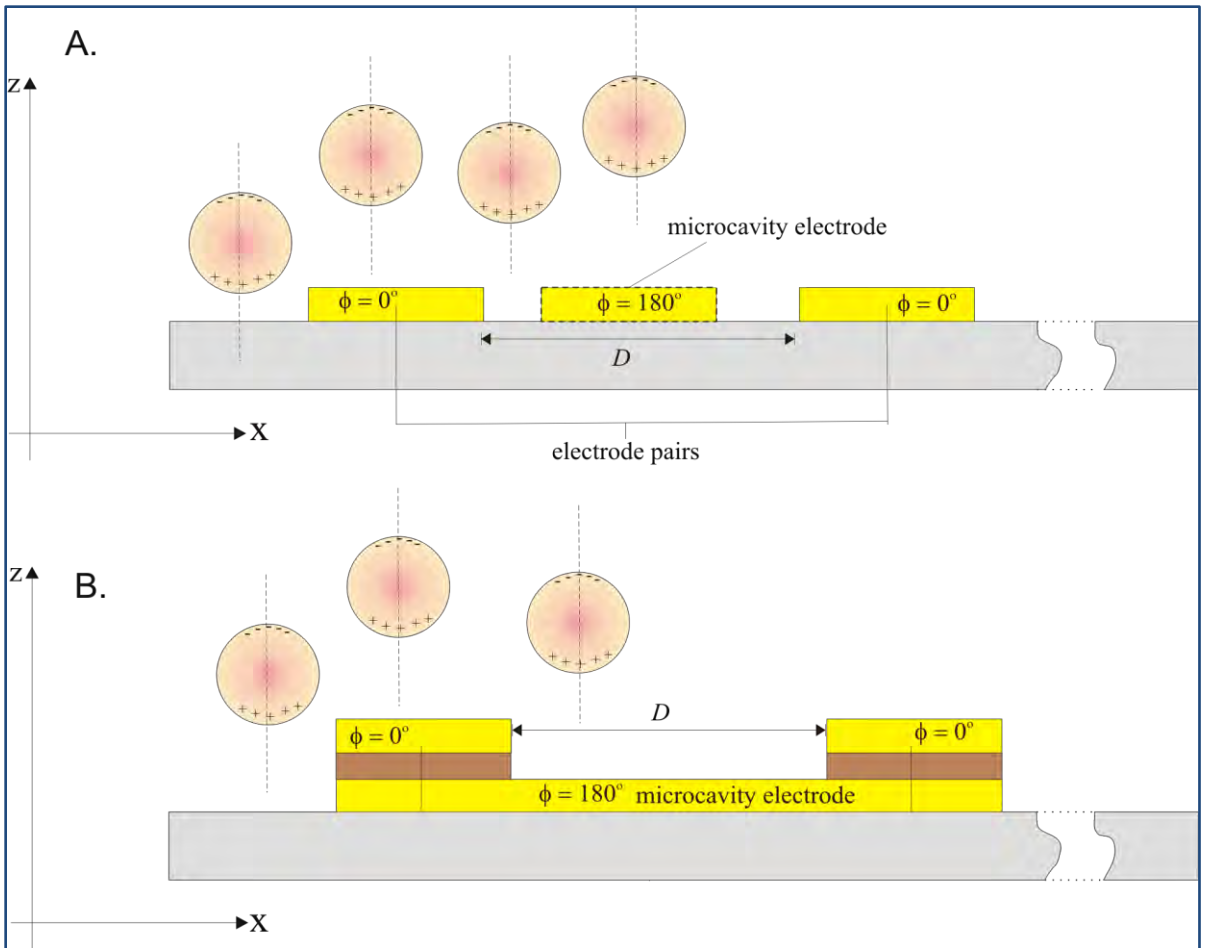

Figure 3.14: (a) The microcavity is fabricated on the same layer with the electrode pairs. (b) The microcavity electrode is fabricated on different layers where DEP force depends on the AC signals magnitude and the depth of the microcavity from the electrode pair layer.

On whether the electric field generated by the microcavity is significant in cell trapping will depends on the fabrication process. If the microcavity electrode is fabricated on the same layer as the electrode pairs as shown in Fig. 3.14(a), the multiple potentials of different phase have to be considered in the time averaged DEP force derivation. While trapping cell occurrences are highly anticipated, electrical connections between the AC supply contact and the

microcavities of each microelectrode arrangements remain complex. Otherwise, without the electrical connections, the microcavity will behave as floating (unbias) electrode.

On the other hand, if the microcavities and the microelectrode patterns are structured on different layers, the multiple potentials effects now depend on the depth between microelectrode and microcavity layers. This means if two layers are too far apart, electric fields from the microcavities are insignificant to cell movements which occur on top of the biochip platform. In order to investigate the conceptual design of SIBC biochip, areas of the high electric field regions on both horizontal plane (x-y axis) and vertical plane (x-z axis) are thoroughly discussed in Chapter Four.

3.3.1 The Microelectrode Analysis using Matlab 7.7.0(2008b)

One common feature of these geometries is the V-shape at the end of each electrode arms described as the polynomial electrode geometry. The shape was introduced by Huang *et al.* to overcome Pohl's isomotive electrode geometry limitations [115], where repelled particles failed to aggregate at the defined region. The polynomial electrode analytical electric field distributions from algebraic expression derivations were further improved by Pethig *et al.*[116]. However, not all microelectrode design field distribution can be calculated directly from its geometry expression, hence a finite element method has to be taken into consideration separately.

This section presents the approximate 2D mathematical models of the dipole, quadrupole and adaptive octupole microelectrodes. Results obtained from these studies are used as references to the finite element solutions in Chapter Four. In general, the polynomial electrodes are confined by the polynomial function of [115]:

$$f_N(x,y) = af_{na} + bf_{nb} \qquad (3.15)$$

with N is the polynomial order, a and b are the constants and f_{na} and f_{nb} are the independent functions defining the electrode geometry. The analytical analysis for the three microelectrodes was conducted using Matlab 7.7.0 (2008b). Results depicted in Fig. 3.15 showed the geometry solutions with d representing the distance between two electrode tips. Subsequently, the electric field distributions generated by the electrodes that profile the DEP trapping force, were estimated.

As expected, high electric field concentrations occur at the central region of electrodes arrangement, as shown in Fig. 3.16. The maximum electric field generated for the dipole, quadrupole, and adaptive octupole arrangements at 10Vpp are $1.21\text{x}10^6$ V/m, $2.0\text{x}10^6$ V/m and

6.325×10^7 V/m respectively. The electric field also decreases as distance increases from the central region.

These results showed that the electric field increases proportionally to the number of electrode acting on a single cell. This is an important finding especially when a strong DEP trapping force is required to maintain cell positionings. It also indicates that strong DEP holding forces generated by high electric field regions at the tips of the electrodes, which in turns justify the location of microcavity at the central of microelectrode arrangements where the 'null field' occured. DEP holding forces on cells are expected to weaken as a cell moves from microelectrodes towards the central region. As a consequence of the microelectrode arrangement, if a microcavity can act as a source of DEP force, the trapping can at 'null field' can be enhanced. From these results, it can be inferred that trapping a single cell can be realised at the central on the SIBC biochip using these microelectrode designs. The Matlab files for these analytical solutions are listed in Appendix C.

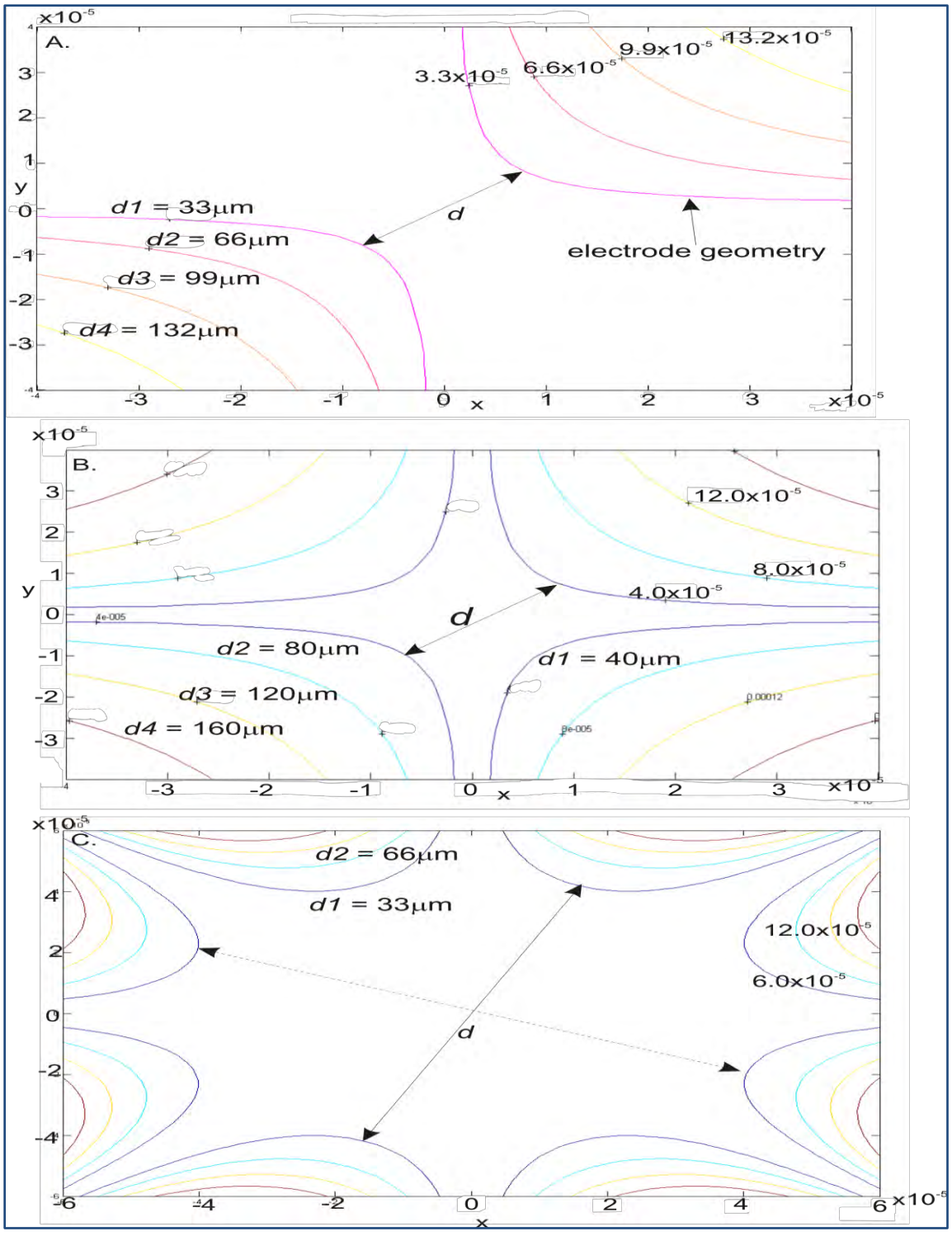

Figure 3.15: The analytical solutions for (a) the dipole, (b) the quadrupole and (c) the adaptive octupole geometry using Matlab 7.7.0(2008b).

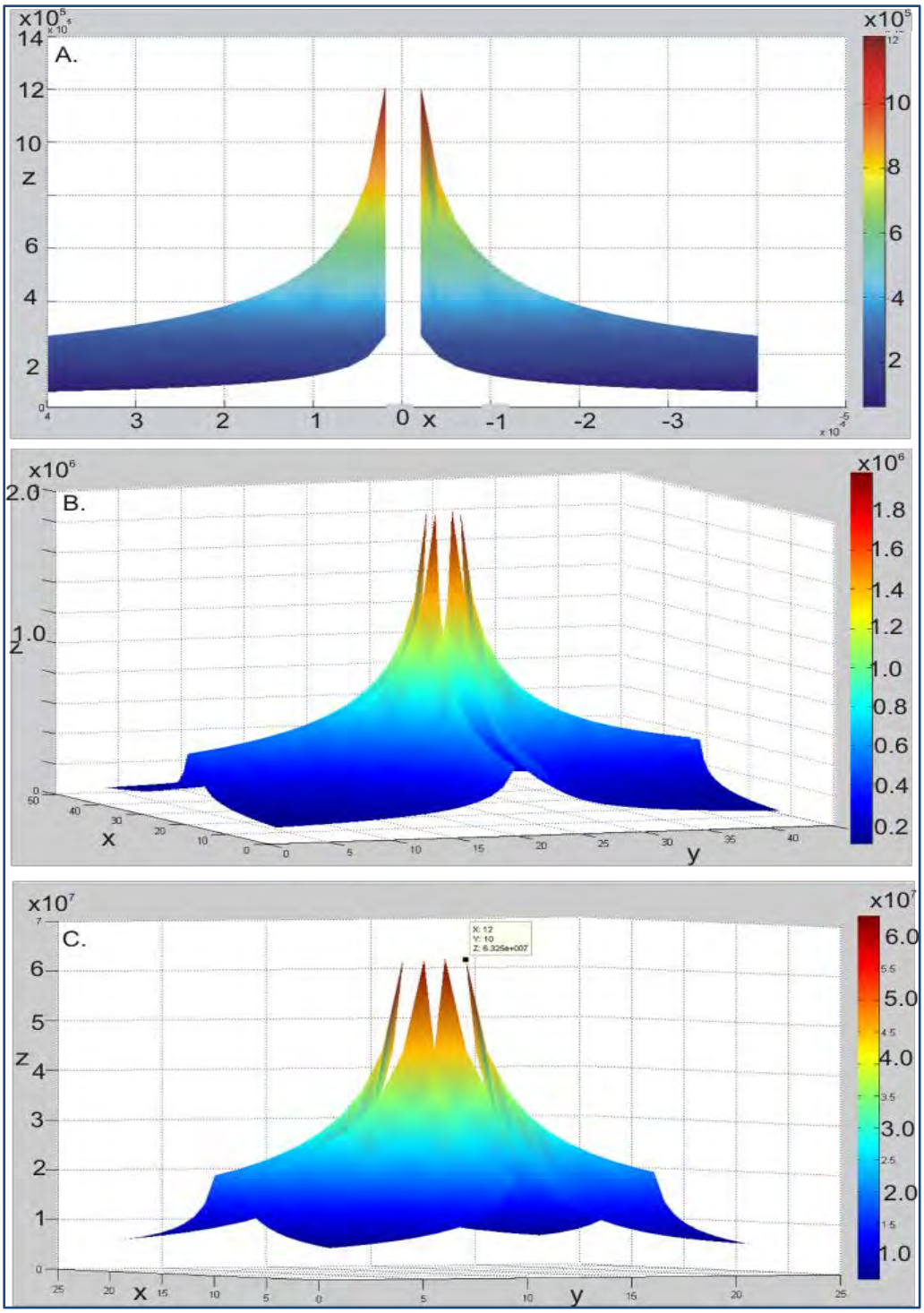

Figure 3.16: Electric field profiles for (a) the dipole, (b) the quadrupole and (c) the adaptive octupole microelectrode.

3.4 Theory of Hydrodynamic Force

The hydrodynamic force plays an important role in cell handling on an analysis platform. In Chapter Two, three types of hydrodynamic force in cell manipulation were explained i.e., suction, laminar flow and electroosmosis, and the benefits of integrating the force with DEP-based biochip were identified. This section outlines the fundamental of the hydrodynamic force on a biochip. It covers the governing equations for cell trapping mechanism, and the integration with DEP-based biochip.

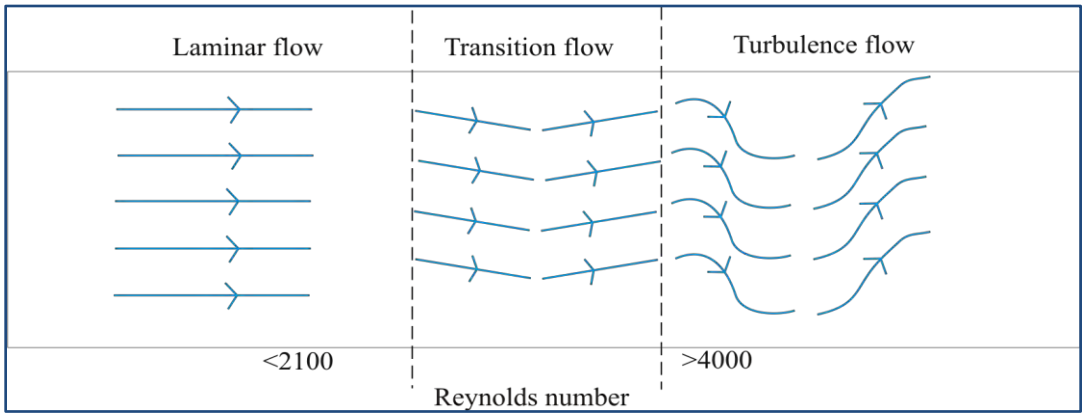

Figure 3.17: Schematic of the Reynolds number and types of fluid flow in a channel.

3.4.1 Hydrodynamic Force Trapping Mechanism

Fluid flow profiles in micro-size channels or microfluidic channels are described by the Reynolds number i.e., the ratio of inertial forces to viscous force in fluid. Since inertial forces are proportional to the flow diameter of a channel or a chamber, the Reynolds number of a biochip is usually very small or less than 0.1 [117]. This implies that in microfluidic channels, the laminar flow profile illustrated in Fig.3.17 is more likely to influence fluid flow than other

type of the flow profiles. There are two key features of a laminar flow: a) no turbulence flow in fluid, and b) the fluid moves according to the streamline. Hence, a laminar flow can be useful in regulating cell movements and transporting cells to the required location accurately with an appropriate microfluidic channel design.

The movements of cell inside a microfluidic channel are related to the fluid velocity. A 2-

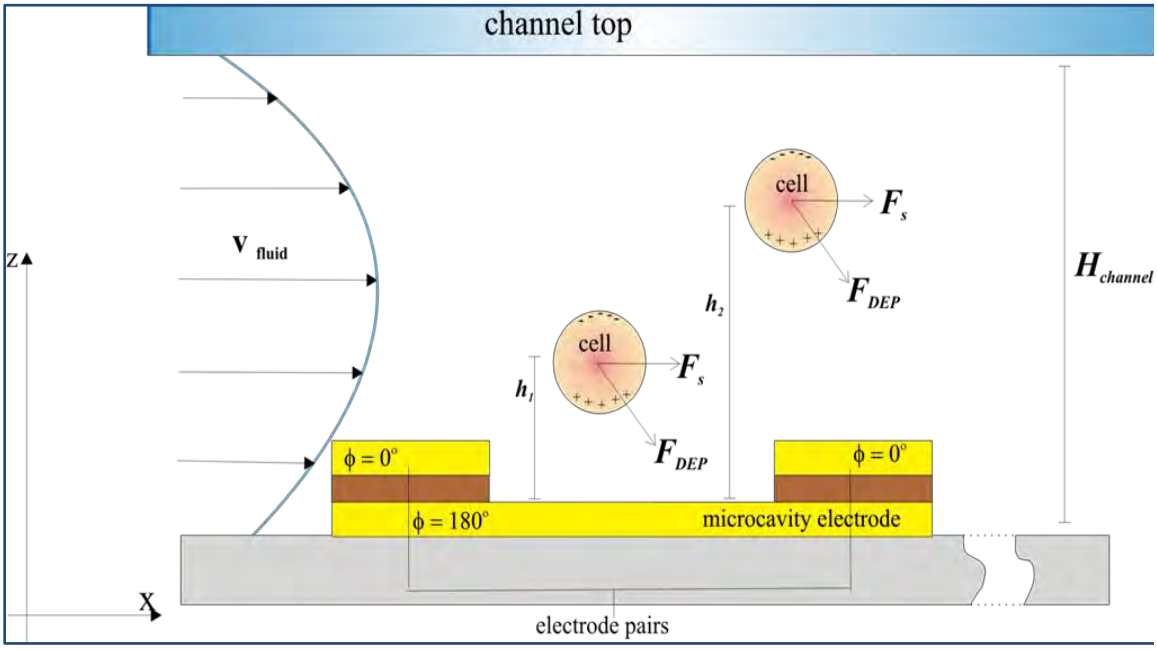

Figure 3.18: Illustration of the particle trapping on top of SIBC biochip and inside the microfluidic channel.

dimensional (2D) cell movement in a microfluidic channel is examined to simplify the velocity profile. Usually, cell movements in microfluidic channels are considered to be incompressible fluid motions with no-slip boundary at the wall of the channels. As illustrated in Fig. 3.18, the fluid flow of a spherical cell type is governed by Stokes equation [118]:

$$F_s = 6\pi \ Rv \qquad (3.16)$$

where F_s is the drag force exerted on cell, is the fluid viscosity, R is the cell radius and v is the fluid velocity. Since the viscosity of a given fluid is constant, cell mobility inside the channel is affected by either fluid velocity or cell size.

For example, an accurate separation by size of cell suspension is done using multiple side-branch channels along a microfluidic channel. Due to hydrodynamic force exerted on cells with different size under specific fluid flow, an accurate separation becomes evident [119-120]. Another way of altering hydrodynamic profiles in a microfluidic channel is through a physical structure or an obstacle. For example, arrays of U-shaped micropost can be placed in a slanted arrangement inside a channel to capture single cells [118, 121]. Another example is by changing the flow resistance using meander-shaped channel, this method leads to sequential filling of trapping sites inside a particular channel [122].

In a microfluidic channel, different DEP force measurement techniques can be applied depending on the fluid conditions of either static or continuous flow. This will exerts a drag force on the cell directly and affects the particle velocity. Consequently, the total effective force for a particle in continuous fluid flow comprises the drag force that pull the cell and DEP force. The slip velocity is then estimated when the cell remains in the static or when $\vec{F}_{DEP} + \vec{F}_s = 0$. Hence, cell velocity with respect to the fluid velocity is [123]:

$$v_{DEP} = \frac{R^2 \varepsilon_m \mathrm{Re}\,[K] \nabla |E^2|}{3} \qquad (3.17)$$

As shown in Fig. 3.18, when a cell that moved inside the microfluidic channel is attracted to the microelectrode, will be dragged into the trap located at the centre of microelectrode's arrangement. With a combination of the microfluidic channel and the

microelectrode, single cells are expected to be trapped and localized for further analysis such as using the Bioimprint process.

3.5 The SIBC Biochip Concept

The main reason for incorporating microfluidic channels on the SIBC biochip is to facilitate cells handling for each of the microelectrode patterns. Figure 3.19 illustrates the schematic of an integrated SIBC biochip with the microfluidic channels for the single cells trapping. The microfluidic channels are made from PDMS, a bio-compatible material, and placed on top of the design SIBC biochip to regulate cells fluid transports i.e., cell nutrients and other soluble factors such as particle's suspension medium or other polymer.

Inside the microfluidic channels, cell flows are directed on the microelectrode arrays which means single cells are focused to the DEP trapping regions. Each pattern has its own dedicated microfluidic channel, hence, observations on cell movements due to the patterns can be conducted easily.

Systematic control over fluid velocity on the integrated SIBC biochip can be implemented by connecting the microfluidic channels to a syringe pump. This will prevent from cells aggregation which usually happened when dispersing cells from micropipette. The advantages of incorporating microfluidic channels on trapping single cells are further discussed in Chapter Six.

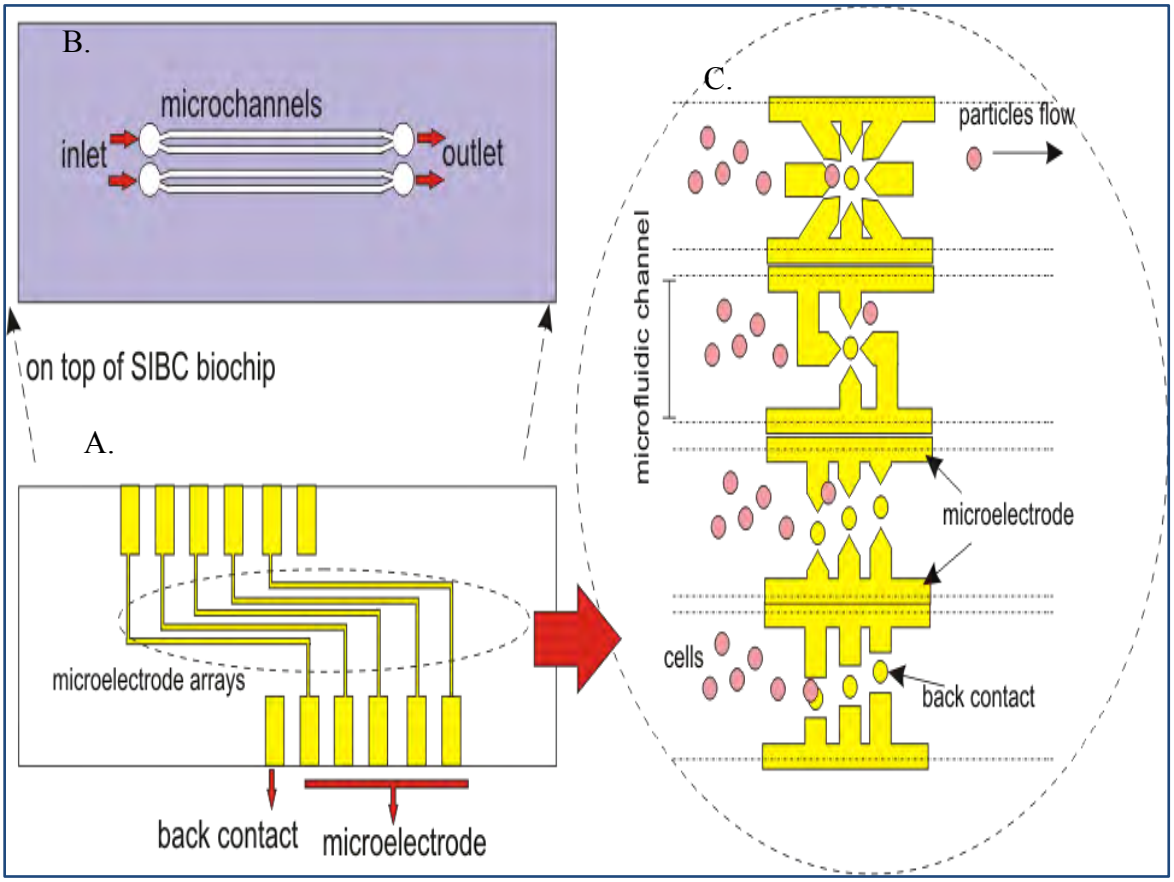

Figure 3.19: The SIBC biochip: (a) the multi layer biochip platform that consists of arrays of microelectrodes illustrated in (c). (b) The PDMS microfluidic channel placed on top of the SIBC biochip to flow cells and imprint polymer. (c) Directions of particle flow inside the 4 different channels.

3.6 Summary

Theoretically, DEP force in a microfluidic channel can be affected by hydrodynamic force, which sometimes can compromise single cells trapping. To achieve a stable holding force of single cells, a proper design of a DEP-based biochip and microfluidic channels are needed. By applying the polynomial equations, 2D models of the V-shaped microelectrodes' tip have been calculated using Matlab7.7.0 (2008b) software. The analysis showed that the electric field

distributions for the three new designed microelectrodes; the dipole, the quadrupole and the adaptive octupole.

As a whole, the results indicated that high electric fields region at the centre of microelectrode arrangements can be used to generate adequate DEP holding force for trapping single cells. Stable trapping can be also facilitated by placing a microcavity that acts as a microelectrode at the centre of arrangements. Following the theoretical aspects in subsection 3.1.1 and analytical solutions of the designed geometries in subsection 3.3.1, the next chapter will discuss the electric field distributions and DEP force profiles generated by the three microelectrodes together with the microcavity as the bottom electrode (the back contact), using a finite element software called COMSOL3.5a.

Chapter Four

Numerical Analysis of the Microelectrode

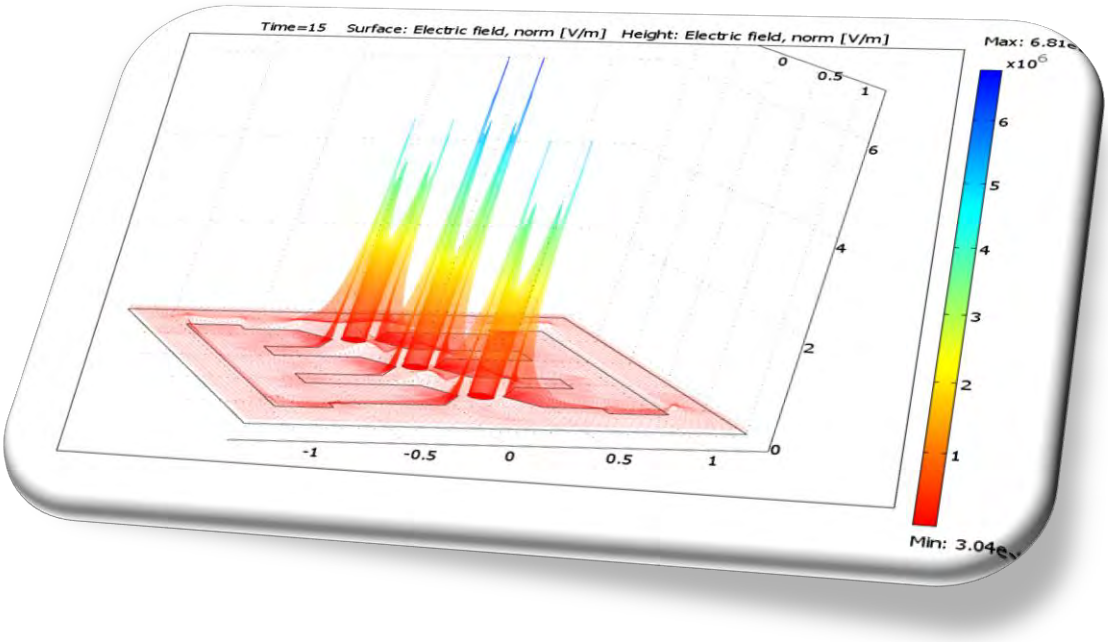

In the previous chapter, three types of microelectrodes were successfully designed and further investigations on these microelectrodes will be performed using finite element analysis. In this chapter, the dipole, quadrupole and adaptive octupole microelectrodes are analysed using COMSOL3.5a software. The electric fields distributions and DEP force profiles produced by each microelectrode patterns are described in section 4.2. Through these studies, locations for DEP trapping on the SIBC biochip are identified. Next, the role of the back contact is presented by comparing the planar two-layer biochip and the SIBC biochip. Results from the simulation are used as the underlying guidelines not only for the fabrication process of the SIBC biochip in Chapter Five but also for the DEP experiments in Chapter Six.

4.1 Microelectrode Design using COMSOL3.5a

Prior to the fabrication stage, the three microelectrodes were designed using finite element software, COMSOL3.5a. One of the main objectives at this stage is to investigate the electric field distributions generated on the platform. The electric field and DEP force in Equation (3.12) of Chapter Three, can be obtained by solving the Maxwell's equations in either electrostatic or quasi-electrostatic approximations. Here, on the assumptions that the dielectric properties are ideal, and the materials only have permittivity and zero conductivity, the microelectrodes were modelled in an electrostatic mode [77][1]. The models were simulated in 2-dimensional (2D) domain and set to the time dependent solution while AC signals were used as the input signals. Then, the electric field was determined by solving the Laplace's equation below:

$$\Delta\varphi = 0 \qquad (4.1)$$

$$E = -\nabla\varphi \qquad (4.2)$$

where φ is the electrical potential and E is the electric field. Here, results from Equation (4.2) are used to find solutions to the DEP force of Equation (3.12). Due to the material homogeneity, where boundary conditions values remain constant, the potential and the electric field solutions only rely on the geometry of the microelectrode model. Furthermore, the gold microelectrodes are considered as isopotential, hence the thickness effect can be neglected in the simulation.

Modelling microelectrode geometry in COMSOL3.5a starts with defining the working space of the model, also known as the model definitions. As shown in Table 4.1, the model working spaces are described by the physics components, the subdomain definitions and the boundary definitions. The software uses values set in the model definitions and then calculates the solution based on pre-defined formulas. Parameters for the model definitions are illustrated in Fig. 4.1. Then, the models were partitioned into small units or meshed to solve Equation (4.2).

The COMSOL3.5a software partitioned a model into small units to determine the nearest variable approximations of a complex equation. Figure 4.2 illustrates the meshing stage of the three microelectrodes in COMSOL3.5a. Following the meshing stage, the equation was solved based on initial values and pre-defined conditions set in the solver manager. In this study, the electrical potential (φ) in x and y domains were determined using Equation (4.2). These results were then used to determine the DEP profiles.

Table 4.1: Models definition of the microelectrode.

Model Studied	Subdomain Definition	Boundaries Definition
i. Dipole ii. Quadrupole iii. Adaptive Octupole	i. Microelectrodes : Gold ii. Suspension : DI water iii. Microcavity : SU8	i. Microelectrodes: Electrical Potential ii. Floating Microelectrodes (octupole): Floating (Unbias) Potential iii. Suspension Plane: Distributed capacitance/impedance

Table 4.2: Parameters used for the COMSOL3.5a simulations from [3].

Parameter	**Polystyrene Microbeads**	**Cells**
Relative Permittivity	2.55	70
Relative Conductivity	0.5 μS/m	0.5 μS/m
Medium Permittivity	78.5	78.5
Medium Conductivity	1.7mS/m (DI water)	1.7mS/m (DI water)
K calculated (Eq. 3.6)	-0.4760269 (nDEP)	-0.037445 (nDEP)
Radius	5μm	5μm
Frequency	1MHz	1MHz
Potential φ	10Vpp	10Vpp

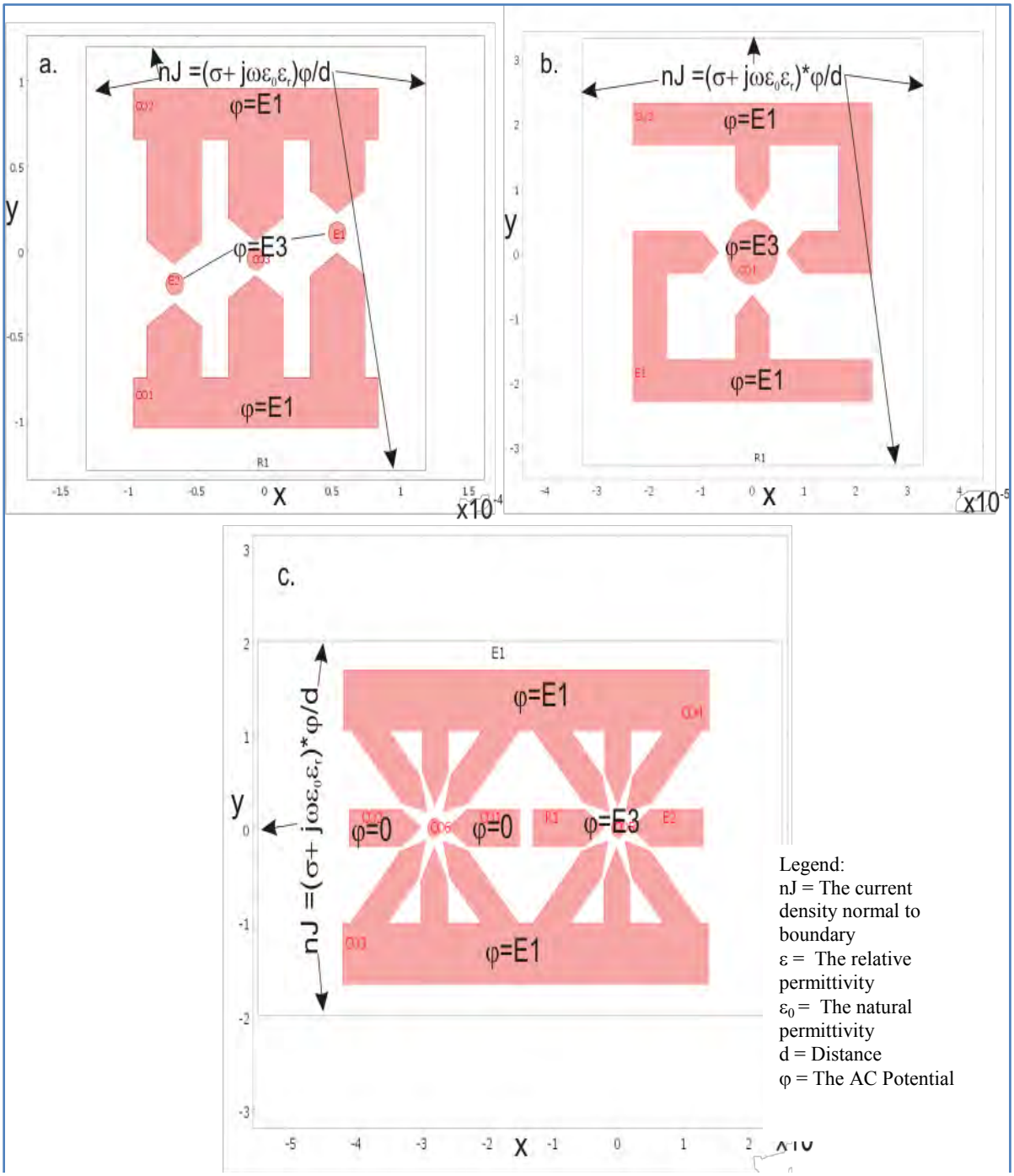

Figure 4.1: Schematics showing the model definitions and boundary conditions for (a) the dipole, (b) the quadrupole and (c) the adaptive octupole microelectrodes.

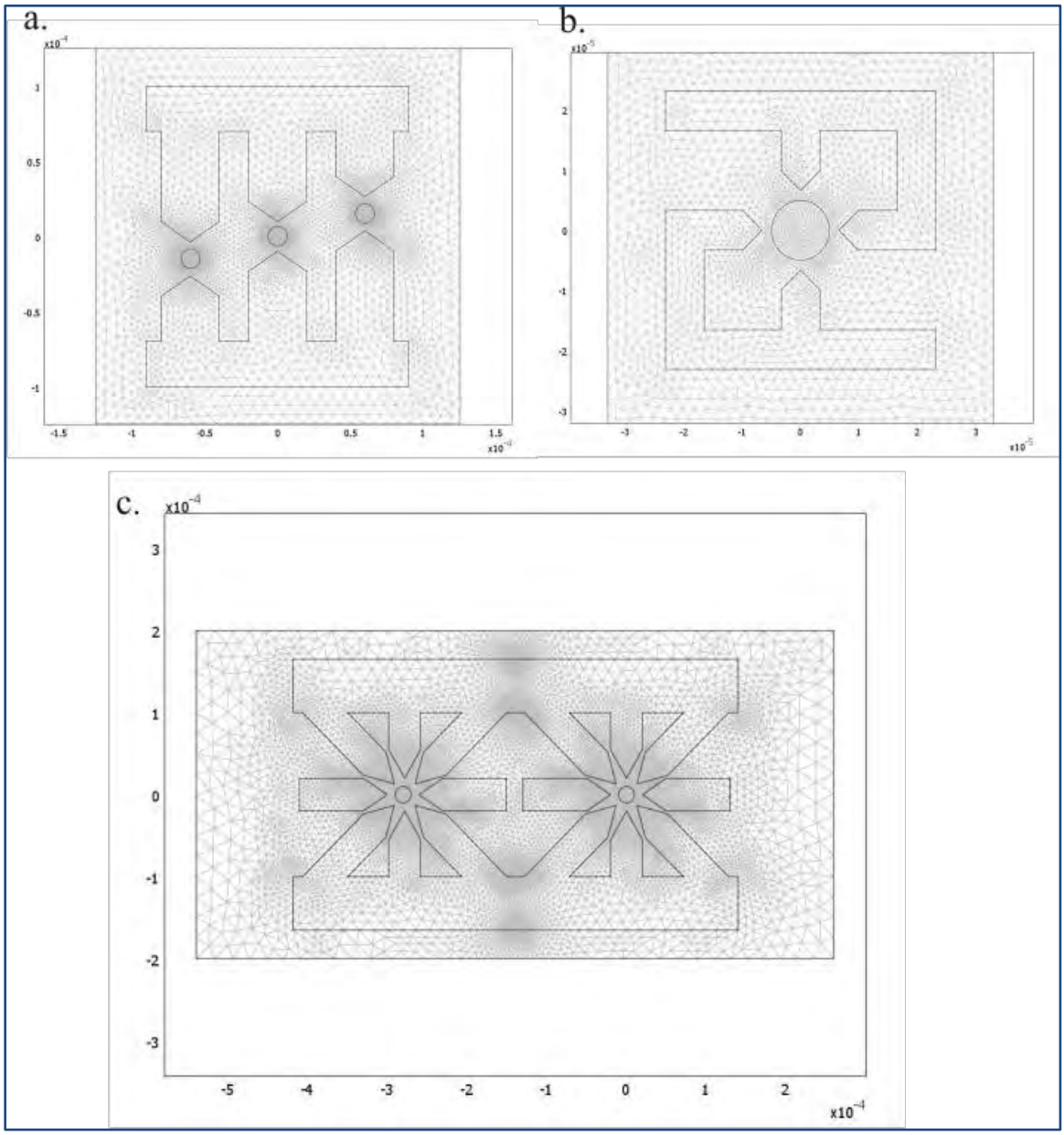

Figure 4.2: Schematics of the meshing stage in COMSOL3.5.a. The microelectrode models were divided into small areas for solving the Maxwell's equation.

4.1.1 Electric Fields Distribution of the SIBC Biochip

Results of the electric field distribution and the DEP force profile for the three microelectrode designs are presented in the following subsections. The purposes of the study are:

1) To identify the trapping regions of the three microelectrode geometries or areas for the DEP force generated on the platform.
2) To obtain the φ that can generate an optimum level of DEP force on the platform and compare the performance of each microelectrode.
3) To study the back contact attributes in enhancing the DEP trapping force.

In order to generate the electric fields for each model, the microelectrode pairs and microcavity were connected with φ of the same or different phase. Results from these simulations are expected to be consistent with the results obtained from the numerical studies conducted using Matlab7.7.0(2008b) in Chapter Three, but with slight increments in electric field intensities due to the additional φ from the back contact.

Trapping regions on the biochip were studied in both horizontal plane (the x-y direction) and the vertical plane (the r-z plane) of the platform. The DEP profiles were calculated using Equation (3.11) and according to the equivalent particle model illustrated in Fig.3.4(a) of Chapter Three. In reality, as explained in Chapter Two, spherical living cells have complex components and are built upon layers of structure. Each of these layers has its own electrical properties and will influence the actual DEP force's cell manipulation on a biochip platform.

With this approximation, the frequency dependent DEP force exerted on a cell can be characterised by modeling the real part of CM factor given in Equation (3.6) in Chapter Three.

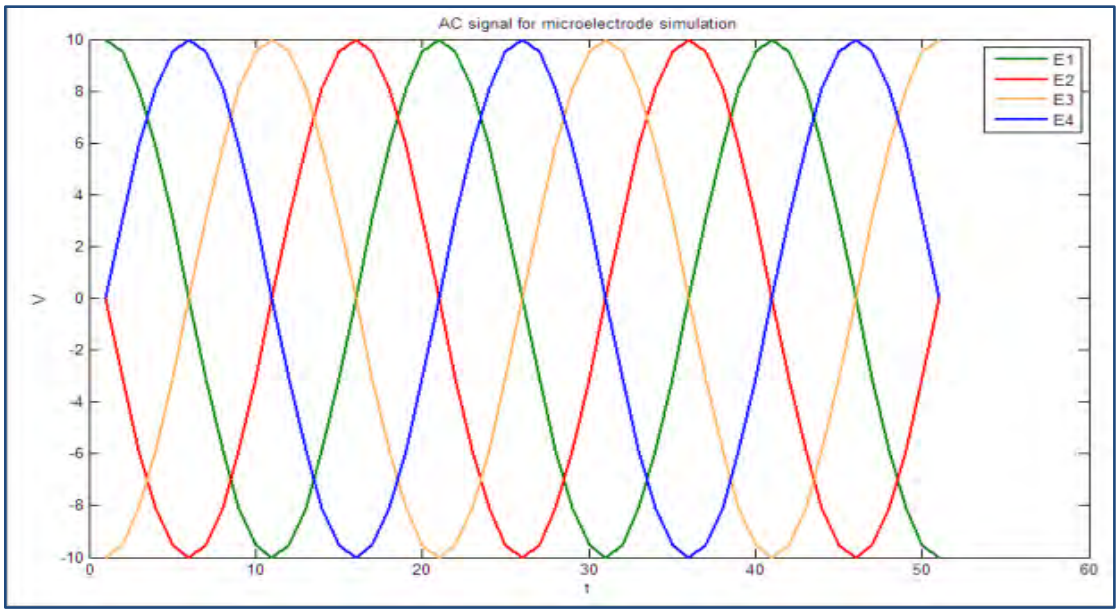

Figure 4.3: The potentials φ used in simulations. Here, E2, E3, and E4 are set to be 90°, 180°, and 270°degree phase different from E1.

The DEP forces for the three geometries were calculated using parameters given in Table 4.2, while variations of the φ used in the simulations are presented in Fig.4.3. Parameters in Table 4.2 were extracted from related literature [124].

4.2 Simulations of the SIBC biochip Horizontal Plane

4.2.1 The Dipole Microelectrode

The electric fields distributions and the DEP force profiles for the microelectrode were calculated based on the polystyrene microbeads dielectric properties (relative permittivity ε_r = 2.55). Figure 4.4 illustrates the electric field profiles when the microelectrode pairs AC potentials were set to be E1 and the microcavity was set to be E3 with 180° phase different from E1 (refer to Fig.4.3).

This setup generated two distinct areas of electric field, one at the microelectrode pair tips, and another inside the microcavity. In Fig.4.4(b), electric fields emerge and peak at the microelectrode tips before decreasing with distance from the electrode tips towards the edge of the microcavity.

Then, another area of electric fields emerge with the maximum is at the edge of the microcavity. Again, the electric field drops with respect to distance and its minimum value is at the centre of the microcavity. Obviously from Equation (3.11), the DEP force is proportional to the electric field generated by the microelectrode. Hence, it can be suggested that the strongest DEP force occurs at the same areas where the high electric field intensities were generated as illustrated in Fig.4.4(a). Results show that the areas of strong DEP forces are within the microcavity proximity, which makes it feasible for trapping particles or single cells on platform. In other words, particles can be navigated towards the traps.

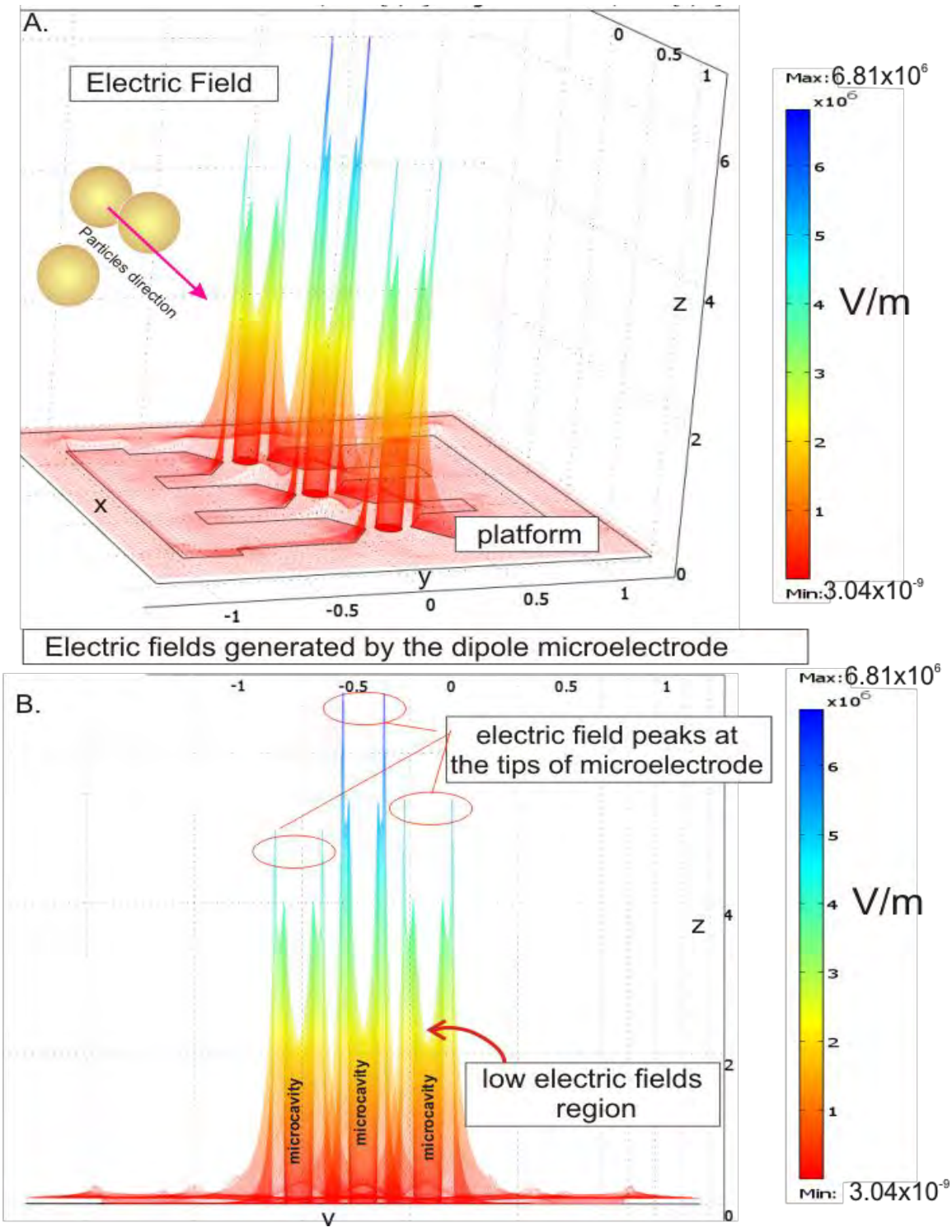

Electric fields generated by the dipole microelectrode

Figure 4.4: Results of the electric field intensity generated by the dipole microelectrode with high peaks occur surrounding the microcavity or at microelectrode tips.

Single cells spatial movements inside a microfluidic channel depend on the dimension (width and height) and shape of the channel. Here, only two directions represent by AB and CD, are discussed due to direction of cells flow in the channel i.e., along the x-plane illustrated in Fig.4.5. When single cells flow along the AB direction, they move towards regions of high electric field intensities generated by the microcavity.

In contrary, single cells moving along CD direction will experience electric fields with phase difference. In this particular case, due to the 180° phase different between potentials (E1 and E3), a single cell may rotate while moving into the microcavity.

As illustrated in Fig.4.5, the asymmetric design of the dipole microelectrode allows

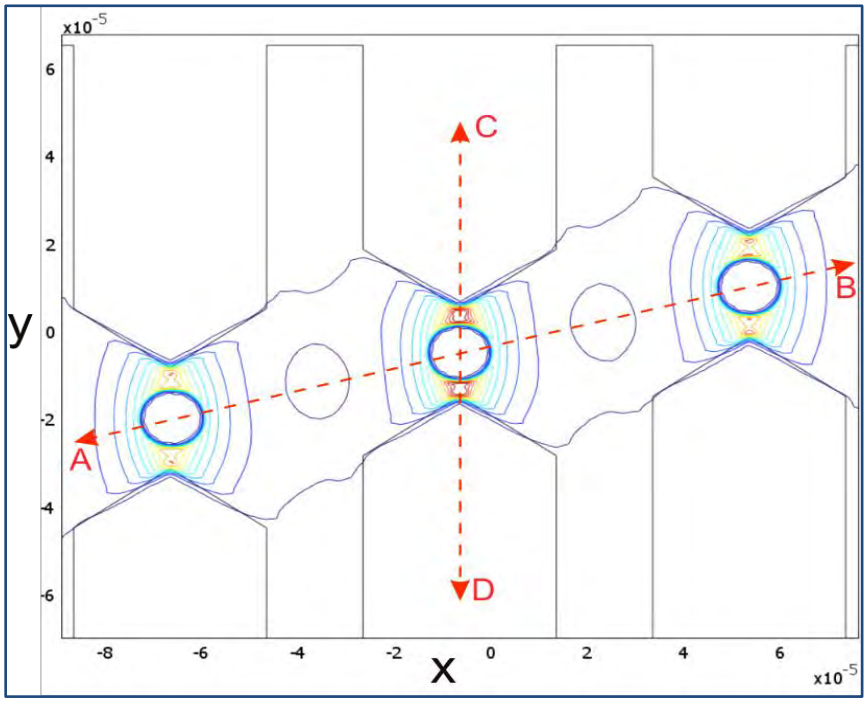

Figure 4.5: The AB and CD lines represent cell movements studied in this chapter. Contours surrounding the microcavities represent the electric field intensities generated by the dipole microelectrode.

single cells that flow horizontally or along AB direction, to be trapped consecutively. To increase trapping yields, one set of dipole microelectrode has three electrodes of different lengths placed in close distance between one another. It is expected that when a single cell is not trapped by the first dipole pair (in the x-direction in Fig.4.5), there are always possibilities that the cell will be trapped by the middle or third dipole electrode pairs.

Apparently, high DEP forces occur between the electrode tips and the microcavity which is similar to the location of high electric fields generated. By connecting to AC signals of 10Vpp at 1MHz, the dipole microelectrode generates 7.82×10^6V/m and 2.69×10^6V/m at high and low electric field regions respectively. The design generates electric field in range of 10^6V/m which is consistent with the values calculated using Matlab7.7.0(2008b) shown in Fig.3.16(a) of Chapter Three.

Results shown in Fig.4.6(a) demonstrate that the high electric field distributions generated by the microelectrode do represent the region of DEP force in Fig.4.6(b). From these results, it can also be deduced that the DEP force is directly proportional to the gradient of electric field squared $\nabla|E|^2$, as depicted in Equation (3.11) in Chapter Three. Using the 10Vpp at 1MHz signal, the maximum DEP force exerted on 10μm microbead (diameter) is approximately 0.67pN. The value is considered to be sufficient to move microbeads inside a microfluidic channel [125]. Depending on the particle size, it is estimated that the DEP forces are within the range of several pico-Newton (pN) to several hundred pN [92, 126].

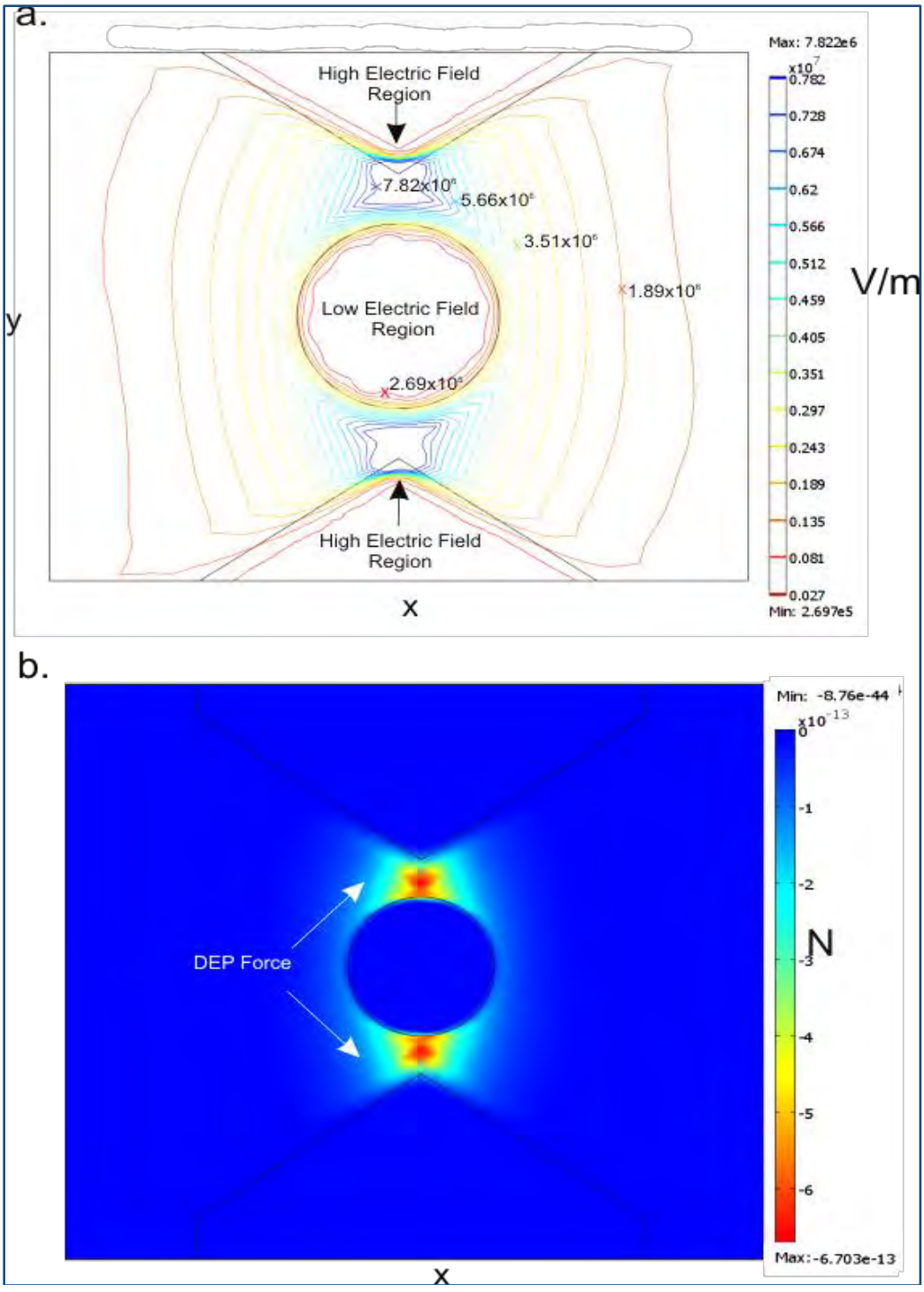

Figure 4.6: (a) The electric field intensities and (b) the DEP forces generated by the dipole microelectrode when it is connected with potentials that have 180º phase difference.

For nDEP trapping, the single cells will repel from the region of high electric fields and attracted to the region of low electric fields, as shown in Fig.4.6(a). Nevertheless, the direction of cell's movements will depend on the frequency and phase of the supplied AC signals. As mentioned previously in Chapter Three, the multilayer structure of SIBC biochip allows many φ to be used simultaneously during DEP trapping experiments. Hence, it is essential to identify the optimum DEP force generated on the SIBC platform through numerical analysis.

Here, the optimum DEP force on the SIBC platform is calculated by setting up several φ values to the back contact (microcavity) and the microelectrode pattern. Then, a cross section analysis between the electrode tip and microcavity edge were used to determine the optimum DEP force. Results in Fig.4.7 show that the optimum DEP force exerted on a microbead or a cell occurs when φ of the back contact is 180° out of phase from the φ of the microelectrode pattern. On the other hand, connecting the microelectrode with φ of the same phase will generate the weakest DEP force.

Data in Table 4.3 also highlight when the microcavity is connected with φ that has 90º and 270º phase different from the electrode pairs, the DEP generated are of the same values. Interestingly, when the back contact (microcavity) is not connected with any φ or is left unbiased, the dipole microelectrode design exerted higher DEP trapping force than when it is connected to the φ of the same phase. Depending on locations, an unbiased electrode will generate induced electric fields that generated by its neighbouring biased electrodes [106]. Therefore, in this situation, the unbiased microcavity which located in between the microelectrodes pair shows significant contributions to the overall DEP force.

The DEP forces calculated in Table 4.3 also showed that the DEP force exerted on cells are less than DEP forces exerted on polystyrene microbeads. The results suggest that particles with higher dielectric property need less DEP force for manipulation. In the literature, different permittivity (ε_r) of cell sizes 4µm to 7µm resulted with DEP force values in the order of pN [127]. Other studies also indicated that 500nm particle resulting in a force of 40pN relative to the microfluidic channel [128]. Hence, results obtained in this section are consistent with DEP force values reported in the literature and considered to be sufficient for trapping single cells.

Table 4.3: Results of DEP force for dipole microelectrode calculated using different φ configurations.

Back contact φ	DEP Force (mean) for Microbead (N)	DEP Force (mean) for Cell (N)
Floating (Unbias)	1.71×10^{-13}	1.71×10^{-14}
No phase shift	1.28×10^{-29}	1.30×10^{-30}
90º	3.42×10^{-13}	3.41×10^{-14}
180º	6.83×10^{-13}	9.07×10^{-14}
270º	3.42×10^{-13}	3.41×10^{-14}

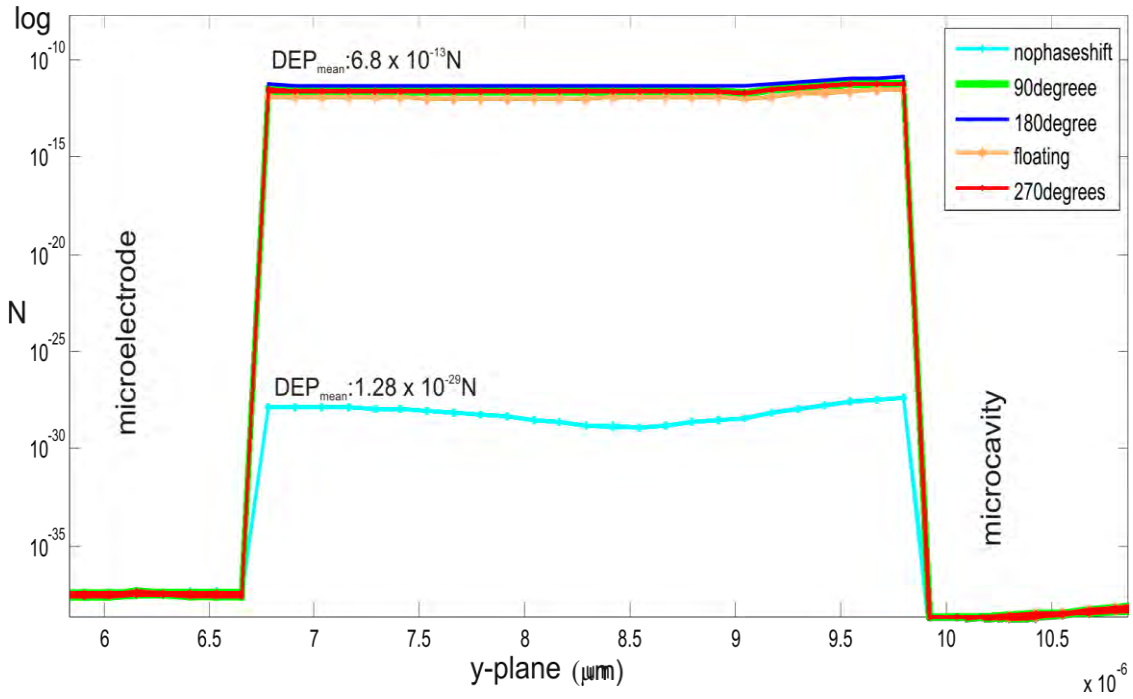

Figure 4.7: (a) The results of DEP force exerted on polystyrene microbeads when the microcavity is set with φ of different phases (ε_r :2.55).

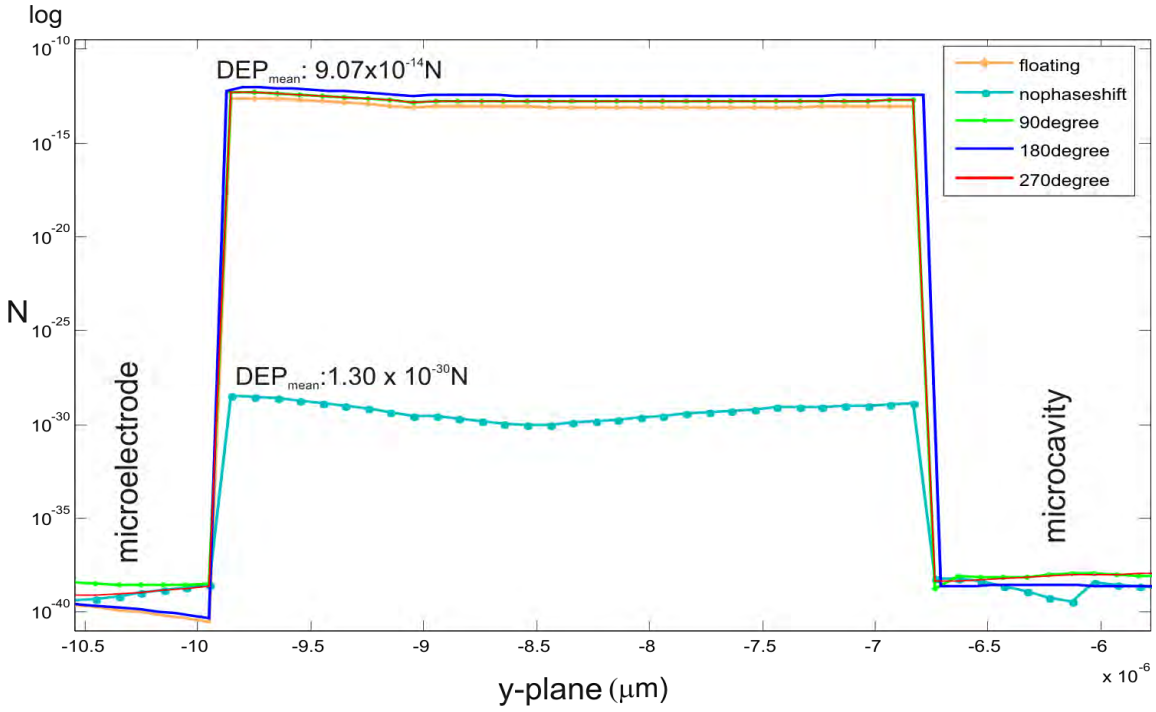

Figure 4.7: (b) Results of the DEP force exerted on cells (ε_r :70).

4.2.2 The Quadrupole Microelectrode

Similar to the dipole design, the quadrupole microelectrode was characterized using the same parameters in Table 4.2. The electric field distributions generated by the quadrupole pattern are illustrated in Fig.4.8. In this figure, areas of high electric field region occur at the tips of electrode while low electric field region occurs at the central area or at the microcavity. Within these two areas (high and low electric field regions), the maximum DEP force occurs but the force decreases as the distance increases towards the central region of the microelectrode. In this particular setup, where φ of the microcavity is 180° out of phase than the φ of the microelectrode pair, the design creates four regions of high electric fields surrounding the microcavity.

Figure 4.8 also exhibits that there are four DEP forces surrounding the microcavity than only two DEP forces generated by the dipole design in Fig.4.6. Therefore, the quadrupole microelectrode design generated higher DEP force to attract single cells toward the trapping region. Due to the four DEP forces surrounding the microcavity, it can be inferred that more single cells will attract to the centre region than the dipole microelectrode. These strong forces are also useful to hold a single cell and to overcome other hydrodynamic forces especially during continuous flow.

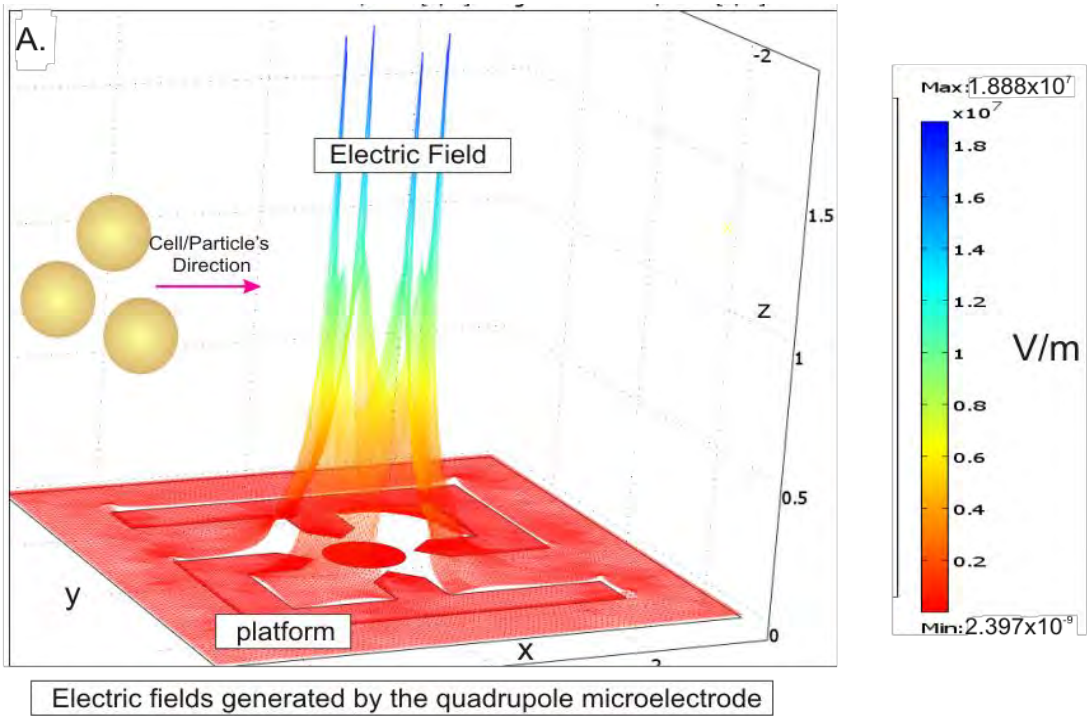

Electric fields generated by the quadrupole microelectrode

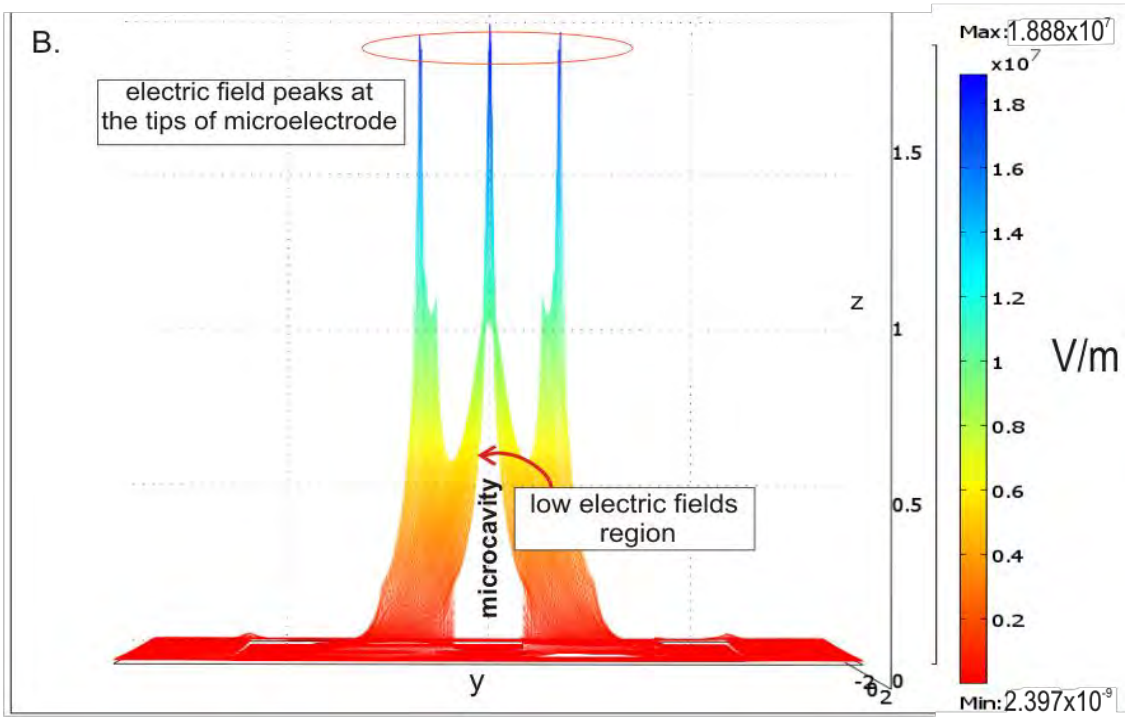

Figure 4.8: The electric field distributions generated by the quadrupole microelectrode using COMSOL3.5a.

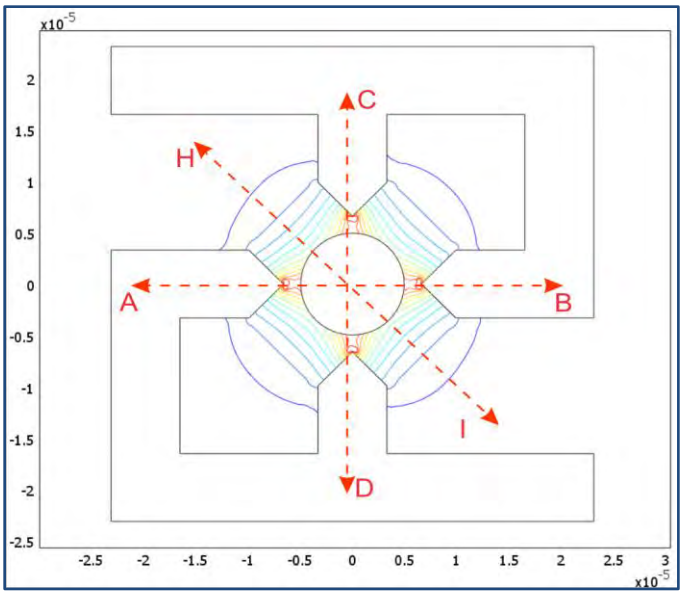

Figure 4.9: AB, CD and HI lines represent directions of single cells movement inside the microchannel with the contour lines represent the electric field intensities produced by the quadrupole microelectrode.

Cell movements along AB and CD directions in Fig.4.9, are from one microelectrode tip to another. In these directions, a cell moves through a region of high electric field before moving into a region of low electric field. Due to the 180° phase difference between potentials (E1 and E3), a single cell may rotate and move towards the microcavity. However, when moving in HI direction, the cells are moving towards low electric field regions at the centre of quadrupole arrangement. It can be inferred that no rotation occurs during the diagonal movement or in the HI direction.

Fig.4.10 illustrates the trapping region for the quadrupole microelectrode. In this instance, the design generates approximately 1.08×10^7V/m at the region of high electric field, and 4.68×10^5V/m at the region of low electric field. The maximum DEP forces value surrounding the microcavity was calculated at 2.04pN.

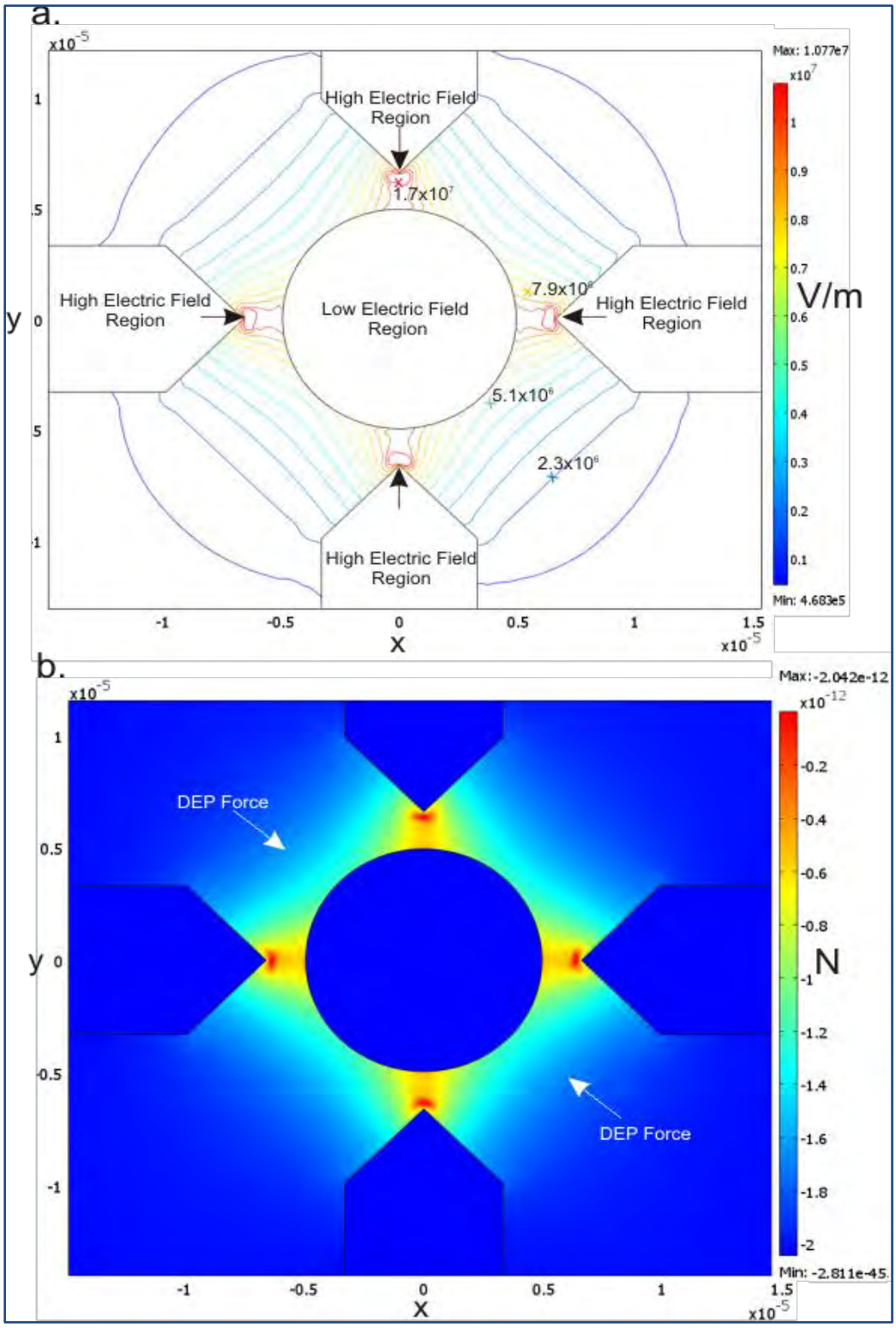

Figure 4.10: (a) The electric field intensities and (b) the DEP forces generated when quadrupole geometry is connected with potentials that have 180º phase different.

Table 4.4 and Fig.4.11 present results for the quadrupole design with AC potentials φ of different phases obtained from measurements between the electrode tip and microcavity edge. The results revealed that the optimum DEP force generated by the quadrupole design is when the φ phase difference is 180°, similar to the results found from previous simulations using the dipole microelectrode. On average, DEP forces generated by this pattern are stronger than forces generated by the dipole microelectrode which indicate stronger holding forces exerted on single cells at the trapping area.

Table 4.4: DEP forces generated by the quadrupole microelectrode.

Back contact φ	DEP Force (mean) AB direction (N)	DEP Force (mean) CD direction (N)	DEP Force (mean) HI direction (N)
Floating (Unbias)	9.22×10^{-13}	9.3×10^{-13}	1.36×10^{-13}
No phase shift	1.45×10^{-22}	83.84×10^{-23}	3.14×10^{-19}
90º	1.86×10^{-12}	1.84×10^{-12}	2.72×10^{-13}
180º	3.68×10^{-12}	3.72×10^{-12}	5.43×10^{-13}
270º	1.86×10^{-12}	1.86×10^{-12}	2.72×10^{-13}

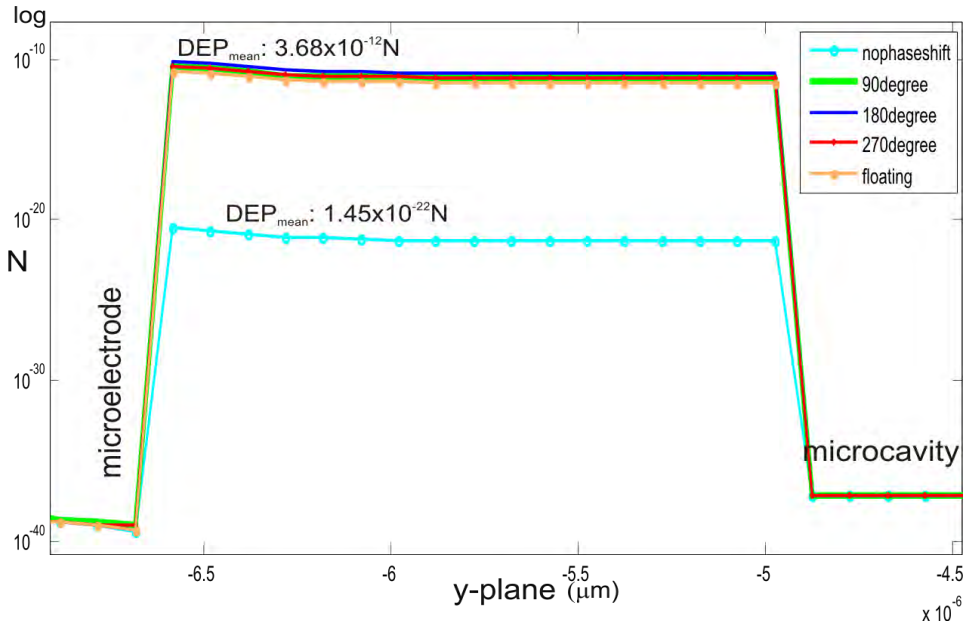

Figure 4.11: (a) Results of the DEP force between tips of the quadrupole microelectrode.

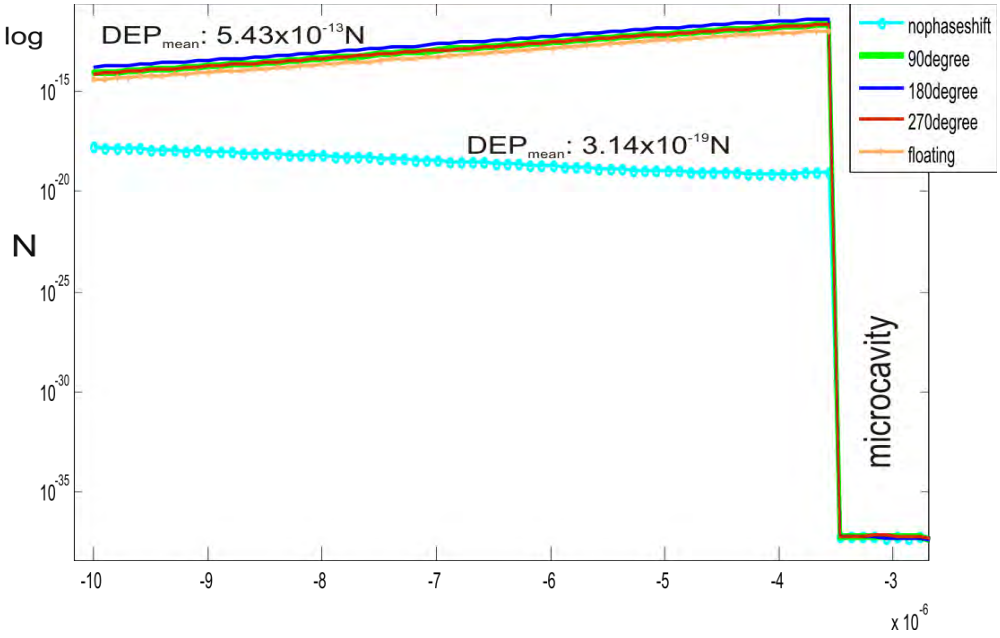

Figure 4.11: (b)The DEP forces along the diagonal direction (HI line of Fig.4.10).

4.2.3 The Adaptive Octupole Microelectrode

The numerical analysis of the adaptive octupole pattern show that the pattern generates six areas of high electric fields surrounding the microcavity, as illustrated in Fig.4.12. Interestingly, the 2-floating-electrode also exhibit high electric fields at its tips. However, the values are less than electric field generated by the microelectrode pairs which were connected (biased) with φ. Due to the existence of high electric field regions from the 3-arm-electrode pair and the 2-floating-electrode, it can be deduced that high magnitude of DEP forces are generated by the adaptive octupole pattern to control cell on biochip platform which results in greater DEP holding force than the dipole and quadrupole microelectrodes.

As depicted in Fig.4.13(b) the DEP trapping regions are surrounding the microcavity. The calculated electric fields at the regions of high and low electric fields are 3.925×10^6V/m and 1.35×10^5V/m respectively. As expected, these electric fields have higher values compared to electric fields generated by the other two microelectrode designs; the dipole and the quadrupole microelectrodes. Using the electric field values, the DEP forces were then calculated, and resulted with 5.277pN for the maximum DEP value.

The 180° phase difference between potentials (E1 and E3) used in this simulation generates the highest DEP force to trap cells within the trapping region. Due to the numbers dipole moment exerted on cells which are proportional to the numbers of electrodes surrounding the microcavity, the adaptive octupole microelectrode is expected to attract more single cells towards the trapping region than the dipole and quadrupole patterns.

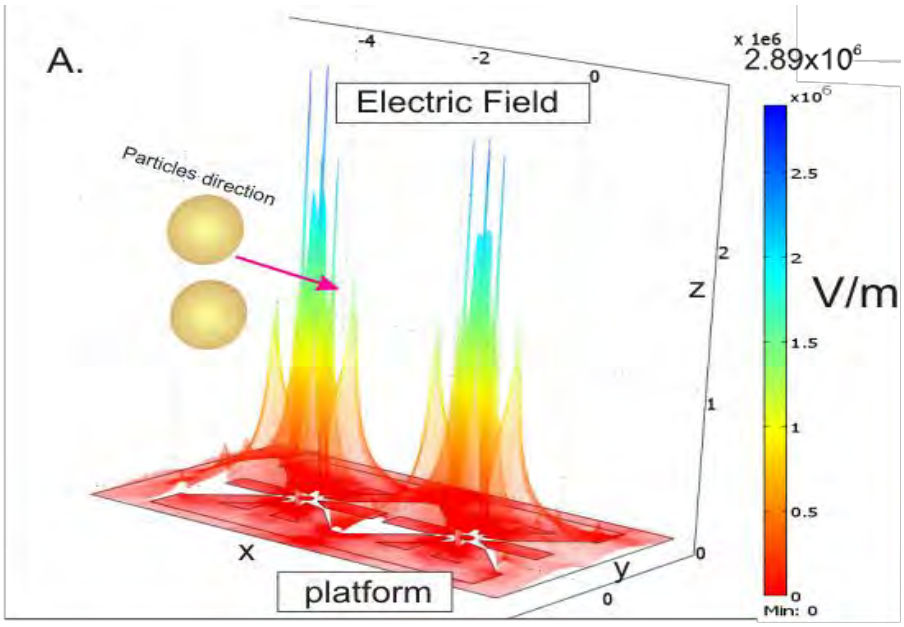

Electric fields generated by the adaptive octupole microelectrode

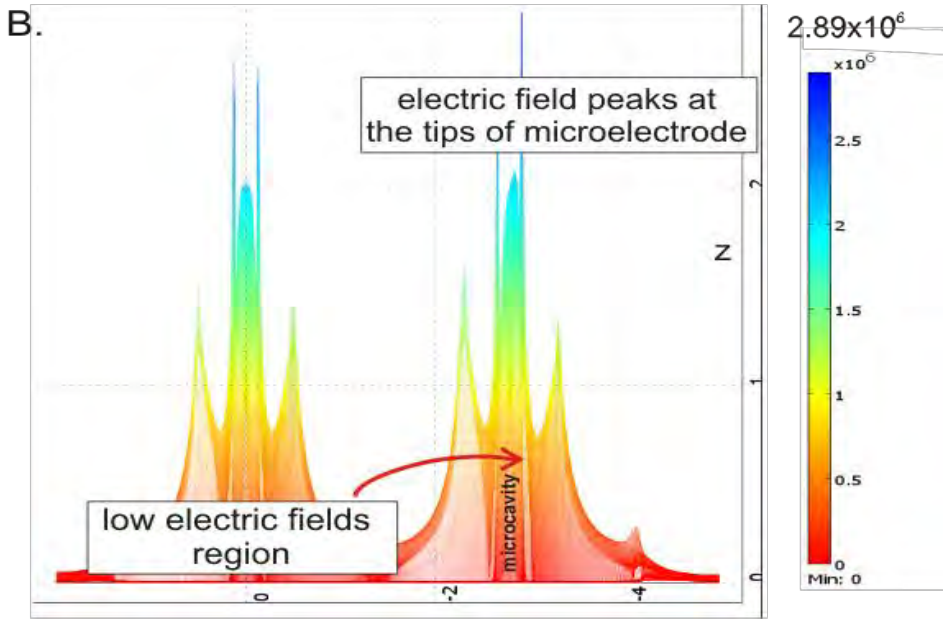

Figure 4.12: The distributions of electric field on biochip generated by the adaptive octupole microelectrode.

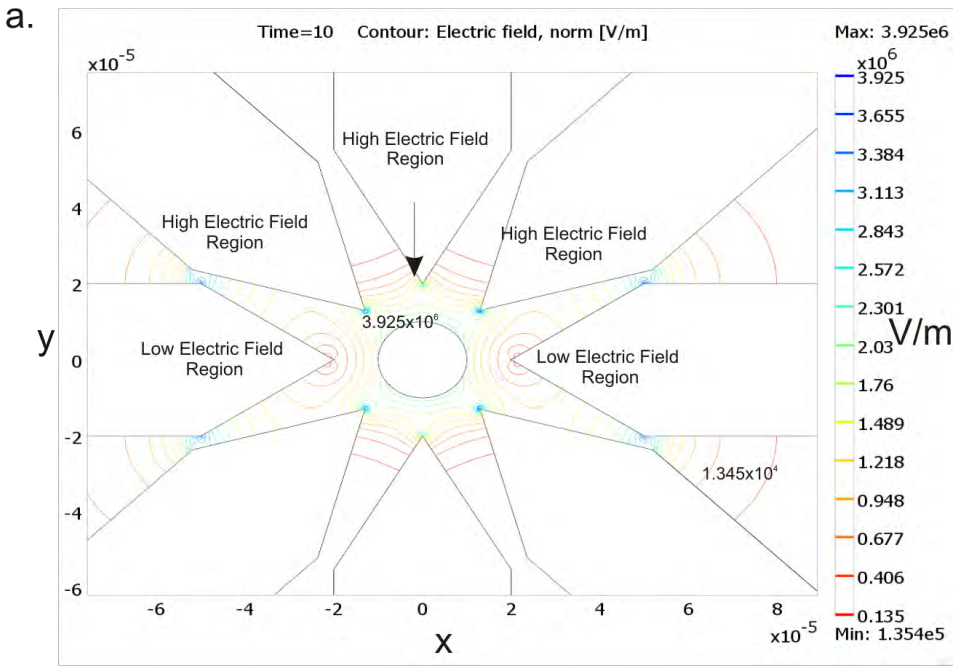

Figure 4.13: (a) Regions of high and low electric fields generated by the adaptive octupole.

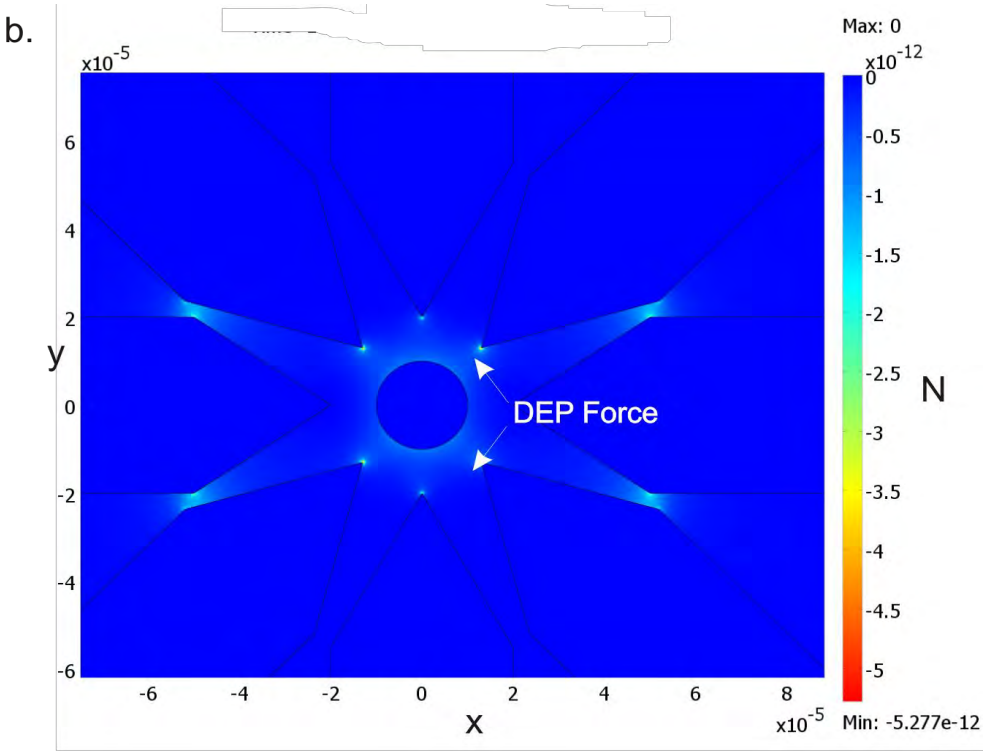

Figure 4.13:(b) The DEP trapping regions generated by the adaptive octupole pattern.

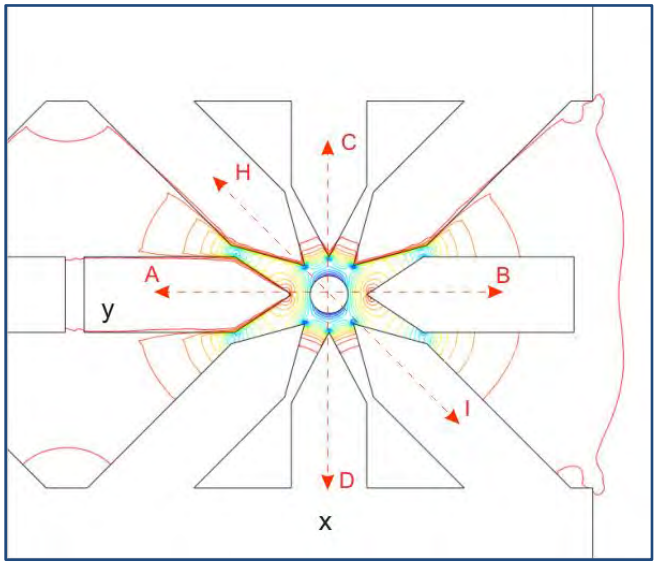

Figure 4.14: The AB, CD and HI lines show directions where the DEP forces are calculated and discussed.

Table 4.5 presents the values of DEP force calculated along AB, CD and HI directions shown in Fig.4.14. The same results are depicted in Figure 4.15. Results in Fig.4.15 demonstrate how φ differences between 3-arm-electrode pair, 2-floating-electrode and microcavity can affect the trapping region. The graph shows that the maximum calculated DEP forces occurred when the back contact is 180° out of phase from the microelectrode pattern layer. Meanwhile, the remainder of the results are consistent with the simulation results of the dipole and the quadrupole pattern with respect to the phase of φ used on SIBC biochip.

Interestingly, the 2-floating-electrode (at the AB direction) generates significant DEP forces that are comparable with results shown in Table 4.5. When the microelectrode and microcavity are connected with the same AC signals, the 2-floating-electrode generates 3.39×10^{-14}N. Due to its location, the 2-floating-electrode induces electric fields generated by both 3-arm-electrode pattern and microcavity which resulted in higher DEP forces compared to other

directions (CD and HI). However, differences in AC signals phase of the 3-arm-electrode pair can reduce the DEP forces generated by the 2-floating-electrode. Nevertheless, the 2-floating-electrode still exhibit high electric field intensity values at it edges and therefore can be useful in controlling cell movements towards the microcavity.

Table 4.5: Results of DEP force exerted on microbead for adaptive octupole design.

Back contact φ condition	DEP Force (mean) AB direction (N)	DEP Force (mean) CD direction (N)	DEP Force (mean) HI direction (N)
Floating (unbias)	4.29×10^{-15}	2.75×10^{-14}	2.60×10^{-14}
No phase shift	3.39×10^{-14}	2.94×10^{-18}	6.89×10^{-16}
90º	3.19×10^{-14}	5.51×10^{-14}	5.01×10^{-14}
180º	2.93×10^{-14}	1.15×10^{-13}	1.01×10^{-13}
270º	3.16×10^{-14}	5.51×10^{-14}	5.01×10^{-14}

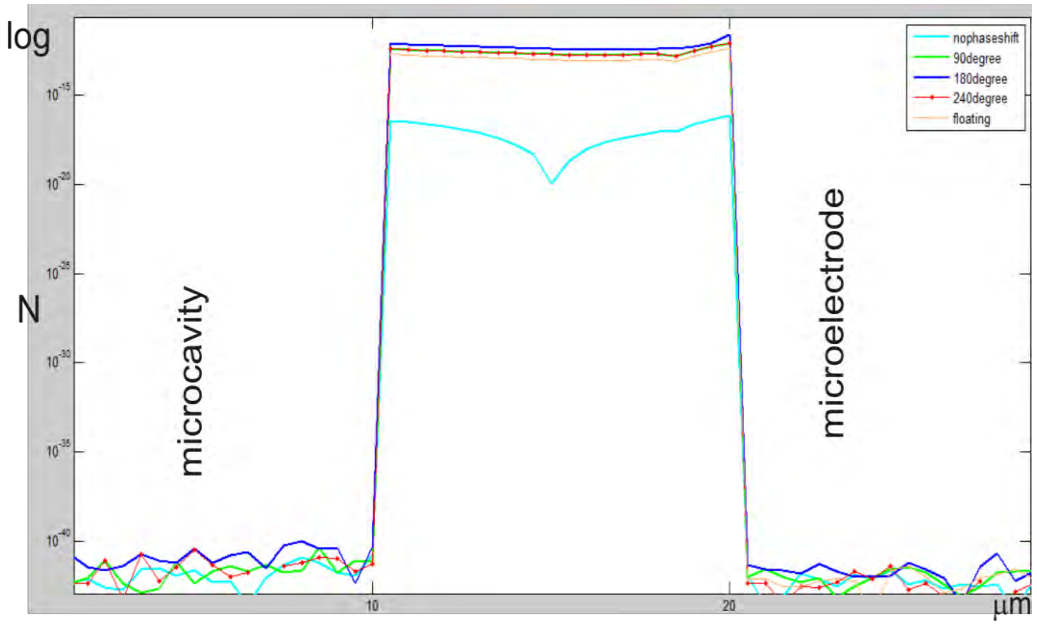

Figure 4.15: (a) The DEP profiles of the adaptive octupole microelectrode design. Results obtained represent single cell movements along the y–plane or CD direction.

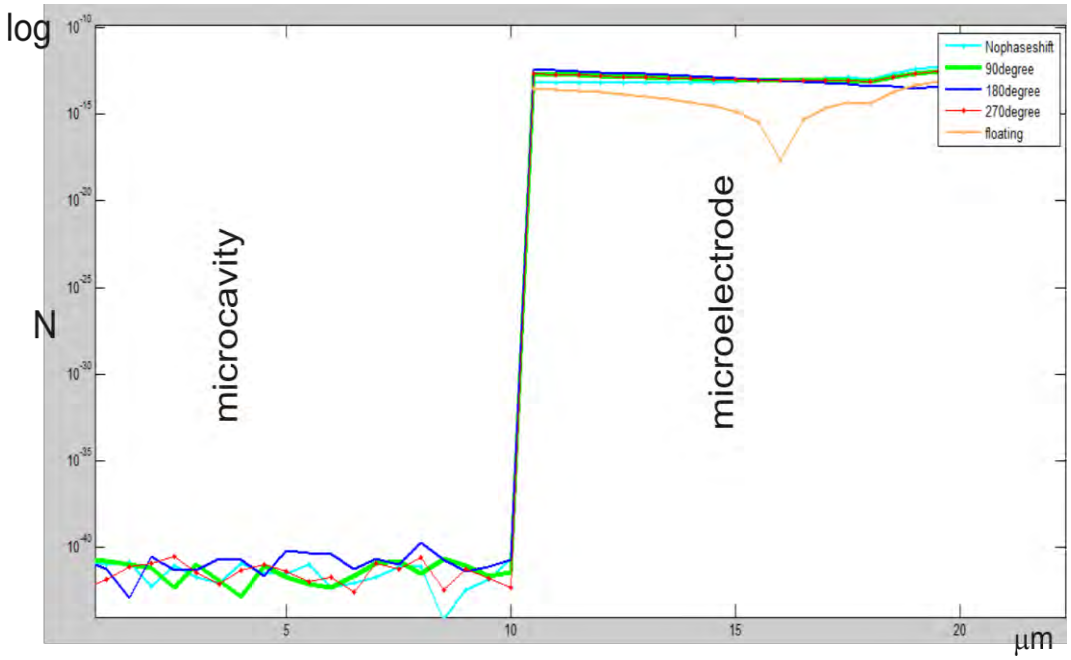

Figure 4.15: (b)The DEP forces along the AB direction of Fig.4.15 or along the 2-floating-electrode.

4.2.4 The amplitude effects on the SIBC microelectrode patterns

The characterization of SIBC biochip continues with a study on the effects of AC signals amplitudes on DEP force. In this analysis, the amplitude of one of the microelectrode pair (on the third layer) was set to 10V, while the opposite microelectrode amplitudes were varied as illustrated in Fig.4.16. Meanwhile, the microcavity is set to be a floating potential, and the phase for φ remains constant with no phase shift. All results were calculated in COMSOL3.5a and plotted using Microsoft Office Excel 2007. Here, only results for the adaptive octupole pattern are discussed since similar results are expected for the quadrupole and the dipole microelectrodes due to the SIBC biochip structure.

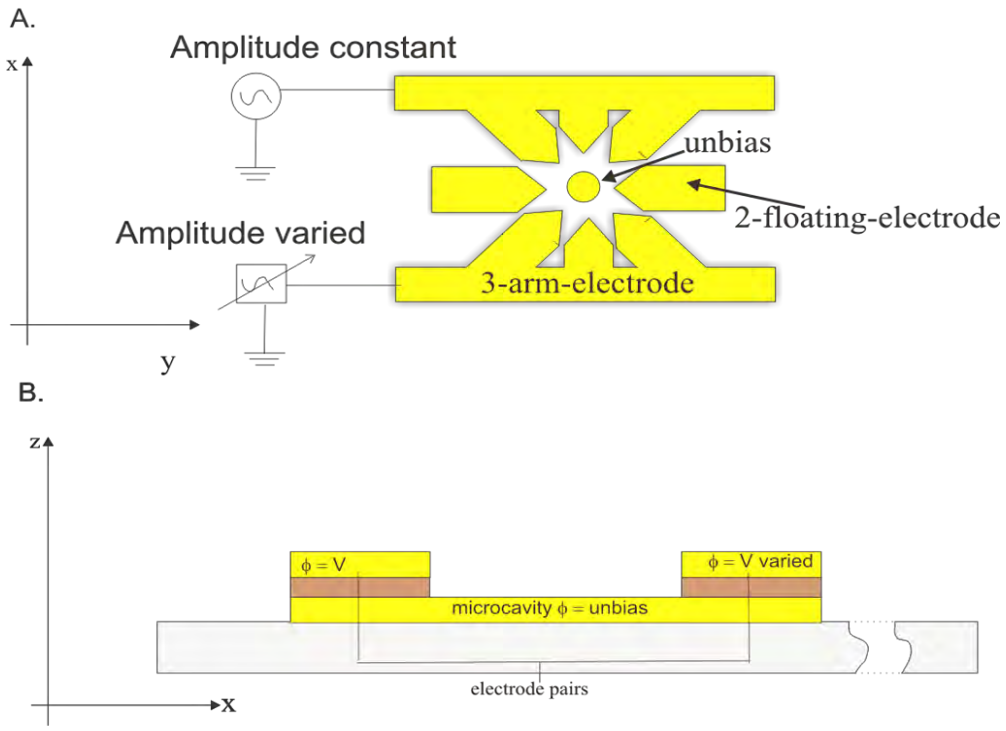

Figure 4.16: The schematic for analysis of amplitude effects on DEP forces.

Results in Fig.4.17 clearly showed that the average DEP force magnitude increases gradually as the amplitude of the φ increases. It can also be predicted that the usage of different amplitudes of φ to bias the microelectrode pattern, is one of the significant factor that increases the magnitude of the DEP forces.

Then the microelectrode potentials were set to have 180° phase different. The reason using different phase is to see whether phase different can increase the DEP force magnitude as indicated by φ combinations in Table 4.5. However, results shown in Fig.4.18 demonstrate that phase difference does not affect the DEP force magnitude generated. It can be inferred that φ phase difference on an alternate microelectrode arrangements, is less significant in increasing the DEP force magnitude. Furthermore, results in Table 4.5 showing higher DEP force for φ of different phase, were obtained between neighbouring microelectrode.

Another useful inference from these results is that the planar two-layer biochip setup, where the microcavity is not an electrode, will generate less DEP force than the SIBC biochip. Results in Fig.4.18 revealed the DEP values of the same order as results using φ of the same phase for alternating microelectrodes as shown in Fig.4.17. For example, the DEP values at 20V along CD direction for both φ conditions (at different phase and at the same phase) are 6.89×10^{-14}N.

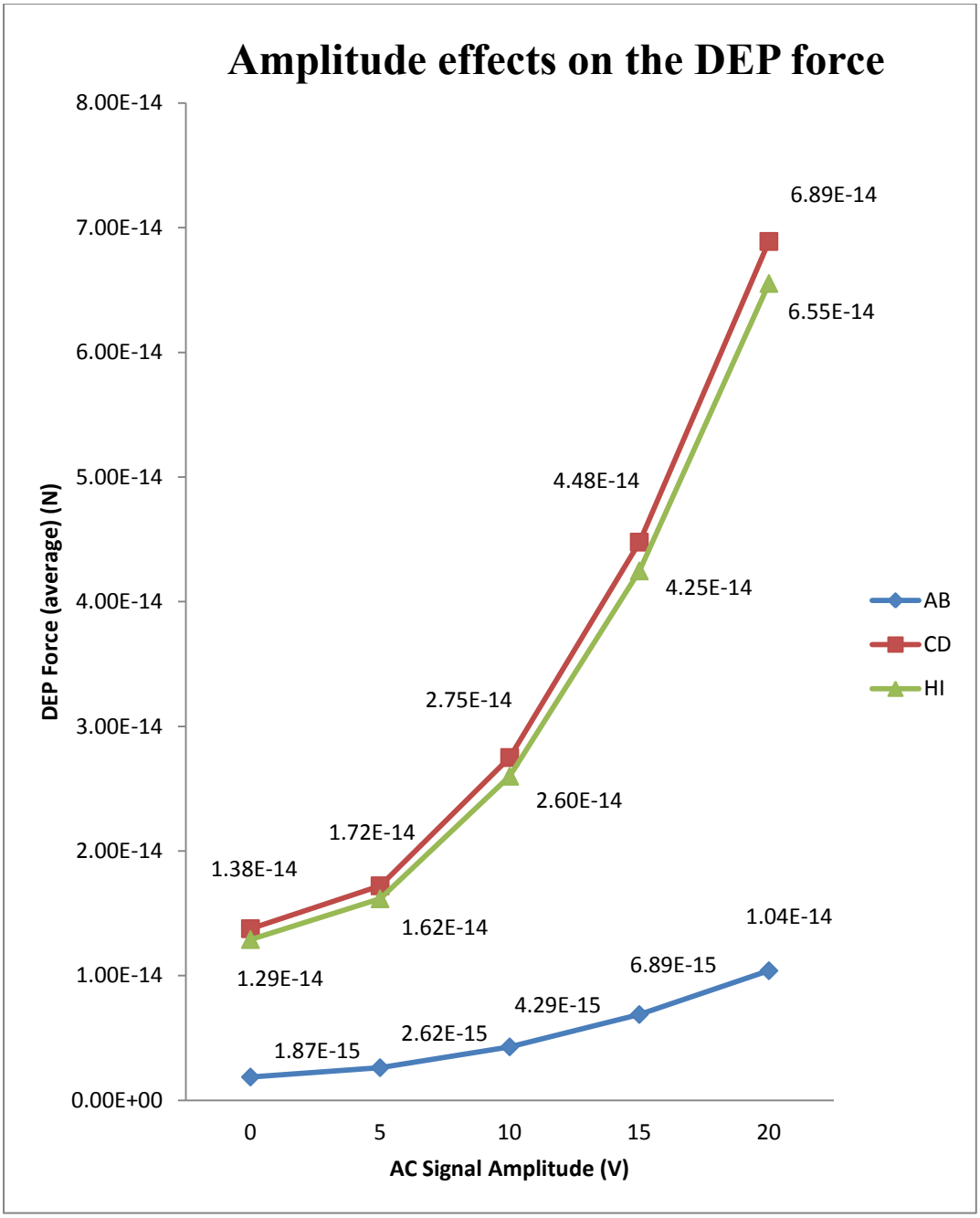

Figure 4.17: Increment of DEP forces magnitude due to the amplitude of AC signals difference by the adaptive octupole.

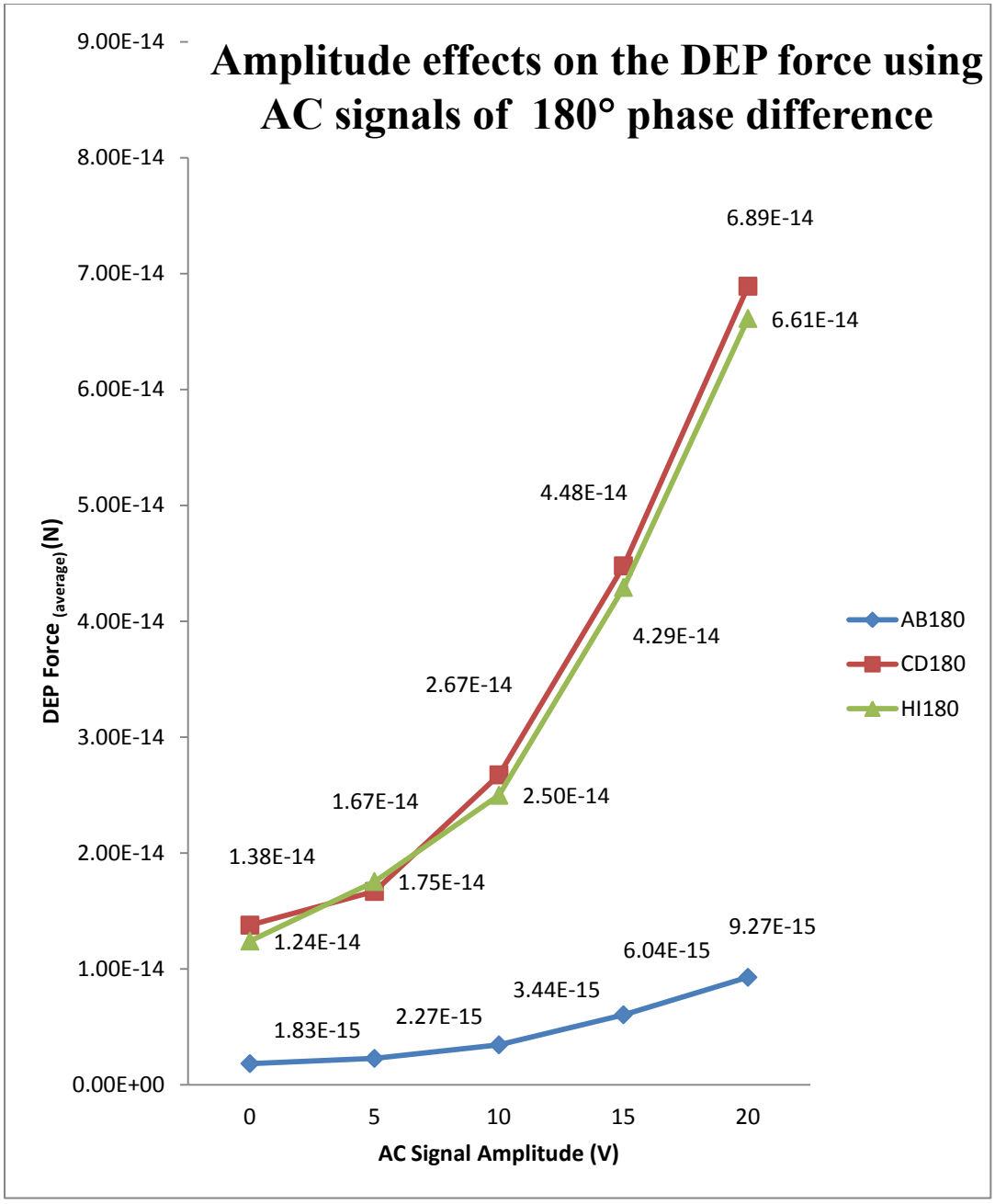

Figure 4.18: The DEP forces generated due to see the effects of AC signals amplitude and 180° phase different.

4.3 Simulations on Vertical Plane of the Microcavity

This subsection presents the back contact attributes on enhancing the DEP force performance in trapping single cells. The simulations were based on model definitions illustrated in Fig.4.19 and by comparing the SIBC biochip and the planar two-layer biochip structures. Here, the channel boundaries were considered to be sufficiently further from the microelectrodes so that the Neumann condition (see Appendix D) can be applied. In the simulations, the AC signals for ML3 were set to be 180° out of phase from AC signals of ML1. However, in the planar two-layer biochip simulations, ML1 was set to be Si and was not connected to any AC signals potential.

Here, the electric fields gradient $\nabla|E|^2$ generated by the SIBC biochip and the planar two-layer biochip were studied. The results in Fig.4.20(a) demonstrate that the gradient of electric fields inside the microcavity, which generated by the back contact, enhanced the overall electric field intensities on the surface of the biochip. On the other hand, the gradient of electric field

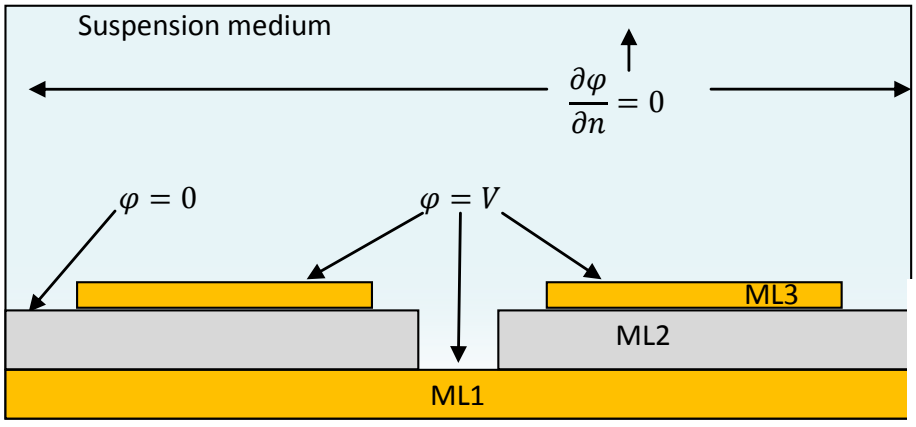

Figure 4.19: The model and boundary definitions for the biochip.

inside the microcavity for the planar two-layer biochip as shown by Fig.4.21 (a), are from the two microelectrode edges. This means that, $\nabla|E|^2$, inside the microcavity of the planar two-layer biochip is less than the $\nabla|E|^2$ generated by the SIBC biochip.

Figure 4.20(a) also reveals the existence of high electric fields gradient at the bottom of the microcavity, an area expected to hold trapped cell inside microcavity. From this result, it can be suggested that the back contact are able to control trapped cell's vertical movement inside the microcavity. However, simulation results in Fig.4.21 showed that the planar two-layer does not generate $\nabla|E|^2$ comparable to the SIBC biochip. At the same time, results of the $\nabla|E|^2$ distribution at the edges of microelectrode, shown in Fig. 4.20(b) and 4.21(b), does not show any significant difference. From these results and comparisons, the SIBC biochip and the planar two-layer generate similar DEP forces at microelectrode edges that surrounding the microcavity.

Figure 4.22 showed the $\nabla|E|^2$ as a function of depth inside the microcavity for both biochips. At 100nm from the surface, the $\nabla|E|^2$ difference values generated by both biochips are in the order of $10(V^2/m^3)$. However, as the depth of a microcavity increases from 100nm to 5μm, the difference values increase from the order of 10 to $10^3(V^2/m^3)$. With these values, it can be concluded that DEP forces inside the microcavity of the SIBC biochip is greater than the planar two-layer biochip in the same order of their $\nabla|E|^2$ respectively.

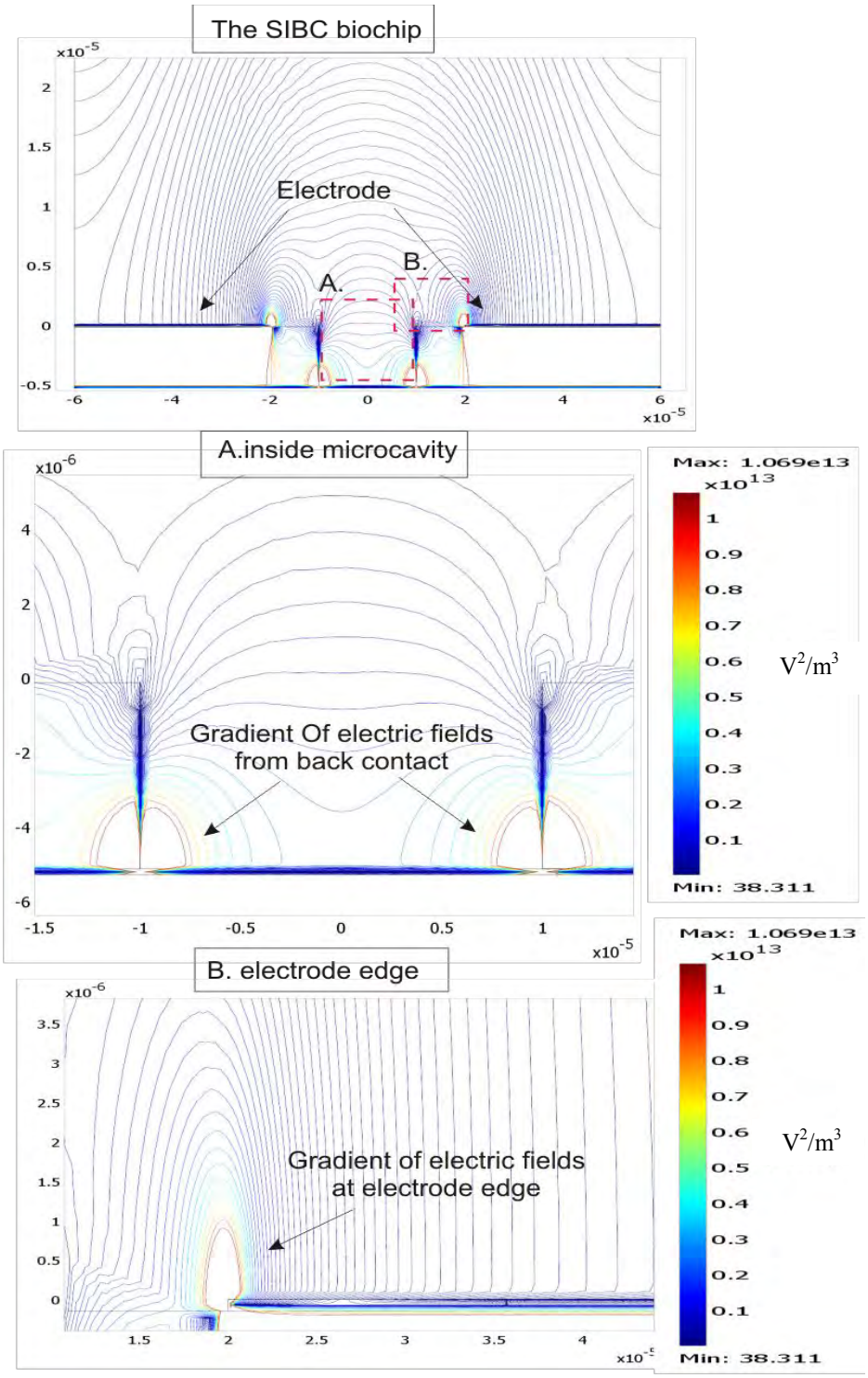

Figure 4.20: (a) On the SIBC biochip, the back contact generates a significant amount of electric field inside the microcavity which can anchor cell inside the trap. b) The electric fields at the edge of microelectrode attract cells into the microcavity.

Results in Fig.4.23 show that the $\nabla|E|^2$ values decrease with distance from the surface of the two platforms. These results suggest that DEP forces exerted on cells will also decrease as the cell located further away from the microelectrodes. Interestingly, the $\nabla|E|^2$ difference between the two types of biochip, which is in the order of 10 to 10^2, are smaller than the difference inside the microcavity, as shown in Fig.4.22. On the SIBC biochip, the occurrence of increasing $\nabla|E|^2$ values can be observed at the microcavity proximity, whereas elsewhere the $\nabla|E|^2$ values are comparable to the planar two-layer biochip.

The results in Fig.4.22 and Fig.4.23 exhibit that the back contact increases the overall DEP forces whether on top of the microelectrodes or inside the microcavity. In view of these results, it can be concluded that the DEP forces generated by the SIBC biochip are greater than DEP forces generated by the planar two-layer biochip.

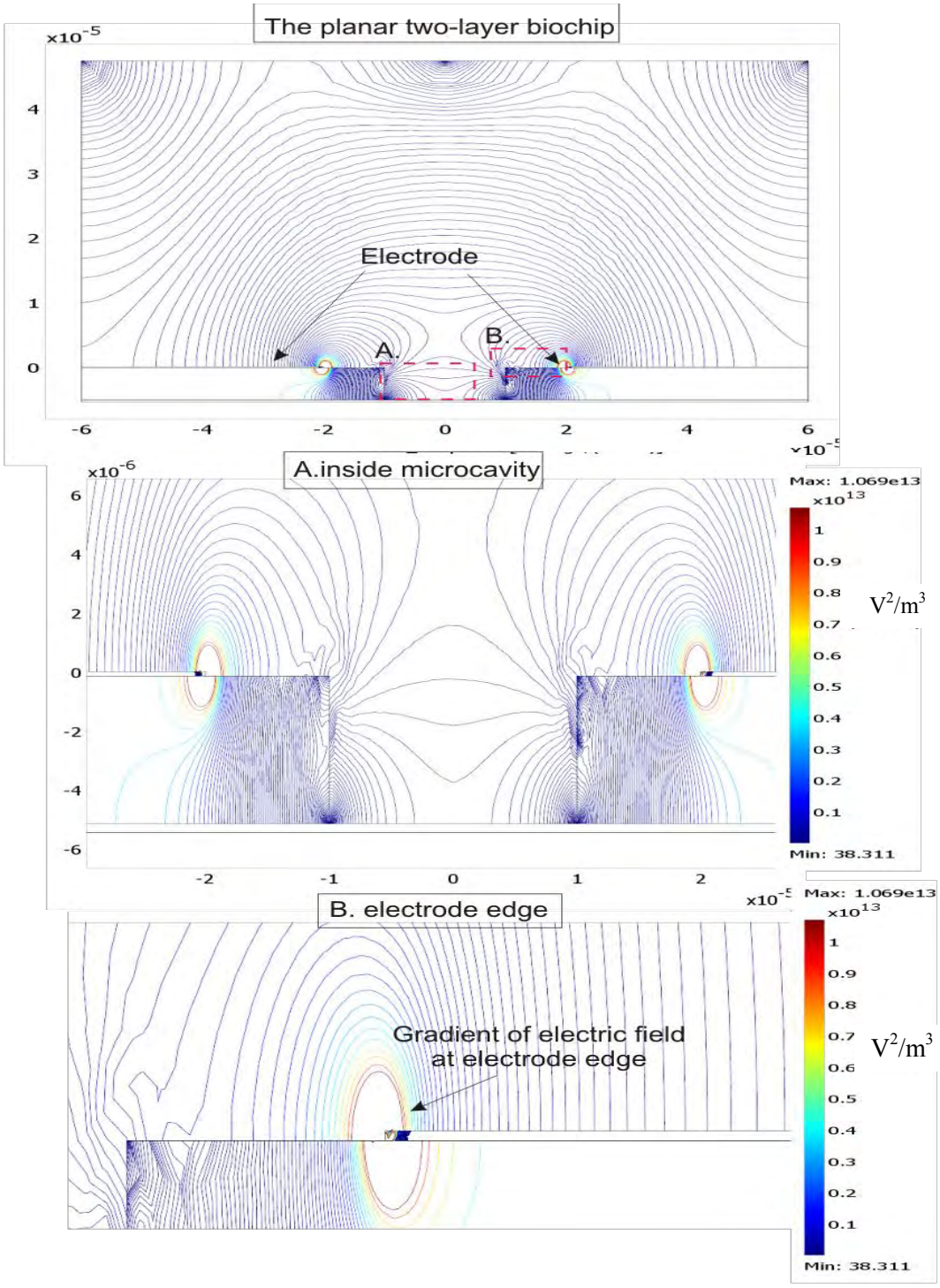

Figure 4.21: Simulations for the planar two-layer biochip where the bottom of microcavity is Si.

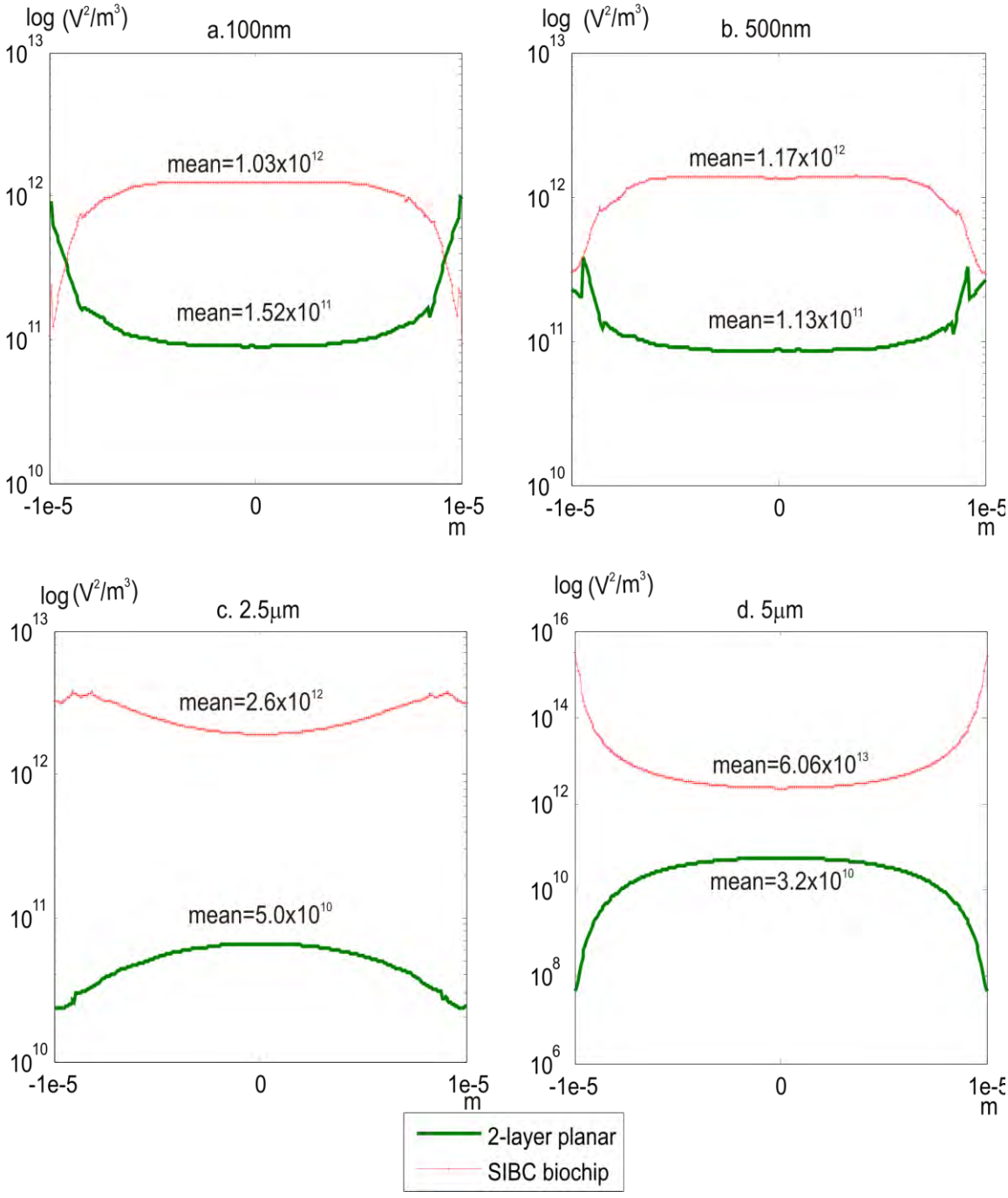

Figure 4.22: The $\nabla|E|^2$ inside the microcavity of the SIBC biochip is greater than the planar two-layer biochip in the order of 10 to 10^3 from the surface of the biochip platform.

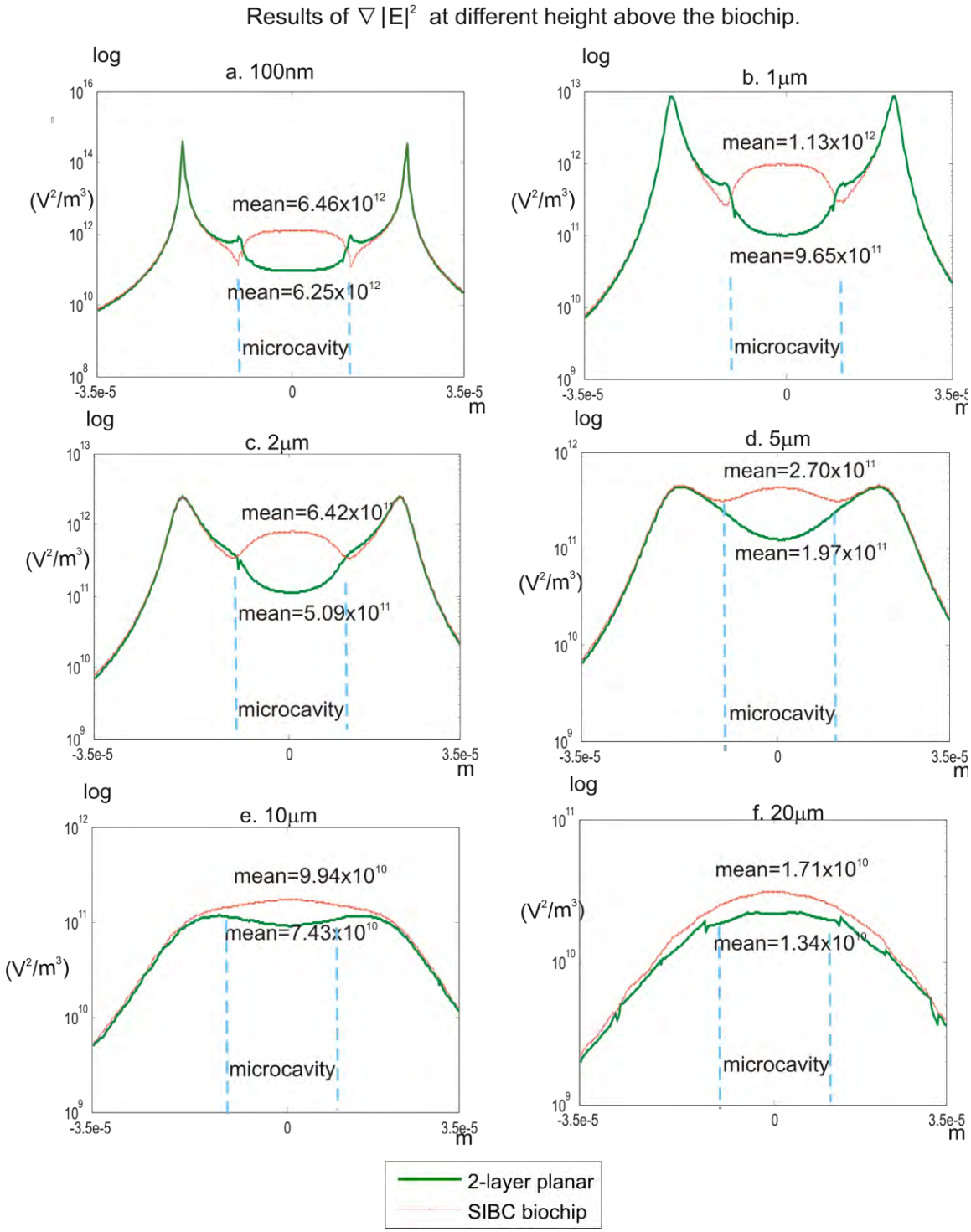

Figure 4.23: Results of $\nabla|E|^2$ as the function of distance from the microelectrode above the biochip platform. These results indicate that the DEP forces exerted on cells weaken as the distance of the cell increases from the microelectrode.

4.4 Summary

Numerical analysis for the three microelectrodes presented in this chapter revealed the trapping region locations defined on the SIBC biochip. The three microelectrode patterns were characterize by studies on electric field distributions, DEP force profiles, φ configurations and amplitude effects as detailed in subsection 4.2.2. Meanwhile, a comparative study on the SIBC biochip and the planar two-layer biochip which relates to the back contact attributes in single cell trapping was presented in subsection 4.2.3.

Results suggested that the DEP trapping regions are located within the microcavity vicinity, provided suitable φ configurations are used to move cells towards these regions. A significant increase in DEP forces were also observed with the increment of numbers of microelectrode from the dipole pattern to the adaptive octupole pattern located within the trapping region.

Results also suggested that the optimum φ setup to power up the microelectrode pairs and the microcavity is when the back contact and the microelectrode pattern has different phase of 180 degree. In contrary, the weakest DEP force is generated when the microelectrode and the microcavity are connected with φ of the same phase. Placing a floating (unbias) electrode on a biochip platform can be useful in facilitating DEP trapping due to its ability to generate induced electric fields and increases the overall DEP force on the biochip.

A trap/microcavity that acts as an electrode place in between microelectrode pairs can increase the total of DEP force on a biochip platform. Results in subsection 4.2.2 revealed that the increment of $\nabla|E|^2$ which is in the order of 10 to $10^3(V^2/m^3)$, point out the probability of the

DEP force increment three times in magnitude. In principle and as demonstrated in numerical analysis, a biochip structure that incorporates cell trap (microcavity) as an electrode can significantly enhance the DEP force generated on the biochip platform.

Chapter Five

Fabrication Process of the SIBC Biochip

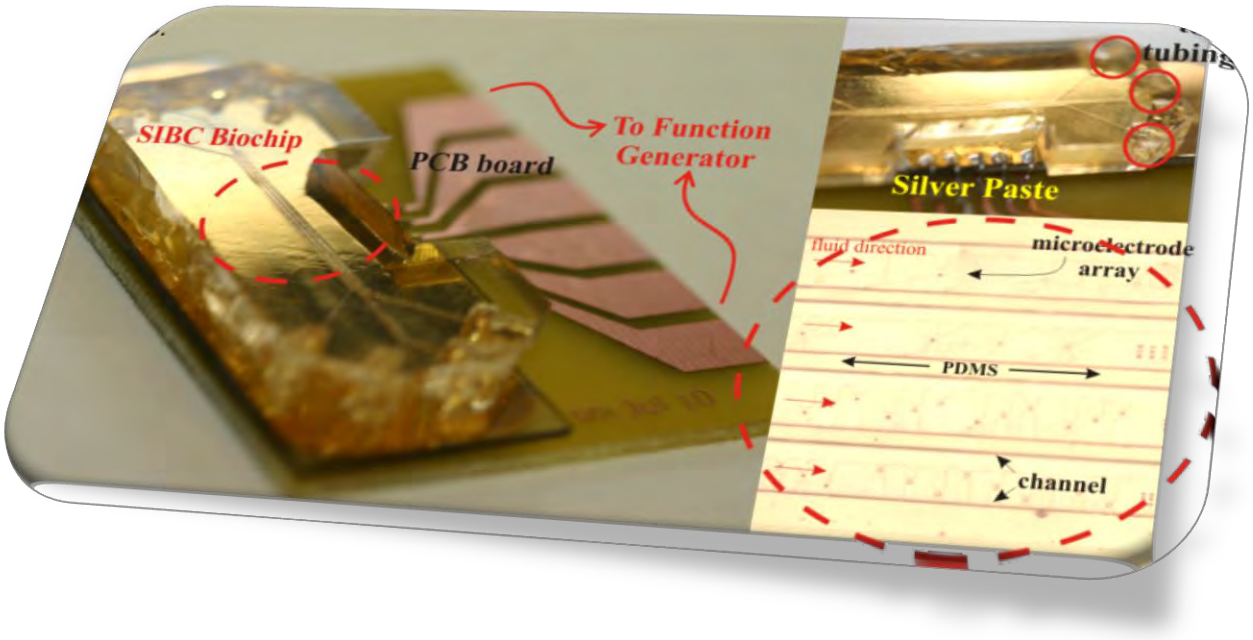

So far, simulations in Chapter Four provide useful insights on the electric field and DEP force of the three microelectrodes. In this chapter, details on fabrication processes employed for structuring the three microelectrodes on the SIBC biochip are presented. The chapter starts with section 5.1, where the fabrication processes of SIBC biochip are explained. This is followed by details on the process of creating PDMS microfluidic channels. The chapter ends with descriptions on the integration of the SIBC biochip and its microfluidic channels.

5.1 Fabrication Process of the SIBC Biochip

The biochip platform is built from two main structures, the SIBC biochip and the microfluidic channels. The former was fabricated using photolithography process while the latter was fabricated using softlithography technique. Photolithography is a pattern transfer technology commonly used in the semiconductor industry. In this technique, micro-size structural patterns on a mask are transferred on photosensitive resists after exposed to the UV (ultra violet) light. A finished device from a photolithography process is actually a result inherited from several fabrication stages. Therefore, using correct parameters in each stage of the process is vital to produce a functioning device.

In this study, the SIBC biochip was fabricated using several processes such as mask design, metallization, resist spreading, photolithography, wet etching and resist stripping as illustrated in Fig.5.1.The following subsections will present details of each process.

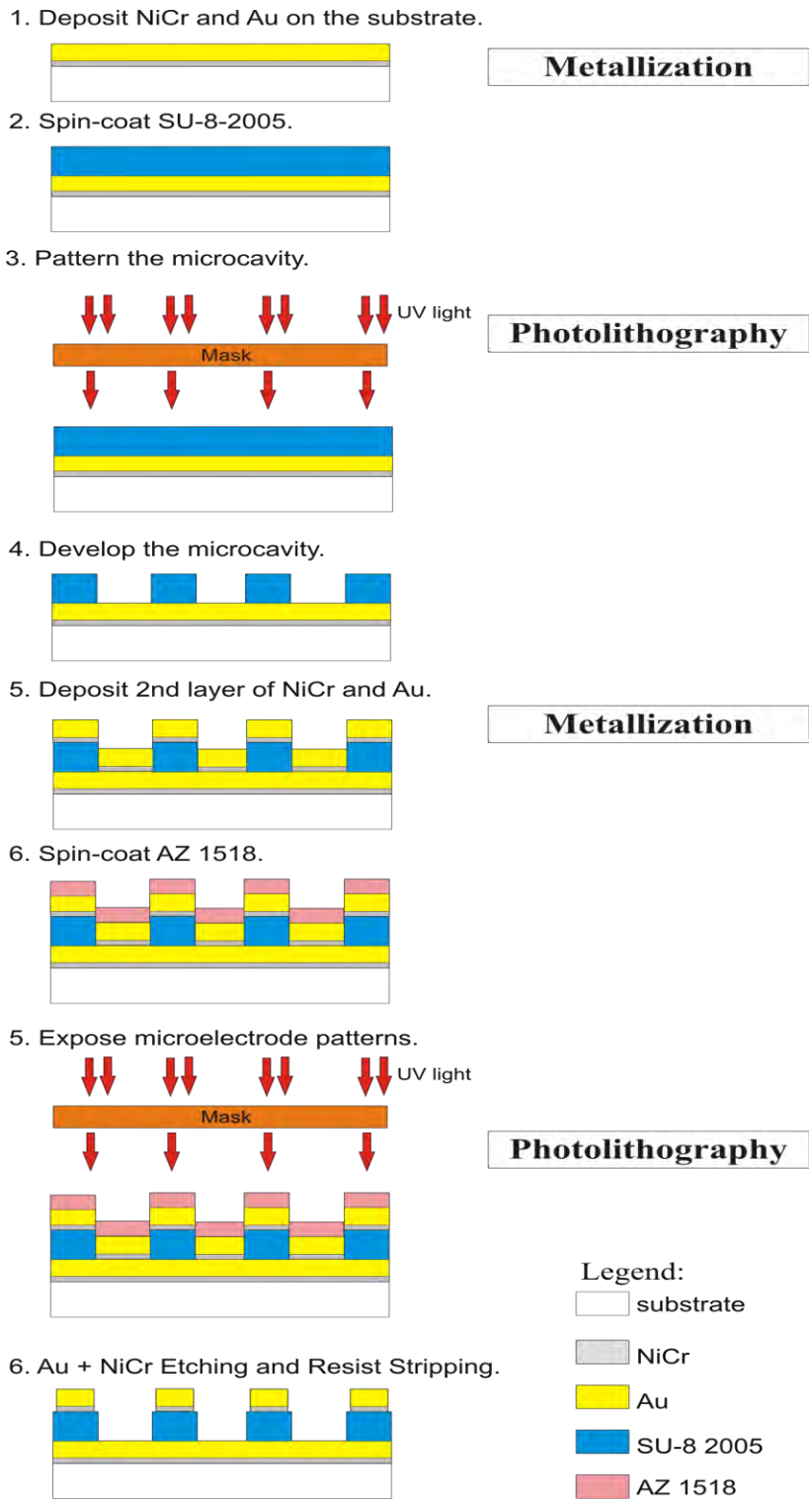

Figure 5.1: The fabrication process of SIBC biochip consists of several stages such as the metallization, the photolithography and the etching process.

5.1.1 The Mask Design

The first step in photolithography is designing the optical mask or photo mask for the microelectrode and microcavity patterns. These patterns were drawn using a CAD software package, L-Edit Pro v14.3 (Tanner Inc.). The software creates layer-by-layer layout of the patterns. In other words, two layouts were created for the SIBC biochip: one layout for the microelectrode layer and another layout for the microcavity layer. Meanwhile, to create the photo mask for the microfluidic channels mould, one layout was created.

Then, the layouts were converted to files in ".dfx" format and uploaded into a mask writer machine (μPG 101 of Heidelberg Instruments). The mask writer machine uses a 375nm wavelength laser beam to transfer patterns onto the mask's substrate. Once exposed to the laser beam, the 4-inch or 3-inch glass substrate which was pre-coated with AZ1518 resist, will be written with the required patterns. Next, the microelectrode and the microcavity masks were developed by immersing in the MIF300 developer for 35 seconds, after which they were etched in the NiCr (Nickel-Chromium) etchant for 30 seconds.

The type of photosensitive resist used for lithography plays an important role in the creation of a photo mask. There are two types of photosensitive resist used in lithography i.e., the positive tone resist (positive resist) and the negative tone resist (negative resist). When a positive resist is exposed to the UV light, the chemical structure of the resist changes and becomes more soluble to the developer solution. Therefore, the patterns that remained on the resist after development process are the exact copy of patterns on the mask. In contrary, the chemical structure of a negative resist will solidify or crosslink when exposed to the UV light. Therefore,

the exposed area of a negative resist will remain on the substrate but not patterns from the mask. Figure 5.2 illustrates the lithography process conducted on both positive and negative resists.

The SIBC biochip uses two types of photosensitive resist, the AZ1518 (a positive resist) and the SU-8-2005 (a negative resist). The AZ1518 was used to transfer microelectrode patterns on the Au metal layer while the SU-8-2005 was used to structure arrays of microcavity on top of the back contact. Meanwhile, the microfluidic channel mould was structure on the SU-8-2100 negative resist. Figure 5.3 and 5.4 depict the masks for the microelectrode, microcavity and microfluidic channels mould. On the microelectrode mask, the first two arrays are for the dipole microelectrodes (sharp and flat tips), followed by the quadrupole and then the adaptive octupole patterns. The microcavity mask has four arrays of 15-20 µm sizes (diameters) microcavity. When the two masks are aligned together, the microcavity will be located at the centre of each microelectrode pattern.

As illustrated in Fig.5.4(a), the microfluidic channels mould photo mask has four 200µm

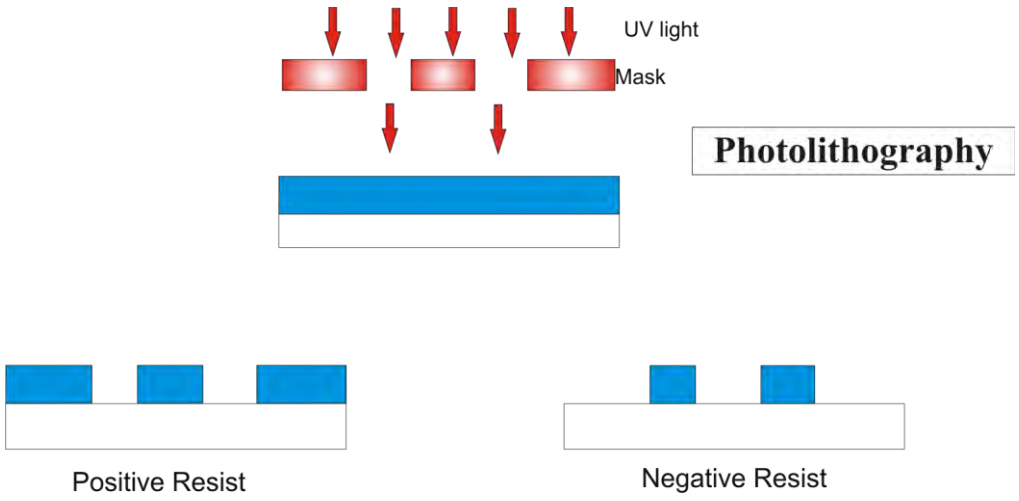

Figure 5.2: By using the same mask, different patterns are transferred on positive and negative resists.

wide channels dedicated for each of the microelectrode design. The channels were created on a SU-8-2100 resist after being exposed to UV light. Upon exposed to UV light, the chemical bonding of SU-8 resist was crosslinked and solidified. This process in turns created long pillars of (200µm x100µm) (width x height). Meanwhile, the microcavity mask was patterned by arrays of circular shape as illustrated in Fig.5.4(b). The circular pattern created holes on the SU-8-2005 resist after immersing the resist in the SU-8 developer. Details of the SU-8 resist development process will be discussed in subsection 5.1.4. Once the photo masks were prepared, the photolithography process can be conducted accordingly.

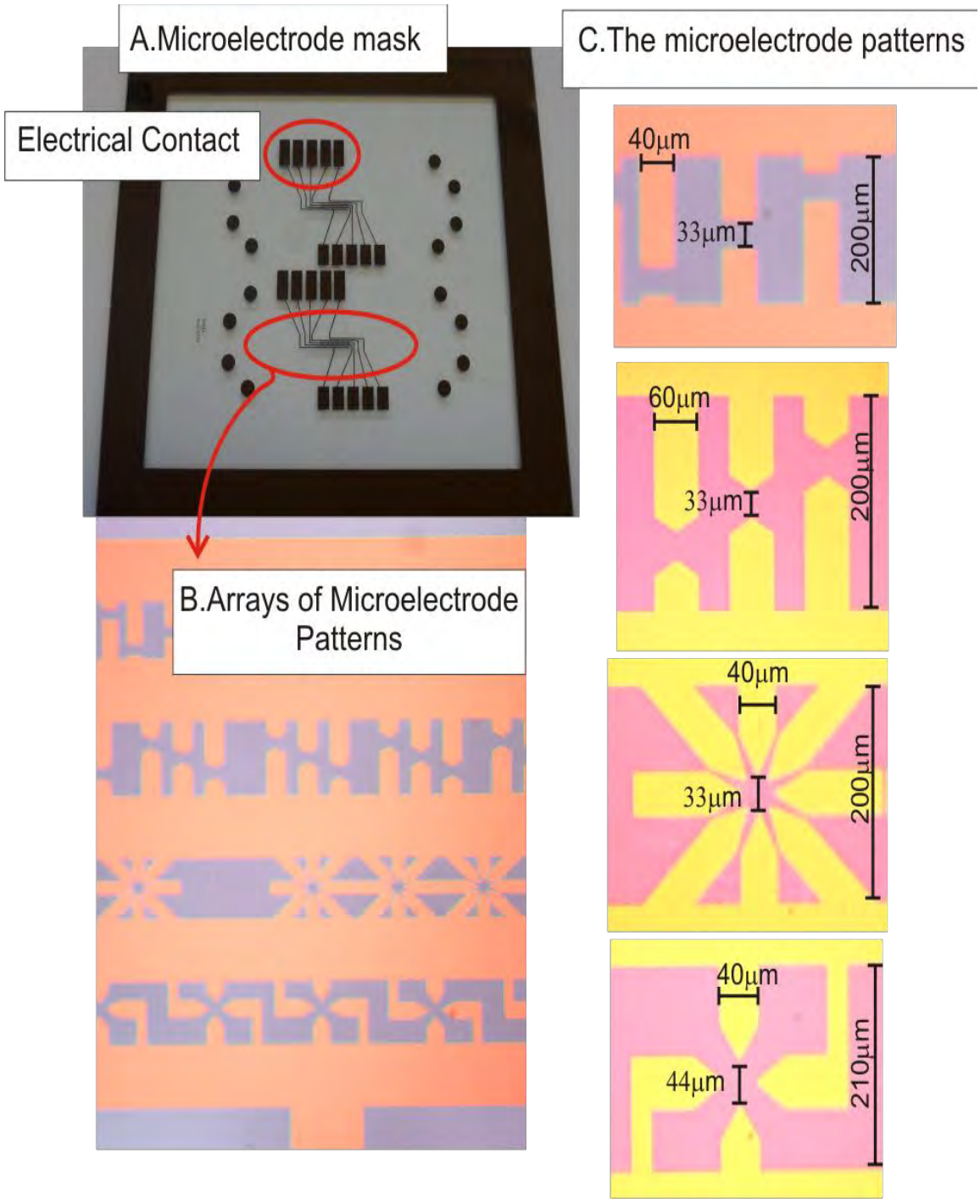

Figure 5.3: (a) Photo mask of the microelectrode patterns. (b) Patterns that will be transferred on the AZ1518 resist. (c) The microelectrode designs.

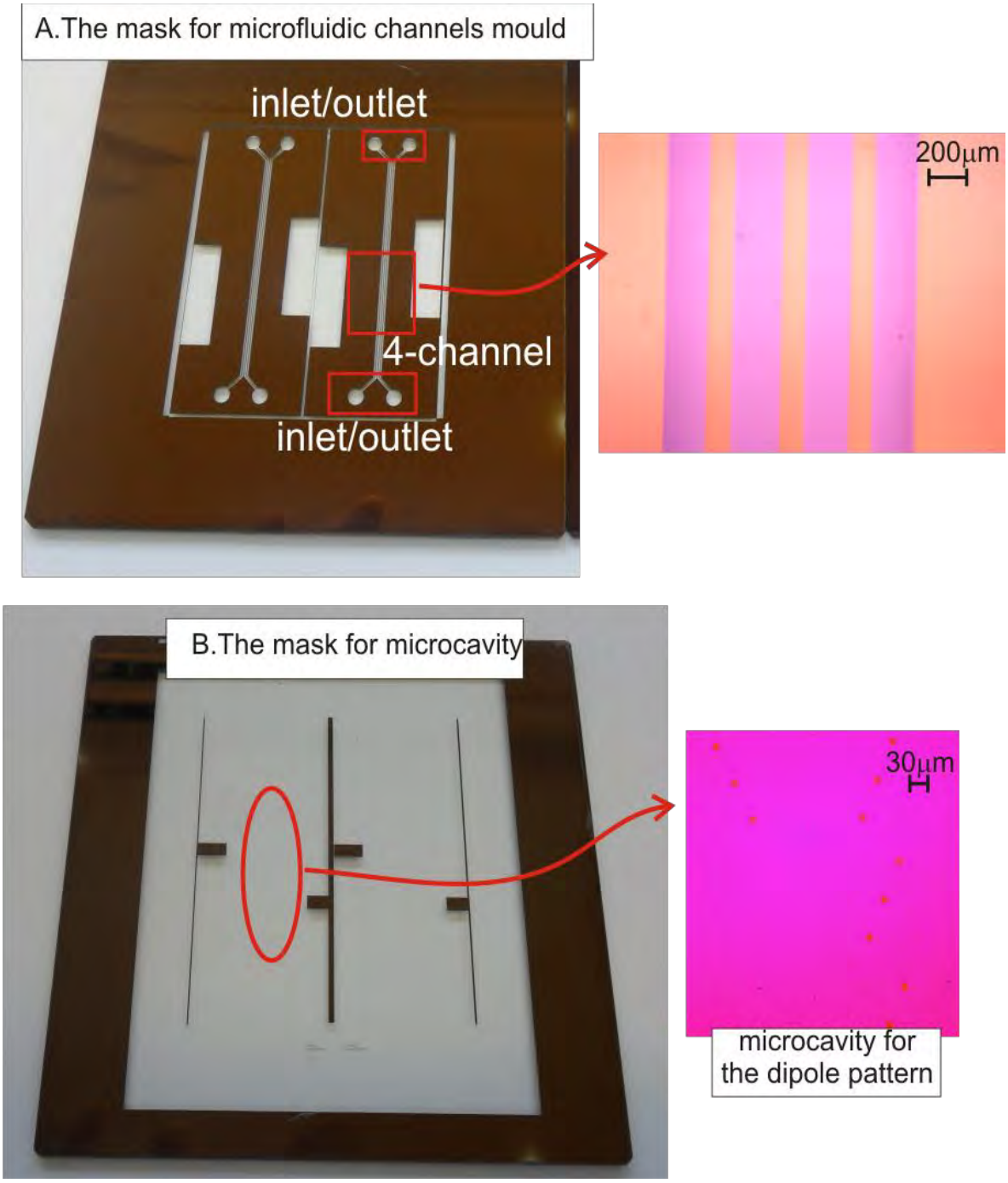

Figure 5.4: Photo masks for the microfluidic channels mould and the microcavity. Patterns on these two masks are transferred on negative-typed resist i.e., SU-8-2100 and SU-8-2005.

5.1.2 The Preparation of Substrate

Choosing a substrate suitable for a biochip platform is essential before starting any fabrication process. In this work, the SIBC biochip uses Silicon Nitride (Si_3N_4) coated Si substrate and glass slide as the base of the platform. Meanwhile, the microfluidic channels for the SIBC biochip are made of polydimethylsiloxane (PDMS) material. Each of these materials has its advantages and disadvantages, particularly in the fabrication of biochip.

The Si substrate, which is the common material in microfabrication technology, can be doped or structure to make electrodes, channels or other biochip components. To structure a multilayer device on a Si substrate however, usually utilizes the Silicon-on-Insulator (SOI)-type substrates such as the Si_3N_4 coated Si substrate. These types of substrate can reduce device's parasitic capacitance and facilitate passivation process between layers. Parasitic capacitance is critical in a biochip design, especially on a DEP-based biochip since the microelectrodes have to be directly in contact with conductive fluids i.e., the particle's suspension medium. This condition creates parasitic capacitance that might affect electrical signals from the microelectrodes, especially when small signals are used on the biochip platform. Furthermore, the parasitic capacitance can affect particle manipulation process on the biochip platform [95]. Having direct contact to a conductively suspension medium on the DEP-based biochip, also means that inert metals such as gold (Au) and platinum (Pt) are more suitable to be used as the microelectrode materials. This is because they are bio-compatible and non-reactive to chemicals [104].

Glass is another commonly used material in a biochip fabrication. One advantage of using glass as a substrate is its transparent nature that makes imaging using optical microscope easy. Glass is also biocompatible and is less reactive to heat. The mechanical property of glass however, which can be very brittle and can break easily depending on the glass ingredients used, has becomes one of its drawback. Therefore, creating the microfluidic channels or other biochip components on a glass substrate by using techniques such as ultra precision diamond turning, chemical wet etching and precision glass moulding, can be very expensive [129]. As the microelectrodes on the biochip are made through metallization process, glass slide is used as one of the substrates for the SIBC biochip platform but not used for creating the microfluidic channels.

Other than Si and glass, organic polymer such as PDMS (polydimethylsiloxane) or PMMA (polymethylmethacrylate) are widely used in microfabrication. By using micromoulding technique, the PDMS material can create complex microfluidic channels or other biochip components such as fluid pumps, valves and mixers either in straight or curve shapes. Furthermore, high aspect ratio structures between 50µm to 200µm dimensions can be easily fabricated using PDMS. Nevertheless, precise alignment between layers of PDMS structure can be very challenging due to its transparent nature.

To resolve the alignment problem of PDMS transparent nature, a mould design using the SU-8 negative photoresist is used. The SU-8 resist, made from epoxy-resin base material, can be patterned via the common photolithography method. The advantages of using SU-8 are: low bonding temperature of less than 80°C, an excellent chemical resistant property and compatible with biological cells [130].

Fabrication of the SIBC biochip starts with cleaning the substrate (Si_3N_4 coated Si substrate and glass) to remove any organic coating and residues. The cleaning process was conducted using piranha solution which is a mixture of 10:1 of sulfuric acid (H_2SO_4) and hydrogen peroxide (H_2O_2).Once the substrates were cleaned, they were kept in an air-tight box and placed in a dry cabinet.

Before depositing the metal or coating with any photoresist, the substrates were cleaned for a second time using acetone-methanol-isopropanol protocol. In this protocol, the substrate was submerged in acetone solvent and placed inside an ultrasonic bath for 5 minutes. Then the substrate was blow-dried using a high pressured nitrogen (N_2) gas. These three steps were then repeated with methanol and isopropanol solvents.

Meanwhile, the microfluidic channels made from PDMS material were cleaned by soaking the substrate into isopropanol (IPA) solution for 5 minutes. Then, the channels have to be blow-dried using high pressured nitrogen gas (N_2) to remove any IPA residues. Before bonding the microfluidic channels, it has to be treated or plasma-ashed with oxygen (O_2) gas to eliminate any moisture. From experience, using untreated microfluidic channels will result in poor bonding with the surface of biochip and poor sealing of the microfluidic channels. After the cleaning process, the substrates i.e., Si_3N_4 coated Si substrate, glass and the PDMS microfluidic channels are ready for other processes.

5.1.3 The Metallization Process

The next step of SIBC fabrication is the metallization process i.e., the deposition of thin metal film on substrate. This process creates the back contact (as the first layer) and the

microelectrodes (as the third layer) of the SIBC biochip. The thin metal films were obtained by applying a current across a resistive crucible made of alumina-coated-molybdenum which is placed inside the chamber of a thermal evaporator (Balzers AG). Once the material reached its melting point, it begins to evaporate and accumulate on the substrate which located directly above the crucible. At the same time, the thickness of the metal film deposit is measured using a quartz crystal oscillator placed in the chamber as illustrated in Fig.5.5.

The back contact layer of the SIBC biochip consists of a 20nm of nickel-chromium (NiCr) and a 100nm of gold (Au) metal layers deposited on a Si_3N_4 coated Si or glass substrate. Here, the thin NiCr film acts as an adhesion layer so that the Au thin film remains on the substrate. Meanwhile, the microelectrode layer comprises of a 20nm of NiCr and a 100nm of Au thin films deposited on a SU-8-2005 layer. The SU-8-2005 layer, where arrays of microcavities were patterned, acts as an insulator separating the two metal layers. The SU-8 layer has to be spin-coated, developed and then crosslinked before deposition of the microelectrode layer can be conducted as details in the following section.

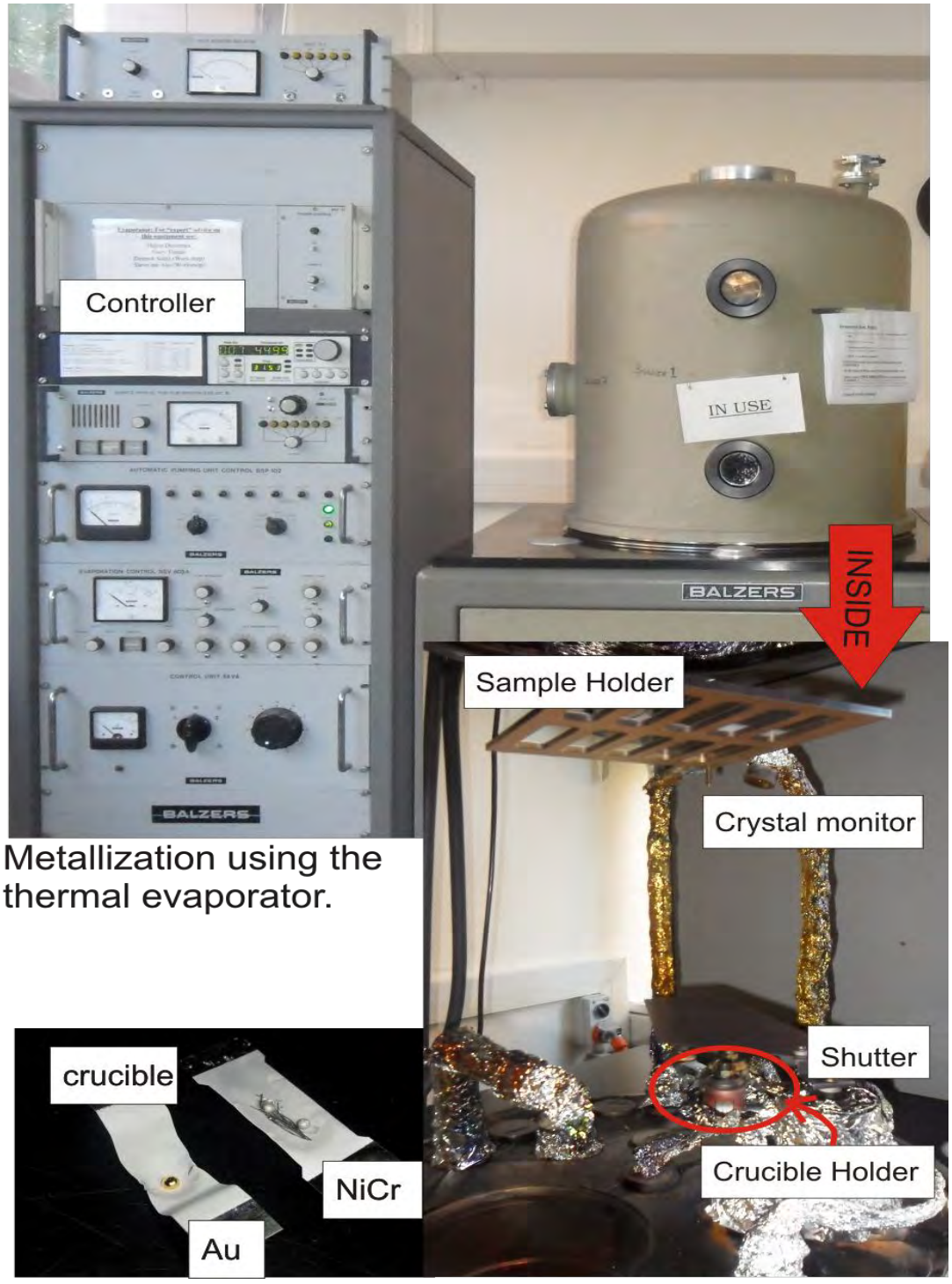

Figure 5.5: Metallization process using the thermal evaporator (Balzers AG). The picture on left (below) shows the crucibles used for Au and NiCr materials. Meanwhile, picture on the right (below) shows the setup inside the evaporator.

5.1.4 The Lithography Process

In the fabrication of SIBC biochip, two types of photosensitive resists are used; the AZ1518 (a positive resist) and the SU-8-2005(a negative resist). The SU-8-2005 was used to structure arrays of microcavities and act as an insulator separating the back contact and the microelectrode layers. Meanwhile, the AZ1518 was used to transfer the three microelectrode patterns on the Au metal layer. In this subsection, processes for the SU-8-2005 listed in Table 5.1 are first discussed. Then, the processes for AZ1518 in Table 5.2 will be described in details.

A photo sensitive resist material can be spin-coated on a substrate by using a spinner machine illustrated in Fig.5.6. The spinner machine uses a high speed rotation and creates centrifugal force to spread resist evenly on a substrate. Critical parameters for the spinner in producing a thin film spread are: rotation speed (rpm), acceleration speed (rpm/s) and spin time.

A. The SU-8-2005 Resist

The SU-8-2005 resist was spin-coated on top of the back contact by using a spinner (Laurell Tech.Corp) of Fig.5.6(b). Even spreading of the SU-8 resist on a substrate is achieved by two consecutive spinning modes. Firstly, the SU-8-2005 was spin-coated at 500rpm with acceleration speed of 85rpm/s for 5 seconds to spread the resist. Then, the rotation speed was ramped up to 4000rpm with acceleration speed of 255rpm/s for 30 seconds to level the SU-8 layer according to the required thickness which is approximately 5μm.

The next step is to softbake the SU-8-2005 resist on a hotplate to eliminate any moisture or solvent from the resist. The process was conducted in three consecutive stages: 1) at 65°C for 1 minute, 2) at 95°C for 3 minutes and 3) at room temperature for 1 hour. The ramping up and

down of the hotplate's temperature in three consecutive stages can reduce surface tension between the resist and the Au layer that might happen once all solvents were eliminated.

Subsequent to the softbake process illustrated in Fig.5.7, the SU-8-2005 was crosslinked using the UV light generated by a mask aligner machine (MA-6 Karl Süss Mask Alinger). As illustrated in Fig.5.8, exposure to the UV light radiation is conducted after aligning the substrate

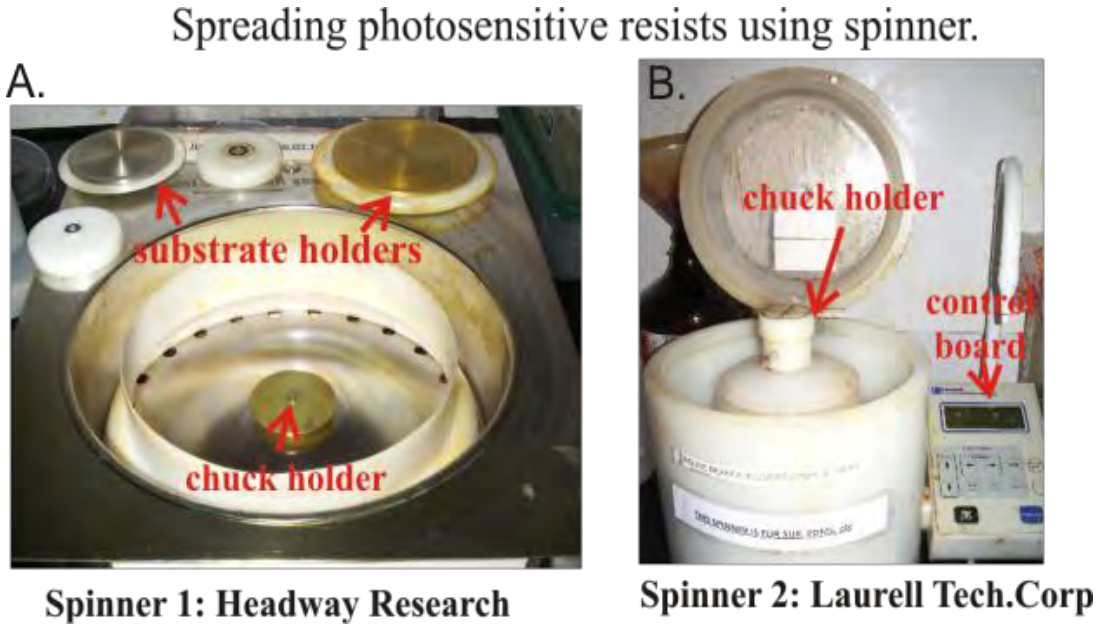

Figure 5.6: (a) The Headway Research spinner used for spin coating the AZ1518 resist. (b) The Laurell Tech. Corp. spinner used spin coating SU-8 resist on the substrate.

and the photo mask together using the vacuum contact mode (the modes available for the MA-6 Karl Süss Mask Alinger are detailed in Appendix D). The microcavity pattern was transferred on the SU-8-2005 resist in 10-cycle exposure using 150mW/cm^2 (measured) UV light intensity. Each exposure consists of 10 seconds of exposure time and 60 seconds of wait time. For the SU-8 type resist, multiple exposure technique is used to reduce thermal stress between the SU-8 resist and the substrate material which occur during exposure.

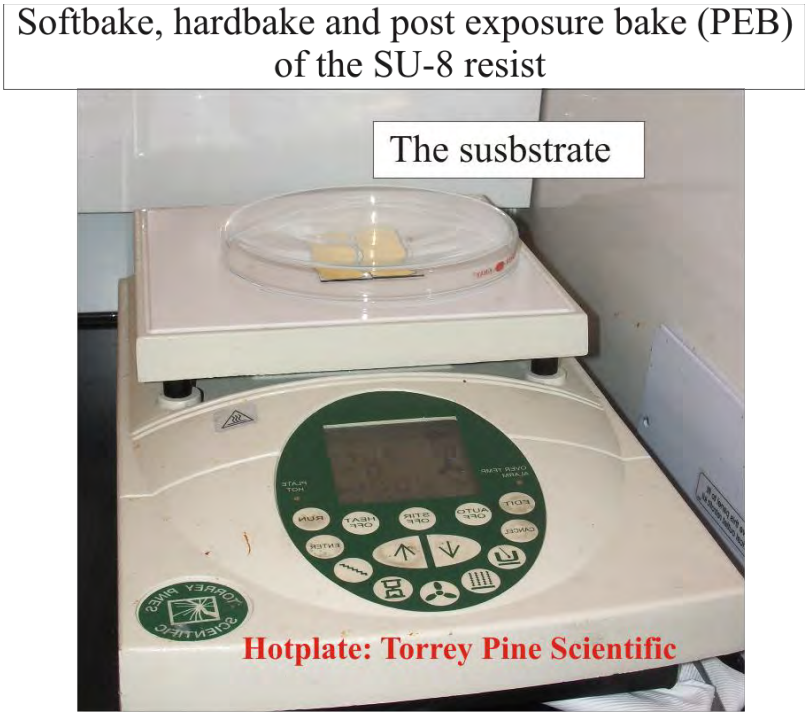

Figure 5.7: Baking the photosensitive resist on a hotplate to eliminate moisture and solvent from the resist.

Following the UV light exposure process, the substrate has to be baked on a hotplate for in three setting : 1) at 65°C for 3 minutes, 2) at 95°C for 5 minutes and 3) at room for 1 hour. After this post-exposure bake (PEB), the substrate was immersed in the SU-8 developer solution or Propylene Glycol Methyl Ether Acetate (PGMEA) for at least 10 minutes or until fully developed. Figure 5.9 illustrates the different between a fully developed microcavity and an under-developed microcavity structure observed using a microscope. Subsequently, the substrate was rinsed using IPA and blow–dried using N_2 gas to remove any unwanted SU-8 residues. After rinsing the substrate with DI water, the transferred patterns on the substrate became visible.

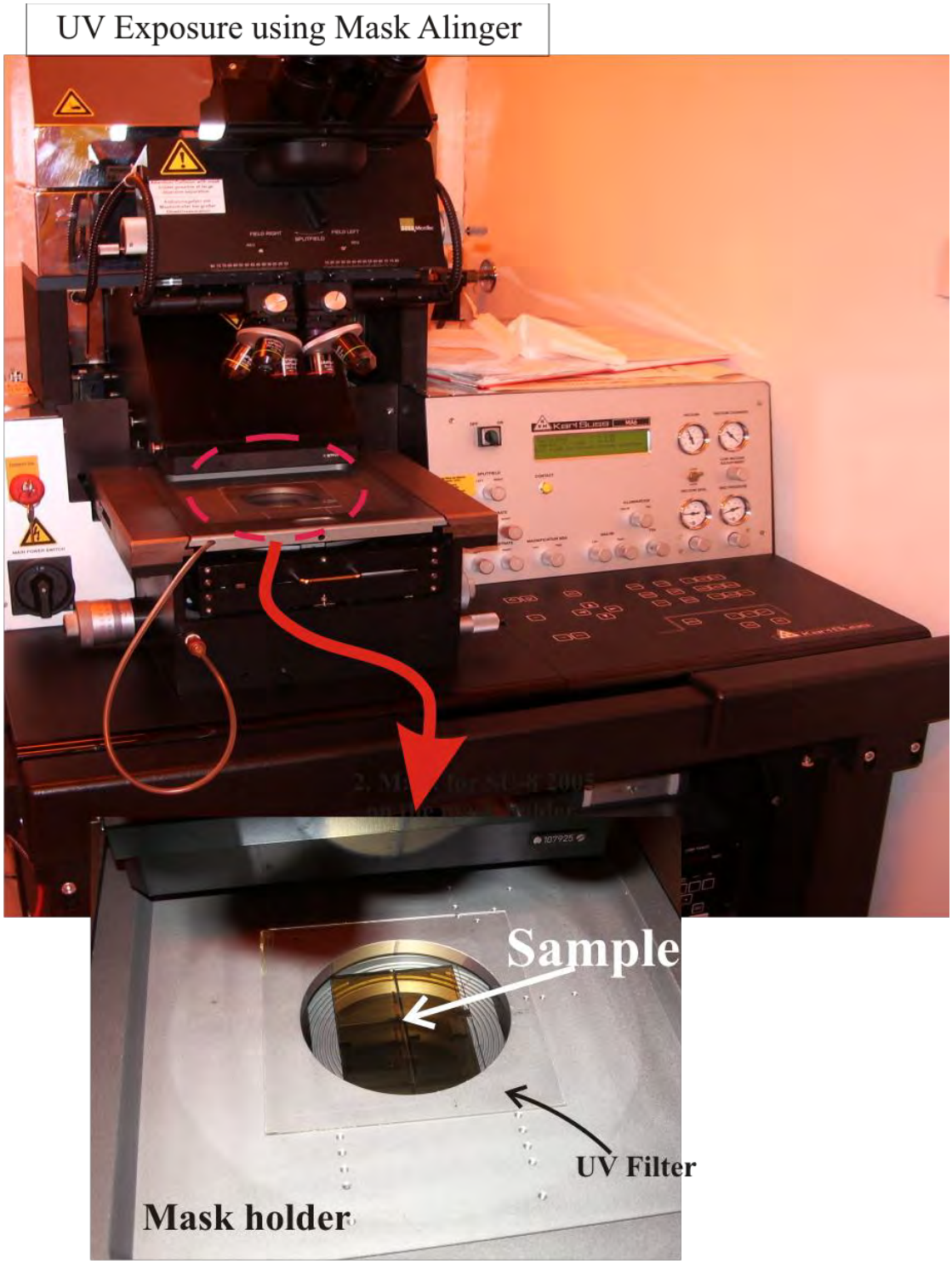

Figure 5.8: Pattern transfer process using the mask alinger (MA-6 Karl Süss Mask Alinger).

There are two additional processes conducted in creating arrays of microcavity structure on the SU-8-2005 layer. First, the SU-8-2005 layer has to be crosslinked for the second time using a flood exposure mode of the mask alinger machine. Then, the substrate has to be hardbaked at 135°C for 10 minutes. These two steps are essential to ensure that the SU-8-2005 was fully crosslinked and cured to prevent shape deformation during the second metal deposition of the microelectrode materials. From experience, during the NiCr and Au thin films deposition on top of SU-8 layer, the microcavity's diameter shrunk and deforming its circular shape. This problem indicates an overflow has occurred during the thermal deposition process. Deformation of microcavity shape occurs due to some areas of the SU-8-2005 material was not fully crosslinked during the UV light exposure stage.

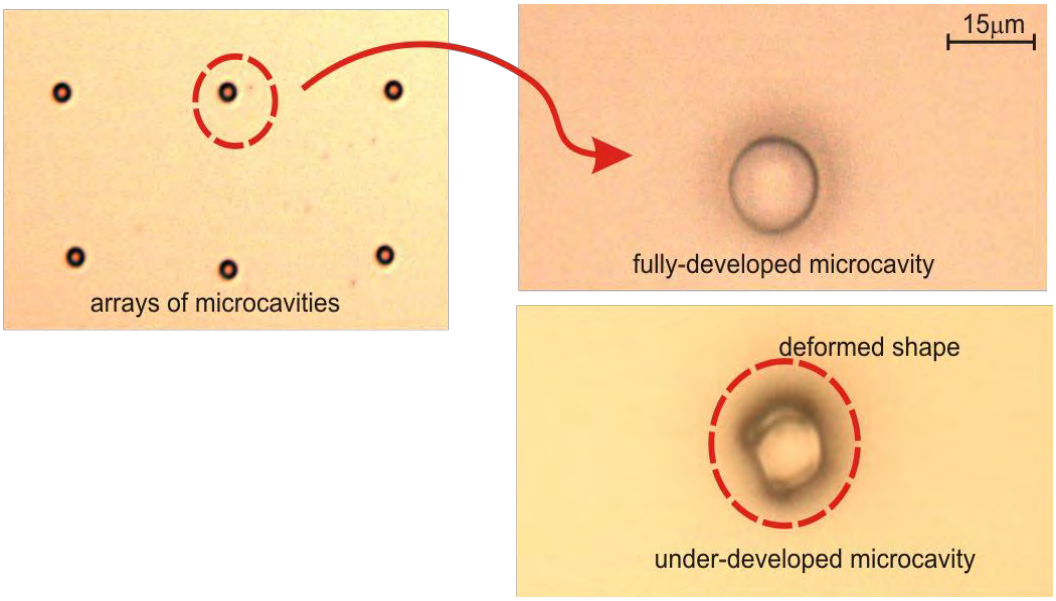

Figure 5.9: The difference between the fully-developed microcavity and the under-developed microcavity.

Conducting hardbake on the SU-8 layer is useful to correct any cracks which are usually found prominent with round edge structure. As shown in Fig.5.10, the cracks on microcavity are

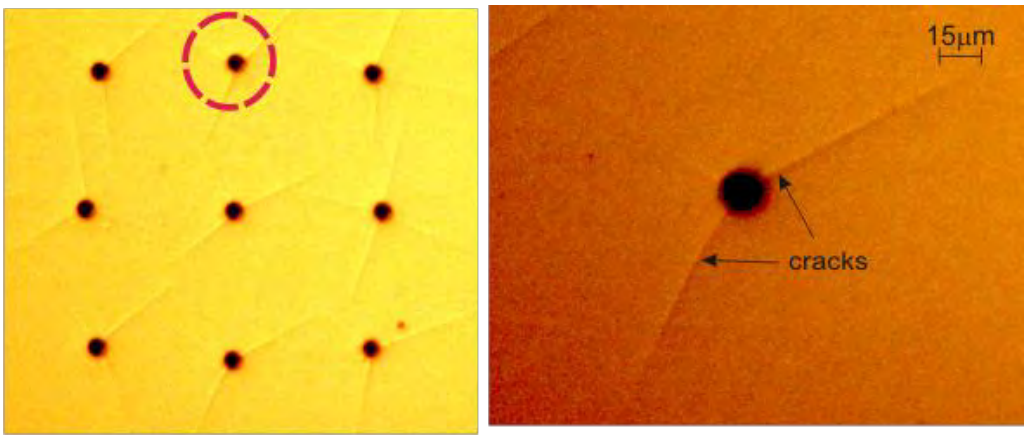

Figure 5.10: Cracks after development of the SU-8 resist. The cracks severity can be minimized by conducting hardbake.

very severe when the pattern is placed in an array and in close proximity to one another. One possible explanation for this problem is the rapid changes of temperature during post exposure bake (PEB). Furthermore, rigorous shaking during the SU-8 development such as using an ultrasonic bath can also contribute towards the severity of the cracks.

The effect of conducting hardbake on a crosslinked SU-8-2005 layer can be observed in Fig.5.11. In Fig.5.11(a), the structure the SU-8 layer has a distinctly high edge bulge with measured thickness between M(green) and R(red) cursors is 4.15µm. After hardbake, the edge bulge reduces and the measured thickness between M and R cursors is 4.53µm shown in Fig.5.11(b).The significant difference in thickness between these two conditions indicates that an overflow effect has to be treated or it can be critical for the microcavity structure.

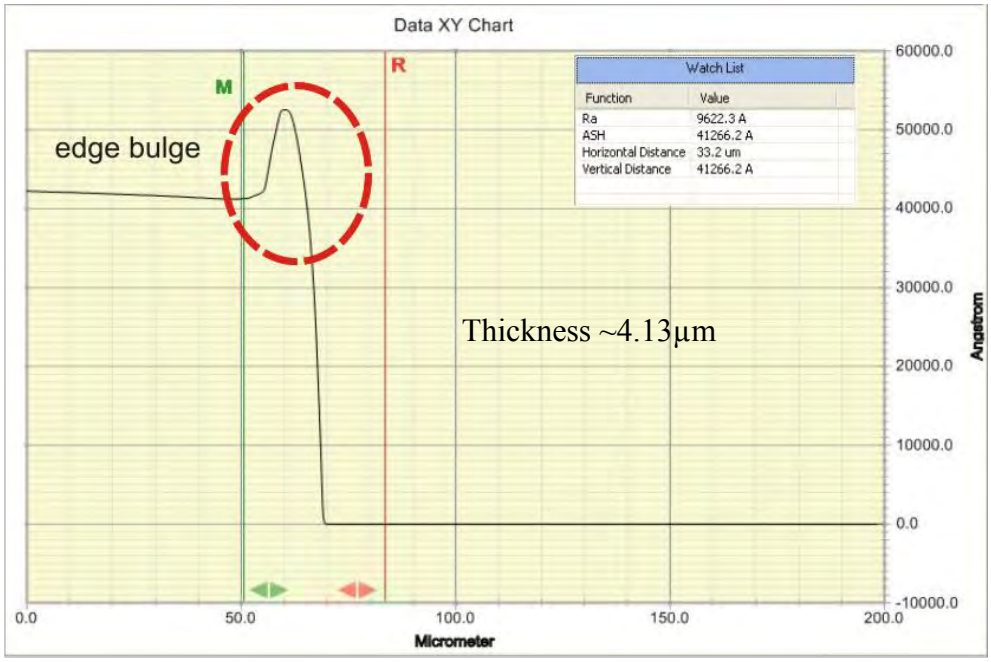

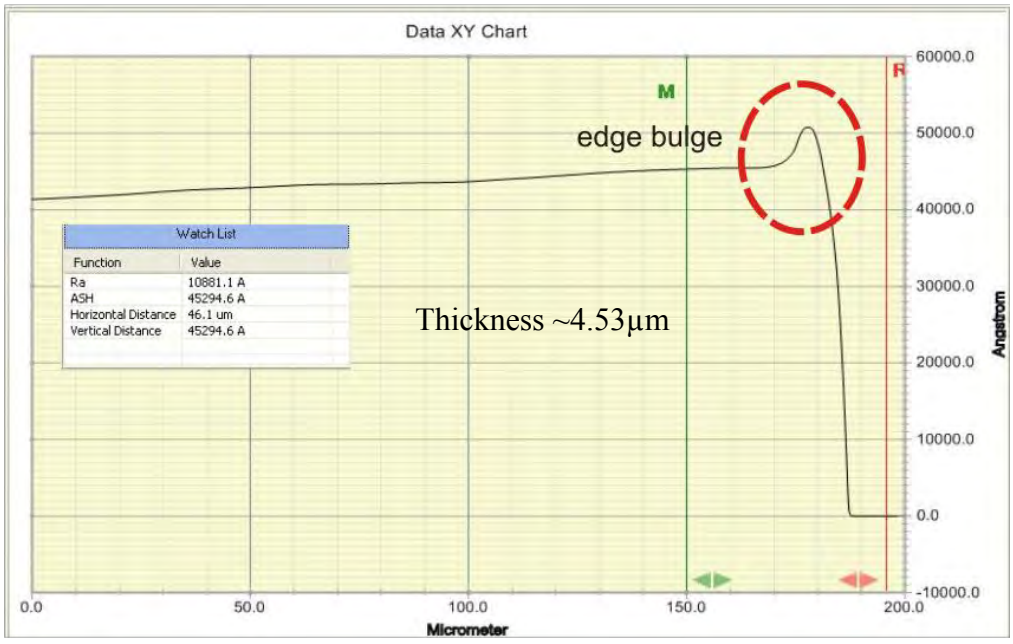

Figure 5.11: The correction of the SU-8 structure after hardbake for 10 minutes at 135ºC.

Table 5.1 presents details of the SU-8-2005 fabrication processes. From these processes, an approximately 5.35µm thick SU-8-2005 insulator layer created on top of the back contact as shown in Fig. 5.12. The height of the microcavity, which is the thickness obtained from the process in Table 5.1, is considered to be adequate for trapping human cells on the biochip. In this design, various diameter of microcavity (15µm, 20µm and 25µm) are used to suit the size of typical human cells which are 10µm–30µm in diameter [12]. The main reason for having a 5µm height trap (microcavity) is to allow trapped cells remain protrusive after the DEP experiments for scanning microscopy, which is important for the Bioimprint process.

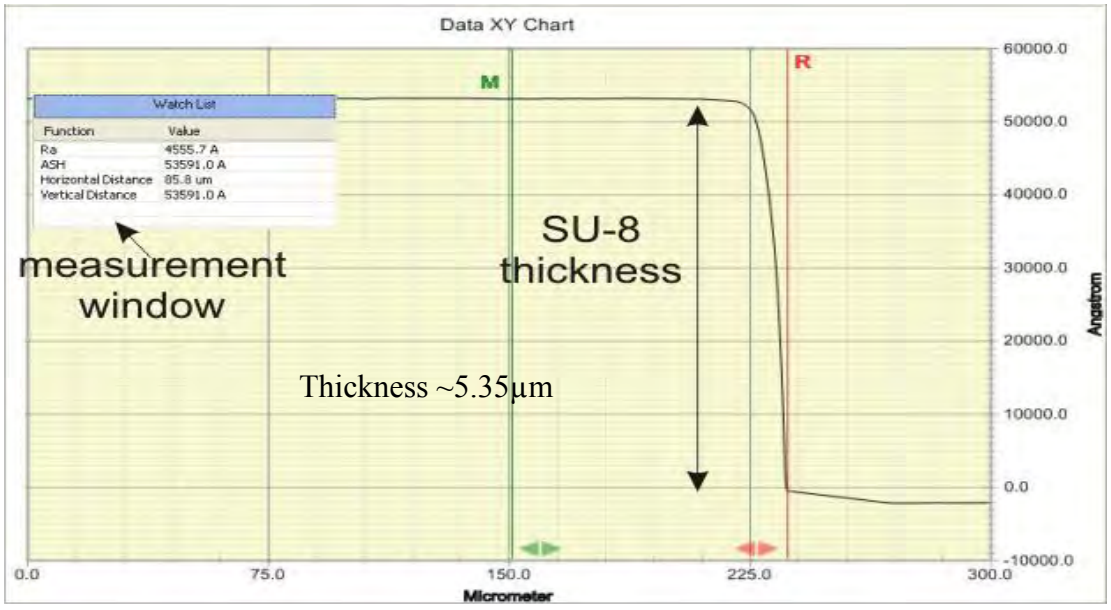

Figure 5.12: The thickness of the SU-8-2005 layer scanned using DEKTAK measured at the edge of a square pattern.

Table 5.1:The SU-8-2005 resist process parameters used in the fabrication.

SU-8-2005			
Process	**Parameter**		
1) Spin Coating	***Rotation speed (rpm)***	***Acceleration speed (rpm/s)***	***Time (s)***
First Spin	**500**	**85**	**5**
Second Spin	**4000**	**255**	**30**
2) Softbake	***Temperature (C)***		***Time (min)***
First Bake	**65**		**1**
Second Bake	**95**		**3**
Third Bake	**Room Temperature**		**60**
3) UV Exposure	***Time (s)***		***Intensity (mW/cm^2)***
	10 * [10 s + 60s (wait)]		**150 (measured)**
4) Post Exposure Bake I	***Temperature (C)***		***Time (min)***
First Bake	**65**		**3**
Second Bake	**95**		**5**
Third Bake	**Room Temperature**		**60**
5) Development	***Time (min)***		
	at least 10		
6) Post Development Exposure	***Time (s)***		***Intensity (mW/cm^2)***
	5 * [10 s + 60s (wait)]		**150 (measured)**
7) Hard Bake	***Temperature (C)***		***Time (min)***
	135		**10**

Legend: * = multiply

To get an evenly spread workable surface with SU-8 resist, great attention is needed when conducting the spinning and the softbake stages. Depending on the SU-8 resist viscosity, edge bulge is usually a critical issue especially when spreading the resist on a small area of biochip substrate such as on a 10mm x 10mm, 15mm x 15mm or 20mm x 20mm (width x length) size sample. The disadvantage of using SU-8 resist on pre-cut substrates is the limitation

of workable area due to the presence of edge bulge. One solution for this issue is to use a glass slide. Not only the glass slide is compatible with a biological cell but it also has larger workable area of 25mm x 75mm (width x length), with respect to the SIBC microelectrode designs. With proper positioning of the design on the glass slide, edge bulge issue becomes negligible. In this work, the SIBC biochip was fabricated on 15mm x 15mm, 20mm x 20mm and 25mm x 75mm (width x length) size substrates.

B. AZ1518 Resist

Once the SU-8-2005 layer was patterned with the microcavity pattern, the fabrication of the SIBC biochip continues with the deposition of another metal layer for the microelectrode patterns. This metallization process creates the third layer on the substrate consists of a 20nm of NiCr and a 100nm of Au films.

After the deposition, the substrate was spin-coated with AZ1518 (positive resist) at 4000rpm for 60 seconds creating an approximately 1μm thick layer. Subsequently, the AZ1518 resist has to be softbaked on a hotplate for 90 seconds to eliminate any solvent from the resist. Microelectrode patterns were transferred on the resist by the UV light exposure for 13 seconds using the mask alinger (vacuum contact mode). Next, the substrate was immersed in the MIF300 developer for 17 seconds and rinsed with DI water, after which the microelectrode patterns became visible. The AZ1518 resist is used to cover the Au and NiCr thin films from being etch away during wet etching process. In other words, pattern that been transferred on the AZ1518 are the exact pattern that going to be structured on the Au and NiCr thin films. Details on the patterning of the three microelectrodes using AZ1518 are presented in Table 5.2.

Table 5.2: The AZ1518 resist process parameters used in the SIBC biochip fabrication.

AZ1518			
Process	**Parameter**		
1) Spin Coating	***Rotation speed (rpm)***	***Acceleration speed(rpm/s)***	***Time (s)***
	4000	**85**	**60**
2) Softbake	***Temperature (C)***	***Time (min)***	
	90	**1**	
3) UV Exposure	***Time (s)***	***Intensity (mW/cm^2)***	
	13	**150 (measured)**	
5) Development	***Time (s)***		
	17		

5.1.5 The Etching Process

Etching processes for the Au and NiCr materials were conducted right after the development process of AZ1518 resist. In this process, unwanted areas of the Au and NiCr materials are removed from substrate. There are two techniques to etch structure onto a substrate: the dry etching and the wet etching technique. In this work, a wet etching technique is used to create isotropic profiles on the substrate by using chemical dissolution. A chemical dissolution or an etchant will selectively remove metallic film areas which are not protected by the photosensitive resist while other non-reactive materials stay intact.

At first, the substrate was immersed in the Au etchant for 10 seconds followed by rinsing with DI water. Once the unwanted areas are removed, the substrate was then immersed in the NiCr etchant and rinsed with DI water to get rid of unwanted NiCr material. From experience, the etching time depends on the patterned surface covered by AZ1518, the thickness of thin films and the concentration of etchant. Finally, after the etching process, the substrate is now consists of microelectrode patterns, microcavity and back contact layers as illustrated in Fig.5.13 and Fig.5.14. From this stage onwards the substrate is called the SIBC biochip.

The three microelectrode patterns which are called the dipole (flat and sharp tip), the quadrupole and the adaptive octupole are fabricated on different array on the SIBC biochip. As illustrate in Fig.5.14, a microcavity is located at the centre of each microelectrode arrangement. The width of one electrode arm for the dipole sharp tip and flat tip is 60µm and 40µm respectively. Similar to the flat tip dipole microelectrode, the quadrupole and adaptive octupole also has 40µm wide electrode. Meanwhile, the lengths of each electrode are varied between

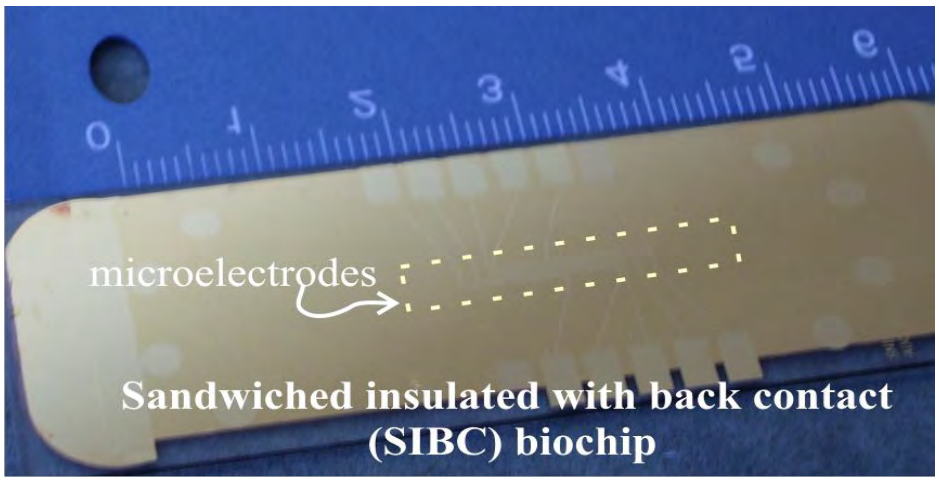

Figure 5.13: The fabricated SIBC biochip on a glass slide used for integration with the microfluidic channels.

40μm to 80μm.

Ideally, the SIBC can be fabricated a 4-inch Si_3N_4 coated Si wafer, before cutting into smaller sizes i.e., 15mm x 15mm, 20mm x 20mm (width x length) etc. But due to the peel-off effect when using dicing saw (Tempress 602) as shown in Fig.5.15(a), a pre-cut substrate has to be used instead. The adhesion problem indicates that the NiCrAu layer is not strong enough to hold layers of thin film (NiCrAu+SU-8-2005+NiCrAu) on the substrate during cutting. From experience, the adhesion of SU-8 layer on a Si_3N_4 coated Si substrate is stronger than adhesion of Au metal layer on a Si_3N_4 substrate, even when using the NiCr as the adhesion layer before depositing the Au metal film.

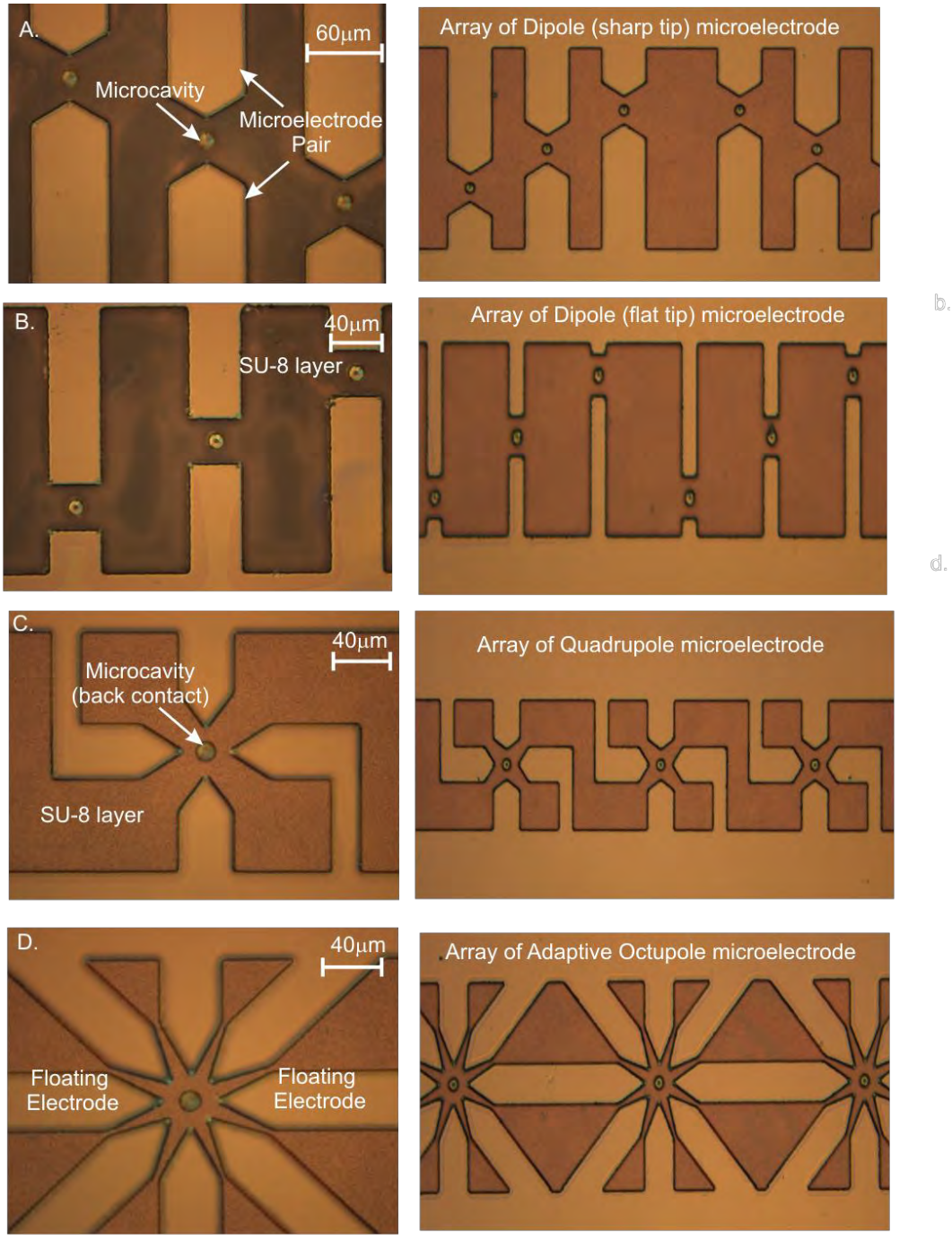

Figure 5.14: The fabricated microelectrode patterns: (a) & (b) the dipole sharp and flat tip, (c) the quadrupole and (d) the adaptive octupole microelectrode.

The 20nm NiCr deposited on the substrate was sufficient to enhance Au adhesion on Si_3N_4 coated Si substrate [9, 131]. Interestingly and from experience, increasing the thickness from 30nm to 50nm and 100nm resulted in the same 'peel-off' effect. An example the SU-8 adhesion on a 4-inch Si_3N_4 coated Si wafer is shown in Fig.5.15(b). Here, the planar two-layer biochip where successfully fabricated and then cut into 25mm x 75mm (width x length) size without affecting the gold microelectrode layer (on top of the SU-8). One possible explanation for this problem may be due to the inert nature of the Au metal which makes deposition of the thin films challenging.

Therefore, an alternative way to fabricate the SIBC biochip on the 4-inch Si_3N_4 coated Si wafer is to pre-cut into the desired size after metallization of the back contact, but before spin-

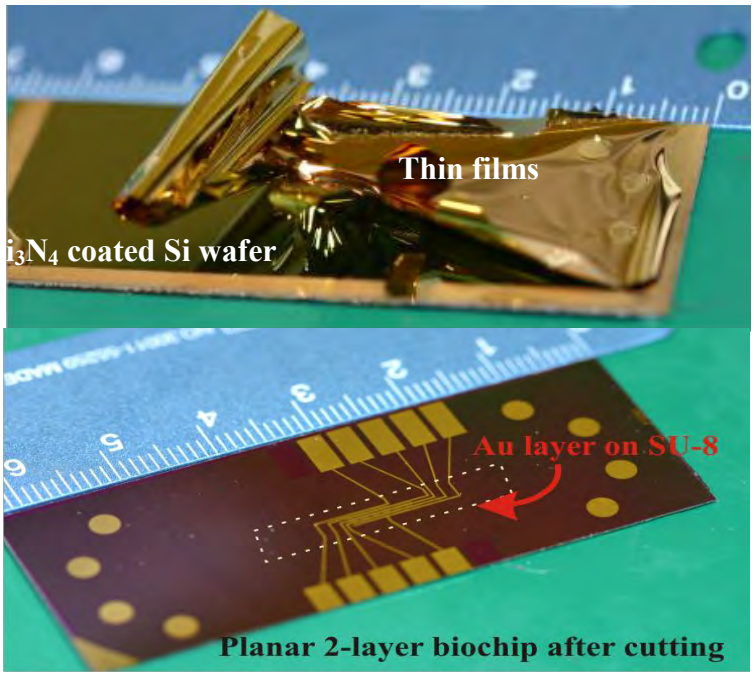

Figure 5.15: 'Peel Off' of thin layers due to the adhesion problem of Au on Si_3N_4 coated Si wafer during dicing the substrate into smaller chip size using dicing saw (Tempress 602).

coating the SU-8-2005 layer. To protect the Au surface from debris and scratching, the 4-inch wafer surface has to be coated with AZ1518 before cutting. Once the cutting process has finished, the substrate must be cleaned with by acetone-methanol-isopropanol protocol (mentioned in subsection 5.1.2) before spin-coating with SU-8-2005. After that, the fabrication process of microcavity layer and the microelectrode layer can be conducted accordingly.

An example of the SIBC biochip fabricated on a pre-cut 15mmx15mm Si_3N_4 coated Si wafer is presented in Fig.5.16. The SIBC biochip fabricated on 15mmx15mm size substrate was used in the initial trapping tests described in subsection 6.1.1 and 6.1.2 of Chapter Six. Meanwhile the 25mm x 75mm (width x length) size SIBC biochip fabricated on glass slide substrate of Fig.5.13 was used in trapping tests using microfluidic channels described in subsection 6.1.3 of Chapter Six.

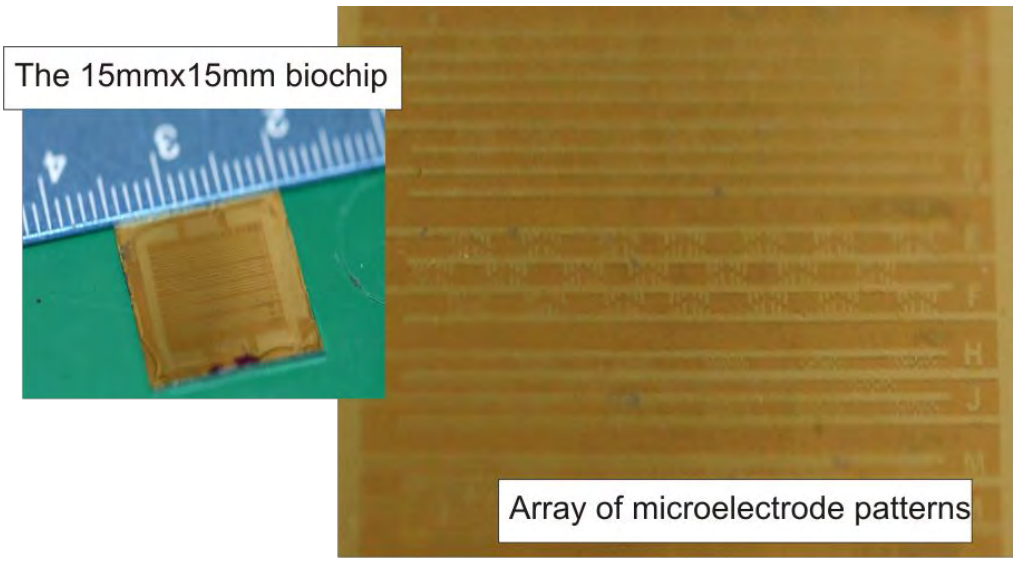

Figure 5.16: The pre-cut 15mm x 15 mm SIBC biochip with arrays of microelectrode pattern.

5.2 Fabrication of the SIBC Microfluidic Channels

The microfluidic channels are fabricated separately from the biochip platform using softlithography technique. Softlithography is a method of replicating structure using elastomeric materials such as the polydimethylsiloxane (PDMS) [132]. PDMS is suitable for the biochip channels due to its biocompatibility and chemical durability natures. This technique is very versatile and cost effective as pattern can be transferred repeatedly. It is also not limited by the wavelength or photoreactive surface. This technique can be useful for a large or non-planar surfaces structure, but pattern sizes are dependent on the designed mask. The following sections will describe the biochip's microfluidic channel fabrication process.

5.2.1 The Process of SU-8 Mould

The fabrication of the microfluidic channels is categorized under softlithography technique. In this process, a master cast made from SU-8 resist containing the microfluidic channel patterns has to be created before spreading the PDMS material, as illustrated in Fig.5.17.

In this process, a standard 4-inch Silicon wafer of mechanical or test grade is used as the substrate. To produce a smooth and an even mould surface, a flat support is needed. The wafer is cleaned using acetone, methanol and isopropanol soaked for 5 minutes in each solvent and blow dried with N_2 gas. Before coating with the SU-8 resist, the substrate was dehydrated in a convection oven at 185°C for at least 12 hours.

Then, the wafer was treated using the oxygen plasma asher to remove any inorganic substance. This step is to ensure the wafer is clean from dust and moisture. The SU-8-2025 was used as the adhesion layer for the mould. From observation and depending on the SU-8 viscosity, structures were observed to peel off after development. This condition occurs due to the surface

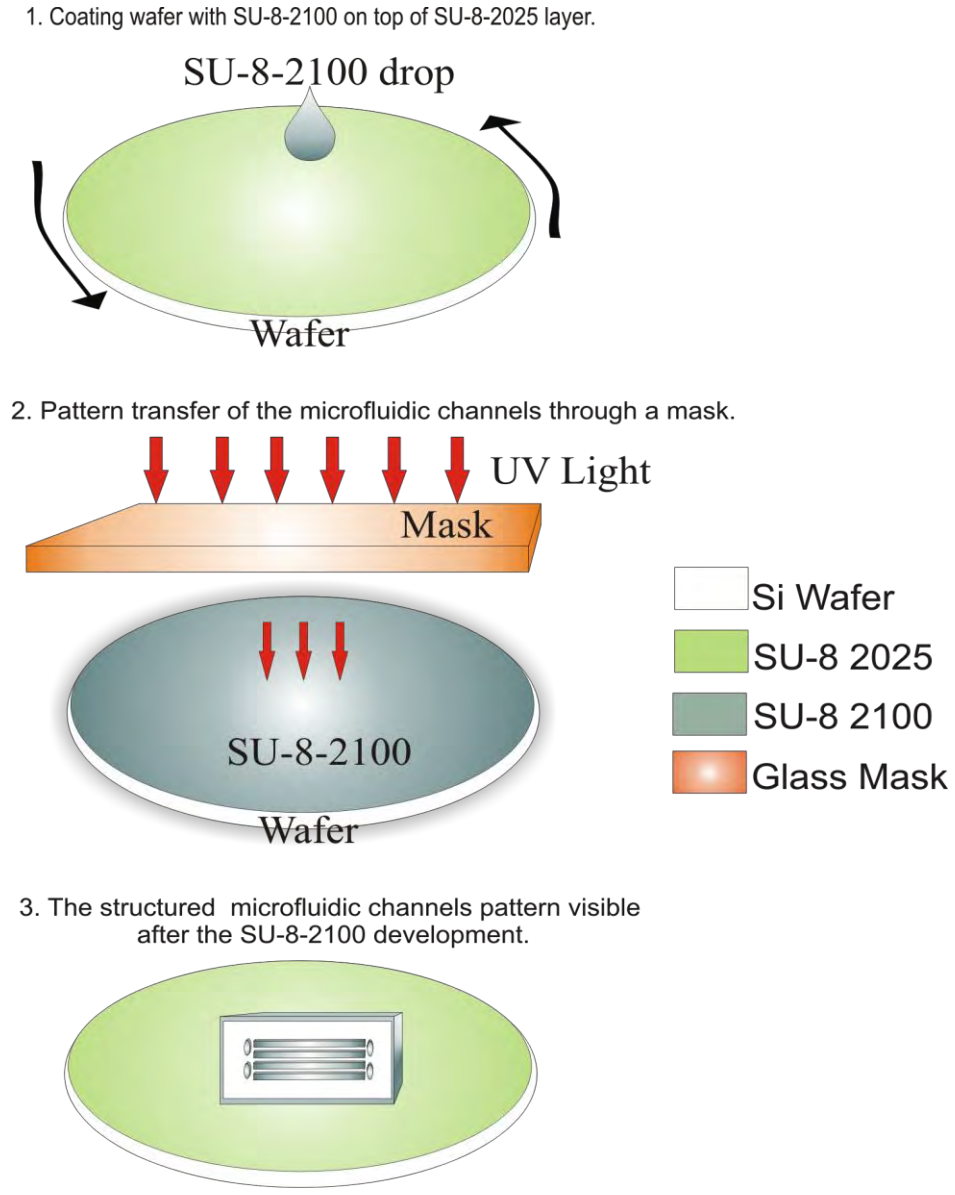

Figure 5.17: Process of creating the SU-8 mould for the microfluidic channels.

tension between wafer and resist, the surface moisture and the thermal stress during processing. Not only the adhesion layer improves the mould durability but it is also useful for easy cleaning of the PDMS from the mould.

Then, the adhesion layer was spread on a wafer using two consecutive spinning programs: 1) the spreading mode at 500rpm with an acceleration of 85rpm/s for 10 seconds and 2) the smoothing mode at 4000rpm with an acceleration of 10030rpm/s for 30 seconds. Next, any excessive resist at the bottom of wafer and edge bulged were cleaned using acetone. Subsequently, the SU-8 resist was softbaked on a contact hotplate using a three-step program. The resist was baked at 65°C for 3 minutes, then at 95°C for 5 minutes and finally cooled at room temperature (RT) for 1 hour. Following the softbake, the resist is now ready to be crosslinked using the UV light.

The SU-8-2025 adhesion layer has to be crosslinked to solidify the resist before spin coating the SU-8-2100 layer, where the microfluidic channels are structured. To crosslink the adhesion layer, the wafer was exposed in flood mode program using 6 times of 10 seconds exposure, with 60 seconds delay period in between each exposure, on a Süss MA6 mask aligner. The advantage of using multiple exposures with delay in between each exposure is to reduce the thermal stress between the resist and the substrate. This was followed by a PEB process at 95°C for 1 hour on a hotplate, and then cooled to room temperature (RT). Details of the SU-8-2025 adhesion layer process are presented in Table 5.3.

Table 5.3:The SU-8 2025 resist (adhesion layer) process parameters.

SU-8-2025			
Process	**Parameter**		
1) Spin Coating	***Rotation speed (rpm)***	***Acceleration speed (rpm/s)***	***Time (s)***
First Spin	**500**	**85**	**10**
Second Spin	**4000**	**10030**	**30**
2) Softbake	***Temperature (C)***		***Time (min)***
First Bake	**65**		**3**
Second Bake	**95**		**7**
Third Bake	**Room Temperature**		**60**
3) UV Exposure	***Time (s)***		***Intensity (mW/cm^2)***
	6 * [10 s + 60s (wait)]		**150 (measured)**
4) Post Exposure Bake I	***Temperature (C)***		***Time (min)***
First Bake	**65**		**10**
Second Bake	**95**		**15**
Third Bake	**Room Temperature**		**60**
5) Development	***Time (min)***		
	at least 10		
6)Plasma Treatment	***Time (min)***		
	20		

Legend: * = multiply

Before spin coating the SU-8-2100, the substrate has to be plasma-ashed for 20 minutes to eliminate any inorganic substance and moisture for the surface. Then the SU-8-2100 was spin-coated on the substrate in two spinning settings: 1) the spreading mode at 500rpm with an acceleration of 85rpm/s for 10 seconds and 2) the smoothing mode at 3000rpm with an acceleration of 10030rpm/s for 30 seconds. This spin-coating step creates an approximately

100μm thick layer of SU-8-2100 on the substrate. After spinning, any excessive resist at the bottom of the substrate and edge bulged were cleaned with acetone.

Subsequent to the spin-coating process, the SU-8-2100 resist was softbaked on a contact hotplate using a three-step program. The resist was baked at 65°C for 10 minutes, then at 95°C for 15 minutes and finally cooled at room temperature (RT) for 1 hour. Following the softbake, now the substrate is ready to be crosslinked using the mask aligner.

Meanwhile the photo mask which contains the microfluidic channels pattern was prepared using steps mentioned in subsection 5.1.1. There are four straight channels for the dipole sharp and flat tips, the quadrupole and the adaptive microelectrode designs. At the end of the straight channel there are outlet and inlet holes. An example of the microfluidic channels' photo mask is illustrated in Fig.5.4(a). During the exposure, a Kopp 3945 (Newport Glass) filter was placed on the photo mask to filter out excessive energy below 350nm from reaching the SU-8 surface.

The filtering is useful to get straighter side wall especially with high aspect ratio structure. Then, the microfluidic channels pattern were transferred on the SU-2-2100 layer using 20 times of 10 seconds exposure, with 60 seconds delay period in between each exposure in the contact mode of the mask aligner. Subsequently, the substrate has to be baked on a hotplate at: 1) at 65°C for 10 minute, 2) at 95°C for 20 minutes and 3) at room temperature for 1 hours. This step is called the post exposure bake (PEB). Details of the SU-8-2100 layer process are presented in Table 5.4.

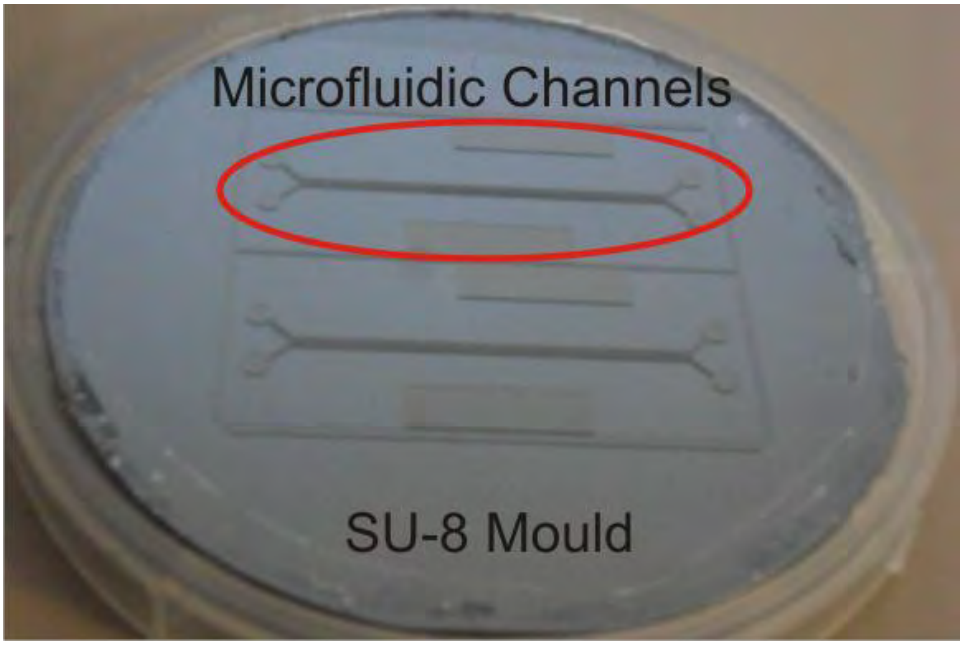

Figure 5.18: An example of the microfluidic channels mould made for the microfluidic channels.

After the PEB, the substrate was then immersed in the SU-8 developer solution or PGMEA and left inside an ultrasonic bath for at least 10 minutes or until fully developed. An indicator of a fully developed SU-8-100 resist is when there are no white residues on the surface of the SU-8 layer. Subsequently, the substrate was rinsed using IPA and blow–dried using N_2 gas to remove any unwanted SU-8 residues, after which the transferred patterns on the substrate become visible. Finally the SU-8 mould consists of the microfluidic channels pattern is ready. An example of the fabricated SU-8 mould is illustrated in Fig.5.18.

Table 5.4: The SU-8 2100 resists process parameters used in microfluidic channel mould.

SU-8-2100			
Process	**Parameter**		
1) Spin Coating	***Rotation speed (rpm)***	***Acceleration speed (rpm/s)***	***Time (s)***
First Spin	**500**	**85**	**10**
Second Spin	**3000**	**10030**	**30**
2) Softbake	***Temperature (C)***		***Time (min)***
First Bake	**65**		**10**
Second Bake	**95**		**15**
Third Bake	**Room Temperature**		**60**
3) UV Exposure	***Time (s)***		***Intensity (mW/cm^2)***
	20 * [10 s + 60s (wait)]		**150 (measured)**
4) Post Exposure Bake I	***Temperature (C)***		***Time (min)***
First Bake	**65**		**10**
Second Bake	**95**		**15**
Third Bake	**Room Temperature**		**60**
5) Development	**Time (min)**		
	at least 20		

Legend: * = multiply

5.2.2 Casting of the PDMS

Once the microfluidic channels mould is ready, the PDMS mixture has to be prepared before casting it on the mould. The PDMS material is a mixture of 10:1 ratio of silicone elastomer and its curing agent (Slygard 184 Silicone elastomer base & curing agent). Firstly, the mixture has to be degassed in a vacuum chamber for about 2 hours to eliminate any gas bubbles that might have been created during the mixing process. Then, the mixture was spread onto the

SU-8 mould and degassed for another 2 hours. Subsequent to the degassing process, the semi-harden PDMS has to be baked on a hot plate for 2 hours at 80°C and then cooled overnight. The fabrication of the PDMS microfluidic channels in this research will follow these softlithography procedures accordingly, unless mentioned otherwise.

Releasing a fully cured PDMS material from its SU-8 mould sometimes can compromise the microfluidic channel structured or the SU-8 mould. Before the pouring in the PDMS, the mould needs to be treated with Trimethylchlorosilane (TMCS) vapour inside a vacuum compartment for 2 hours. The surface silanization process makes the cured PDMS's release from the SU-8 mould easier [133]. The TMCS interacts with the hydroxyl ions part of SU-8 and balance the surface tension of the SU-8 resist, making the surface more hydrophobic. The hydrophobic surface condition makes releasing process of the cured PDMS from its SU-8 mould easy.

Next, a mixture of PDMS according to procedures defined in section 5.3 is prepared. The PDMS mixture is then poured onto the SU-8 mould within a metal ring boundary. In this setup, a metal ring is placed on top of the mould so that the surface can solidify evenly. A metal weighting approximately 20N was placed on top of the metal ring to prevent the PDMS mixture from flowing out of the mould. Then, the setup is left inside a vacuum chamber. It was left to solidify for at least 2 hours before further cured on a hotplate at 80°C for another 2 hours. Then, the PDMS was left to cool at room temperature for at least another 2 hours. An example of the PDMS microfluidic channels is shown in Fig.5.19. The sample is then kept in a clean box to prevent any dust from clogging the microfluidic channels before bonding it with the SIBC biochip.

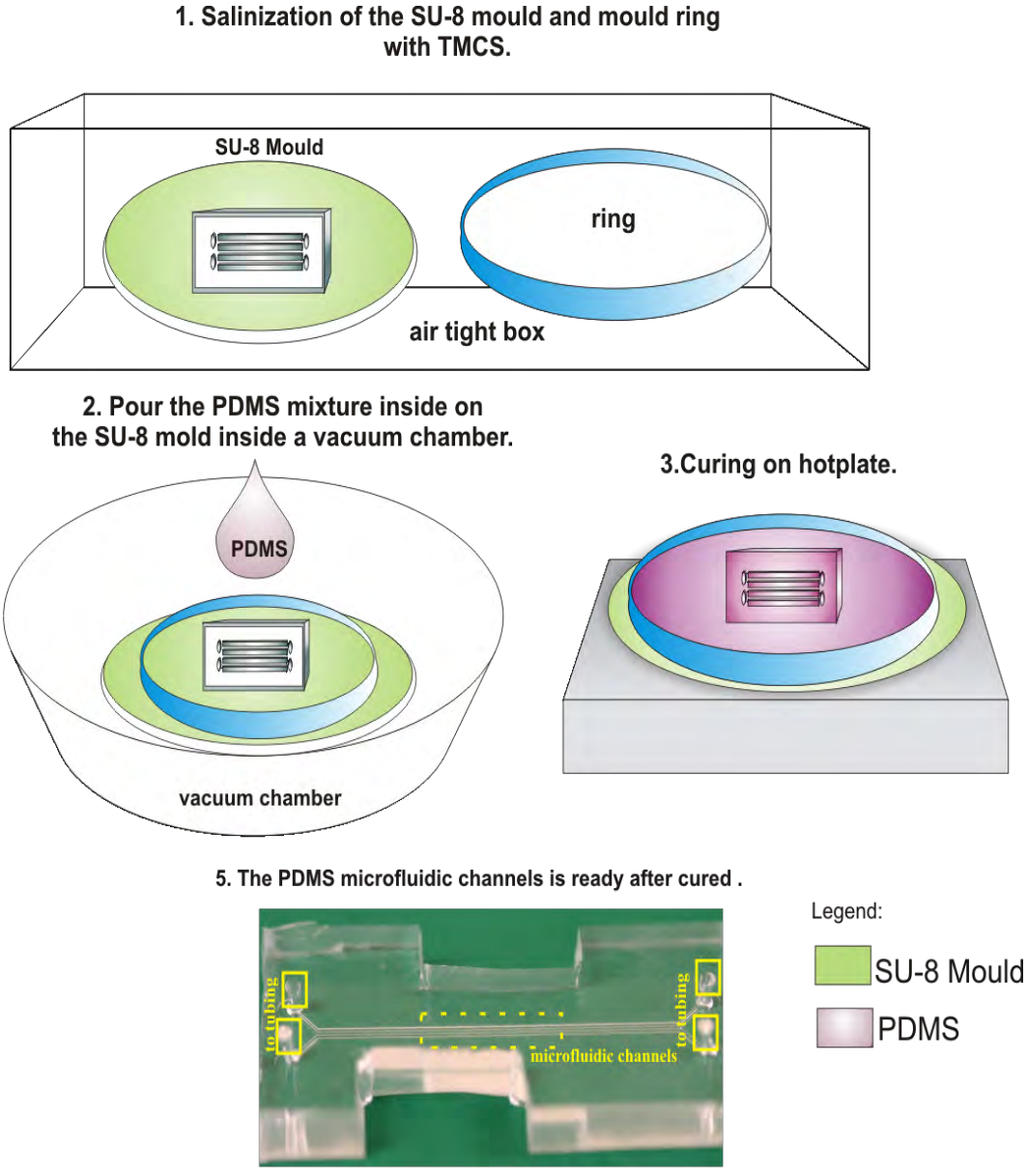

Figure 5.19: The process of PDMS casting on the SU-8 mould.

5.3 Integration of the SIBC Biochip and the Microfluidic Channels

After the SIBC biochip and its microfluidic channels are fabricated, they are placed on top of a printed circuit board (PCB) illustrated in Fig. 5.20, in preparation for the DEP experiments. But prior to that, the SIBC biochip and microfluidic channels have to be bonded together. There are two possible bonding methods: 1) the irreversible bonding, and 2) the reversible bonding. The irreversible bonding can be achieved by using 3-aminopropyltriethoxysilane (APTES) as the bonding agent. The APTES solvent interacts with the SU-8 hydroxyl chemical structure and then changes the SU-8 surface's chemistry to be more hydrophilic. One way to silanize SU-8 is by using the APTES vapour in vacuum chamber [134]. Another surface silanization technique is immersing the substrate in 1% (v/v) APTES –Acetone solution for 15 minutes [135].

Before attaching the microfluidic channels and the SU-8 surface (of the SIBC biochip)

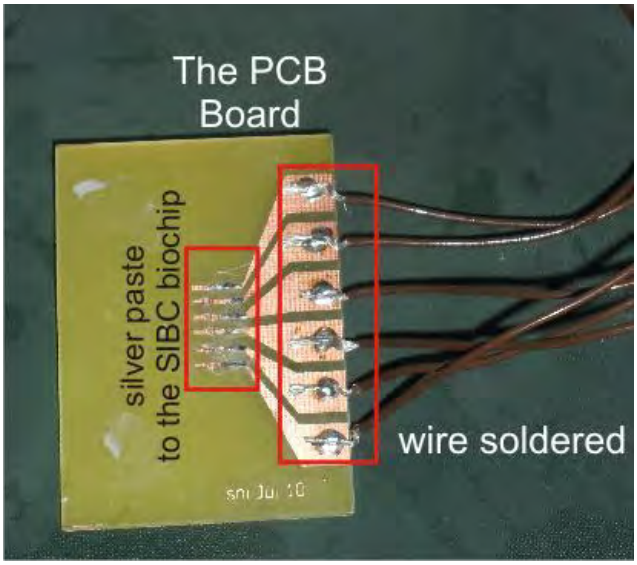

Figure 5.20: PCB board which connects the SIBC biochip with the function generator.

together, they need to be plasma ashed to eliminate any moisture that can hinder successful surface bonding. This technique creates a permanent bonding between the PDMS and the SU-8 surface due to the strong Si-O-Si covalent bond created through the silanization process. As a consequence, any attempt to separate the PDMS and the SIBC biochip after bonding will cause permanent damage to both structures.

An in-house bonding test was conducted by varying the percentage of APTES in acetone solution. The APTES percentage was varied from 1% (v/v), 2%(v/v), 5%(v/v), 10%(v/v), 15%(v/v) and 20%(v/v). In this test, six Si_3N_4 coated Si substrates (15mmx15mm) were coated with SU-8-2005 resist. After PEB stage, each substrate was immersed into the APTES-Acetone solution for 15 minutes. Then, the substrate was rinsed with DI water and dried in convection oven at 95ºC for 5 minutes. After the silanization process, the substrate was bonded with PDMS. Results from this test demonstrated that the strongest binding of PDMS on SU-8 surface occurred when the SU-8 surface was immersed in the 20% (v/v) APTES –Acetone solution.

Using the 20% (v/v) APTES–Acetone solution, the SIBC biochip was irreversibly bond together with PDMS as shown in Fig.5.21. The main advantage of irreversible bonding is that leakage between channels can be prevented. Furthermore, the setup is less complicated without the need for fabricating a customised holder for the biochip system. However, great attention is needed to ensure the microelectrode arrays and the microfluidic channels are accurately aligned because any misalignment cannot be corrected.

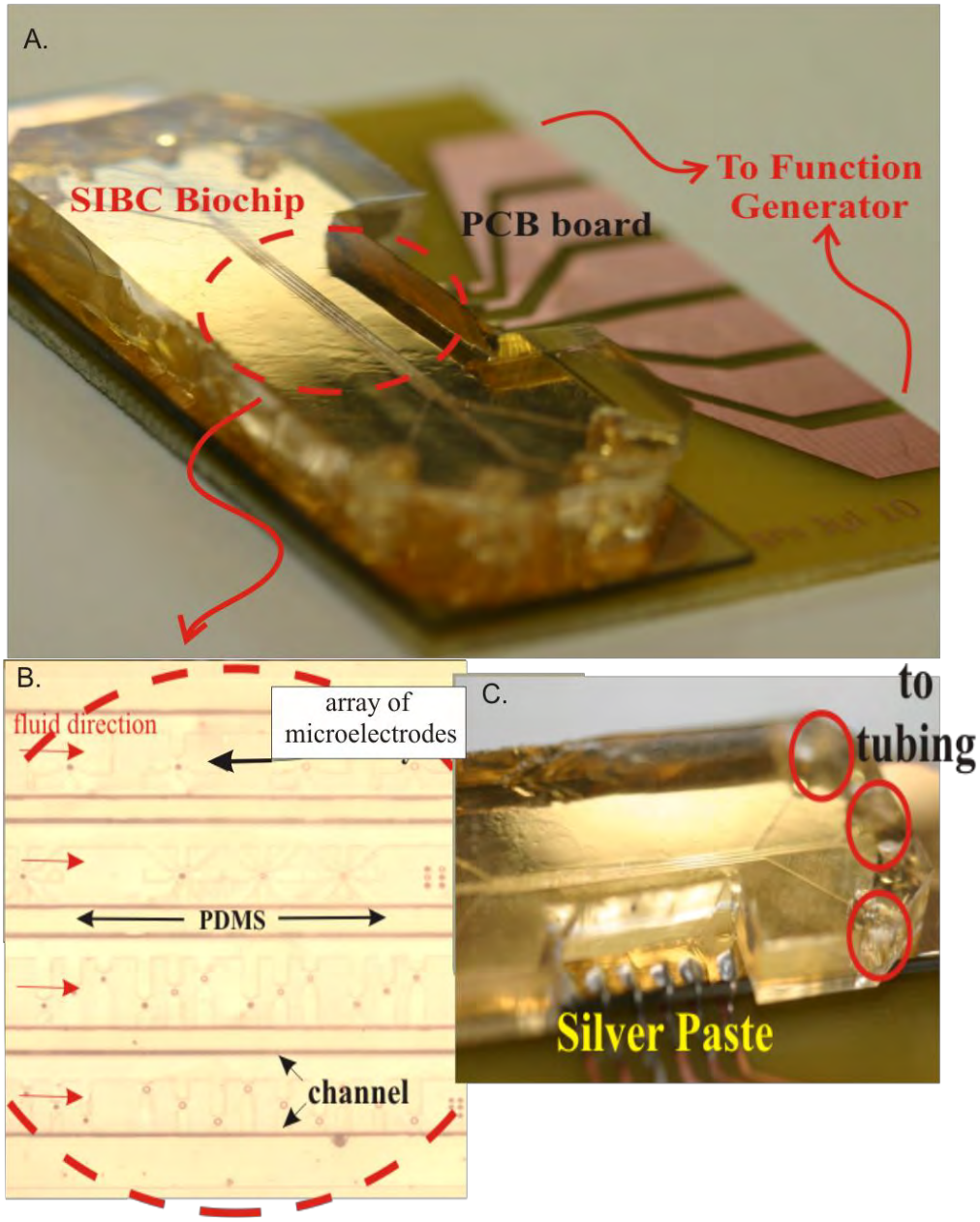

Figure 5.21: The SIBC biochip and its microfluidic system.

Alternatively, the SIBC biochip and the microfluidic channels can be placed between transparent holders creating a reversible bonding. These holders can be made from a transparent material such as perspex and can be customised according to the microfluidic channels design. However, the inlet and outlet connectors at the holders need to be precisely aligned with the inlets and outlets of the microfluidic channels to prevent any leakage. Reversible bonding promotes reusability of the device as cleaning the microfluidic channels and the SIBC biochip can be done easily. Figure 5.22 illustrates an example of the reversible bonding concept used in this thesis.

After experimenting with both bonding techniques, the SIBC and PDMS microfluidic channels were reversibly bonded together but without the perspex holder. At first, the microfluidic channels were plasma-ashed to eliminate any moisture. Then, both structures have to be carefully aligned by ensuring that the microelectrode patterns were inside their dedicated channels. A weight of approximately 10N was placed on top of the PDMS and the SIBC biochip to establish bonding. Despite the flexibility of a reversible setup, it is limited by the fluid force and is more appropriate for a non-continuous flow experiment. The maximum fluid velocity that can be used during fluid loading is 70μL/min. Fluid velocity greater than the maximum limit will result in inter-channel leaking. Nevertheless, this reversible bonding setup is adequate for the DEP trapping experiments and further experimental setup will be described in Chapter Six.

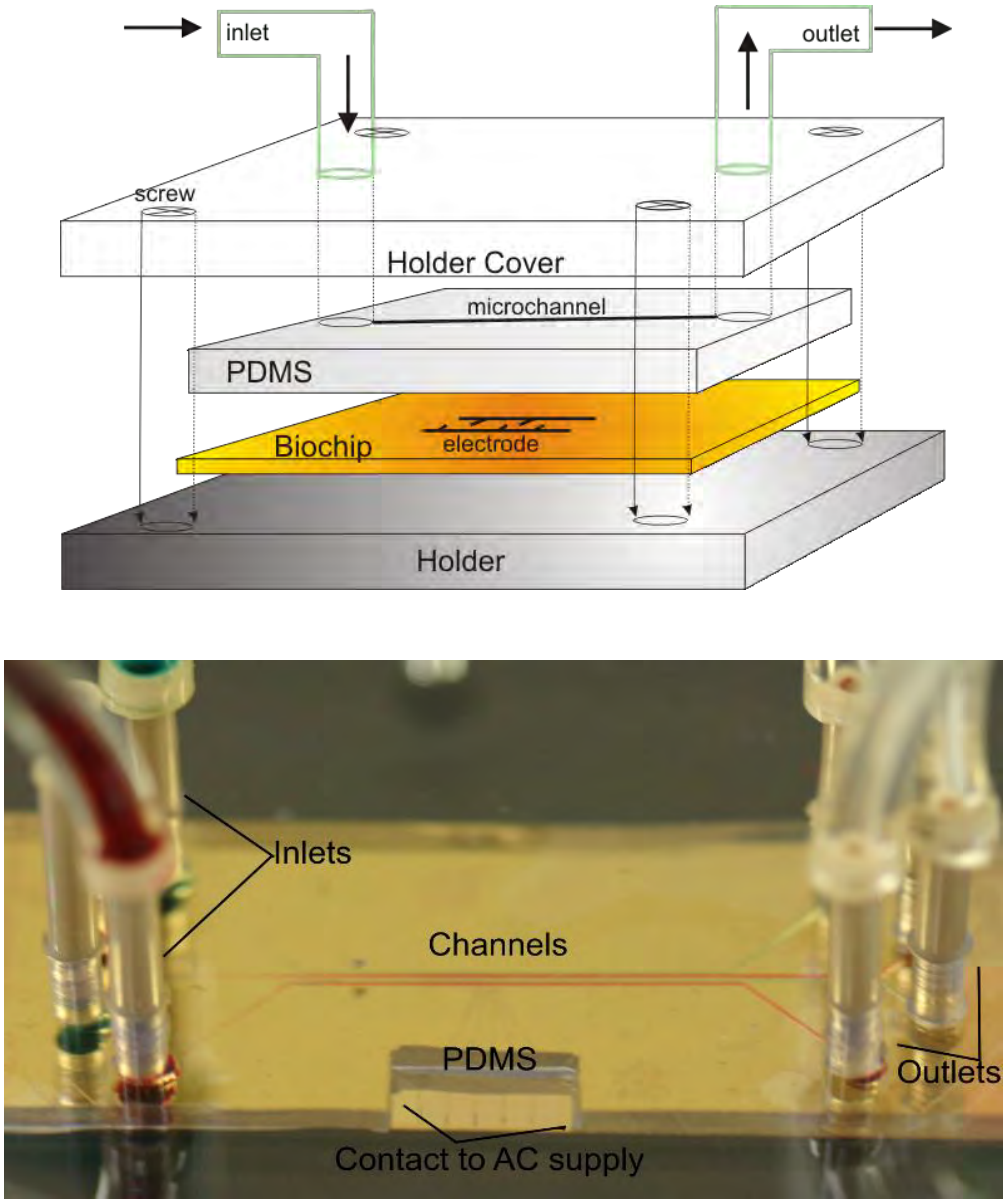

Figure 5.22 (a): Schematic of the reversible bonding. (b) An example of reversible bonding using perspex to hold both SIBC biochip and microfluidic channel together and prevent leaking during experiment.

5.4 Summary

This chapter has presented the fabrication processes of SIBC biochip and its microfluidic channels. It revealed several issues encountered during the fabrication process, and how the processes were modified and adapted to resolve fabrication problems from affecting the results.

Following the fabrication process in section 5.1, the designed microelectrode patterns were successfully fabricated on the metal-insulator-metal layer. Meanwhile, the PDMS microfluidic channels were fabricated by conducting processes in section 5.2. Integration between the SIBC biochip and the microfluidic channels was achieved in two ways: irreversible and reversible bonding. Following the fabrication of integrated SIBC biochip and microfluidic system, the designed microelectrodes are ready for testing with particles or cells. Details on the experimental setup and the DEP experiments on the SIBC biochip are detailed in Chapter Six.

Chapter Six

Experimental Setup and Results

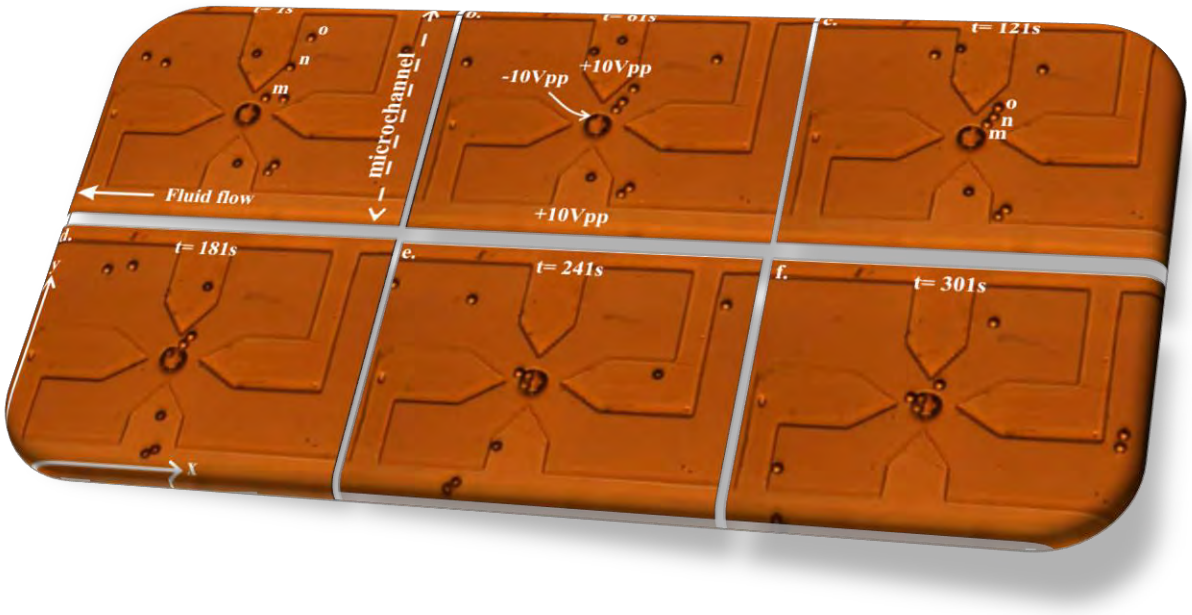

Subsequent to the fabrication stage, assessments on the microelectrode's functionality and trapping ability are essential to ensure performance of the SIBC biochip. The chapter starts with details on the experimental setup and the procedures used in the assessments. This is followed by section 6.2 where the results of DEP experiment using polystyrene microbeads and Ishikawa cancer cells are presented. Meanwhile, subsection 6.2.6 presents the back contact attributes toward the DEP trapping performance, which is followed by discussions of the result in section 6.3. The chapter ends with a brief summary of the experimental results.

6.1 The DEP Experimental Setup

Conducting experiments on the SIBC biochip with particles and real cells are important to evaluate the trapping regions identified in Chapter Four using COMSOL3.5a software. It is known that different types of biological cells have different dielectric properties, for example, the relative permittivities (ε_r) of yeast cells, human red blood cells and T-lymphocytes are 2657.7, 1859.4 and 5529.3 respectively [127]. In other words, two types of cell may have different polarization effects. Therefore, the actual response of the Ishikawa endometrial cell line by DEP force can only be observed through an experimental approach.

Assessments on the SIBC biochip are important not only to evaluate the trapping region but also to demonstrate the back contact trapping attributes on the performance of the SIBC biochip. The actual cell response due to the back contact can be obtained by comparing the three microelectrode designs fabricated on two different platform i.e., the SIBC biochip and the planar two-layer biochip (a platform without the back contact as the bottom electrode). This

comparative study demonstrated that a microcavity used as an electrode or back contact can increase trapping yields.

Figure 6.1 illustrates the DEP experiments setup. Before conducting the DEP experiments, the SIBC biochip is placed on a PCB board which was soldered with wires for electrical connections. Silver paste is used to create electrical connections between the SIBC biochip and the printed circuit board (PCB) board. Subsequently, the microfluidic channels are aligned on top of the SIBC biochip. In this setup, clips are used to reversibly bind the microfluidic channels and the SIBC biochip (on the PCB board). The reversible bonding technique allows effortless cleaning of residues and contaminants after each experiment.

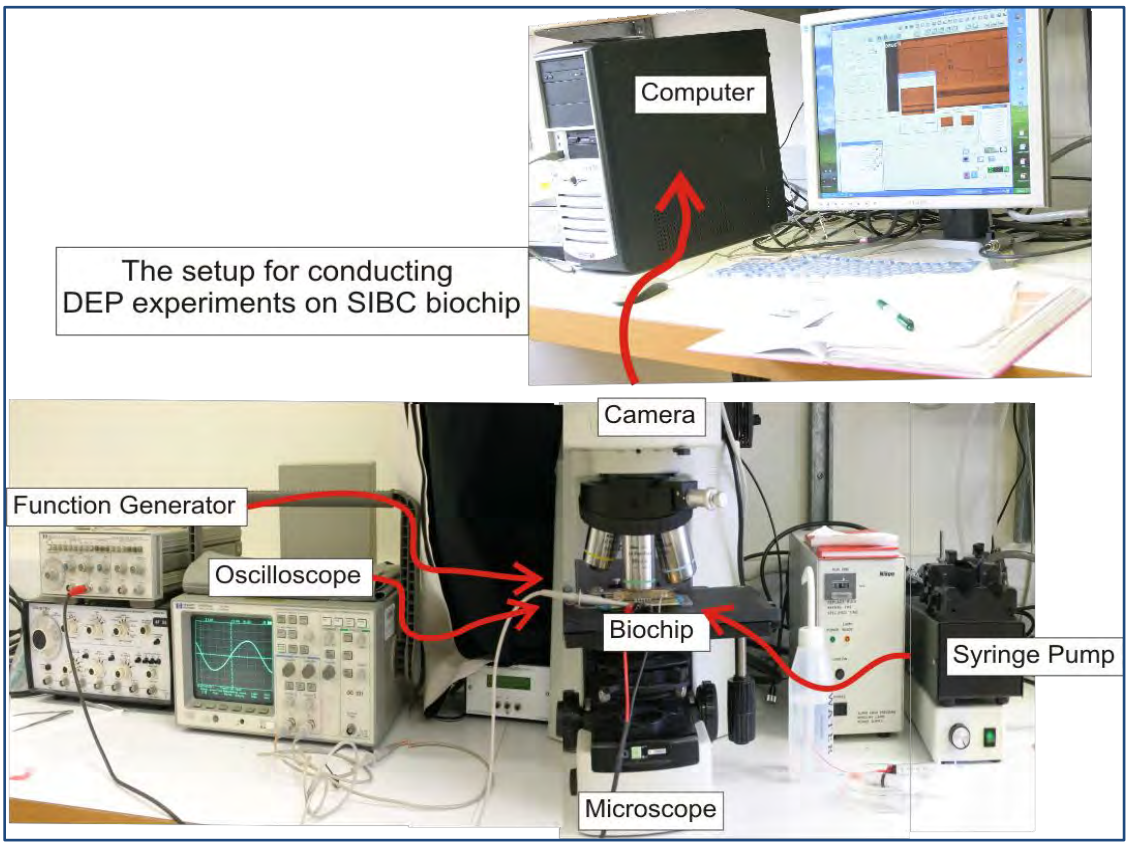

Figure 6.1: The equipments and setup used to test the SIBC biochip.

Moreover, it also allows post-trapping analysis to be conducted after particles are trapped inside the microcavities on the SIBC biochip.

After the setting of SIBC biochip on the PCB board, tubes are fitted at the inlets and outlets of the microfluidic channels. Unless otherwise stated, suspension media flowed into the SIBC biochip through transparent Masterflex tubings (Tygon Lab, Cole-Parmer) and a 5ml/cc syringe (Terumo) regulated by a syringe pump (PHD 2000, Harvard Apparatus). Due to the reversible bonding, care needs to be taken when assays were flowed into the channel. In order to prevent leakage, the maximum flow rate was set to be 50μL/min. This is achieved by using the syringe pump as it precisely regulates the flow rate from 0.0001μl/hr to 220.82 ml/min with ±1% accuracy [136].

In Fig.6.1, the microelectrode and back contact of the SIBC biochip are biased with the AC signals (φ) generated from a function generator (HP3312A). Meanwhile, the frequency and voltage of the AC signals are monitored using an oscilloscope (HP54600A). Movements of particle or cell are monitored through a microscope (Nikon Eclipse 80i) equipped with a CCD camera (Nikon digital Sight DS-U1) which is mounted on the microscope. The CCD camera is used for recording video clips of the movements. Then, the videos are captured into the ACT-2U software and saved in .avi format for analysis.

Conducting the DEP experiments in a non-continuous fluid flow is crucial to ensure that all movements observed are due to the DEP forces. Therefore, a flow from the syringe pump can be stopped after filling the microfluidic channels with the particle's suspension medium. After 1 to 3 minutes of 'waiting time', the DEP experiment starts by biasing the SIBC biochip with AC

signals from the function generator. The 'waiting time' is useful to allow particles or cells to settle inside the microfluidic channels and to ensure movements of cell are not due to other forces such as the hydrodynamic force. During the experiments, frequency of φ was set from 1kHz to 15MHz. Meanwhile, the amplitude of φ was set from 2V to 25V to find one set of frequency and amplitude combination that will initiate cell movement.

The three microelectrodes have demonstrated their trapping abilities when tested using 10μm polystyrene microbeads (Polysciences Inc.) suspended in DI water. The polystyrene microbead resembles the equivalent cell model of Fig.3.4 (in Chapter Three) and shows the actual DEP response of a particle with constant dielectric permittivity. Following confirmation of the SIBC biochip trapping ability, DEP experiments on living cells were conducted using Ishikawa endometrial cancer cells. The Ishikawa cells were obtained from the Cell and Protein Regulation, Department of Obstetrics and Gynaecology, Christchurch School of Medicine, University of Otago. Protocols for preparing the Ishikawa cancer cell line listed are listed in Appendix E.

The Ishikawa cells were harvested after 48 hours of culture time with an average size of 20μm to 40μm in diameter. Before conducting the experiments, the total concentration of cells and microbeads are calculated using haemocytometer. Meanwhile, the conductivity of particle/cell suspension medium was measured using a conductivity meter (Waterproof Cyberscan PC300).The results of DEP experiment are presented in section 6.2.

The following subsections present three techniques used in conducting the DEP experiments. The setup in subsections 6.1.1 and 6.1.2 were optimized to find the best way of

observing cell movements during experiments and finally led the integration of microfluidic channels on the SIBC biochip platform.

6.1.1 DEP Experiment on an Open Biochip Platform

Initially, the DEP experiments were conducted on an open biochip platform setup illustrated in Fig.6.2. In this setup, polystyrene microbeads in suspension were dispensed directly from a micropipette at the centre of the biochip platform. The DEP experiments were conducted on a 15mm x 15mm or 20mm x 20mm (width x length) SIBC biochip. For electrical connections, the biochip was placed on a biochip holder made of glass slide. After dispensing a droplet of polystyrene microbeads onto the platform, the function generator supplying was switched 'ON'. The convex shape of the droplet, however, creates difficulty to image the cells due to poor focusing and therefore affecting observations on the movements of cell. Hence, it is difficult to differentiate between movements of cell controlled by DEP forces and movements of strayed cells.

Another issue with this setup is that the droplet may not remain on top of the platform during experiments due to surface tension between the suspension medium and the biochip platform. Another possible problem is that the movements of microscope platform during imaging can affect the droplet's positions on biochip. These issues can disrupt the DEP experiments. Moreover, suspended particles/cells on the open biochip platform are exposed to contaminations. Based on these reasons, the setup was changed to a method called the close biochip platform described in the following subsection

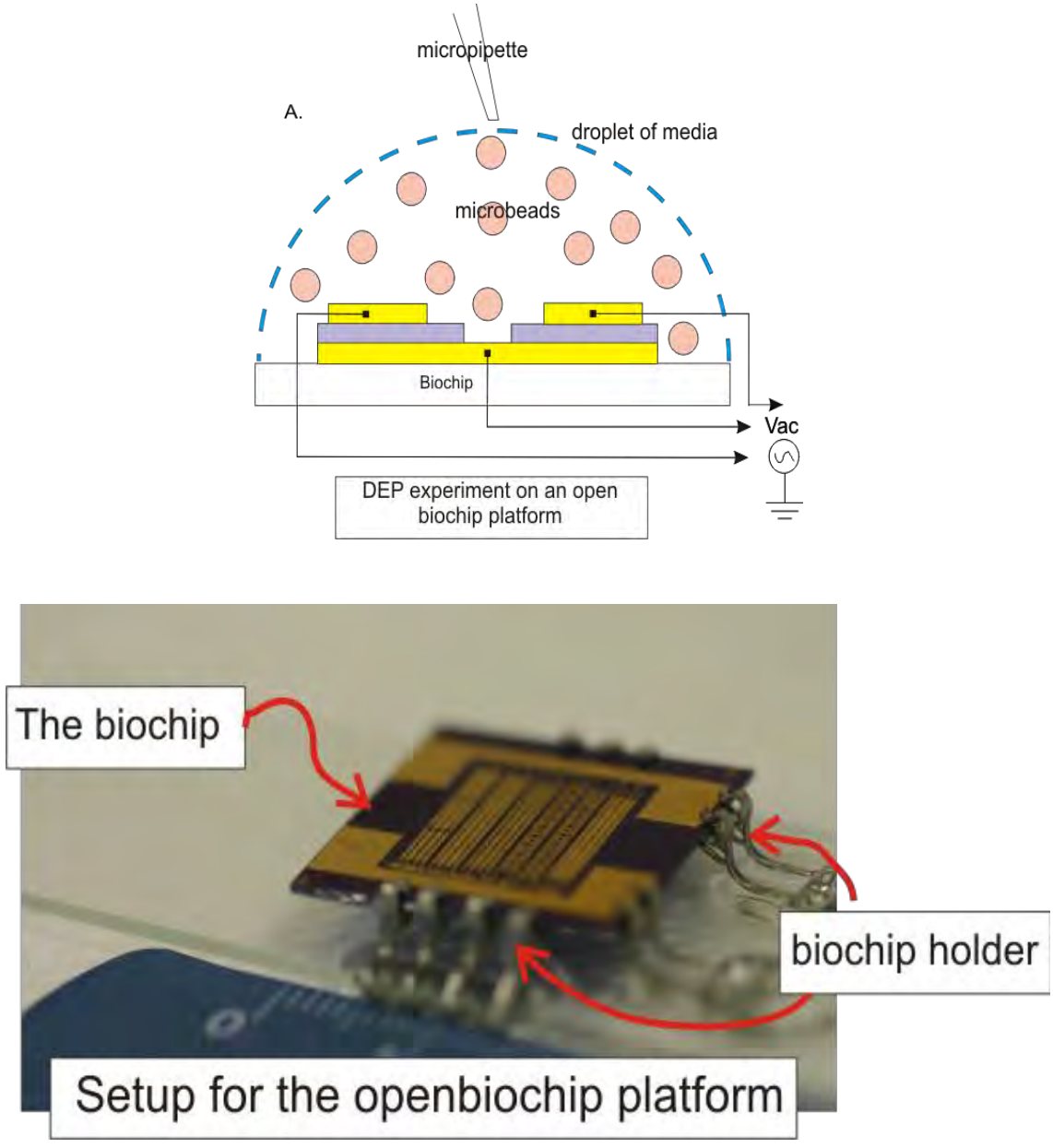

Figure 6.2: Schematic diagram of the DEP trapping experiments on an open biochip platform.

6.1.2 DEP Experiment on a Close Biochip Platform

Figure 6.3 shows the setup used to improve observations on cell movement when conducting DEP experiments on a 15mm x 15mm (width x length) size biochip. This setup uses a 1mm height rectangular PDMS spacer to contain suspension medium on the platform and a cover slip to level the droplet after dispensed from a micropipette. With this setup, observations on cell movements become clearer than the previous setup described in subsection 6.1.1. Using this method, cells' movements due to the DEP forces can be easily distinguished from the cells that are floating in the medium. Moreover, this technique contains particle/cell's suspension medium inside the PDMS space throughout the experiments and protects it from contaminants. Once the DEP experiments are completed, then the cover slip can be removed, and unwanted cells or particles are washed away.

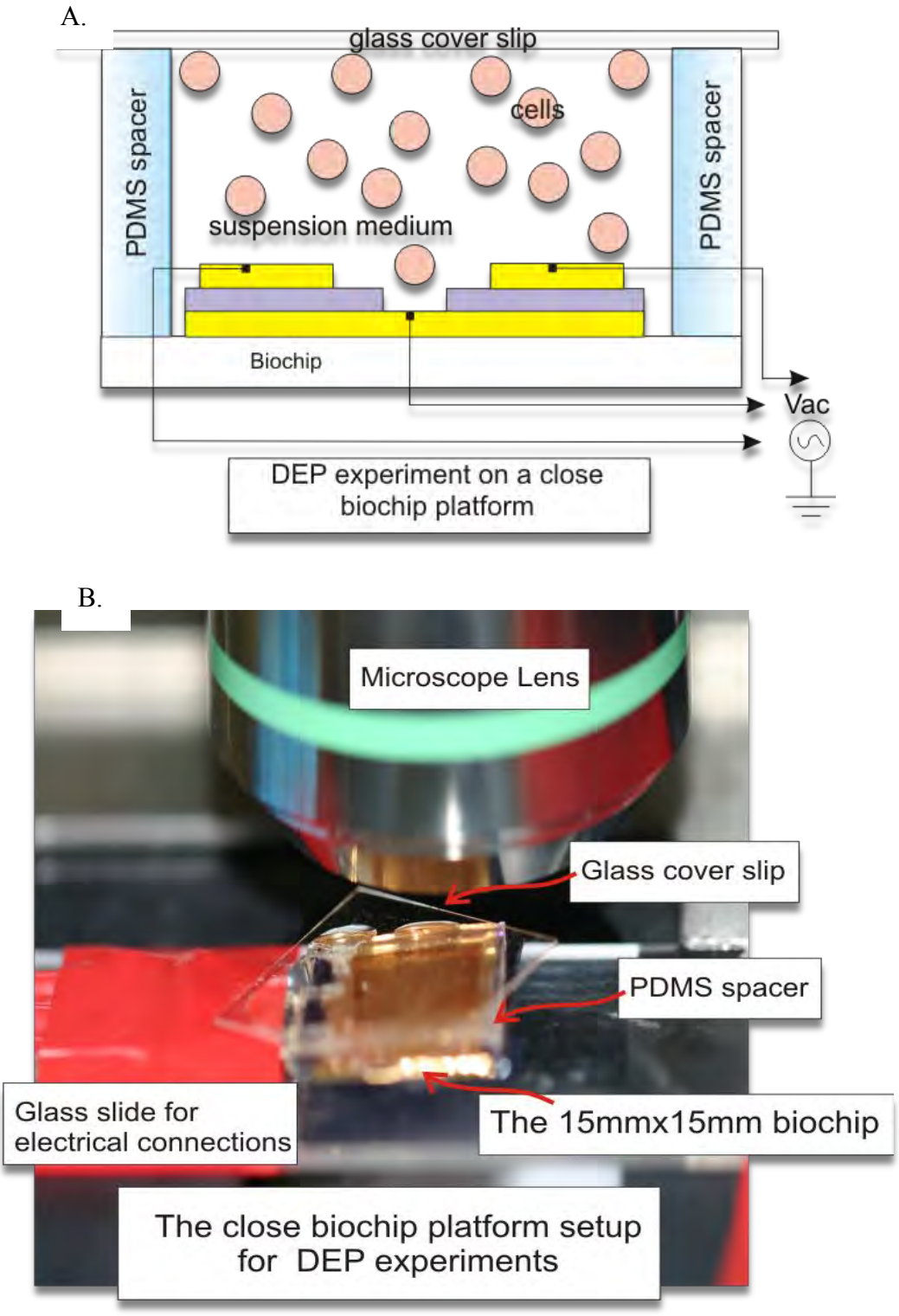

Figure 6.3: Spacer and cover slip are used to create an enclosure for the biochip platform which improved visibility of cell movements due to the DEP forces.

6.1.3 DEP Experiment inside a Microfluidic Channel

Uneven spreading of microbeads on a biochip platform may occur when dispensing suspension medium using a micropipette. This condition resulted in the microbeads' tendency to aggregate at various locations on top of the biochip platform, as shown in Fig.6.5(a). Aggregation of microbeads can overcrowd the biochip platform and impede observation on the movements of individual microbead into a microcavity. One solution to eliminate the condition is by limiting the amount of suspension mediums used during experiments. This in turn has led to the integration of microfluidic channels on the biochip platform.

As illustrated in Fig.6.4, a microfluidic channel can be used to limit the amount of suspension mediums flowed onto a biochip platform. The microfluidic channel made from PDMS material can be fabricated according to the required dimensions. For example, a 100µm x100µm x 1mm (width x height x length) channel can be easily fabricated using the softlithography technique described in Chapter Five.

By comparing the microbeads distribution in Fig.6.5(a) and (b), the advantage of using microfluidic channels for flowing particles on a biochip platform becomes apparent. Here, a DEP experiment conducted inside the microfluidic channel has better visibility and therefore, movements of particle microbeads inside toward the cell traps can be clearly observed. Experiments that incorporate microchannel have to be conducted on a bigger biochip platform than the 15mm x 15mm (width x length) SIBC biochip. For the SIBC biochip design, a 25mm x 75mm (width x length) glass slide was used as the substrate. Meanwhile, for the planar two-layer design, a 25mm x 75mm (width x length) of Si_3N_4 coated Si was used as the substrate. A bigger

platform is used to accommodate the areas required for bonding the SIBC biochip and its microfluidic channels.

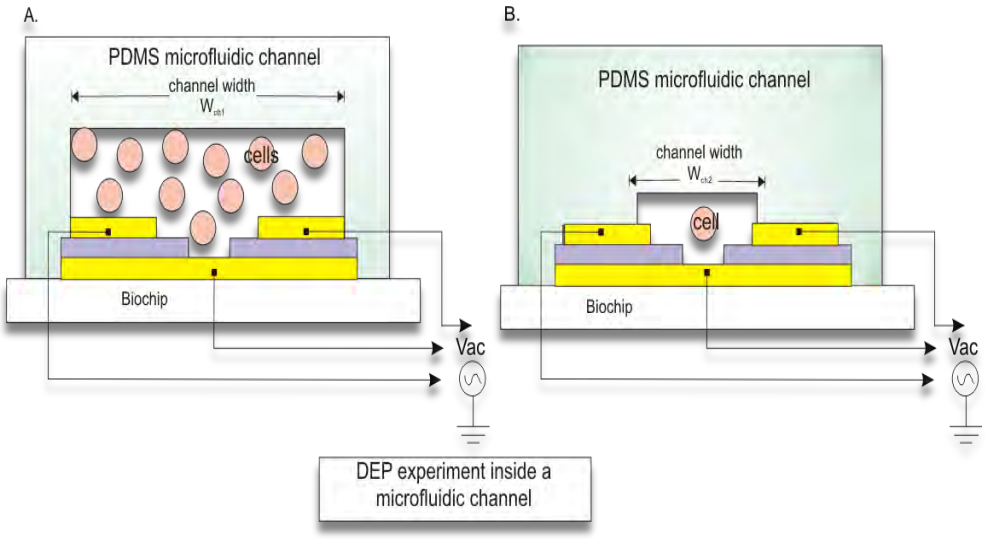

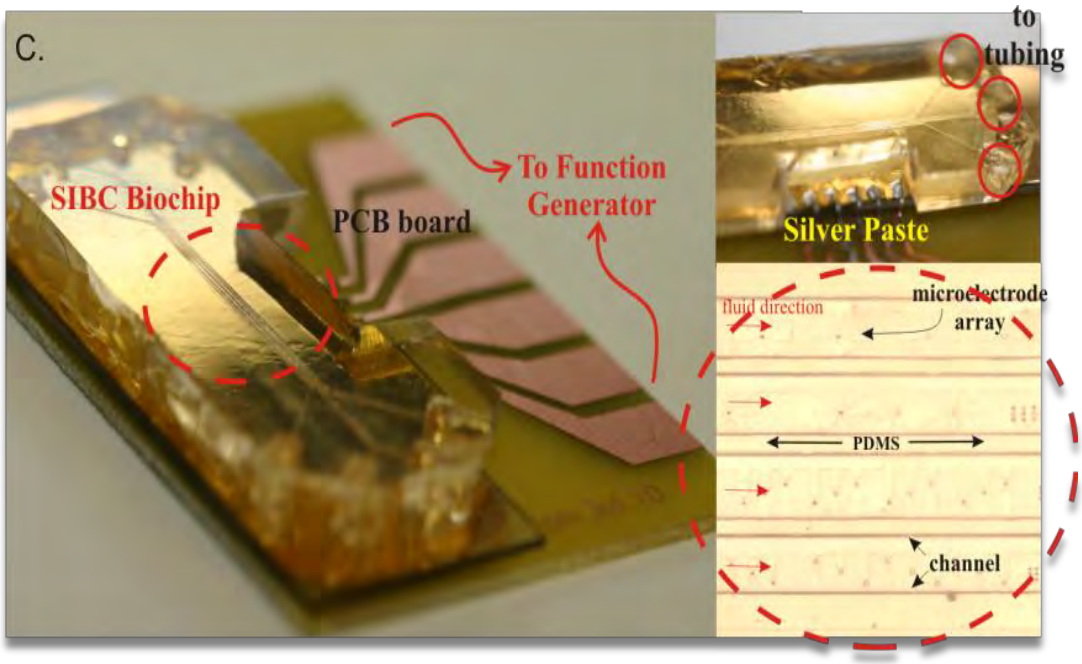

Figure 6.4: (a) The conceptual diagram of conducting DEP trapping experiments inside a microchannel. (b) The dimension and shape of the microfluidic channels are easily designed according to the required cell manipulation technique. (c) The setup for SIBC biochip with microfluidic channels.

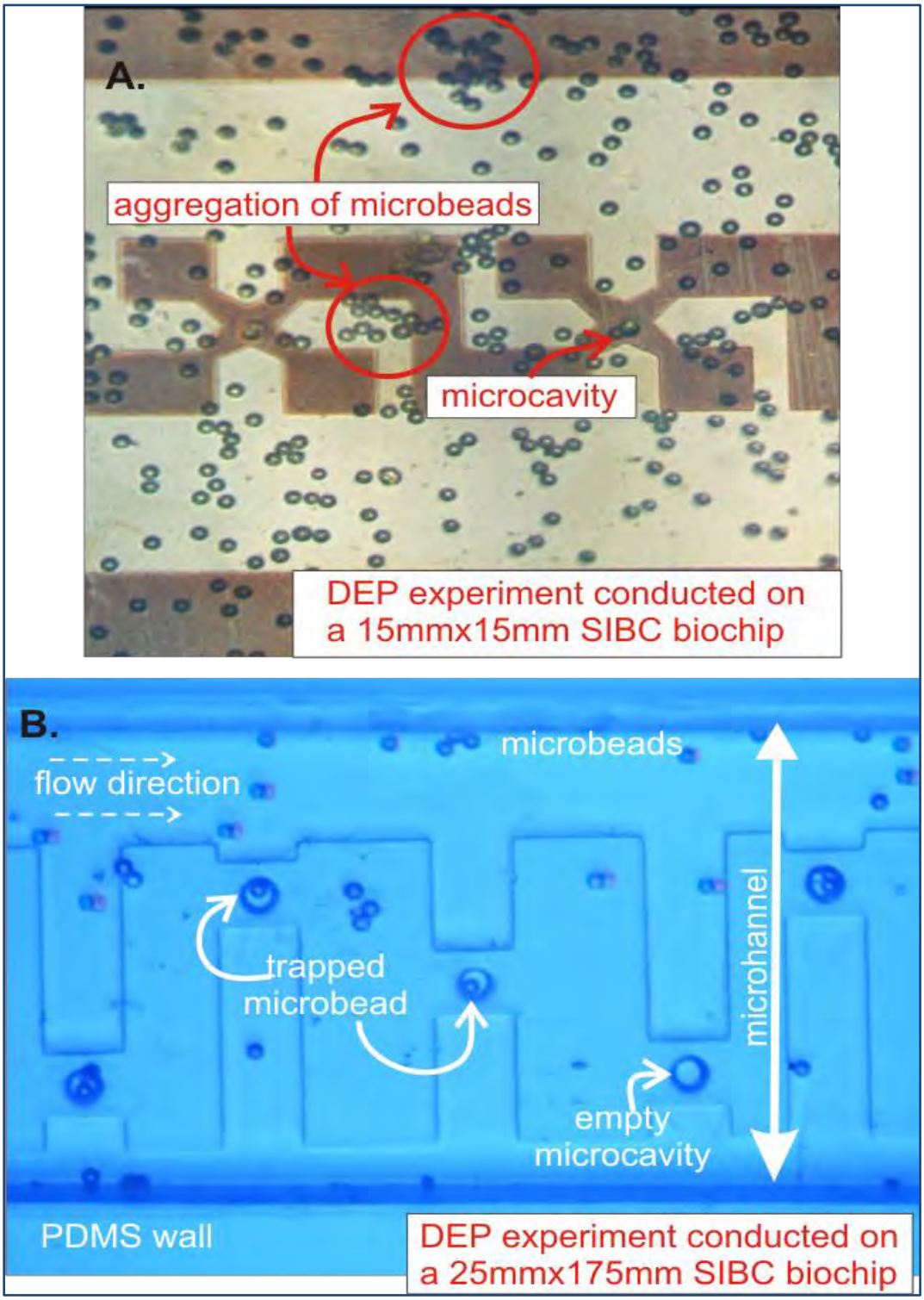

Figure 6.5: (a) Uneven spreading of microbeads on a biochip platform increases the possibility of aggregation at various locations. (b) Microfluidic channel is used to prevent the aggregations.

6.2 The result and Discussion of DEP Experiments

6.2.1 Introduction

This section presents the results obtained from conducting DEP manipulation tests on the three microelectrodes. The movement of microbeads and cells (Ishikawa cancer cells) were observed at different frequencies and amplitudes of the supplied φ and in various conductivity of the suspension medium.

At first, the trapping ability test was conducted as it represents the microelectrode's trapping behaviour inferred from the results of numerical simulation in Chapter Four. These results indicated that each pattern possesses distinct trapping behaviour due to the numbers of moments created inside the particle, which in turns polarizes the particle. As explained in Chapter Three, the moments are proportional to the electric fields generated by the electrodes.

Conducting DEP experiments in a medium of very low conductivity such as the DI water indicates that the relative particle conductivity (σ_p*), is insignificant on the actual DEP force [77]. Furthermore, by using particle that has a constant relative permittivity ε_r like polystyrene microbeads, the only significant factor in the actual DEP force is the gradients of electric field. Therefore, in the initial testing, the movements of microbead towards the DEP trapping regions represent the microelectrode's trapping pattern. Following the trapping ability tests with polystyrene microbeads, the three microelectrodes were then tested with Ishikawa cancer cells.

As to date, no evidence has been reported in the literature on DEP trapping cell manipulation using Ishikawa cancer cells, hence results from the experiment is novel. The Ishikawa cancer cells were cultured according to protocols listed in Appendix E at the Cell and

Protein Regulation Laboratory, Department of Obstetrics and Gynaecology, Christchurch School of Medicine, University of Otago. Unless stated otherwise, DEP experiments using the Ishikawa cancer cells were conducted inside the microfluidic channels.

During the experiments, movements of particle towards the regions of high electric field intensity (pDEP) or the regions of low electric field intensity (nDEP) controlled by the supplied φ become apparent. Subsequently, the characterization of SIBC microelectrode continues with experiments on various frequencies and amplitudes. The microelectrodes and the back contact were connected to φ with amplitudes ranging from 5V to 25V and frequency ranging from 10kHz to 5MHz.

The DEP experiments were conducted on 15mm x 15mm (width x length) size SIBC biochip using the close biochip platform setup in Fig.6.3, and 25mm x 75mm (width x length) SIBC biochip with setup in Fig.6.4(c). During the experiment, a specific frequency and voltage setting was maintained until a trapping event occurs. Movements of particle (microbeads and cells) were recorded and compiled using Windows Movie Maker software, after which the video files were later studied. The following subsections present results of the DEP experiment conducted on the three microelectrodes.

6.2.2 Trapping Results of the Dipole Microelectrode

The trapping behaviour of dipole microelectrode was demonstrated on a 15mm x 15mm size SIBC biochip using the setup illustrated in Fig.6.3(b). In this test, polystyrene microbeads with concentrations of 1.45×10^6/ml, were suspended in DI water (measured conductivity of 1960μS/m) and dispensed onto the SIBC biochip platform manually using a micropipette. After

two minutes of 'waiting time', the SIBC biochip was connected with an AC signals (φ). The dipole microelectrode pairs were connected to 10Vpp, whereas the microcavity was connected with φ that has 180°phase difference from the microcavity. Note that, particle mobility factors on the DEP force such as time and velocity, and trapping yield were negligible in the experiments. Therefore, these assessments were conducted to demonstrate the actual trapping region highlighted in Chapter Four.

Table 6.1 presents trapping results of the dipole microelectrode designs with the respective trapping frequency. As depicted in Table 6.1, the dipole microelectrode showed successful trapping at all tested frequency. Successful trappings were achieved due to the movement of microbeads toward regions of low electric fields intensity on the platform. The regions of low electric field inside the microcavities were consequences of connecting the back contact with φ that has 180° phase difference from the microelectrode pairs. Evidently, these movements were caused by nDEP.

Table 6.1: Trapping results of the dipole microelectrode using polystyrene microbeads.

Microelectrode	Frequency of the AC signal						
	50 kHz	100 kHz	250 kHz	500 kHz	1 MHz	2 MHz	5 MHz
Dipole Flat Tip	Yes	Yes	Yes	Yes	Yes	Yes	Yes
Dipole Sharp Tip	Yes	Yes	Yes	Yes	Yes	Yes	Yes

Another important finding from Table 6.1 is that both types of dipole microelectrodes i.e., the flat tip and the sharp tip dipole microelectrode, successfully trapped microbeads in all occasions. It means that when two microelectrodes have the same number of electrodes

generating DEP forces, the shape of an electrode tip is insignificant in determining the DEP trapping performance with respect to the trapping frequency. Therefore, tests on the sharp tip dipole microelectrode can also represent the performance of flat tip dipole microelectrode and vice versa. With successful trapping occurrences at all tested frequencies above 50kHz, undoubtedly, the dipole microelectrode pattern is capable of trapping particles or cells on the SIBC biochip.

The video snapshots showing movement of microbeads toward the trapping regions are illustrated in Fig.6.6 Here, the microelectrode pairs were connected with a 10Vpp AC signal at 1MHz, while the back contact was connected to AC signal that was 180° out of phase from the microelectrode. At t=0, there were few microbeads on the surface of the platform indicating that many of the microbeads were floating in the medium. This is probably due to the volume created by the spacer from its 10mm x 10mm x 1mm (width x length x height) dimensions.

After three minutes, more microbeads can be seen on the surface of the platform, which means the generated DEP forces are attracting more microbeads to the surface of the platform. As more microbeads moved towards the surface of the biochip, more microbeads are attracted to the trapping region in between the tips of electrode and the edge of microcavity. The effects of DEP force on movement of microbeads are demonstrated in Fig. 6.6(b) to (g). From these observations, sequences of trapping using the dipole microelectrode on the SIBC biochip are:

1) Attract the microbeads from suspension towards the surface of biochip platform.

2) Bring the microbeads closer to the trapping area in between the tips of electrode and the edge of microcavity.

3) Trap the microbeads inside the microcavities.

Once trapped, the microbeads were anchored by the electric fields generated by the back contact. Due to the low conductivity of DI water, the overall microbeads' movements on the SIBC biochip were very slow.

Following the testing on the SIBC biochip, the dipole microelectrode was then tested on a planar two-layer biochip. This comparison is studied to understand the microelectrode's trapping behaviour and demonstrate the back contact attributes on trapping performance. In the design of planar two-layer biochip, the microcavity was made of SU-8-2005 with access to the Silicon Nitride (Si_3N_4) coated Si substrate.

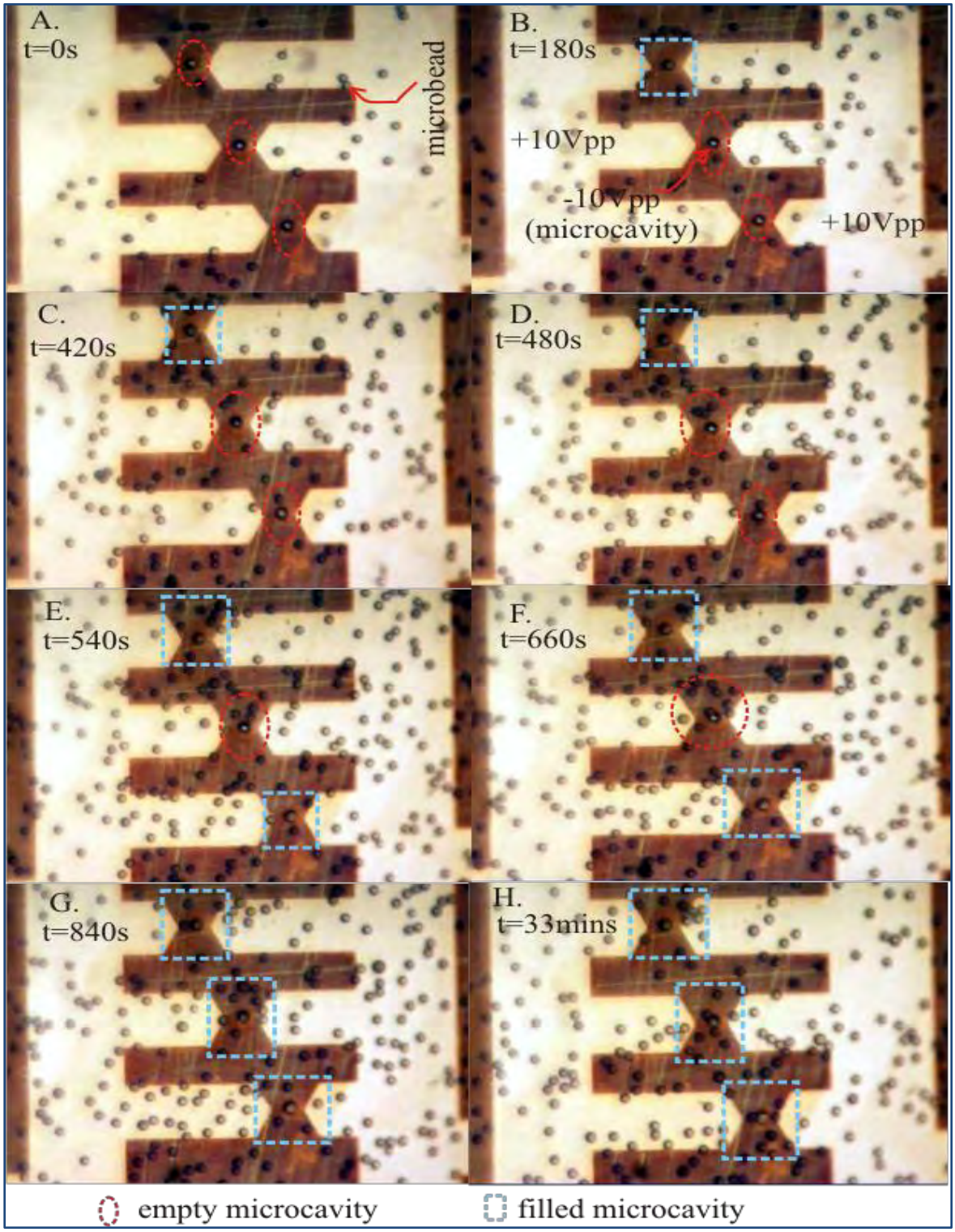

Figure 6.6: Sequences of microbead movements at 1MHz. At t=840s all three microcavities were filled with microbeads. The back contact which was connected to AC signals, anchors the three microbeads inside the microcavities as shown in (h).

To create a gradient of electric fields between the microelectrode pairs of the planar two-payer biochip, one side of the electrode was connected to 10Vpp of φ, while the other electrode was connected to 10Vpp that has 180° phase difference. The amplitude of φ was maintained at 10Vpp throughout the experiment. From experience, applying potentials beyond 10Vpp would only benefit particle mobility in a conductive suspension medium.

Video snapshots in Fig.6.7, showed the results of microbeads' movements on the planar two-layer biochip tested with frequencies from 10kHz to 1MHz. From these snapshots, the dipole microelectrode showed a common nDEP characteristic where microbeads were attracted toward regions of low electric field intensity at the electrode gap. The common sequences of positioning observed during experiments on the planar two-layer biochip are as follows:

1) Microbeads moved to the surface of the biochip platform, scattered either on top of the microelectrode or on the SU-8 surface.

2) As more microbeads resided on the surface, they travelled either to the edge of microelectrode or to the microelectrode gap.

3) The microbeads aggregated and aligned themselves in direction of φ, forming long chains of microbead on the platform.

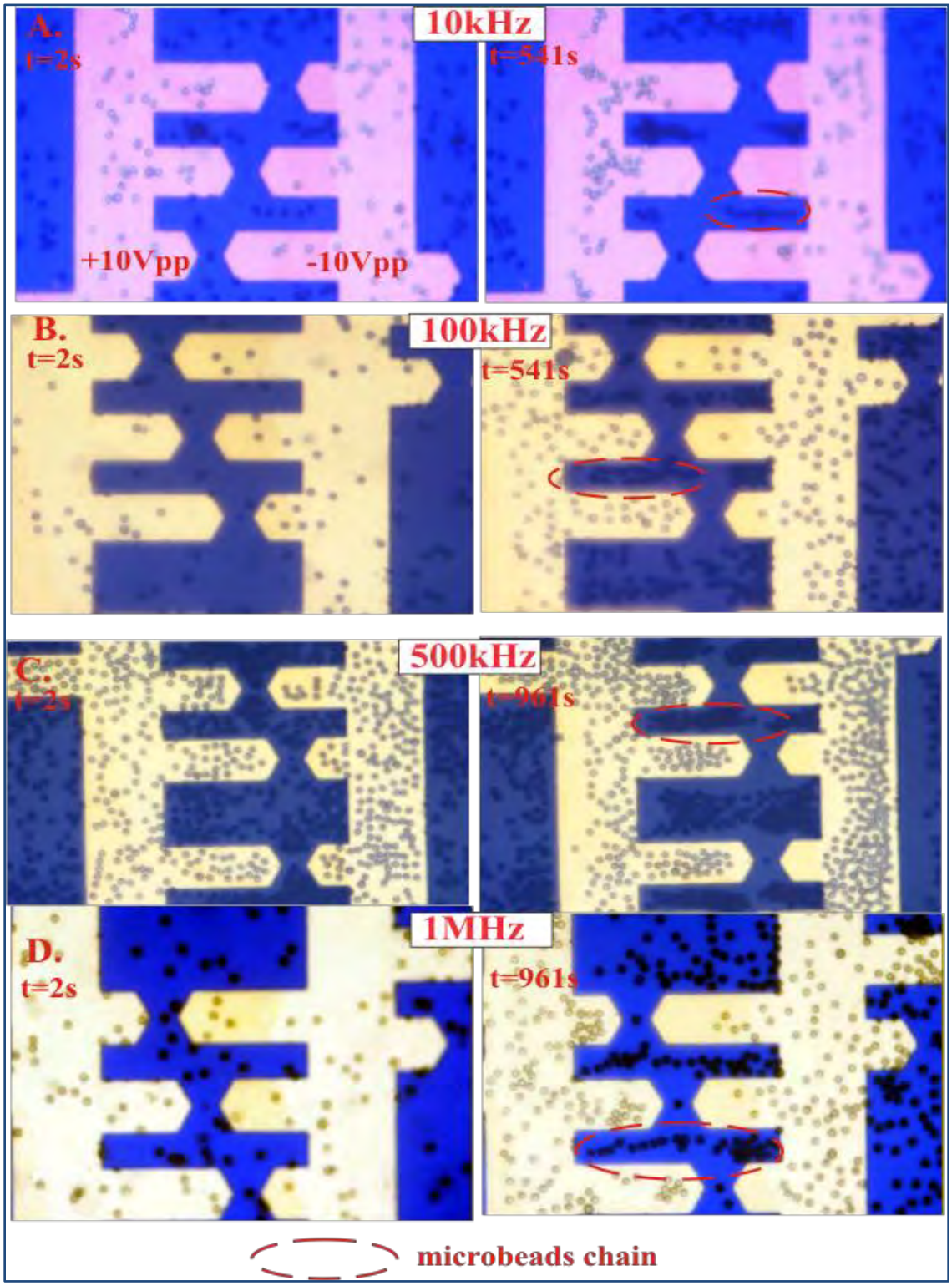

Figure 6.7: Movements of the microbeads on the planar two-layer biochip. The polystyrene microbeads tend to aggregate and create chains of microbead in the region of low electric field (in between microelectrode pairs).

These results exhibit distinct movements of the microbeads at two areas of the platform: 1) at the surface of SU-8, and 2) on top of the microelectrode. On top of the dipole microelectrode, movements of microbead were confined by the electrode's shape. For example at 500kHz of Fig.6.8, the microbeads did not move further beyond the V-shaped tips, where the DEP force is high, but only resided at approximately 10μm to 20μm from the edge instead.

Apparently in this condition, the microbeads repelled from regions of high electric fields and therefore no microbeads were trapped inside the microcavities. Since the microbeads did not move beyond the electrode tips, there were no microbead chains created between the two electrode tips or at the trapping region, as denoted by (i.) in Fig.6.8. Hence, the possibilities of microbeads or cells trapped inside the microcavities on the planar two-layer platform were very low.

On the contrary, microbeads that resided on the SU-8 surface (indicated by the blue coloured area in Fig.6.8) formed chains of microbead from the electrode of high electric field intensity to the electrode of low electric field intensity. These chains connected two microelectrode pairs by filling the gap in between them.

Therefore, it can be concluded that on the planar two-layer biochip, microbeads reside on either top part of the dipole microelectrode or in the gap of the dipole microelectrode shown in (i.) of Fig.6.8. The results demonstrated that on the planar two-layer biochip, trapping regions are located at the microelectrode gap instead of in between the microelectrode tips or the expected trapping region for the dipole microelectrode mentioned in Chapter Four.

Consequently, the only way to drive microbeads toward the trapping region (in the case

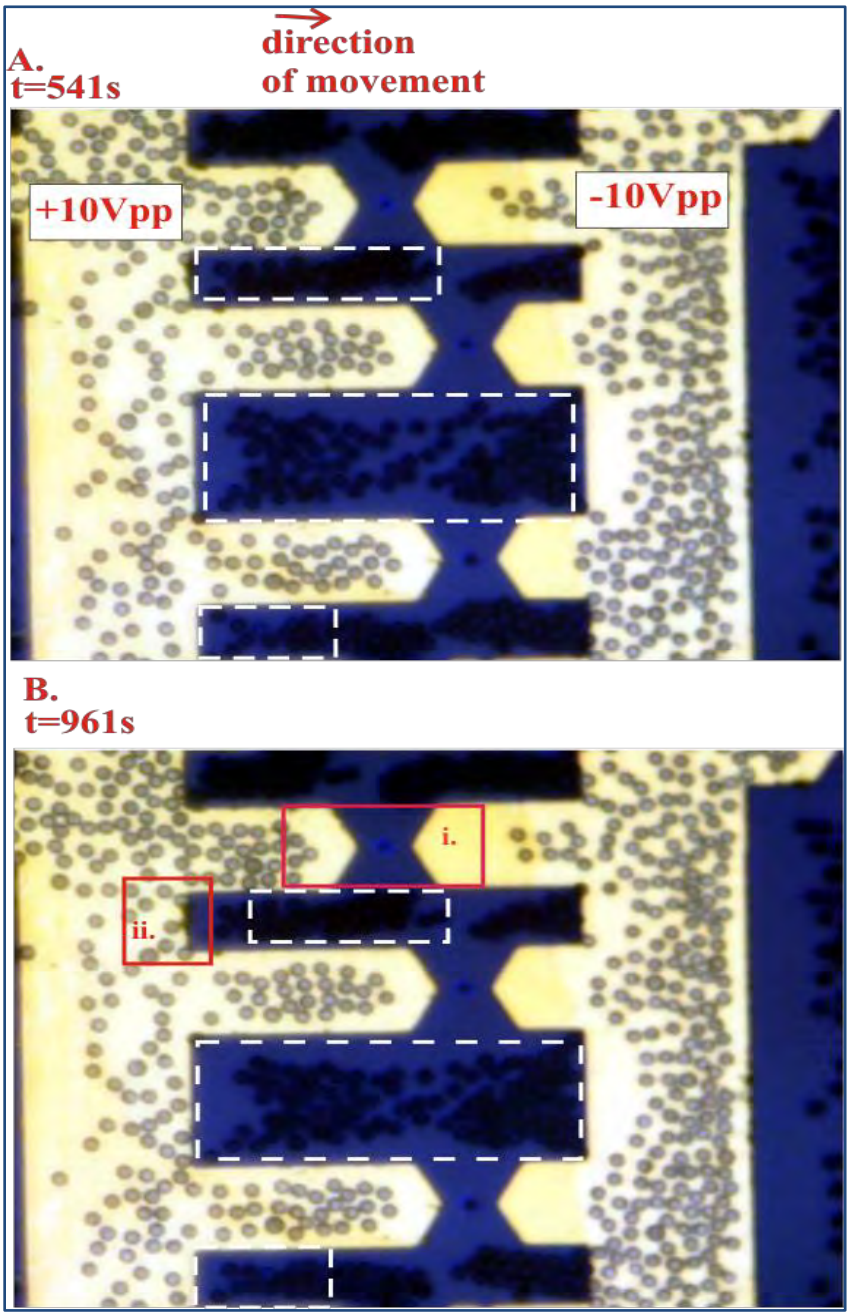

Figure 6.8: Movements of the microbeads on the planar two-layer biochip. On top of the microelectrode, microbeads aligned according to the shape of microelectrode but created a 10-20 µm gap near the borders. Meanwhile, the microbeads aligned horizontally and created chains that closing the gap on the SU-8 surface in (b).

of trapping with nDEP), is by turning the microcavity to be the only area of low electric fields intensity on the biochip platform. Otherwise, the objective of trapping cells inside the microcavity cannot be achieved. In other words, the microelectrode pairs have to be connected with φ of the same phase while the microcavity is connected with φ with different phase from the microelectrode pairs.

After testing the dipole microelectrode trapping behaviour using polystyrene microbeads, the dipole microelectrode was then tested using the Ishikawa cancer cells. The experiments were conducted inside a microfluidic channel integrated on the SIBC biochip. The mature Ishikawa cancer cells in 20µm to 30µm sizes were obtained after subcultured in the M199 media for 72 hours.

The DEP experiment uses M199 as the suspension medium with measured conductivity

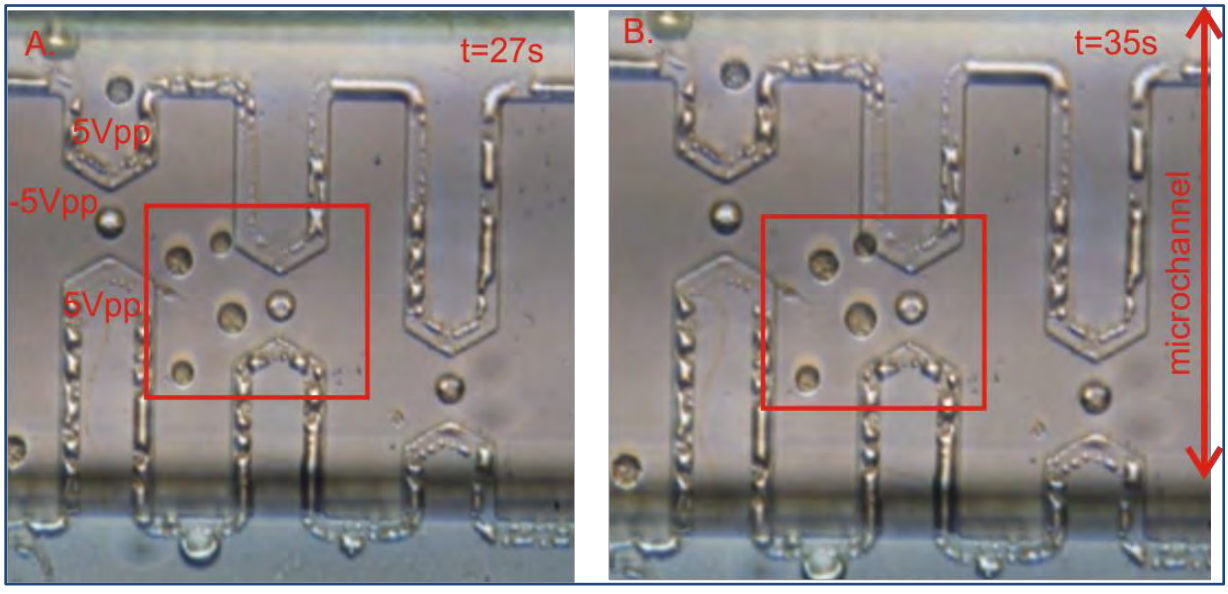

Figure 6.9: Video snapshots of Ishikawa cancer cell's movements inside a microfluidic channel using the dipole microelectrode.

of 13.55mS/m. The cells were then flowed into the microfluidic channel using a 5ml syringe. After two minutes of 'waiting time', the function generator was switched 'ON'. Due to the nature of cell's suspension medium is more conductive than the DI water, so, different trapping frequency is expected. Similar to the initial SIBC test using microbeads, the dipole microelectrode was connected with φ that had 180° phase difference between the back contact and the microelectrode pairs. Because of the medium's conductivity, the amplitude of φ was maintained at 5Vpp.

In this experiment, movements of the Ishikawa cancer cells were observed at 2.5MHz. Figure 6.9 presents video snapshots of the Ishikawa cancer cells inside a microfluidic channel. As expected, the cells moved to the trapping region in the microcavity where a low electric field was generated. From this observation, the movements exhibited have similar pattern to the movement of microbeads presented in Fig.6.6. Therefore, it can be concluded that the dipole microelectrode is capable of trapping single cells while the trapping regions demonstrated through the DEP experiments concur with the simulation results in Chapter Four.

6.2.3 Trapping Results of the Quadrupole Microelectrode

This section presents the results obtained from DEP experiments on the quadrupole microelectrode. Initially, the microelectrode's trapping ability was tested using polystyrene microbeads suspended in DI water. Table 6.2 depicts successful trapping of microbeads occur at 100kHz, 500kHz and 5MHz respectively. As the trapping events occurred at certain frequencies, therefore, segregation between two types of cell SIBC biochip is more likely possible using the quadrupole than the dipole microelectrode design.

An example of the movements of microbeads toward the microcavity is illustrated in Fig.6.10. In this figure, the microbeads were attracted to the trapping region and moved towards the region of low electric field which is in between the microelectrode gap. After 120 seconds, the microcavity was filled with a microbead while at t=540 seconds, three more microbeads

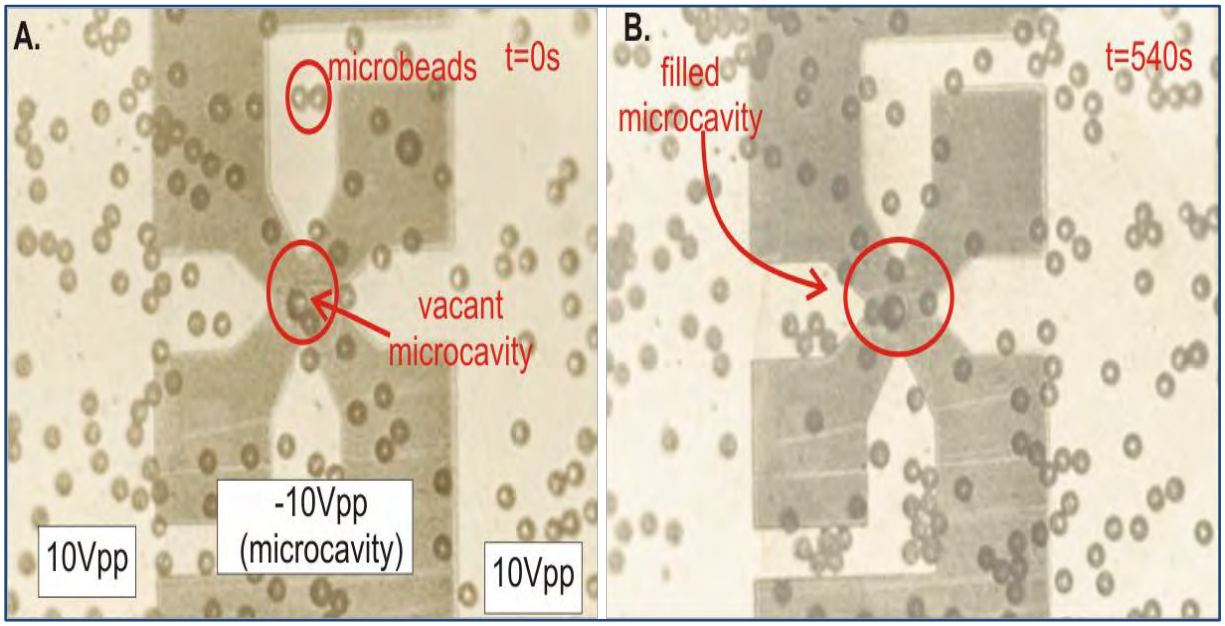

Figure 6.10: The quadrupole microelectrode trapping ability was demonstrated using polystyrene microbeads suspended in DI water at 5Mhz.

attached themselves at the tips of the electrode illustrated in Fig.6.10(b).

Table 6.2: Trapping results of the quadrupole microelectrode using polystyrene microbeads.

Microelectrode	Frequency of the AC signal						
	50 kHz	100 kHz	250 kHz	500 kHz	1 MHz	2 MHz	5 MHz
Quadrupole	Aggregate	Yes	No	Yes	No	No	Yes

Following the initial assessment using close platform method in subsection 6.3.1 and 6.3.2, the DEP experiments were then conducted inside a microfluidic channel. As illustrated in Fig. 6.11, the setup consists of a biochip platform and microfluidic channel made from PDMS. The microbeads, with concentrations of $1.5x10^6$/ml in suspension, were diluted to a ratio of 1:5 with DI water. Then, the medium's flow was regulated into a microfluidic channel using a syringe pump with a flow rate of 50µL/min.

The quadrupole microelectrode pairs were given φ of the same phase. Meanwhile, the microcavity was connected with φ that was 180º out of phase from the microelectrode pairs. Finally, after the microbeads settled inside the microfluidic channel, the function generator was switched 'ON'.

Due to the laminar flow, loading of microbeads through a microfluidic channel eliminates aggregations of microbeads at the trapping regions. Movements of microbead were caused by the DEP force's at the V-shape tip as illustrated in Fig.6.11. Initially, one microbead (m), can be seen to reside in the trapping region, as shown in Fig.6.11(a). Then, more microbeads (n and o) from the medium, started to reside at the edge of microelectrode, as seen in Fig.6.11(c).

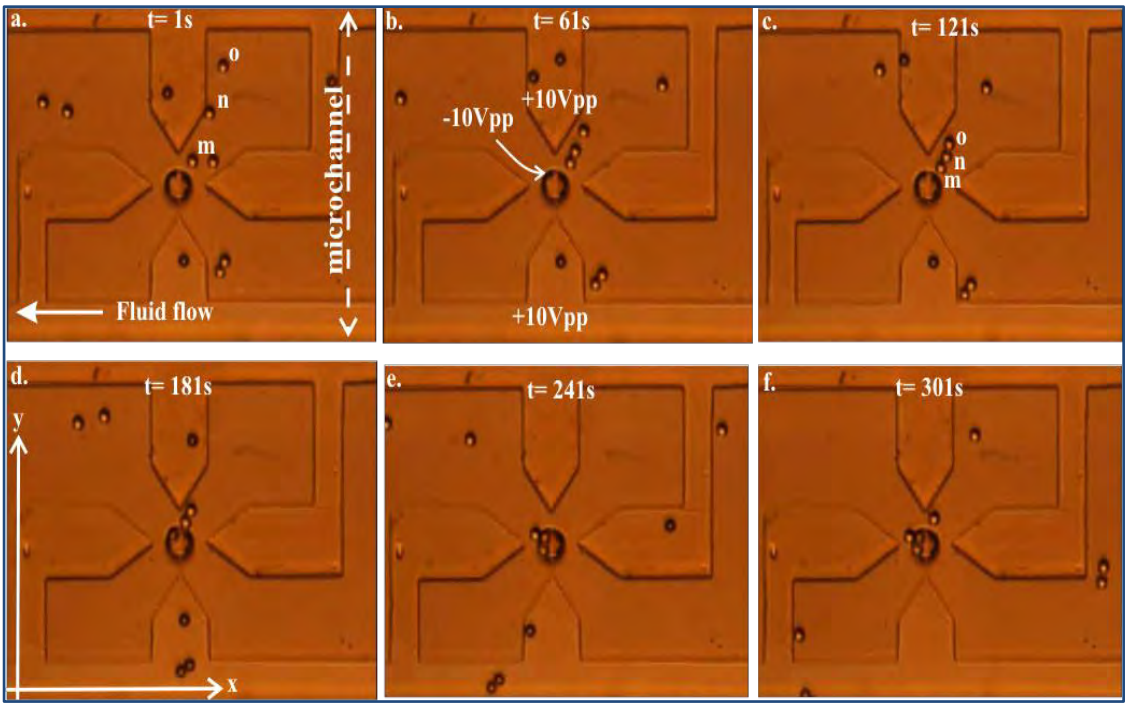

Figure 6.11: Movements of the microbeads inside a microfluidic channel at 5MHz using the quadrupole microelectrode.

Subsequently, the three aligned microbeads (m, n and o) moved together into the microcavity, which can be seen in Fig.6.12(d).

As demonstrated, observations on movements of individual microbead have been improved when the DEP experiment was conducted inside a microfluidic channel. The trapping mechanism starts with DEP force attracting the microbeads to the edge of microelectrode tip. However, it is interesting to see that the microbead (m) stayed at the tip and did not move into the microcavity by itself, until there were more microbeads (n and o) aggregated behind it. This observation suggests there were some form of an induced force generated from the aggregations of microbeads, which then accelerated microbead movement into the microcavity. It also can be

inferred that particle-particle interactions due to the AC signals, can determine the movements of a microbead or cell on a DEP-based biochip platform.

After testing with the polystyrene microbeads, the quadrupole microelectrode design is ready to be tested with biological cells. The Ishikawa cancer cells were cultured with measured the M199 cell media and the conductivity was 13.55mS/m. From the experiments, the frequency at which Ishikawa cancer cells in M199 media started moving was at 2.5MHz, while the

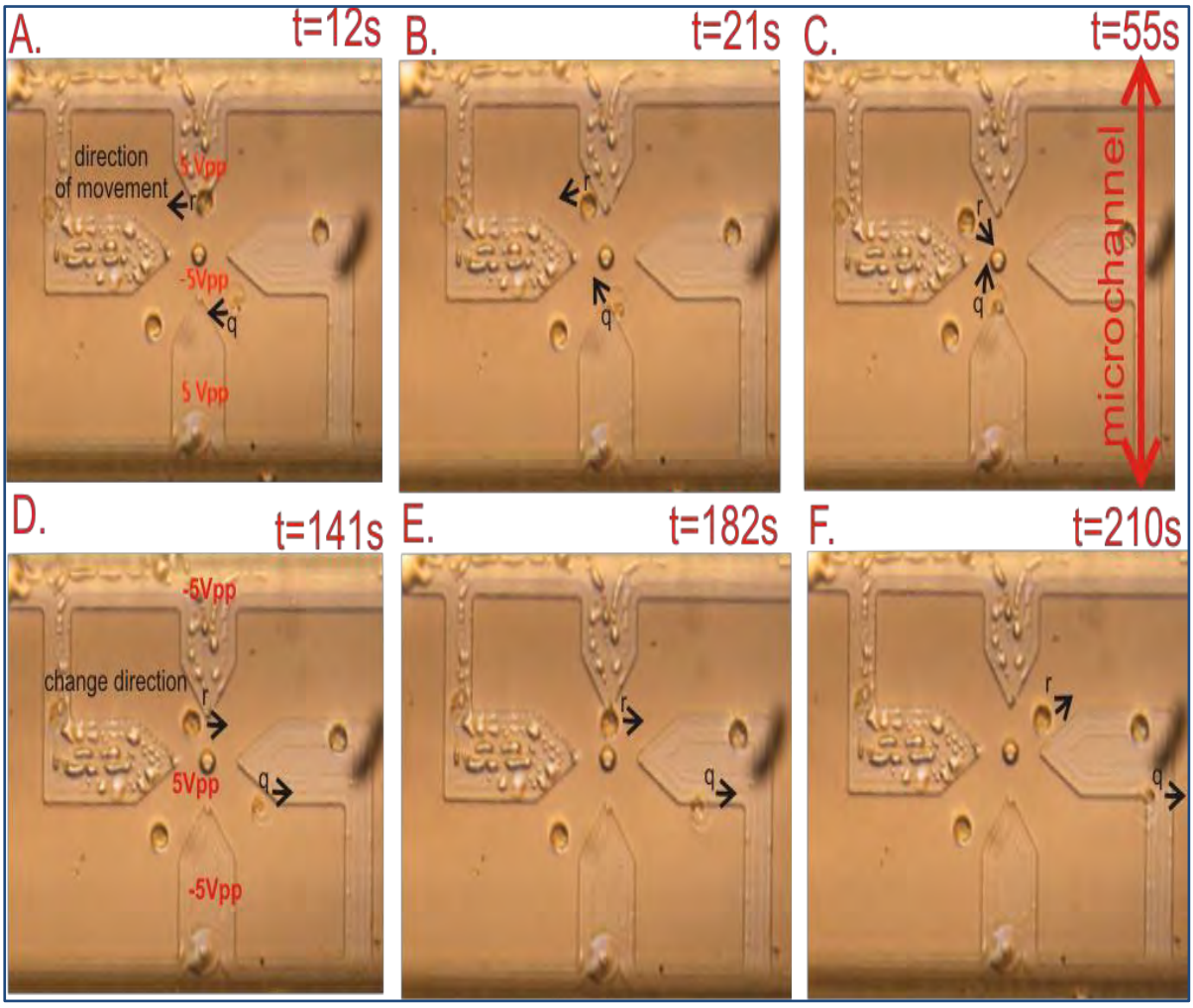

Figure 6.12: Movements of the Ishikawa cancer cells at 2.5MHz inside a microfluidic channel on the SIBC biochip.

amplitude of the φ was maintained at 5Vpp.

Figure 6.12 presents video snapshots of the Ishikawa cancer cell's movements (denoted as r and q) inside a microfluidic channel. Similarly, the φ of the microelectrode pairs was set to be 5Vpp while the back contact was connected with φ that has a 180° phase difference. With this setting, the two Ishikawa cells moved horizontally to the left before moving in diagonal directions, as shown in Fig.6.12(b). At this point, both cells are moving toward the low electric fields' areas and subsequently, to the microcavity at the centre of the quadrupole microelectrode, as shown in Fig.6.12(c).

In Fig.6.12(d), the φ setting was changed to a different polarity and interestingly, the two Ishikawa cells moved horizontally toward the opposite of their previous directions. However, one of the Ishikawa cancer cell (denoted as 'r') started to move diagonally once it reached the V-shape tip, as shown in Fig.6.12(f).

The effect of DEP forces on the Ishikawa cancer cell were demonstrated by the movements of cell denoted as 'q'. In Fig.6.12(a) to Fig.6.12(c), the polarization effect inside the membrane drags the cell towards the direction of low electric field region. The same situation happened when the polarity of φ changes where the membrane polarized and moved the cell. The organelles inside the Ishikawa cancer cells however, tend to adhere to the surface of microelectrode as illustrated in Fig. 6.12(f).

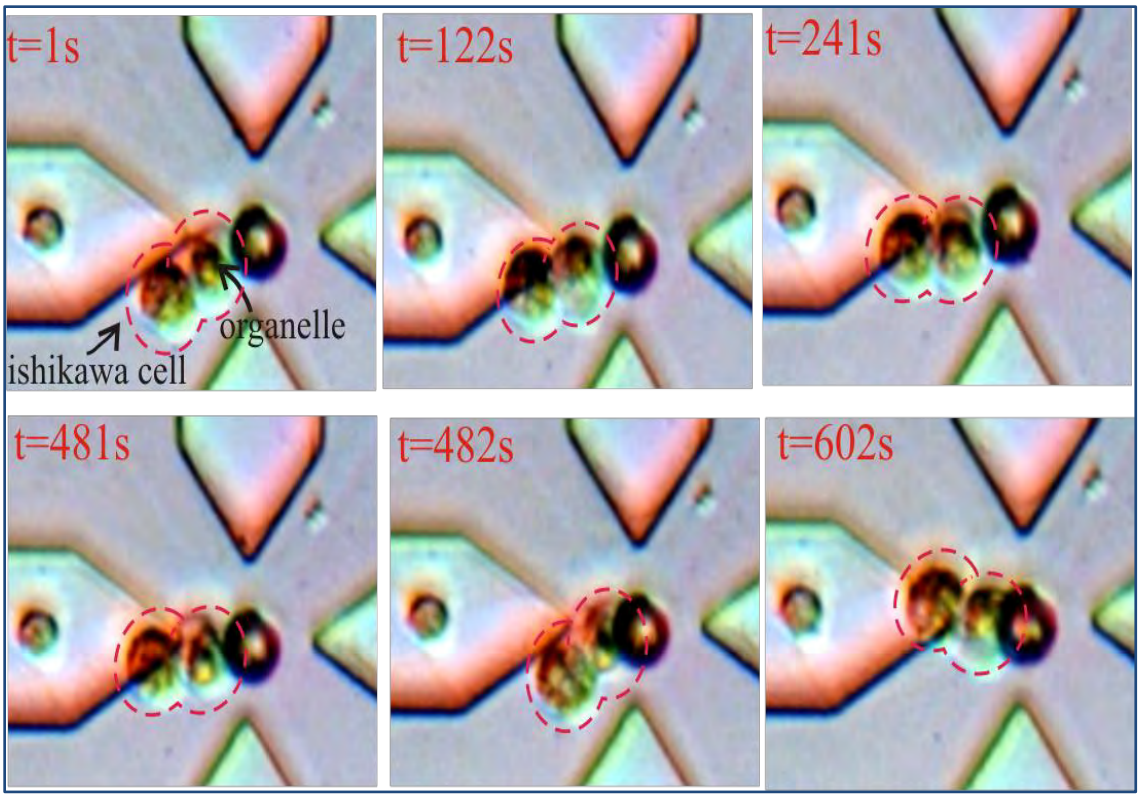

Figure 6.13: Movements of organelles inside the two infused Ishikawa cells due to the DEP force at 250Hz and medium's conductivity of 12mS/m. At t=602s, the two cells moved into the microcavity.

Another example of the DEP force effects is illustrated Fig.6.13. Here, the Ishikawa cancer cells were suspended in minimum essential media (MEM) with conductivity of 12.8mS/m and flowed inside a microfluidic channel. In this figure, two Ishikawa cancer cells were infused during loading and were attracted to the trapping region at 250Hz. From t=1 to t= 481 seconds, the Ishikawa cell organelles moved within the membrane's compound as the infused cells making their way into the microcavity. It also can be inferred that movements of the Ishikawa cancer cells into the microcavity were predominantly led by the cell's membrane that was polarized toward the low electric field region of the microcavity at t=482 to t=602 seconds.

The results presented in this section have demonstrated the trapping ability of the quadrupole microelectrode using polystyrene microbeads and Ishikawa cancer cells. DEP forces generated by the quadrupole microelectrode on the SIBC biochip, provide adequate holding force to attract single cells toward its trapping region. The results also substantiated the presence of the trapping region on the SIBC biochip. As demonstrated through the movements of polystyrene microbeads and Ishikawa cancer cells, the area between the edge of microcavity and the electrode's tips is essential in DEP trapping mechanism. Nevertheless, a particle's direction on the SIBC biochip platform can be controlled by the frequency and phase of supplied AC signals (φ).

6.2.4 Trapping Results of the Adaptive Octupole Microelectrode

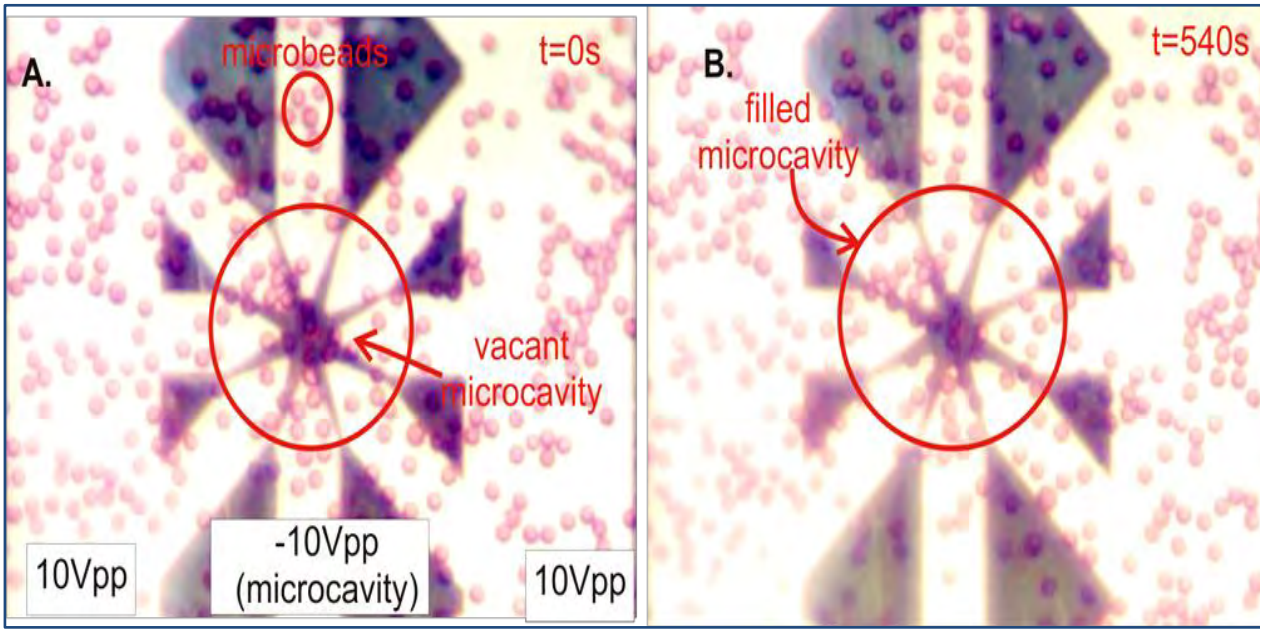

Figure 6.14: The adaptive octupole microelectrode trapping ability was demonstrated using polystyrene microbeads suspended in DI water at 5Mhz.

The adaptive octupole traps only at 2MHz in the trapping ability test as depicted in Table 6.3. These tests were conducted using polystyrene microbeads suspended in DI water with a similar setting to the previous trapping ability tests for the dipole and quadrupole microelectrodes. Hence, the AC signals used were of 180° phase difference between the back contact and the microelectrode pairs on the uppermost layer of the SIBC biochip

Table 6.3: Trapping results of the adaptive octupole microelectrode using polystyrene microbeads.

Microelectrode	Frequency of the AC signal						
	50 kHz	100 kHz	250 kHz	500 kHz	1 MHz	2 MHz	5 MHz
Adaptive Octupole	No	No	No	Aggregate	Aggregate	Yes	Aggregate

During the first 60 seconds, the microbeads moved toward the central region of the adaptive octupole microelectrode. The movements are due to the DEP forces generated at the tips of microelectrodes. At t= 540 seconds as shown in Fig.6.14(b), a microbead has successfully trapped inside the microcavity. The microbeads however, tend to concentrate in the trapping region if the DEP forces were exerted for a longer period. The same condition occurred at 500kHz, 1MHz and 5MHz frequencies, where the microbeads aggregated at the trapping region but failed to move into the microcavity.

One possible reason for the aggregation of microbeads in this manner is there were too many microbeads dispensed on top of the adaptive microelectrode. Furthermore, the numbers of electrode surrounding the microcavity in the adaptive octupole design tend to attract too many particles and behave as a particle concentrator. On the other hand, as the trapping only occurred at 2Mhz, it can be inferred that the adaptive octupole can be useful in separating two types of cell SIBC biochip than the quadrupole and dipole designs. Comparing the experimental results from Table 6.1, 6.2 and 6.3, the trapping frequencies were narrowing as the number of microelectrode moments on particles increases namely, from dipole to octupole.

At the same time, the adaptive octupole microelectrode demonstrated different trapping behaviours on the planar two-layer biochip. By using AC signals setup shown in Fig.6.15, the

adaptive octupole was capable of trapping microbeads inside the microcavities. The microbeads also tend to aggregate at the middle electrode tip and align themselves according to the shape of the tip. In the adaptive octupole experiments, microbeads were attracted to the regions of high electric fields at the microelectrode tips instead of showing the common nDEP behaviour.

Figure 6.15 illustrates that movement of microbeads were from the regions of high electric field intensity, on the right electrode, to the regions of low electric field intensity at the central region. As more microbeads are concentrated at the tips, as opposed to the low electric field region, the microbeads trapped themselves at the microcavity. From these results, trapping at the microcavity became evident in all occasions tested at 10kHz, 100kHz, 500kHz and 1MHz.

Another important finding was the location of the microbead chains. At 10kHz and 100kHz, the chains were formed on top of the floating electrode, whereas at higher frequencies of 500kHz and 1MHz, the chains were formed at the edge of floating electrode instead. Here, the floating electrode created induces electric fields [106, 137] and attracted microbeads to align at its edge shown in Fig.6.15(c) and Fig.6.15(d). With proper design, a floating electrode can be useful in DEP trapping single cells as it reduces electrical connections needed on a biochip platform, especially for arrayed microelectrode.

Following the trapping ability test, the adaptive octupole microelectrode was then tested with the Ishikawa cancer cells. The DEP experiments were conducted on 15mm x 15mm (width x length) size using the close biochip platform setup in Fig.6.3. The Ishikawa cancer cells were suspended in cell minimum essential media (MEM) with conductivity of 12.8mS/m and dispensed on top of the SIBC biochip using a micropipette. Upon switching ‘ON’ the function generator, the Ishikawa cancer cells started to move toward the microcavities.

Figure 6.16 shows the trapping of Ishikawa cancer cells in the trapping region. Interestingly, the cells aggregated and clumped at the trapping region, which make observations on the movement of single cells difficult. To overcome this problem, and as demonstrated previously with the dipole and the quadrupole microelectrodes, conducting the DEP experiments inside a microfluidic channel will result in better observation on single cells. Furthermore, with the help of a laminar flow, flowing cells using a microfluidic channel promotes random distribution on the biochip platform.

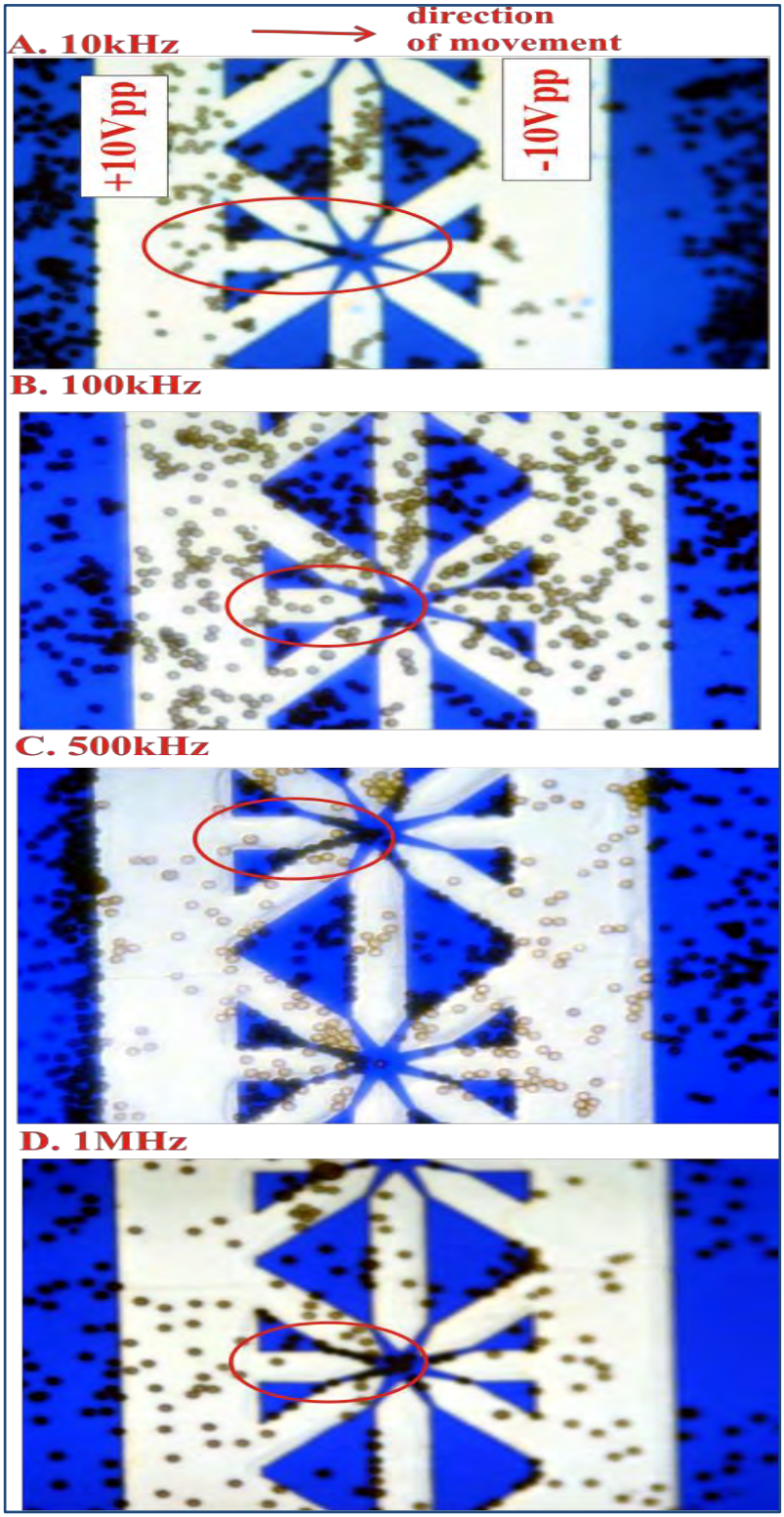

Figure 6.15: At t=10 minutes, the microbeads aligned themselves and moved toward microcavity from the middle electrode tip of the microelectrode that was connected with the 10Vpp (on the right hand side).

Results from these experiments have demonstrated the adaptive octupole microelectrode's trapping ability and the presence of DEP trapping regions surrounding the microcavity. The adaptive octupole has demonstrated the ability to trap single cells and also act like a particle concentrator.

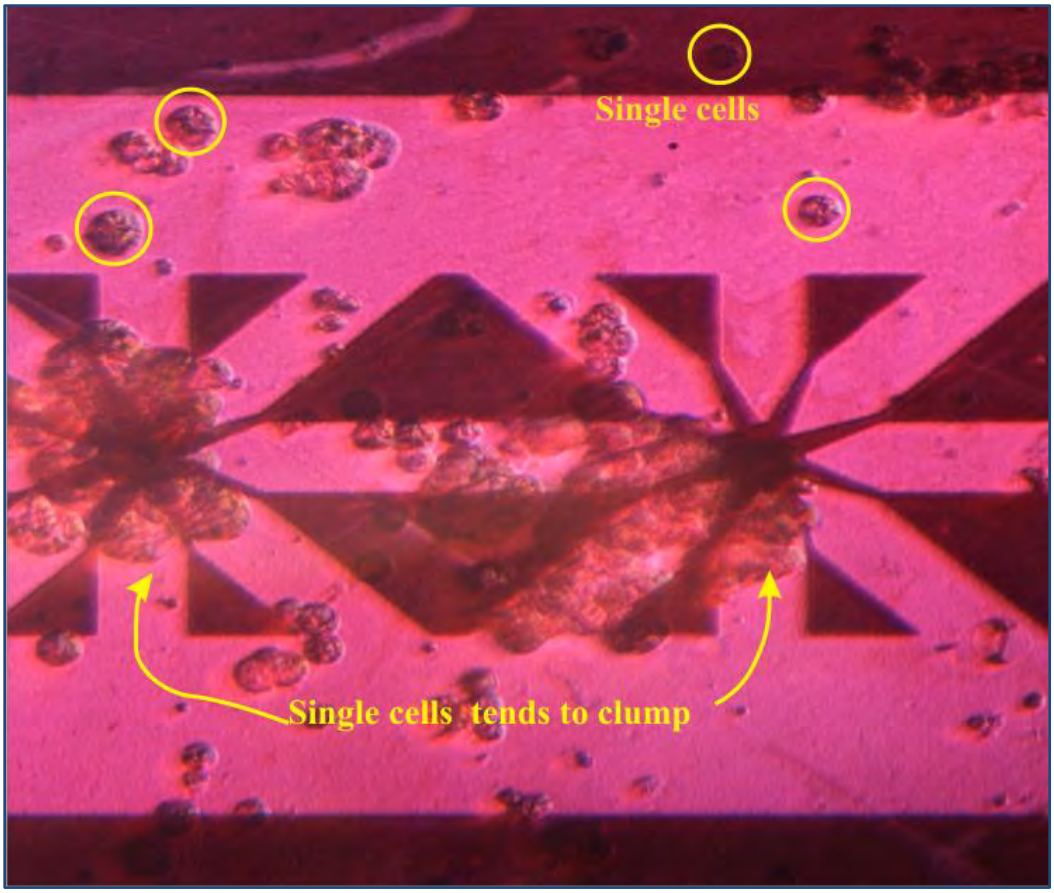

Figure 6.16: Trapping of the Ishikawa cancer cells using the adaptive octupole microelectrode on a 15mm x 15mm SIBC biochip.

6.2.5 The Effects of Amplitude and Frequency on DEP Experiments

In this section, the effects of amplitude and frequency on DEP experiments conducted inside a microfluidic channel are presented. The objective of this study is to characterize the working frame of the SIBC biochip. The measured conductivity of the cell minimum essential media (MEM) in Appendix E, was 12.8mS/m. Firstly, the frequency was maintained at 5MHz while the amplitude of AC signals was slowly increased from 0V to 20V. From the initial observations, there were no significant changes when the amplitude of AC signals was set below 10V. As the amplitude was increased to 13V, the microbeads started to show some vibration movements.

Then, as the amplitude reached 15V, the vibrations on the microbeads became stronger and small bubbles started to form. Within 10 seconds, these small bubbles increased in size, which forced the microbeads to move randomly inside the microfluidic channel as illustrated in Fig.6.13. When the amplitude was increased to 20V, the microelectrode was damaged within 3 seconds of the amplitude increment. The microbead vibrations and the forming of bubbles from the suspension mediums are signs of the electrothermal force inside the microfluidic channel.

To investigate the frequency limit of DEP experiments, the amplitude was maintained at 10V and the frequency was varied gradually from 5MHz down to 10Hz. At a frequency less than 100Hz, the conductive medium started to oxidise. As a result, the microelectrodes were damaged. At low frequency, the conductive medium created a very capacitive environment within the channel and increases the potentials between the microelectrodes.

On the contrary, varying the frequency at a high frequency range showed no significant changes. Nevertheless, the amplitude and frequency limits are dependents of the medium conductivity. Therefore it can be concluded that for conductivity of 12.8mS/m, the SIBC biochip can be operated using AC signals with amplitude ranging from 1V to 13V and frequency ranging from 101 Hz up to 5MHz.

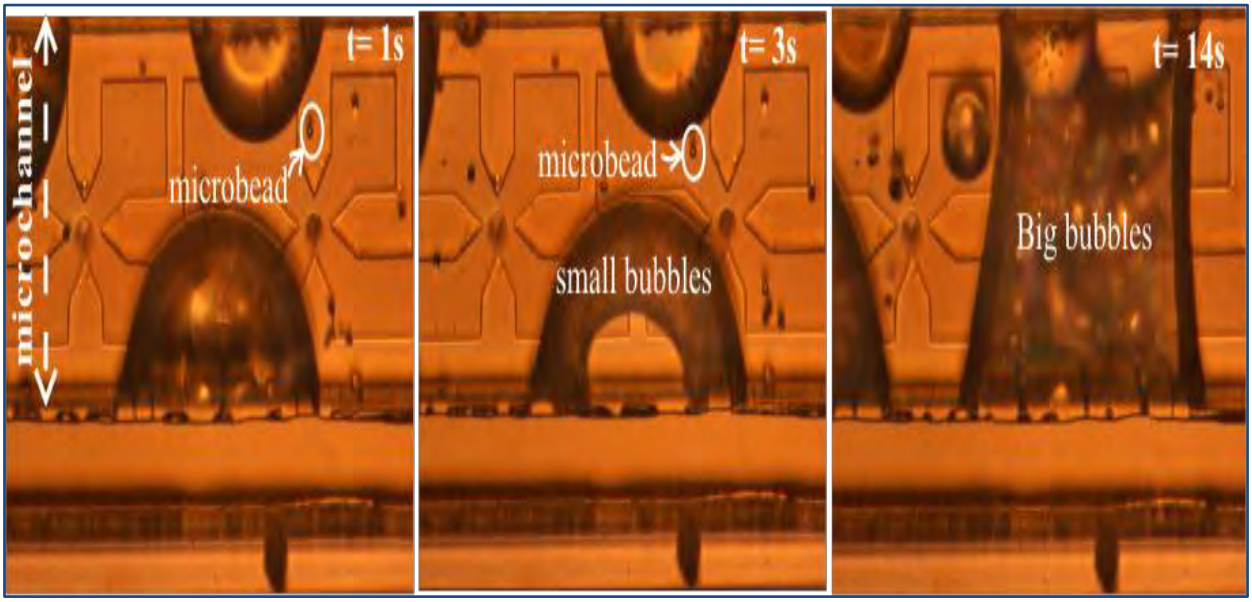

Figure 6.17: The effects of electrothermal inside the microfluidic channel with medium conductivity of 12.8mS/m at 15V, 5 MHz.

6.2.6 The Back Contact Attributes on Single Cells Trapping

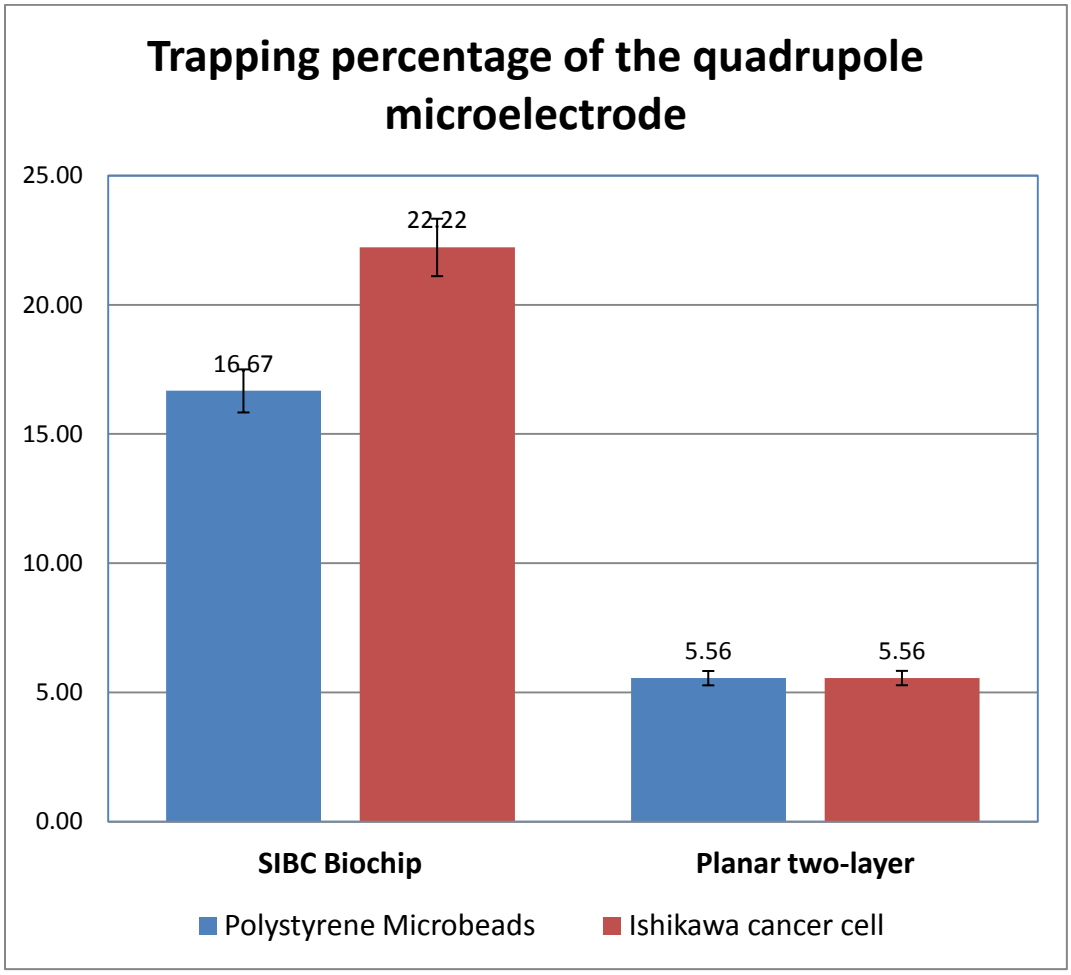

Figure 6.18: The trapping percentage of DEP experiments conducted on the SIBC and the planar two-layer biochips.

This section presents an experiment on the SIBC back contact attribute in enhancing the trapping of single cells. The DEP experiments were conducted using the quadrupole microelectrode structured on two types of biochip platform: the SIBC biochip and the planar two-layer biochip. The main objective is to observe the back contact performance in trapping

single cells. Here, two types of specimens were used, the polystyrene microbeads as the control specimen and the Ishikawa cancer cells as the live cells specimen.

The Ishikawa cancer cells (concentration of $3.4x10^6$cell/mL) were suspended in Eagle minimum essential media (Sigma Aldrich) diluted in a ratio of 1:5 with DI water, which resulted in a measured conductivity (σ_{eagle}) of 8.04mS/m. Meanwhile, the polystyrene microbeads (concentration of $1.45x10^6$cell/mL) were suspended in a sodium chloride (NaCl) medium with measured conductivity (σ_{NaCl}) of 8.2mS/m.

Trapping efficiency of the SIBC biochip is defined as the ratio of traps with trapped cells from the total traps available on the platform. There were 18 traps or microcavities located from 18 quadrupole microelectrodes. In these experiments, AC signal's frequency was varied from 500Hz to 5MHz while the amplitude was sustained at 10Vpp, until one frequency that initiate the movement was observed. The trapped single cells were counted after 10 minutes from the moment of the AC signal was switched 'ON'. Then, the microfluidic channels were flushed with deionised (DI) water to clean and remove any residues. For consistency, the experiments were repeated three times. Results in Fig.6.18 represent the average trapping events.

The results revealed that the SIBC biochip traps more particles than the planar two-layer biochip. Figure 6.18 showed that the SIBC biochip traps 16 percent of polystyrene microbeads and 22 percent of Ishikawa cancer cells. In contrary, the planar two-layer trapped only 5 percent of both specimens. Therefore, it can be suggested that the back contact enhanced particles trapping on a biochip platform.

The SIBC biochip also shows the ability to trap more living particles (22 percent of Ishikawa cells) than non-living particles (16 percent of polystyrene microbeads). This is due to the polarization effects on Ishikawa cell membranes towards the nDEP region. On the other hand, the polystyrene microbeads depend solely on the suspension medium dielectric polarization for moving towards microcavities. As a conclusion, the presence of back contact on SIBC biochip has significantly improved particle trapping of the quadrupole microelectrode.

6.3 Discussion

Results in section 6.2 showed that the trapping behaviour of the three microelectrodes. Works in that section, justify the significance of microelectrode geometry design has on cell trapping. Therefore, it can be inferred that cell movements on DEP-based biochip, are outcomes from the cumulative effects of microelectrode moments and dielectric properties towards the frequency of the supplied AC signals.

Results also show that trapping frequency of specific cell will differ, depending on the microelectrode patterns. For instance, at 2MHz, the dipole and the adaptive octupole microelectrodes demonstrated successful trapping events but the quadrupole pattern did not show any successful trapping. Another example, at 250kHz, only the dipole pattern showed evidence of trapping. This condition is probably due to the frequency dependency of electric field imaginary parts in Equation (3.13) [138], which results in selective trapping.

Nevertheless, the findings in Table 6.1, Table 6.2 and Table 6.3 demonstrated trapping ability of the three microelectrodes. However, results for the quadrupole and adaptive octupole patterns were inconclusive in terms of response towards frequency dependency. At 50kHz, the

polystyrene microbeads happened to cluster in the trapping region without moving into the microcavity pattern for the quadrupole microelectrode. Similar results were observed at 500 kHz, 1 MHz and 5 MHz for the adaptive octupole pattern. These results were probably due to the uneven spreading of microbeads on the biochip platform. To improve cell localization on the platform, the DEP experiments were then conducted in microfluidic channels, as explained in subsection 6.1.3. All three microelectrodes have created high electric fields surrounding the microcavities, in accord with the simulation results in Chapter Four, making it possible to attract single cells toward the trapping regions.

DEP experiments are limited by the frequency and amplitude of the applied voltage. Results in subsection 6.2.5 demonstrate common electrothermal effects induced by the Joule heating and the AC electro-osmosis. These effects on particles and/or cells contributed to the electro-convective flow or the acceleration of particle's movement which is more prevalent as the power dissipated to the fluid increases [139-140].

Another issue that limits the microelectrode's working range is the 'Faradaic rectification' effect. Apparently, AC and DC polarization have different effects on the electrode-medium boundary [141]. At high frequency, the interface of microelectrode-medium acts as a double-layer capacitance while at low frequency the boundary interface acts more likely as DC polarization. Therefore at a frequency less than 100Hz, the interface acts as a rectifier allowing one direction of current and resulted with irreversible corrosions of the microelectrode. As a consequence, depending on the electrochemical properties of the medium, the effect of polarization on the interface boundary can facilitate cell's movement into the trap or kill the cell.

Results in subsection 6.2.6 depict the advantage of having a back contact on the SIBC biochip. Clearly, the back contact can trap more cells than the planar two-layer biochip. Therefore, creating the microcavities or cell traps with electrodes that generate electric field does contribute to the total DEP trapping force, which in turn increases the trapping yield on the SIBC biochip.

6.4 Summary

This chapter has detailed the setup suitable for the DEP experiments and trapping results of the three microelectrodes. The experimental setup has evolved from the open biochip platform test to the close biochip platform test, and finally led to the use of microfluidic channels as explained in section 6.1. Clearly, observations on DEP experiments conducted inside a microfluidic channel were better when compared to the other two setups.

Assessments on the trapping ability for the three microelectrode patterns are vital to characterise cell manipulations on the SIBC biochip platform. The experiments have highlighted interesting trapping patterns between the three microelectrodes. As expected, moments exerted on the microbeads reflect on the distinct trapping pattern of the three microelectrodes and has a significant effect on DEP trapping. It can be concluded that trapping microbeads suspended in a specific medium may occur at different frequency from one microelectrode pattern to another pattern.

In subsection 6.2.6, results indicated that the back contact on the SIBC biochip enhances the trapping of Ishikawa cancer cells than when trapping using the planar two–layer biochip. Therefore, having microcavities or cell traps that also act as electrodes on a biochip can

contribute to the total DEP trapping force which in turn increases the trapping yield on the SIBC biochip. To summarize, this chapter presents experiments completed to assess SIBC biochip functionality. Future works will be discussed in Chapter Seven, with suggestions for improvement in the trapping yield and trapping behaviour of each microelectrode pattern.

Chapter Seven

Conclusions and Future Works

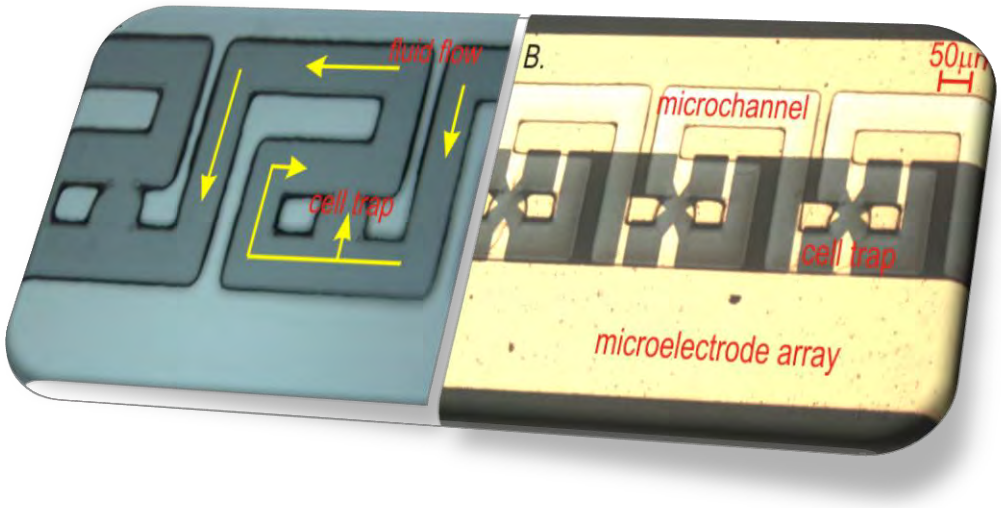

This chapter begins by summarising the work completed during the doctoral research. Then, discussion on contributions made by this work is presented in section 7.2. The chapter ends with an outline on future works for continuing research using the SIBC biochip platform.

7.1 Research Summary

The thesis presents a study on three new microelectrode patterns, the dipole, the quadrupole and the adaptive octupole microelectrode pattern, specifically for trapping single cells using Dielectrophoretic (DEP) force on a biochip platform. Arrays of these microelectrodes were fabricated on a multilayer (metal-insulator-metal layer) platform which is called the Sandwiched Insulator with Back Contact (SIBC) biochip. The microelectrodes were designed and simulated using COMSOL3.5a, fabricated using photolithography technique and tested using polystyrene microbeads and Ishikawa cancer cells.

In this study, the DEP force is used to control cell movements and directions on the biochip platform. Hence, the three patterns need to create a trapping region with a strong DEP holding force for trapping single cells, before a chemical stimulus or other studies on the trapped cell can be conducted. The three patterns have one similarity which is a cell trap (microcavity) surrounded by a numbers of electrode. This strategy is used to generate high DEP forces and create a DEP trapping region around the cell trap. The number of electrodes used are two-electrode (the dipole), four-electrode (the quadrupole) and eight-electrode (the adaptive octupole), in order to compare trapping behaviour between patterns. The multilayer structure allows the back contact which is formed by the first metal layer, to generate a DEP force within the microcavity. This is useful for anchoring trapped cell inside the trap.

Cells movements on the platform is achieved by connecting AC signals (φ) to the microelectrode patterns and the back contact. Directions on a platform are controlled by manipulating the phase and frequency of φ. Inside the cell membrane, charges polarize toward high (pDEP) or low (nDEP) electric field regions, in response to the supplied φ and the suspension media's dielectric properties. Therefore, great attention has to be given in defining the areas of nDEP or pDEP trapping regions, with respect to the shape of the microelectrodes during the design stage of SIBC biochip. Details on the background studies of DEP force and the three microelectrode designs are described in Chapter Three.

Studies on the electric field intensities and the DEP force profiles of the three microelectrode patterns described in Chapter Four, represents the actual trapping behaviour on the biochip. Results from these studies suggested that the DEP trapping regions occurred at locations between the tips of microelectrode and the edge of microcavity. Knowledge on the frequency of φ, the dielectric properties of cell membrane and suspension medium, can be used to predict cell's direction on the SIBC biochip. In reality, however, many cells demonstrate the nDEP behaviour since the effective conductivity and permittivity usually are much lower than that of the suspension media [142].

The SIBC biochip structure start with the back contact layer which consists of 20nm NiCr and 100nm Au layers deposited on a substrate. This study uses two types of substrate: the Silicon Nitride coated Silicon substrate and the glass slide as the biochip platform. Then, arrays of microcavities are formed on an insulator layer made of SU-8-2005 resist. This is followed by the three microelectrode patterns layer which consists of 20nm NiCr and 100nm Au layers deposited

on top of the SU-8 insulation layer. A resist called AZ1518 is used to define the microelectrode patterns. Then, two consecutive wet etching processed are conducted to remove unwanted area from the Au and NiCr layers.

Meanwhile, microfluidic channels used for regulating fluid and cell flows on the SIBC biochip are fabricated using softlithography technique. In this technique, SU-8-2100 is used to define the microfluidic channel structures on a Silicon wafer. Then, a mixture of PDMS is spread on the mould forming the microfluidic channels. Finally, the SIBC biochip and the microfluidic channels are bonded together in preparations for the trapping experiments. Descriptions on fabrication processes and issues encountered during fabrication of the SIBC biochip are detailed in Chapter Five.

The three microelectrode patterns on the SIBC biochip have demonstrated the ability of trapping particles using DEP forces. In Chapter Six, the trapping tests were conducted on polystyrene microbeads and the Ishikawa cancer cells using various frequencies and amplitudes of the φ. In order to study the back contact effects on single cells movement, trapping experiments were also conducted on a planar two-layer biochip structured with the three microelectrode patterns.

Results showed that on the SIBC biochip, there were significant differences on microbeads movement due to the DEP force generated by the back contact. The results also exhibit higher trapping yields on the SIBC biochip than the planar two-layer biochip. Overall, controlling living cell movements on both biochip platforms are not as easy and predictable as

movements of polystyrene microbeads. Hence, unprecedented results are always expected from the experiments, but can be minimised with proper experiment arrangements and repetitions.

7.2 Research Contributions

There are two key contributions made by this research as a result of the new microelectrodes design and experiments carried on the SIBC biochip platform. These contributions are:

1) The designs of three new microelectrode patterns for trapping single cells using DEP forces. The microelectrodes were specified according to the number of moments created within the cell membrane by the electrodes. In principal, and as demonstrated in results of section 6.2 of Chapter Six, these microelectrodes have distinct trapping patterns with respect to the frequency of the φ. Therefore, a specific configuration with respect to the frequency and phase of the φ, can generate DEP forces and direct single cells toward the microcavity on the SIBC biochip.

Movements of particles i.e., polystyrene and Ishikawa cells due to the DEP on SIBC biochip were demonstrated in Chapter Six and showed good agreements with numerical analysis results. From observations, particle trapping mechanism occurs in two steps; firstly, the particles were attracted to the tips of microelectrode and secondly, the particles moved from the tips into the microcavity.

The numbers of microelectrode generating the DEP force plays an important role in particle trapping particularly in the trapping yield. Yet, effects of the DEP force can only be observed through experimental approach due to the unique match of cells dielectric properties, the microelectrode design, the polarization factor (α) and the Claussius Mosotti factor ($K(\omega)$).

Therefore, a thorough study on microelectrode designs has to be conducted using numerical analysis for any DEP-based biochip, as it provides insights over the actual DEP effects.

2) Another contribution of the SIBC biochip is the multilayer design used to enhance trapping efficacy. Results in subsection 6.2.6 exhibit that trapping on SIBC biochip resulted with higher trapping yield than trapping on a planar two-layer biochip. Due to the multilayer structure, the φ configurations can move and direct single cells using nDEP or pDEP generated at areas between the microelectrode patterns and the back contact (at trapping region).

The flexibility in generating DEP force allows manipulation of various types of cell on the SIBC platform. By comparing results in Fig.6.6 and Fig. 6.7, the dipole microelectrode was able to trap single cells when the back contact was connected with φ. Undoubtedly, the back contact enhances single cells trapping on the SIBC biochip. Fig.4.22 and 4.23 also indicate that the gradients of electric field can be increased by the order of 10^3 on the SIBC biochip if compared to the planar two-layer biochip.

Another important aspect from the DEP experiments is the trapping regions on biochip. Findings showed that these trapping areas are dependent of φ phases which explained why it can limit the DEP force cell trapping manipulation on a biochip platform.

Interestingly, there were some unprecedented results shown in Table 6.2 and Table 6.3. Instead of going into the microcavity, the polystyrene microbeads concentrated at trapping region for the quadrupole and the adaptive octupole microelectrodes. Furthermore, the common nDEP and pDEP behaviour and the particle positioning sequences, were not observed during

experiments with the adaptive octupole microelectrode. One possible reason for these conditions is the higher moment effects on the particle.

In Equation (3.13), for electric field generated from more than one source, the imaginary part was omitted to simplify calculations of the microelectrode designs. The designed microelectrode generated electric field from the microelectrode pairs and inside the microcavity, which means the imaginary cross product of the setup might not be zero. Thus effects from the imaginary parts which been neglected in numerical studies may have significant effect on the trapping and trapping of the same particle type becomes more selective as demonstrated during experiments. However, more experiments are needed to better understand the effects of higher moment in controlling DEP force cell manipulations and characterize the three microelectrode designs.

7.3 Applications and Future Works

This section presents future works that can be implemented on the SIBC biochip. While the SIBC biochip platform provides a flexible trapping platform particularly in single cells trapping, its benefits to live science analysis can be expended through integration with other cell manipulation techniques. Therefore, continuing research on the SIBC biochip is aimed at maturing the platform functionalities and cells response towards DEP force. One aspect that needs improvement is the single cells trapping yield on the SIBC biochip, which can be further investigated through the alteration on the microfluidic channel design.

7.3.1 Future work I: Effects of the DEP Force on Organelles

One of the reasons of using a microfluidic channel on the SIBC biochip is to maintain cell viability. In Chapter Six, advantages of conducting DEP trapping experiments inside the microfluidic channels became evidence. Results in subsection 6.1.3 demonstrated that movement of polystyrene microbeads into the microcavity was clearly observed when experiments were conducted inside the microfluidic channel. Furthermore, the movement of nucleus and organelles of Ishikawa cancer cells in subsection 6.2.3 demonstrated that cell's membrane structure rupture due to the high DEP holding force can be avoided.

Undoubtedly, DEP force is a very flexible cell manipulation technique which can be used to navigate single cells on the SIBC biochip. Despite DEP force ability to trap cell, concerns over cell mortality after trapping was not studied during experiments. Up to this point, the cells conditions whether they are still alive or dead, have not been addressed. In Fig.6.13, the nucleus and organelles within the Ishikawa cell's membrane demonstrated some movements due to the DEP force. Therefore, there is no guarantee that the DEP force from the microelectrode designs will not damage the cell's structure. A way to confirm cell viability is through Trypan blue exclusion test. Future work should therefore concentrate on the effects of DEP force on cell's nucleus and other organelles trapped on the SIBC biochip. One way to study the DEP effects on nucleus is by using microfluidic channel traps shown in Fig.7.1. In this design, single cells are trapped inside the cell trap so that DEP force is used to observe the movements of nucleus and organelle.

7.3.2 Future work II: Enhancement of Trapping Yield using Microfluidic Traps

It is expected that the DEP force on SIBC biochip can accurately trap every single cell that flows in each microfluidic channel at the trapping region. However results in subsection 6.2.6 show that the trapping percentage was 22 percent. One of the possible reasons for the reduction in trapping yields is the DEP force reduces by distance from the source. Due to the microfluidic channel's height i.e., approximately 100 µm, many cells remain floating and were not affected by the effective DEP trapping force, which usually occurs on the surface of the SIBC biochip. Therefore, by reducing the channel heights proportionally to cell size, the trapping inside the microfluidic channel can be increased.

Another solution to increase the trapping yield is through the hydrodynamic component on the SIBC biochip or the microfluidic channels design. The microfluidic channels can be designed so that it can also functions as a cell trap. Studies have shown that trapping of cells was up to 97% trapping efficiency using non adherent mammalian cells when the microfluidic

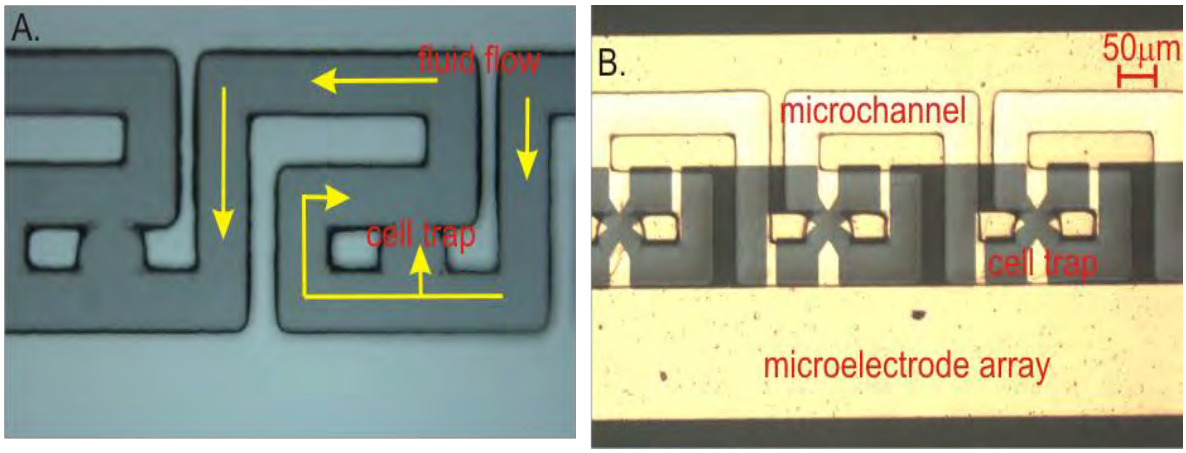

Figure7.1: The proposed microfluidic channel design to enhance trapping yield on the SIBC biochip.

channel was designed as a trapping channel [143]. One implication of the design is that trapping on SIBC biochip can be increased through combinations of the hydrodynamic effects and the DEP force.

In this design, each trap can only be filled with one cell. As illustrated in Fig.7.1, the single trap design, each microfluidic channel trap needs to be aligned with each microelectrode on the SIBC biochip. This design is useful for measuring a cell's membrane capacitance especially when only a single cell can be trapped inside each microcavity. Thus, the effect of a DEP force on the membrane capacitance of a single cell can be explored. Furthermore, it is possible to observe the relations between intracellular activities and the measured membrane's capacitance.

7.3.3 Future work III: Integration of Bioimprint Process on the SIBC Biochip

The main objective of the SIBC biochip is to produce a trapping platform for the implementation of Bioimprint technology [144] as detailed in subsection 2.3.1 of Chapter Two. Thus, the conceptual development of SIBC biochip has been focused on trapping single cells, as described in Chapter Three. The integration with the Bioimprint application can easily be implemented through regulated flow between the suspension medium and the polymer for imprint controlled by syringe pump.

Trapped cells inside microcavities can be replicated using photosensitive polymer flowed into the microfluidic channel. By using UV light, the imprint polymer is solidified which creates replica of the trapped cell inside the microfluidic channel. However, a technique to retrieve cured replica of trapped cells inside the microfluidic channel is one issue to be addressed. Another

important issue is material incompatibility between the imprint polymer and material used for structuring the SIBC biochip which can leads to permanent damage on the SIBC biochip. Therefore, integrating Bioimprint on the SIBC biochip has to be thoroughly studied.

7.4 Final Remarks

The SIBC described by the thesis has been designed to create a cell trapping platform, particularly for single cells studies. The SIBC biochip achieved its objective via three microelectrode designs, the dipole, the quadrupole and the adaptive octupole on a multilayer structure. In this study, the DEP force controls cell movements on the biochip while the microfluidic channels maintain the environment that promotes cell viability. In addition to the two features, the back contact enhances trapping ability of the designed microelectrodes.

The results produced so far are promising and demonstrate that the SIBC biochip platform can enhance single cells trapping. Research into the biochip is ongoing, and the next stages will involve integration of the biochip platform with other cell manipulation techniques and/or microfluidic designs. The works on SIBC biochip has demonstrated with precise controlled over cell movements, cell can be trapped at the required locations. Overall, the SIBC biochip has huge potentials in facilitating observation on single cells intercellular interactions.

APPENDIX A

% Calculating the CM factor

```
clear all
R=10e-6 ;                       %Particle Radius
f=logspace(2,10,1000);          % Generates 1000 points between decades 10^2 and 10^9.
Eps0=8.85e-12;                  %Natural Permittivity
%Condm1=1.960e-3;               % Material Conductivity in S/m from Nanoelectromechanics book (DI water
                                %approx  0.055u/S
Condm1 =4.52e-3;
Epsm=78*Eps0;                   % Permittivity Material from Nanoelectromechanics

Condp=5e-3;                      % Konduktiviti Particle (latex microbeads) in DI water
Epsp=2.55*Eps0;                 % Permittivity Particle
                                % frekuensi dalam log ( 10^2 to 10^9 dlm 1000 point)
mu=1e-3;                        % dynamic viscosity Pa.s
delD=10e-6;

%********** Calling KiraCm function**********
% KiraCm once
 [cmstop,output,fc]= CMa(Condm1,Condp,Epsp,Epsm)

% transform output into 1x1 matrix to be plotted in figure
 one = (output).';

 %calculate CM function with increment of medium conductivity 1mS each iteration
% calculate CM function dgn different medium conductivity

%The  KiraCm function
function [cmstop,output,fc]=KiraCm(Condm1,Condp,Epsp,Epsm)

%-------------------- Setting the frequency scale ----------------------
f=logspace(2,10,1000);
w=2*pi*f;
j=sqrt(-1);
fstop=250;
wstop=2*pi*fstop;

%-------------------- increment of the medium conductivity ------------
% ------------------- then calculate the Cm factor,fc -------------------
 % the  formula ./  allows operation between array for complex numbers

   Epspc=(Epsp-j*Condp./w);
   Epsmc=(Epsm-j*Condm1./w);
   Deno1=Epspc;
   Deno2=2*Epsmc;
   cm=(Epspc-Epsmc)./(Deno1+Deno2)                  % the Cmulm factor is...
```

```
% Set variable for real and imagenary CM  factor
output=real(cm);
output1=imag(cm);

%------------------checking the results-----------------------
Epspstop=(Epsp-j*Condp./wstop);
Epsmstop=(Epsm-j*Condm1./wstop);
Deno3=Epspstop;
Deno4=2*Epsmstop;
cmstop=(Epspstop-Epsmstop)./(Deno3+Deno4)      % the Cmulm factor is...

% Set variable for real and imagenary CM  factor
outputstop=real(cm);
outputstop1=imag(cm);

fc=D*C            % The cross over frequency for stipulated medium conductivity

% checking the crossover frequency

fc =(1/(2*pi))*sqrt(((Condm1-Condp)*(Condp+2*Condm1))/((Epsp-Epsm)*(Epsp+2*Epsm)))

 %----------------------Plotting result----------------------
 figure(1);
 semilogx(f,output,f,output1);

%set('String',[35])
h = legend('real(CM)','imag(CM)',-1);
hold all;

title('Claussius Mossotti factor Plot')
xlabel('frequency (Hz)');
ylabel('Re[k(w)]');
```

APPENDIX B

DEP Force expression with spatially dependent phase from [78]

In application of multiple potential of different phase, the derivation of DEP is needed. Given the electric field is $E\,(x,t) = Re\left[\vec{E}(x)e^{j\omega t}\right]$ and $\vec{E} = -\nabla\vec{\emptyset} = -(\nabla\emptyset_R + j\nabla\emptyset_I)$ is the corresponding complex phasor, the time-averaged force is then, $\langle F_{\mathrm{DEP}}\rangle = \frac{1}{2}\,V\,Re\left[\tilde{\alpha}\;(\vec{E}.\nabla)E^*\right]$. The electric field is simplified using vector identities and the fact that it has the same phase i.e. no rotation ($\nabla \times \vec{E} = 0$) and from Gauss's law that it has zero divergence, the expression becomes:

$$\langle F_{\mathrm{DEP}}\rangle = \frac{1}{4}\,V\,Re\,[\tilde{\alpha}\,]\nabla(\vec{E}.E^*) - \frac{1}{2}\,V\,Im\,[\tilde{\alpha}\,](\nabla \times (\vec{E} \times E^*))$$

$$\langle F_{\mathrm{DEP}}\rangle = \frac{1}{4}\,V\,Re\,[\tilde{\alpha}\,]\nabla\left|\vec{E}\right|^2 - \frac{1}{2}\,V\,Im\,[\tilde{\alpha}\,]\left(\nabla \times \left(\mathrm{Re}\,[\vec{E}] \times Im[\vec{E}]\right)\right)$$

where $\left|\vec{E}\right| = \left|\mathrm{Re}\left[\vec{E}\right]\right|^2 + \left|Im[\vec{E}]\right|^2$.

In no spatial varying phase condition, the phasor can be taken to be real i.e, $\left|Im\left[\vec{E}\right]\right|^2 = 0$. The derivations are following the vector identity:

$$\nabla(A.B) = (A.\nabla)B + (B.\nabla)A + B \times (\nabla \times A) + A \times (\nabla \times B)$$

$$\nabla \times (A \times B) = (B.\nabla)A - (A.\nabla)B + (\nabla.B)A - (\nabla.A)\mathrm{B}$$

Table for the Electric field distributions analytical solutions from [115] .

Note:	V_1 and V_2 : electrode potentials h_n : the constant for defining electrode size.	
n (n=1,2,..)	$\lvert E\rvert = \sqrt{(E_x^2 + E_y^2)}$	$\nabla \lvert E\rvert^2$
2	$2\frac{V_2 - V_1}{2h_2}\sqrt{x^2 + y^2}$	$8\left(\frac{V_2 - V_1}{2h_2}\right)^2 \sqrt{x^2 + y^2}$
4	$4\frac{V_2 - V_1}{2h_4}(x^2 + y^2)^{1.5}$	$96\left(\frac{V_2 - V_1}{2h_4}\right)^2 (x^2 + y^2)^{2.5}$
8	$8\frac{V_2 - V_1}{2h_8}(x^2 + y^2)^{3.5}$	$896\left(\frac{V_2 - V_1}{2h_8}\right)^2 (x^2 + y^2)^{6.5}$
n	$n\frac{V_2 - V_1}{2h_n}(x^2 + y^2)^{0.5\,(n-1)}$	$2(n-1)n^2\left(\frac{V_2 - V_1}{2h_n}\right)^2 (x^2 + y^2)^{n-1.5}$
Note:	V_1 and V_2 : electrode potentials h_n : the constant for defining electrode size.	

APPENDIX C

Matlab Code for the polynomial electrodes (Dipole)

```
clear all

x = -40e-6:2e-6:40e-6;      %creates x- array with values from -40x10^-6 in 0.2 x10^-6 step up to 40x10^-6
y = -40e-6:2e-6:40e-6;      %creates y- array with values from -40x10^-6 in 0.2 x10^-6 step up to 40x10^-6
y (1:4)                     %Print the first four values of the y array for inspection
[xx,yy] = meshgrid(x,y);     %meshgrid creates an x-y grid with the coordinates
                             %of the point given by the vectors  x and y;
                            %the matrices xx and yy contain the x-values at the grid points.
xx(14:16,14:16)
yy(14:16,14:16)

Vrms= 10;                   % Assuming the Vrms = 10
r=sqrt(xx.^2+yy.^2);
d=(sqrt((yy.*xx).*17));     %Distance between tips of hyperbola function

Z=(2.*Vrms)./(2.*abs(d));              %Electric field for dipole electrode
Zc=(2.*Vrms)./(2.*abs(d)).*r;  %Dipole |E| formula from Huang 1990 for negative DEP for the centre region at (0,0)
E2=gradient(Z.^2);                    %  Electric field gradient
E2c=gradient(Zc.^2);                  % Electric field gradient at centre of electrode

% ***************Contour of the analytical solutions**********************
figure(1)
[C,h] = contour(x,y,d,4);colormap spring;              %plot the contour of the xy between two tips
clabel(C);
xlabel('x');ylabel('y');
title('Hyperbola tips geometry analytical solutions i.e. xy=(d^2/17)');     % a=constant=17 to get 33um distance

% ***************Surf of |E| gradient of the dipole  analytical solutions**********
figure(2)
[U,V,W] = surfnorm(xx,yy,Zc);                          % surface normal to DEP component
quiver3(Zc,U,V,1);                                     %arrow of DEP components
view(180,0)

% ***************Surf of |E| of the dipole  analytical solutions**********
figure(3)
g = surf(xx,yy,Zc,'LineStyle','none', ...
  'FaceLighting','gouraud', ...
  'FaceColor','interp');
colormap jet
view(180,0)
hold off

ans =
```

```
 1.0e-004 *
  -0.4000   -0.3800   -0.3600   -0.3400

ans =
 1.0e-004 *
  -0.1400   -0.1200   -0.1000
  -0.1400   -0.1200   -0.1000
  -0.1400   -0.1200   -0.1000
ans =
 1.0e-004 *
  -0.1400   -0.1400   -0.1400
  -0.1200   -0.1200   -0.1200
  -0.1000   -0.1000   -0.1000
Published with MATLAB® 7.6
```

Matlab Code for the polynomial electrodes (Quadrupole)

```
% polynomial electrode in x-y plane is defined as |x^2-y^2|=k^2
%and 2k = distance between apposing electrode
%************* The Electric field ***************
clear all

g=20e-6;
x = -40e-6:2e-6:40e-6;      % creates x- array with values from -40x10^-6 in 2 x10^-6 step up to 40x10^-6
y = -40e-6:2e-6:40e-6;      % creates y- array with values from -40x10^-6 in 2 x10^-6 step up to 40x10^-6
y(1:4)                      %Print the first four values of the y array for inspection

[xx,yy] = meshgrid(x,y);    %meshgrid creates an x-y grid with the coordinates
                            %of the point given by the vectors  x and y;
                            %the matrices xx and yy contain the x-values at the grid points.
xx(1:20,1:20)
yy(1:20,1:20)

Vrms= 10; % Assuming the Vrms = 10
a=2;

r=(xx.^2+yy.^2).^1.5;               % r (0,0) for quadrupole
d=abs(sqrt((xx.*yy))./0.2);         %polynomial electrode geometry in x-y plane for 40um
Zc=((4.*Vrms)./(2.*abs(d))).*r;     %Quadrupole |E| formula from Huang 1990 for negative DEP for the centre
                                        % region at (0,0)
Z=((4.*Vrms)./(2.*abs(d)));         %|E| field at the tips of electrode
E2=gradient(Z.^2);                  %  Electric field gradient
E2c=gradient(Zc.^2);                % Electric field gradient at centre of electrode

% ***************Contour of the analytical solutions**********************
figure(1)
[C,h]=contour(x,y,d,4)
clabel(C);
hold on
```

```
% ***************Surf of |E| of the quadrupole analytical solutions**********
figure(2)
s = surf(Z,'LineStyle','none', ...
  'FaceLighting','gouraud', ...
  'FaceColor','interp');
colormap jet
hold on

% ***************Surf of |E|  at central region (0,0) *********************
figure(3)
s = surf(Zc,'LineStyle','none', ...
  'FaceLighting','gouraud', ...
  'FaceColor','interp');
colormap hsv
hold off

figure(4)
[U,V,W] = surfnorm(xx,yy,Zc);% surface normal to DEP component
quiver3(Zc,U,V,1);%arrow of DEP components
view(180,0)
```

Matlab Code for the polynomial electrodes (Octupole)

```
% polynomial electrode in x-y plane is defined as |x^2-y^2|=k^2
%and 2k = distance between apposing electrode
%************* The Electric field ***************
clear all

x = -20e-6:2e-6:20e-6;      % creates x- array with values from -20x10^-6 in 2 x10^-6 step up to 20x10^-6
y = -20e-6:2e-6:20e-6;      % creates y- array with values from -20x10^-6 in 2 x10^-6 step up to 20x10^-6

y(1:4)  %Print the first four values of the y array for inspection

[xx,yy] = meshgrid(x,y); %meshgrid creates an x-y grid with the coordinates
                          %of the point given by the vectors  x and y;
                          %the matrices xx and yy contain the x-values at the grid points.
xx(10:10,10:10)
yy(10:10,10:10)

% setting the components of polynomial electrode equation for n=4 (octupole)
Vrms=10;
p=(xx.^2).*(yy.^2);                 % define the p  variable
v=(xx.^3).*yy;                      % define the v  variable
q=xx.*(yy.^3);                      % define the q variable

a=12;                               %a constant value
b=200;                              %a constant value
```

```
r=(xx.^2+yy.^2).^3.5;                          % r (0,0) for octupole
d=abs((xx.*yy)./10).^0.5;                      %distance between two opposing electrodes
j=(a.*(xx.^4 -(6.*p)+ yy.^4)+ b.*(v - q));     %c=sqrt((xx.^2+yy.^2));      % microcavity

Zc=((8.*Vrms)./(2.*d)).*r;   %Octupole |E| formula from Huang 1990 for negative DEP for the centre region at (0,0)
Z=((8.*Vrms)./(2.*d));        %|E| field at the tips of electrode
T=conj(Z);
E2=gradient(Z.^2);            %  Electric field gradient
E2c=gradient(Zc.^2);          % Electric field gradient at centre of electrode

% ***************Contour of the analytical solutions**********************
figure(1)
[C,h] = contour(x,y,j,4);       %plot the contour of the octupole electrode
hold on

% ***************Surf of |E| of the quadrupole analytical solutions**********
figure(2)
s = surf(Z,'LineStyle','none', ...
  'FaceLighting','gouraud', ...
  'FaceColor','interp');
colormap jet
hold on

% ***************Surf of |E|  at central region (0,0) *********************
figure(3)
s = surf(Zc,'LineStyle','none', ...
  'FaceLighting','gouraud', ...
  'FaceColor','interp');
colormap hsv
hold off

figure(4)
[U,V,W] = surfnorm(xx,yy,Z);% surface normal to DEP component
quiver3(Z,U,V,1);%arrow of DEP components
view(180,0)

ans =
  1.0e-004 *
   -0.2000   -0.1800   -0.1600   -0.1400
ans =
 -2.0000e-006
ans =
 -2.0000e-006
```

APPENDIX D

1.Maxwell's Equations in AC electrokinetics in electrostatic:

$E = -\nabla \phi$, the electric field is irrotational

$\nabla . J + \frac{\partial \rho}{\partial t} = 0$, the charge conservation equation

$\nabla . D = \rho$, The Gauss's equation

J is the conduction current,ρ is the free charge density and D is the electric flux density or the displacement vector.

2.Neumann condition:

Boundary condition imposed on an ordinary or a partial differential equation. The value is specified by the derivative of a solution taken on the boundary of the domain. In the case microelectrode design, the boundary condition is specified as:

$\frac{\partial \phi}{\partial \mathrm{n}} = 0$.

APPENDIX E

Preparation of Ishikawa Cancer Cells

1.Basal Media

1. Dissolve 5 packs of MEM powder in 5 liters of autoclaved DI water.
2. Then, add Na_2CO_3 according to instructions (at the pack).
3. Adjust pH to about 7.2
4. Filter the media into 1-liter bottle. (total basal media prepared = 5 bottles).
5. Then stores at 4 degree for at least 24 hrs before usage.

2.Working Media (ex. 400 ml; v/v%)

1. Add 4 ml of Sodium Pyruvate (P/S) making 1% of medium content.
2. Add 4 ml of Glutamax making 1% of medium content.
3. Add 40 ml of Fetal Bovine Serum (FBS) making 10% of medium content.

Optional: add Fungizone at 2 ug/ml final concentration.

4. Top up with basal media up to 400 ml.
5. Store the medium at store at 4ºC.

Note : The prepared medium need to be used within one month.

3. Cells preparation for storing in N_2

1. Trypsinise cells and centrifuge at 1600 rpm for 5 min.
2. Collect cell pellets and add 10 ml of PBS.
3. Centrifuge at 1600 rpm for 5 min
4. Discard solution and add media solution containing 10% DMSO, 90% FBS.
5. Pipette 1 ml into cytotubes.
6. Put in -80 ºC for 24 hr.

7. Put cells in liquid N_2 for long term storage.

4.Preparation for solution containing 10% DMSO, 90% FBS (5 ml).

1. Pipette 4.5 ml FBS into 15 ml tube.
2. Add 0.5 ml Dimethyl sulfoxide (DMSO).
3. Mix properly.
4. Add solution to cell pellet.

5.Preparation for 200ml M199 solution

1. 2ml penicillin streptomycin + 2ml glutamax + 20ml fbs + 176ml base media.
2. Mix properly.
3. Add solution to cell pellet.

REFERENCES

[1] D.R. Reyes, D. Iossifidis, P.-A. Auroux, and A. Manz, "Micro Total Analysis Systems : 1. Introduction,Theory, and Technology," *Anal. Chem. 2002,* vol. 74, pp. 2623-2636, 2002.

[2] A. Manz, "Miniaturizing Conventional Analytical Methods: Electrophoresis, Chemical Reactors and Detection," vol. 2, pp. 1638-1639 vol.1632, 2002.

[3] C. Chia-Fu and F. Zenhausern, "Electrodeless Dielectrophoresis for Micro Total Analysis Systems," *Engineering in Medicine and Biology Magazine, IEEE,* vol. 22, pp. 62-67, 2003.

[4] A. VandenBerg, P. Bergveld, D.N. Reinhoudt, M. Elwenspoek, and J.H.J. Fluitman, "Miniaturized Chemical Analysis Systems," in *The 5th International Symposium on Micro Machine and Human Science*, 1994, p. 181.

[5] M.J. Madou, *Fundamentals of Microfabrication : The Science of Miniaturization*, 2 ed.: CRC Press 2002.

[6] K. Chakrabarty and J. Zeng, "Design Automation for Microfluidics-Based Biochips," *ACM Journal of Emerging technologies in Computing Systems,* vol. 1, pp. 186-223, 2005.

[7] S.P. Forry, D.R. Reyes, M. Gaitan, and L.E. Locascio, "Cellular Immobilization within Microfluidic Microenvironments: Dielectrophoresis with Polyelectrolyte Multilayers," *J. Am. Chem. Soc.,* vol. 128, pp. 13678-13679, 2006.

[8] H. Lee, Y. Liu, D. Ham, and R.M. Westervelt, "Integrated Cell Manipulation System--Cmos/Microfluidic Hybrid," *Lab on a chip,* vol. 7, pp. 331-337, 2007.

[9] J. Muys, "Cellular Analysis by Atomic Force Microscopy," PhD, Electrical and Computer Engineering, University Of Canterbury, Christchurch, 2006.

[10] M. Bocchi, M. Lombardini, A. Faenza*, et al.*, "Dielectrophoretic Trapping in Microwells for Manipulation of Single Cells and Small Aggregates of Particles," *Biosensors and Bioelectronics,* vol. 24, pp. 1177-1183, 2009.

[11] L.S. Jang, P.H. Huang, and K.C. Lan, "Single Cell Trapping Utilizing Negative Dielectrophoretic Quadrupole and Microwell Electrodes," *Biosensors and Bioelectronics,* vol. 24, pp. 3637-3644, 2009.

[12] A.C. Guyton, *Textbook of Medical Physiology* 8th ed. Philadelphia: Saunders, 1991.

[13] E.N. Marieb, *Essentials of Human Anatomy and Physiology* 5th ed. ed. Menlo Park, Calif. : Benjamin/Cummings Pub. Co., c1997.

[14] A.I. Lamond, "Molecular Biology of the Cell, 4th Edition," *Nature,* vol. 417, pp. 383-383, May 2002.

[15] M. Jenkner, M. Tartagni., A. Hierlemann, and R. Thewes, "Cell-Based Cmos Sensor and Actuator Arrays," *IEEE Journal Of Solid-State Circuits,* vol. 39, pp. 2431-2437, December 2004.

[16] J.J. Muys, M.M. Alkaisi, and J.J. Evans, "Cellular Replication and Atomic Force Microscope Imaging Using a Uv-Bioimprint Technique," *Nanomedicine: Nanotechnology, Biology and Medicine,* vol. 2, pp. 169-176, 2006.

[17] J.J. Muys, M.M. Alkaisi, and J.J. Evans, "Bioimprint," in *International Conference on Nanoscience and Nanotechnology ICONN '06.*, 2006.

[18] J.V. Sweedler and E.A. Arriaga, "Single Cell Analysis," in *Analytical & Bioanalytical Chemistry* vol. 387, ed: Springer Science & Business Media B.V., 2007, pp. 1-2.

[19] S. Yue and Y. Xue-Feng, "Novel Multi-Depth Microfluidic Chip for Single Cell Analysis," *Journal of Chromatography A,* vol. 1117, pp. 228-233, 2006.

[20] E.A. Arriaga, *Single Cell Heterogeneity*: Wiley-VCH Verlag GmbH & Co. KGaA, 2009.

[21] M. Sakaguchi, "Eukaryotic Protein Secretion," *Current Opinion in Biotechnology,* vol. 8, pp. 595-601, 1997.

[22] B. Polzer, C.H. Hartmann, and C.A. Klein, *Genome and Transcriptome Analysis of Single Tumor Cells*: Wiley-VCH Verlag GmbH & Co. KGaA, 2009.

[23] V.V. Abhyankar and D.J. Beebe, "Spatiotemporal Micropatterning of Cells on Arbitrary Substrates," *Analytical Chemistry,* vol. 79, pp. 4066-4073, 2007.

[24] A. Folch and M. Toner, "Microengineering of Cellular Interactions," *Annual Review of Biomedical Engineering,* vol. 2, pp. 227-256, 2000.

[25] H. Kaji, T. Kawashima, and M. Nishizawa, "Patterning Cellular Motility Using an Electrochemical Technique and a Geometrically Confined Environment," *Langmuir,* vol. 22, pp. 10784-10787, 2006.

[26] J. El-Ali, P.K. Sorger, and K.F. Jensen, "Cells on Chips," *Nature,* vol. 442, pp. 403-411, 2006.

[27] K.G. Klemic, J.F. Klemic, M.A. Reed, and F.J. Sigworth, "Micromolded Pdms Planar Electrode Allows Patch Clamp Electrical Recordings from Cells," *Biosensors and Bioelectronics,* vol. 17, pp. 597-604, 2002.

[28] F.J. Sigworth, J.F. Klemic, and K.G. Klemic, "An Air-Molding Technique for Fabricating Pdms Planar Patch-Clamp Electrodes," *Pflügers Archiv European Journal of Physiology,* vol. 449, pp. 564-572, 2005.

[29] T. Lehnert, M.A.M. Gijs, R. Netzer, and U. Bischoff, "Realization of Hollow Sio2 Micronozzles for Electrical Measurements on Living Cells," *Applied Physics Letters,* vol. 81, pp. 5063-5065, 2002.

[30] F.J. Sigworth and K.G. Klemic, "Patch-Clamp Technologies for Ion Channel Research," in *Biological Membrane Ion Channels*, S.-H. Chung, O.S. Andersen, and V. Krishnamurthy, Eds., 1 ed: Springer New York, 2007, pp. 571-593.

[31] R.M. Johann, "Cell Trapping in Microfluidic Chips," *Analytical And Bioanalytical Chemistry,* vol. 385, pp. 408-412, 2006.

[32] M.D. Armani, S.V. Chaudhary, R. Probst, and B. Shapiro, "Using Feedback Control of Microflows to Independently Steer Multiple Particles," *Journal of Microelectromechanical Systems,* vol. 15, pp. 945-956, 2006.

[33] S.S. Kohles, D.C. Tretheway, N. NÃ¨ve, and S.R. Winn, "Manipulation of Suspended Single Cells by Microfluidics and Optical Tweezers," *Cellular and molecular bioengineering,* vol. 3, pp. 213-228, 2010.

[34] J. Scrimgeour, W. Timp, K. Beck*, et al.*, "Live Cell Lithography: Using Optical Tweezers to Create Synthetic Tissue," *Lab on a Chip,* vol. 8, pp. 2174-2181, 2008.

[35] X.B. Wang, Y. Huang, P.R.C. Gascoyne, and F.F. Becker, "Dielectrophoretic Manipulation of Particles," *IEEE Transactions on Industry applications,* vol. 33, pp. 660-669, May/June 1997.

[36] D. Trinh Chu, L. Gih-Keong, and P.M. Sarro, "Polymeric Thermal Microactuator with Embedded Silicon Skeleton: Part 2 Fabrication, Characterization, and Application for 2-D of Microgripper," *Journal of Microelectromechanical Systems,* vol. 17, pp. 823-831, 2008.

[37] D. Trinh Chu, L. Gih-Keong, J.F. Creemer, and P.M. Sarro, "Electrothermal Microgripper with Large Jaw Displacement and Integrated Force Sensors," *Journal of Microelectromechanical Systems,* vol. 17, pp. 1546-1555, 2008.

[38] B. Solano and D. Wood, "Design and Testing of a Polymeric Microgripper for Cell Manipulation," *Microelectronic Engineering,* vol. 84, pp. 1219-1222, 2007.

[39] R.M. Johann and P. Renaud, "Microfluidic Patterning of Alginate Hydrogels," *Biointerphases,* vol. 2, pp. 73-79, 2007.

[40] T. Braschler, R. Johann, U. Seger, H. Van Lintel, and P. Renaud, "Single Cell Study in a Hydrogel," in *Cell Technology for Cell Products*, R. Smith, Ed., ed: Springer Netherlands, 2007, pp. 291-295.

[41] W.-H. Tan and S. Takeuchi, "Dynamic Microarray System with Gentle Retrieval Mechanism for Cell-Encapsulating Hydrogel Beads," *Lab on a Chip,* vol. 8, pp. 259-266, 2008.

[42] J.R. Rettig and A. Folch, "Large-Scale Single-Cell Trapping and Imaging Using Microwell Arrays," *Analytical Chemistry,* vol. 77, pp. 5628-5634, 2005.

[43] T. Melikhan, E.M. Johnson-Chavarria, and C.M. Schroeder, "Hydrodynamic Trap for Single Particles and Cells," *Applied Physics Letters,* vol. 96, p. 224101, 2010.

[44] A.L. Hodgkin and A.F. Huxley, "Resting and Action Potentials in Single Nerve Fibres," *The Journal of physiology,* vol. 104, pp. 176-195, 1945.

[45] W. Losert, K. Okamoto, D. English, and C. Poole, "Probing Local and Large Scale Membrane Stiffness of Giant Unilamellar Vesicles with Holographic Laser Tweezers," *Biophysical journal,* vol. 88, p. 414A, 2005.

[46] T. Muller, A. Pfennig, P. Klein, G. Gradl, M. Jager, and T. Schnelle, "The Potential of Dielectrophoresis for Single-Cell Experiments," *Engineering in Medicine and Biology Magazine, IEEE,* vol. 22, pp. 51-61, 2003.

[47] N. Manaresi, A. Romani, G. Medoro*, et al.*, "A Cmos Chip for Individual Cell Manipulation and Detection," *IEEE Journal Of Solid-State Circuits,* vol. 38, p. 2297, 2003.

[48] H.A. Pohl, "The Motion and Precipitation of Suspensoids in Divergent Electric Fields," *J. Appl. Phys.,* vol. 22, p. 869, 1951.

[49] H.A. Pohl, *Dielectrophoresis*: Cambridge University Press, 1978.

[50] J.S. Crane and H.A. Pohl, "A Study of Living and Dead Yeast Cells Using Dielectrophoresis," *Journal of The Electrochemical Society,* vol. 115, pp. 584-586, 1968.

[51] L. Benguigui and I.J. Lin, "Experimental Analysis of Dielectrophoretic Forces," *Journal of Applied Physics,* vol. 49, pp. 2536-2539, 1978.

[52] T.B. Jones and G.W. Bliss, "Bubble Dielectrophoresis," *Journal of Applied Physics,* vol. 48, pp. 1412-1417, 1977.

[53] A.S. Bahaj and A.G. Bailey, "Dielectrophoresis of Microscopic Particles," *Journal of Physics D: Applied Physics,* vol. 12, p. L109, 1979.

[54] T. Schnelle, T. Müller, G. Gradl, S.G. Shirley, and G. Fuhr, "Paired Microelectrode System: Dielectrophoretic Particle Sorting and Force Calibration," *Journal of Electrostatics,* vol. 47, pp. 121-132, 1999.

[55] S. Fiedler, S.G. Shirley, T. Schnelle, and G. Fuhr, "Dielectrophoretic Sorting of Particles and Cells in a Microsystem," *Analytical Chemistry,* vol. 70, pp. 1909-1915, 1998.

[56] J. Cheng, E.L. Sheldon, L. Wu, M.J. Heller, and J.P. O'Connell, "Isolation of Cultured Cervical Carcinoma Cells Mixed with Peripheral Blood Cells on a Bioelectronic Chip," *Analytical Chemistry,* vol. 70, pp. 2321-2326, 1998.

[57] T. Matsue, N. Matsumoto, S. Koike, and I. Uchida, "Microring-Ring Electrode for Manipulation of a Single Cell," *Biochimica et Biophysica Acta (BBA) - General Subjects,* vol. 1157, pp. 332-335, 1993.

[58] J. Suehiro and R. Pethig, "The Dielectrophoretic Movement and Positioning of a Biological Cell Using a Three-Dimensional Grid Electrode System," *Journal of Physics D: Applied Physics,* vol. 31, p. 3298, 1998.

[59] F.F. Becker, "Separation of Human Breast-Cancer Cells from Blood by Differential Dielectric Affinity," *Proc. Natl Acad. Sci. USA,* vol. 92, pp. 860-864, 1995.

[60] X.-B. Wang, J. Vykoukal, F.F. Becker, and P.R.C. Gascoyne, "Separation of Polystyrene Microbeads Using Dielectrophoretic/Gravitational Field-Flow-Fractionation," vol. 74, pp. 2689-2701, 1998.

[61] J. Rousselet, G.H. Markx, and R. Pethig, "Separation of Erythrocytes and Latex Beads by Dielectrophoretic Levitation and Hyperlayer Field-Flow Fractionation," *Colloids and Surfaces A: Physicochemical and Engineering Aspects,* vol. 140, pp. 209-216, 1998.

[62] A. Docoslis, N. Kalogerakis, L.A. Behie, and K.V.I.S. Kaler, "A Novel Dielectrophoresis-Based Device for the Selective Retention of Viable Cells in Cell Culture Media," *Biotechnology and Bioengineering,* vol. 54, pp. 239-250, 1997.

[63] G.H. Markx and C.L. Davey, "The Dielectric Properties of Biological Cells at Radiofrequencies: Applications in Biotechnology," *Enzyme and Microbial Technology,* vol. 25, pp. 161-171, 1999.

[64] Y. Ghallab and B. Badawy, "Sensing Methods for Dielectrophoresis Phenomenon: From Bulky Instruments to Lab-on-a-Chip," *IEEE Circuits and Systems Magazine,* p. 5, 2004.

[65] E.G. Cen, C. Dalton, Y. Li, S. Adamia, L.M. Pilarski, and K.V.I.S. Kaler, "A Combined Dielectrophoresis, Traveling Wave Dielectrophoresis and Electrorotation Microchip for the Manipulation and Characterization of Human Malignant Cells," *Journal of Microbiological Methods,* vol. 58, pp. 387-401, 2004.

[66] D.J. Bakewell and M. Hywel, "Dielectrophoresis of DNA: Time- and Frequency-Dependent Collections on Microelectrodes," *IEEE TRANSACTIONS ON NANOBIOSCIENCE, ,* vol. VOL. 5, pp. 1-8, 2006

[67] S. Claudio, G. Carlotta, B. Luca*, et al.*, "A Fully Electronic Label-Free DNA Sensor Chip," *Sensors Journal, IEEE,* vol. 7, pp. 577-585, 2007.

[68] M. Hoeb, J.O. Radler, S. Klein, M. Stutzmann, and M.S. Brandt, "Light-Induced Dielectrophoretic Manipulation of DNA," *Biophys. J.,* vol. 93, pp. 1032-1038, August 1, 2007 2007.

[69] S. Nedelcu and J.H.P. Watson, "Size Separation of DNA Molecules by Pulsed Electric Field Dielectrophoresis," *Journal of Physics D: Applied Physics,* vol. 37, p. 2197, 2004.

[70] T. Kawabata and M. Washizu, "Dielectrophoretic Detection of Molecular Bindings

" *IEEE Transactions on Industry Applications,* vol. 37, pp. 1625-1633, 2001.

[71] L. Zheng, S. Li, P.J. Burke, and J.P. Brody, "Towards Single Molecule Manipulation with Dielectrophoresis Using Nanoelectrodes," *IEEE,* vol. 03, 2003.

[72] S. Gagliardi, B. Rapone, L. Mosiello, D. Luciani, A. Gerardino, and P. Morales, "Laser-Assisted Fabrication of Biomolecular Sensing Microarrays," *NanoBioscience, IEEE Transactions on,* vol. 6, pp. 242-248, 2007.

[73] N. Flores-Rodriguez and G.H. Markx, "Flow-through Devices for the Ac Electrokinetic Construction of Microstructured Materials," *Journal of Micromechanics and Microengineering,* vol. 16, p. 349, 2006.

[74] D. Aristides and A. Paschalis, *One, Two, and Three Dimensional Organization of Colloidal Particles Using Nonuniform Alternating Current Electric Fields* vol. 23. Berlin,Allemagne: Wiley-VCH, 2002.

[75] R. Pethig, M.S. Talary, and R.S. Lee, "Enhancing Traveling-Wave Dielectrophoresis with Signal Superposition," *Engineering in Medicine and Biology Magazine, IEEE,* vol. 22, pp. 43-50, 2003.

[76] P. Gascoyne, "Microsample Preparation by Dielectrophoresis: Isolation of Malaria," *Lab Chip,* vol. 2, pp. 70-75, 2002.

[77] R.S. Thomas, H. Morgan, and N.G. Green, "Negative Dep Traps for Single Cell Immobilisation," *Lab on a Chip,* vol. 9, pp. 1534-1540, 2009.

[78] H. Michael Pycraft, "Ac Electrokinetics: Applications for Nanotechnology," *Nanotechnology,* vol. 11, p. 124, 2000.

[79] T. Müller and et al., "Trapping of Micrometre and Sub-Micrometre Particles by High-Frequency Electric Fields and Hydrodynamic Forces," *Journal of Physics D: Applied Physics,* vol. 29, p. 340, 1996.

[80] C. Jun, P. Chen, and F.J. Hong, "Applications of Electrohydrodynamics and Joule Heating Effects in Microfluidic Chips: A Review," *Science in China Series E Technological Sciences,* vol. 52, p. 3477, 2009.

[81] T. Schnelle, T. Müller, and G. Fuhr, "Trapping in Ac Octode Field Cages," *Journal of Electrostatics,* vol. 50, pp. 17-29, 2000.

[82] J. Chun-Ping and C. Teng-Wen, "Trapping of Cells by Insulator-Based Dielectrophoresis Using Open-Top Microstructures," *Microsystem Technologies,* vol. 15, p. 1141, 2009.

[83] E. Martínez, E. Engel, J.A. Planell, and J. Samitier, "Effects of Artificial Micro- and Nano-Structured Surfaces on Cell Behaviour," *Annals of Anatomy - Anatomischer Anzeiger,* vol. In Press, Corrected Proof, 2008.

[84] H. Morgan, N.G. Green, M.P. Hughes, W. Monaghan, and T.C. Tan, "Large-Area Travelling-Wave Dielectrophoresis Particle Separator," *J. Micromech. Microeng.,* vol. 7, pp. 65-70, 1997.

[85] B.G. Kim, K.S. Yun, and E. Yoon, "Active Positioning Control of Single Cell Microbead in a Micro-Well Array Chip by Dielectrophoresis," *IEEE,* pp. 702-705, 2005.

[86] C. Cheng-Hsin, W. Ching-Hua, H. You-Ming, and L. Jian-Tang, "Multilayer Electrodes Dep Chip for Single-Cell Level Impedance Measurement," in *Nano/Micro Engineered and Molecular Systems, 2007. NEMS '07. 2nd IEEE International Conference on*, 2007, pp. 821-825.

[87] R.-Z. Lin, C.-T. Ho, C.-H. Liu, and H.-Y. Chang, "Dielectrophoresis Based-Cell Patterning for Tissue Engineering," *Biotechnology Journal,* vol. 1, pp. 949-957, 2006.

[88] L.C. Hsiung, C.H. Yang, C.L. Chiu*, et al.*, "A Planar Interdigitated Ring Electrode Array Via Dielectrophoresis for Uniform Patterning of Cells," *Biosensors and Bioelectronics,* vol. 24, pp. 869-875, 2008.

[89] J. Chun-Ping and et al., "Hydrodynamic Separation of Cells Utilizing Insulator-Based Dielectrophoresis," *Microsystem Technologies,* 2009.

[90] C. Iliescu, L. Yu, F.E.H. Tay, and B. Chen, "Bidirectional Field-Flow Particle Separation Method in a Dielectrophoretic Chip with 3d Electrodes," *Sensors and Actuators B: Chemical,* vol. 129, pp. 491-496, 2008.

[91] J.H. Kang and J.-K. Park, "Technical Paper on Microfluidic Devices —Cell Separation Technology," *APBN,* vol. 9, pp. 1135-1146, 2005.

[92] I. Doh and Y.-H. Cho, "A Continuous Cell Separation Chip Using Hydrodynamic Dielectrophoresis (Dep) Process," *Sensors and Actuators A: Physical,* vol. 121, pp. 59-65, 2005.

[93] H. Tsutsui and C.-M. Ho, "Cell Separation by Non-Inertial Force Fields in Microfluidic Systems," *Mechanics Research Communications,* vol. 36, pp. 92-103, 2009.

[94] P.R.C. Gascyone and J.V. Vykoukal, "Dielectrophoresis-Based Sample Handling in General-Purpose Programmable Diagnostic Instruments," vol. 92, pp. 22-42, 2004 Jan.

[95] P.S. Bangalore and P. Abshire, "On-Chip Capacitance Sensing for Cell Monitoring Applications," *Sensors Journal, IEEE,* vol. 7, pp. 440-447, 2007.

[96] P.M. Patel, A. Bhat, and G.H. Markx, "A Comparative Study of Cell Death Using Electrical Capacitance Measurements and Dielectrophoresis," *Enzyme and Microbial Technology,* vol. 43, pp. 523-530, 2008.

[97] P. Patel and G.H. Markx, "Dielectric Measurement of Cell Death," *Enzyme and Microbial Technology,* vol. 43, pp. 463-470, 2008.

[98] A. Romani , N. Manaresi , L. Marzocchi*, et al.*, "Capacitive Sensor Array for Localization of Bioparticles in Cmos Lab-on-a-Chip," pp. 224-225 Vol.221, 2004.

[99] J. Gimsa and D. Wachner, "A Unified Resistor-Capacitor Model for Impedance, Dielectrophoresis, Electrorotation, and Induced Transmembrane Potential," *Biophys. J.,* vol. 75, pp. 1107-1116, August 1, 1998 1998.

[100] T.B. Jones, "Basic Theory of Dielectrophoresis and Electrorotation," *IEEE Engineering in Medicine and Biology Magazine,* pp. 33-41, 2003 November/December.

[101] H. Morgan and N.G. Green, *Ac Electrokinetics : Colloids and Nanoparticles*: Baldock, Hertfordshire, England. Research Studies Press., 2003.

[102] P.R.C. Gascoyne and J. Vykoukal, "Particle Separation by Dielectrophoresis," *Electophoresis,* vol. 23, pp. 1973-1983, 2002.

[103] M. Hywel, G.I. Alberto, B. David, and G.G. Nicolas, "The Dielectrophoretic and Travelling Wave Forces Generated by Interdigitated Electrode Arrays: Analytical Solution Using Fourier Series," *Journal of Physics D: Applied Physics,* p. 2708, 2001.

[104] M. Castellarnau, N. Zine, J. Bausells*, et al.*, "Integrated Cell Positioning and Cell-Based Isfet Biosensors," *Sensors and Actuators B: Chemical,* vol. 120, pp. 615-620, 2007.

[105] S. Golan, D. Elata, and U. Dinnar, "Hybrid Dielectrophoresis Devices That Employ Electrically Floating Electrodes," *Sensors and Actuators A: Physical,* vol. 142, pp. 138-146, 2008.

[106] S. Golan, D. Elata, M. Orenstein, and U. Dinnar, "Floating Electrode Dielectrophoresis," *Electrophoresis,* vol. 27, pp. 4919-4926, 2006.

[107] L. Zheng, J.P. Brody, and P.J. Burke, "Electronic Manipulation of DNA, Proteins, and Nanoparticles for Potential Circuit Assembly," *Biosensors and Bioelectronics,* vol. 20, pp. 606-619, 2004.

[108] P. Pham, I. Texier, A.S. Larrea*, et al.*, "Numerical Design of a 3-D Microsystem for Bioparticle Dielectrophoresis: The Pyramidal Microdevice," *Journal of Electrostatics,* vol. 65, pp. 511-520, 2007.

[109] A. Ajdari, "Electrokinetic `Ratchet' Pumps for Microfluidics," *Applied Physics A : Materials Science & Processing,* vol. 75, p. 271, 2002.

[110] J.G. Kralj, M.T.W. Lis, M.A. Schmidt, and K.F. Jensen, "Continuous Dielectrophoretic Size-Based Particle Sorting," *Anal. Chem.,* vol. 78, pp. 5019-5025, 2006.

[111] M.P. Hughes, "Numerical Simulation of Dielectrophoretic Ratchet Structures," *Journal of Physics D: Applied Physics,* vol. 37, p. 1275, 2004.

[112] D.S. Gray, J.L. Tan, J. Voldman, and C. S.Chen, "Dielectrophoretic Registration of Living Cells to a Microelectrode Array," *Biosensors and Bioelectronics,* pp. 1765-1774, 2004.

[113] V. Joel, B. Rebecca A, T. Mehmet, G. Martha L, and S. Martin A, "Holding Forces of Single-Particle Dielectrophoretic Traps.," *Biophys J.,* vol. 80(1), pp. 531-541., 2001

[114] L. Altomare, M. Borgatti, M. Medoro*, et al.*, "Levitation and Movement of Human Tumor Cells Using a Printed Circuit Board Device Based on Software-Controlled Dielectrophoresis," *Biotechnology and Bioengineering,* vol. 82, pp. 474-479, 2003.

[115] Y. Huang and R. Pethig, "Electrode Design for Negative Dielectrophoresis," *Measurement Science and Technology,* vol. 2, p. 1142, 1991.

[116] R. Pethig, Y. Huang, X.B. Wang, and J.P.H. Burt, "Positive and Negative Dielectrophoretic Collection of Colloidal Particles Using Interdigitated Castellated Microelectrodes " *J. Phys. D: Appl. Phys.,* vol. 25, p. 881, 1992.

[117] A.P. Lee, T. Yung-Chieh, J. Collins, H. Lung-Hsin, and H. Tsung-Hsi, "Micro and Nano Fluidic Chips for Biosensors," p. 5 pp., 2005.

[118] S.M. Kim, S.H. Lee, and K.Y. Suh, "Cell Research with Physically Modified Microfluidic Channels: A Review," *Lab on a Chip - Miniaturisation for Chemistry and Biology,* vol. 8, pp. 1015-1023, 2008.

[119] J. Nilsson, M. Evander, B. Hammarström, and T. Laurell, "Review of Cell and Particle Trapping in Microfluidic Systems," *Analytica Chimica Acta,* vol. 649, pp. 141-157, 2009.

[120] S.A. Vanapalli, M.H.G. Duits, and F. Mugele, "Microfluidics as a Functional Tool for Cell Mechanics," *Biomicrofluidics,* vol. 3, pp. 12006-12006, 2009.

[121] A.M. Skelley, O. Kirak, H. Suh, R. Jaenisch, and J. Voldman, "Microfluidic Control of Cell Pairing and Fusion.(Report)," *Nature Methods,* vol. 6, p. 147(146), 2009.

[122] W.-H. Tan and S. Takeuchi, "A Trap-and-Release Integrated Microfluidic System for Dynamic Microarray Applications," *Proceedings of the National Academy of Sciences,* vol. 104, pp. 1146-1151, January 23, 2007 2007.

[123] J.K. Park and S. Choi, "Microfluidic System for Dielectrophoretic Separation Based on a Trapezoidal Electrode Array," *Lab on a chip,* vol. 5, pp. 1161-1167, 2005.

[124] Y Huang, R Holzel, R Pethig, and X.B. Wang, "Differences in the Ac Electrodynamics of Viable and Non-Viable Yeast Cells Determined through Combined Dielectrophoresis and Electrorotation Studies," *Physics in Medicine and Biology,* vol. 37, p. 1499, 1992.

[125] H. Imasato and T. Yamakawa, "Measurement of Dielectrophoretic Force by Employing Controllable Gravitational Force," *Journal of Electrophoresis,* vol. 52, pp. 1-8, 2008.

[126] X. Hu, P.H. Bessette, J. Qian, C.D. Meinhart, P.S. Daugherty, and H.T. Soh, "Marker-Specific Sorting of Rare Cells Using Dielectrophoresis," *Proceedings of the National Academy of Sciences of the United States of America,* vol. 102, pp. 15757-15761, November 1, 2005 2005.

[127] S. Burgarella, S. Merlo, B. Dell'Anna, G. Zarola, and M. Bianchessi, "A Modular Micro-Fluidic Platform for Cells Handling by Dielectrophoresis," *Microelectronic Engineering,* vol. 87, pp. 2124-2133, 2010.

[128] M.A.M. Gijs, "Magnetic Bead Handling on-Chip: New Opportunities for Analytical Applications," *Microfluidics and Nanofluidics,* vol. 1, pp. 22-40, 2004.

[129] C.-Y. Huang, C.-H. Kuo, W.-T. Hsiao, K.-C. Huang, S.-F. Tseng, and C.-P. Chou, "Glass Biochip Fabrication by Laser Micromachining and Glass-Molding Process," *Journal of Materials Processing Technology,* vol. 212, pp. 633-639, 2012.

[130] L. Hong, C. Sung-Hoon, J.-B. Lee, L. Cauller, M. Romero-Ortega, and G. Hughes, "Su8-Based Micro Neural Probe for Enhanced Chronic in-Vivo Recording of Spike Signals from Regenerated Axons," *Proc. 5th IEEE Sensors Conf.,* 2006.

[131] C. Dalton and K.V.I.S. Kaler, "A Cost Effective, Re-Configurable Electrokinetic Microfluidic Chip Platform," *Sensors and Actuators B: Chemical,* vol. 123, pp. 628-635, 2007.

[132] Anderson J R, Chiu D T, Jackman R J*, et al.*, "Fabrication of Topologically Complex Three-Dimensional Microfluidic Systems in Pdms by Rapid Prototyping," *Anal. Chem.,* vol. 72, p. 3158, 2000.

[133] J.F. Zhong, Y. Chen, J.S. Marcus*, et al.*, "A Microfluidic Processor for Gene Expression Profiling of Single Human Embryonic Stem Cells," *Lab on a chip,* vol. 8, p. 68, 2008.

[134] S. Talaei, O. Frey, P.D. van der Wal, N.F. de Rooij, and M. Koudelka-Hep, "Hybrid Microfluidic Cartridge Formed by Irreversible Bonding of Su-8 and Pdms for Multi-Layer Flow Applications," *Procedia Chemistry,* vol. 1, pp. 381-384, 2009.

[135] L.M. Lee, R.L. Heimark, J.C. Baygents, and Y. Zohar, "Self-Aligned Immobilization of Proteins Utilizing Peg Patterns," *Nanotechnology,* vol. 17, p. S29, 2006.

[136] Insteclabs.com. (2012, 6 June 2012). *Phd 2000 Syringe Pump Series User's Manual*. Available: http://www.instechlabs.com/Support/manuals/PHD2000manual.pdf

[137] J.D. Yantzi, J.T.W. Yeow, and S.S. Abdallah, "Multiphase Electrodes for Microbead Control Applications: Integration of Dep and Electrokinetics for Bio-Particle Positioning," *Biosensors and Bioelectronics,* vol. 22, pp. 2539-2545, 2007.

[138] T. Schnelle, T. Muller, S. Fiedler, and G. Fuhr, "The Influence of Higher Moments on Particle Behaviour in Dielectrophoretic Field Cages," *Journal of Electrostatics,* vol. 46, pp. 13-28, 1999.

[139] K. Khoshmanesh, S. Baratchi, F. Tovar-Lopez*, et al.*, "On-Chip Separation of Lactobacillus Bacteria from Yeasts Using Dielectrophoresis," *Microfluidics and Nanofluidics,* vol. 12, pp. 597-606, 2012/01/01 2012.

[140] K. Khoshmanesh, N. Kiss, S. Nahavandi*, et al.*, "Trapping and Imaging of Micron-Sized Embryos Using Dielectrophoresis," *ELECTROPHORESIS,* vol. 32, pp. 3129-3132, 2011.

[141] B. Kannan, D.E. Williams, K. Khoshmanesh, G.A. Bowmaker, and J. Travas-Sejdic, "The Electrochemical Growth of Conducting Polymer “Nanowires”," *Journal of Electroanalytical Chemistry,* vol. 669, pp. 82-89, 2012.

[142] T. Schnelle, T. Müller, C. Reichle, and G. Fuhr, "Combined Dielectrophoretic Field Cages and Laser Tweezers for Electrorotation," *Applied Physics B: Lasers and Optics,* vol. 70, pp. 267-274, 2000.

[143] S. Kobel, A. Valero, J. Latt, P. Renaud, and M. Lutolf, "Optimization of Microfluidic Single Cell Trapping for Long-Term on-Chip Culture," *Lab on a Chip,* vol. 10, pp. 857-863, 2010.

[144] F. Samsuri, M.M. Alkaisi, J.S. Mitchell, and J.J. Evans, "Replication of Cancer Cells Using Soft Lithography Bioimprint Technique," *Microelectronic Engineering,* vol. 87, pp. 699-703, 2010.